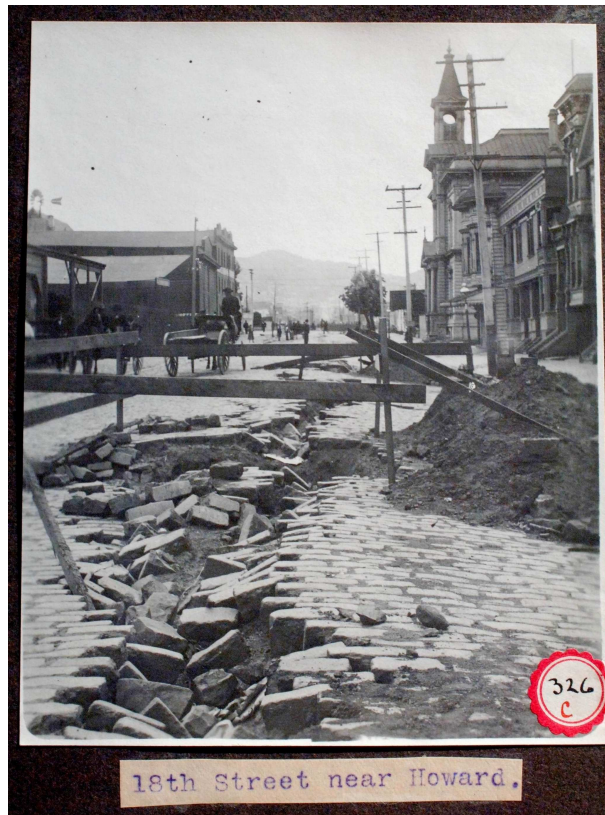


Berkeley Seismological Laboratory



Annual Report
July 2005 - June 2006

Berkeley Seismological Laboratory
Annual Report
July 2005 - June 2006

Cover Picture

Photograph of damage to 18th Street near Howard St. in San Francisco due to the 1906 earthquake. This photograph, from the archives of the Berkeley Seismological Laboratory was one of many taken by H.C. Branner in his efforts to document the effects of the quake for the *Report of the State Earthquake Investigation Commission*

Contents

1	Director's Report	1
1.	Background and Facilities	2
2.	Highlights of 2005-2006	3
3.	BSL staff news	6
4.	Acknowledgements	7
2	In Memoriam: Bruce Bolt	8
3	Research Studies	11
1.	Is Earthquake Rupture Deterministic?	12
2.	Periodic Pulsing of the San Andreas Fault: An Update	15
3.	Monitoring Nonvolcanic Tremor on the San Andreas Fault	17
4.	Repeating Earthquakes on an Imbricated Thrust Fault in the Arc-Continent Collision Boundary of Eastern Taiwan	19
5.	Subsurface Creep From Repeating Earthquakes at the Juncture of the San Andreas and Calaveras Faults	21
6.	Kinematic Modeling of the 2004 Parkfield Earthquake	22
7.	Identifying Isotropic Events Using an Improved Regional Moment Tensor Inversion Technique	24
8.	3D Simulations of Ground Motions of the 1989 Loma Prieta Earthquake Using the USGS SF06 Velocity Model	28
9.	Toward Earthquake Early Warning in Northern California	30
10.	Identifying and Removing Noise from the Monterey Ocean Bottom Broadband Seismic Station (MOBB) Data	33
11.	The Orinda Earthquake Sequence: Complexity in Small Earthquakes	36
12.	Northern California Seismicity Project	38
13.	Seismogram Scanning Project	40
14.	Regional Attenuation Method Comparison for Northern California	43
15.	Geodetically Constraining Indian Plate motion and Implications for Plate Boundary Deformation	46
16.	Large Scale Ground Deformation of Etna Observed by GPS Between 1994 and 2001	48
17.	Parkfield-Hollister Electromagnetic Monitoring Array	50
18.	Observation and Analysis of Vertical Electric Fields in the Earth	53
19.	Surface Deformation and Fault Kinematics of the San Francisco Bay Area from PS-InSAR Analysis	57
20.	Slip of the 2004 Sumatra-Andaman Earthquake from Joint Inversion of Long Period Global Seismic Waveforms and GPS Static Offsets	61
21.	Inversion for the Velocity Structure of the Santa Clara Valley, California	63
22.	A Study of the Relation between Ocean Storms and the Earth's Hum	65
23.	Physically Constrained Inversion of Long-Period Seismic Data: Insights on the Nature of the Transition Zone	67
24.	The Fate of the Juan de Fuca Plate	71
25.	Applying the Spectral Element Method to Model 3D Attenuation in the Upper Mantle	73
26.	Radial and Azimuthal Anisotropic Structure of the North American Upper Mantle From Inversion of Surface Waveform Data	76
27.	Improvements in Waveform Modeling and Application to Eurasian Velocity Structure	78
28.	Toward Constraints on Lateral S Wave Velocity Gradients around the Pacific Superplume	80
29.	Joint Inversion for 3D Velocity Structure of the Broader Africa-Eurasia Collision Region	81

30.	A Three Dimensional Radially Anisotropic Model of Shear Velocity in the Whole Mantle	83
31.	Short Wavelength Topography on the Inner Core Boundary	85
32.	Long Period Seismology on Europa	87
33.	Tidal Excitation of Free Oscillations of Icy Satellites	89
34.	A Comparison of Standard Inversion, Neural Networks and Support Vector Machines	92
BSL Operations		96
4	Berkeley Digital Seismic Network	97
1.	Introduction	97
2.	BDSN Overview	97
3.	2005-2006 Activities	102
4.	Acknowledgements	107
5.	References	107
5	California Integrated Seismic Network	108
1.	Introduction	108
2.	CISN Background	108
3.	2005-2006 Activities	109
4.	Statewide Integration	111
5.	Acknowledgements	114
6.	References	115
6	Northern Hayward Fault Network	116
1.	Introduction	116
2.	NHFN Overview	116
3.	2005-2006 Activities	121
4.	Acknowledgments	125
5.	References	125
7	Parkfield Borehole Network (HRSN)	126
1.	Introduction	126
2.	HRSN Overview	126
3.	2005-2006 Activities	132
4.	Acknowledgments	136
5.	References	136
8	Bay Area Regional Deformation Network	137
1.	Introduction	137
2.	BARD overview	137
3.	2005-2006 Activities	141
4.	Data Analysis and Results	142
5.	Acknowledgements	142
6.	References	143
9	Northern California Earthquake Data Center	146
1.	Introduction	146
2.	2005-2006 Activities	146
3.	Data Collections	146
4.	NCEDC Operations	153
5.	Data Quality Control	154
6.	Database Development	154
7.	Data Distribution	155
8.	Acknowledgements	157

10 Data Acquisition and Quality Control	158
1. Introduction	158
2. Data Acquisition Facilities	158
3. Data Acquisition	159
4. Seismic Noise Analysis	160
5. Sensor Testing Facility	161
6. STS-1 Electronics Development	161
7. Acknowledgements	162
8. References	162
11 Northern California Earthquake Monitoring	163
1. Introduction	163
2. Northern California Earthquake Management Center	163
3. 2005-2006 Activities	164
4. Routine Earthquake Analysis	166
5. Acknowledgements	168
6. References	168
12 Outreach and Educational Activities	171
1. Introduction	171
2. Highlights of 2005-2006	171
3. On-Going Activities	172
4. Acknowledgements	173
13 Glossary of Common Acronyms	174
Appendix I Publications, Presentations, and Panels 2005-2006	175
Appendix II Seminar Speakers 2005-2006	186
Appendix III Organization Chart 2005-2006	188

Chapter 1

Director's Report

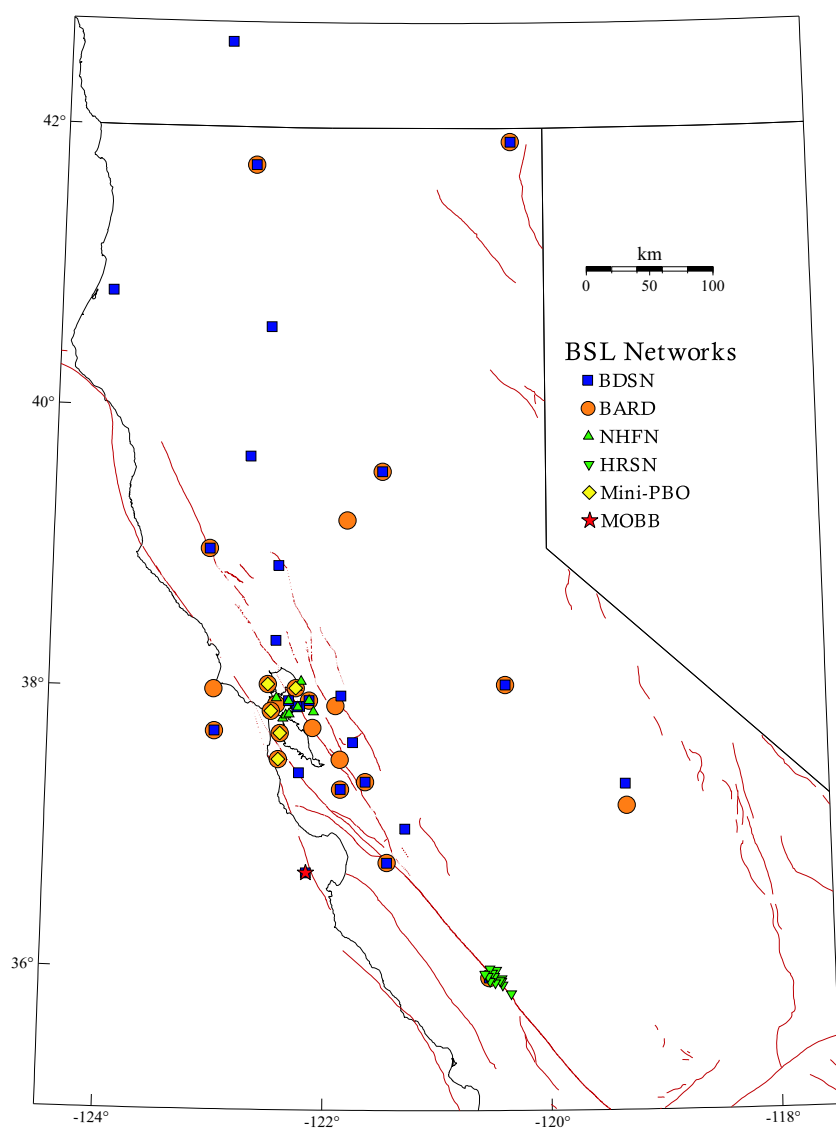


Figure 1.1: Map illustrating the distribution of stations in the BDSN, NHFN, HRSN, BARD, and Mini-PBO networks in northern and central California. A star indicates the location of the MOBB deployment.

1. Background and Facilities

The Berkeley Seismological Laboratory (BSL), formerly the Berkeley Seismographic Station (BSS), is the oldest Organized Research Unit (ORU) on the UC Berkeley campus. Its mission is unique in that, in addition to research and education in seismology and earthquake-related science, it is responsible for providing timely information on earthquakes (particularly those that occur in northern and central California) to the UC Berkeley constituency, the general public, and various local and state government and private organizations. The BSL is therefore both a research center and a facility/data resource, which sets it apart from most other ORUs. A major component of our activities is focused on developing and maintaining several regional observational networks, and participating, along with other agencies, in various aspects of the collection, analysis, archival, and distribution of data pertaining to earthquakes, while maintaining a vigorous research program on earthquake processes and Earth structure. In addition, the BSL staff spends considerable time with public relations activities, including tours, talks to public groups, responding to public inquiries about earthquakes, and, more recently, World-Wide-Web presence (<http://www.seismo.berkeley.edu/seismo/>).

UC Berkeley installed the first seismograph in the Western Hemisphere at Mount Hamilton (MHC) in 1887. Since then, it has played a leading role in the operation of state-of-the-art seismic instruments and in the development of advanced methods for seismic data analysis and interpretation. Notably, the installation, starting in 1927, of Wood-Anderson seismographs at 4 locations in northern California (BKS, ARC, MIN and MHC) allowed the accurate determination of local earthquake magnitude (M_L) from which a unique historical catalog of regional earthquakes has been maintained to this day, providing crucial input to earthquake probabilities studies.

Over the years, the BSS continued to keep apace of technological improvements. The first centrally telemetered network using phone lines in an active seismic region was installed by BSS in 1960. The BSS was the first institution in California to operate a 3-component “broadband” system (1963). Notably, the BSS played a major role in the early characterization of earthquake sources using “moment tensors” and source-time functions, and made important contributions to the early definitions of detection/discrimination of underground nuclear tests and to earthquake hazards work, jointly with UCB Engineering. Starting in 1986, the BSS acquired 4 state-of-the-art broadband instruments (STS-1), while simultaneously developing PC-based digital telemetry, albeit with limited resources. As the telecommunication and computer technology made rapid progress, in parallel with broadband instrument development, paper record reading could be completely abandoned in favor of largely

automated digital data analysis.

The current modern facilities of BSL have been progressively built over the last 14 years, initiated by significant “upgrade” funding from UC Berkeley in 1991-1995. The BSL currently operates and acquires data, continuously and in real-time, from over 60 regional observatories, housing a combination of broadband and strong motion seismic instrumentation installed in vaults, borehole seismic instrumentation, permanent GPS stations of the Bay Area Regional Deformation (BARD) network, and electromagnetic sensors. The seismic data are fed into the BSL real-time processing and analysis system and are used in conjunction with data from the USGS NCSN network in the joint earthquake notification program for northern California, started in 1996. This program capitalizes on the complementary capabilities of the networks operated by each institution to provide rapid and reliable information on the location, size and other relevant source parameters of regional earthquakes. In recent years, a major emphasis in BSL instrumentation has been in densifying the state-of-the-art seismic and geodetic networks, while a major on-going emphasis in research has been the development of robust methods for quasi-real time automatic determination of earthquake source parameters and predicted strong ground motion, using a sparse network combining broadband and strong motion seismic sensors, as well as permanent geodetic GPS receivers.

The backbone of the BSL operations is a regional network of 25+ digital broadband and strong motion seismic stations, the Berkeley Digital Seismic Network (BDSN), with continuous telemetry to UC Berkeley. This network provides the basic regional data for the real-time estimation of location, size and rupture parameters for earthquakes of M 3 and larger in central and northern California, within our Rapid Earthquake Data Integration (REDI) program and is the Berkeley contribution to the California Integrated Seismic Network (CISN). It also provides a fundamental database for the investigation of three-dimensional crustal structure and its effects on regional seismic wave propagation, which is ultimately crucial for estimating ground shaking for future earthquakes. Most stations also record auxiliary temperature/pressure channels, valuable in particular for background noise quality control. Complementing this network is a ~ 25 station “high-resolution” network of borehole seismic sensors located along the Hayward Fault (HFN) and under the Bay Area bridges, operated jointly with the USGS/Menlo Park and linked to the Bridge Safety Project of the California Department of Transportation (Caltrans). The latter has facilitated the installation of sensor packages at 15 bedrock boreholes along 5 east-bay bridges in collaboration with Lawrence Livermore National Laboratory (LLNL). A major science goal of this network is to collect high signal-to-noise data

for micro-earthquakes along the Hayward Fault to gain insight into the physics that govern fault rupture and its nucleation. The BSL is also involved in the operation and maintenance of the 13 element Parkfield borehole seismic array (HRSN), which is yielding enlightening results on quasi-periodic behavior of micro-earthquake clusters and important new constraints on earthquake scaling laws and is currently playing an important role in the characterization of the site for the future San Andreas Fault Observatory at Depth (SAFOD). Since April 2002, the BSL is also involved in the operation of a permanent broadband ocean bottom station, MOBB, in collaboration with MBARI (Monterey Bay Aquarium Research Institute).

In addition to the seismic networks, the BSL is involved in data archival and distribution for the permanent geodetic BARD Network as well as the operation, maintenance, and data processing of 22 out of its 70+ sites. Whenever possible, BARD sites are collocated with BDSN sites in order to minimize telemetry costs. In particular, the development of analysis methods combining the seismic and geodetic data for the rapid estimation of source parameters of significant earthquakes has been one focus of BSL research.

Finally, two of the BDSN stations (PKD, SAO) also share data acquisition and telemetry with 5-component electromagnetic sensors installed with the goal of investigating the possibility of detection of tectonic signals. In 2002-2003, an automated quality control software was implemented to monitor the electromagnetic data.

Archival and distribution of data from these and other regional networks is performed at the Northern California Earthquake Data Center (NCEDC), operated at the BSL in collaboration with USGS/Menlo Park. The data reside on a mass-storage device (current holdings ~ 10 TerraBytes), and are accessible "on-line" over the Internet (<http://www.quake.geo.berkeley.edu>). Among others, data from the USGS Northern California Seismic Network (NCSN), are archived and distributed through the NCEDC. The NCEDC also maintains, archives and distributes the ANSS/CNSS earthquake catalog.

Core University funding to our ORU has suffered from permanent budget cuts to research programs from the State of California, and currently provides salary support for 2 field engineers, one computer expert, 2 data analysts, 1 staff scientist and 2 administrative staff. This supports a diminishing portion of the operations of the BDSN and provides seed funding for our other activities. All other programs are supported through extramural grants primarily from the USGS and NSF, and in the past five years, the Governor's Office of Emergency Services (OES). We acknowledge valuable recent contributions from other sources such as Caltrans, the CLC program and PEER, as well as our Earthquake Research Affiliates.

2. Highlights of 2005-2006

2.1 Research Accomplishments

Chapter 3 documents the main research contributions of the past year. Research at the BSL spans a broad range of topics, from the study of microseismicity at the local scale to global deep earth structure, and includes the use of seismological, geodetic, and remote sensing (InSAR) techniques.

Richard Allen and his students have continued to develop a methodology for earthquake early warning (1.,9.), documenting, in particular, that, for large earthquakes, the frequency content of radiated seismic energy within the first few seconds of rupture scales with the final magnitude of the event.

Bob Nadeau and collaborators continued to work on characteristically repeating micro-earthquakes (2.,5.). In particular, Nadeau has extended the study published in 2004 to investigate if the time varying patterns of periodic pulsing of deep slip, extends through an additional 5 years. The successful prediction of time periods with increased likelihood for larger earthquakes based on his earlier data suggest that there is significant potential in his approach to refine time dependent earthquake forecasts, at least for the central San Andreas Fault segment (2.). Nadeau and collaborators are also studying repeating earthquakes in other tectonic settings, such as Taiwan (4.).

Studies of data generated by the M6 2004 Parkfield earthquakes continue. Nadeau and collaborators have been further documenting the time and space distribution of non-volcanic tremors on the San Andreas fault near Parkfield (3.). Graduate student Karl Kappler has been refining EM data analysis procedures (17., 34., 18.). Doug Dreger and his student Ahyi Kim have developed a kinematic model of the Parkfield earthquake using jointly GPS and seismic data (6.).

Doug Dreger and his students and collaborators have also worked on a variety of source and structure topics including the development of a promising method to identify seismic events with a strong isotropic component, very relevant to the recent nuclear test in North Korea (7.), new earthquake ground motion simulations using the recently developed USGS SF06 velocity model (8.), the determination of structure in the Santa Clara Valley using both teleseisms and microearthquake data (21.), and evaluation of methodologies to constrain attenuation models in northern California (14.).

Geodetic studies include work by Roland Bürgmann and his students and post-docs on the surface deformation in the San Francisco Bay Area using InSAR data (19.) and on the motion of the Indian plate (15.), as well as work by Nicolas Houlié and collaborators on the deformation of the Etna volcano, using GPS (16.). In a collaborative effort involving three BSL faculty members

(Dreger, Bürgmann and Romanowicz), separate tools developed by each of them were combined by graduate student Junkee Rhie to obtain a slip model for the great M9 2004 Sumatra earthquake, based on teleseismic and near field geodetic data (20.).

Other regional studies include continuation by Bob Uhrhammer of the study of Bay Area historical seismicity (12.) and, in particular, scanning of old seismograms with the help of undergraduates (13.); the study by Peggy Hellweg of an unusual sequence of earthquakes near Orinda, CA (11.); and the development of a methodology to reduce long period ocean noise at the broadband ocean bottom station MOBB(21.).

On the topic of relation of oceanography and seismology, Romanowicz and her student Junkee Rhie have continued their study of the relation of ocean storms to the earth's long period noise known as "hum", and followed a particular sequence of storms across the Pacific (22.), showing how the generation of the hum involves a three stage process (ocean waves, infragravity waves, seismic waves).

Deep earth structure studies start in the upper mantle, with work by graduate student Mei Xue with Richard Allen on a regional tomographic model beneath northwestern US, tracking the fate of the Juan de Fuca plate down to 400 km (24.), while post-doc Federica Marone, working with Barbara Romanowicz, has developed a tomographic model of S velocity and anisotropy beneath the entire North American continent, documenting the presence of two layers of anisotropy beneath the stable continent, one in the lithosphere and one in the asthenosphere (26.). Federica has also been working, with collaborators at Northwestern Univ., on a similar model for the Mediterranean region (29.). Also on the regional scale, graduate student Ahyi Kim, working with post-doc Mark Panning and Barbara Romanowicz, has developed a regional upper mantle 3D model for southeast Asia (27.). This model is the first step towards developing a higher resolution model of this region using more sophisticated tools for 3D wave propagation.

As in previous years, Romanowicz and her group have continued their work on refining tomographic models of mantle structure at the global scale (30.,28.) and have started to obtain results from a new approach, combining seismic and mineral physics constraints to map lateral variations of temperature and composition in the upper mantle (23.). Also, graduate student Ved Lekic has started constructing a new global 3D model of attenuation in the upper mantle, using the spectral element method to compute synthetic seismograms in an elastic model (25.). With post-doc Aimin Cao, Romanowicz also continues work on core structure, one example of which is given in this report, documenting the possible presence of short wavelength topography on the inner core boundary (31.).

Finally, combining expertise in seismology and geodynamics, a study of the constraints on the structure of Jupiter's satellite Europa that could be obtained with seismic data has given rise to two publications (32.), while Ved Lekic, working with Michael Manga, has been investigating tidal excitation of free oscillations on Saturn's moon Enceladus (33.).

2.2 Infrastructure and Earthquake Notification

Highlights in 2005-06 include the BSL's participation in the commemoration activities of the 1906 earthquake's centennial anniversary (see Chapter 12). These activities included a joint SSA/EERI/DRC conference which was held in San Francisco in April 2006. The BSL, and specifically Dr Peggy Hellweg, were heavily involved in its organization. The BSL also helped develop many exhibits, classes, and a series of public lectures on the UC Berkeley Campus, which were held between October 2005 and April 2006. Richard Allen and Barbara Romanowicz taught a Freshman Seminar on the subject of the 1906 earthquake and earthquake preparedness, which resulted in an informational movie, put together by the students, and targeted at incoming Berkeley freshmen. This movie is available through several websites on Campus, in particular: <http://seismo.berkeley.edu/~rallen/BEAR>

Another new activity began in February 2006, with funding from NSF through the IRIS/GSN program (Global Seismic Network). It is a collaborative project with Tom VanZandt of Metrozet on the design and testing of new electronics for the STS-1 very broadband seismometer which occupies several hundred sites around the world, and in particular 10 of the Berkeley sites. The manufacturer of this sensor of unsurpassed quality has discontinued its production, but no equivalent new instrument of any design is available. Meanwhile the STS-1s, many of which have been around for 15-20 years, are deteriorating with age. In the Spring of 2006, significant effort was deployed at BSL to set up a testbed at the Byerly Vault to test successive iterations of new electronics developed by Metrozet.

As in the previous year, BSL's infrastructure development efforts have centered around several major projects:

- operation and enhancement of the joint earthquake notification system with USGS/Menlo Park.
- the continuing development of the California Integrated Seismic Network
- participation, at various levels, in three components of the national Earthscope program: the deployment in northern California of the *BigFoot* component of USArray, archival of borehole strainmeter data in the framework of the Plate Boundary Observatory (PBO), and the preparation for archival

of the data from the San Andreas Fault Observatory at Depth (SAFOD).

- development of borehole networks at Parkfield and along the Hayward Fault
- operation and further enhancements of the BARD network of continuous GPS
- operation of the Northern California Earthquake Data Center

The main goal of the CISN (see Chapter 5) is to ensure a more uniform system for earthquake monitoring and reporting in California. The highest priority, from the point of view of emergency responders in California, is to improve the robustness of statewide real-time notification and to achieve a uniform interface across the State to the California OES and other emergency responders. This represents a major challenge, as the CISN started as a heterogeneous collection of networks with disparate instrumentation, software systems and culture. Much effort has gone over the past few years to develop coordinated software between southern and northern California and in northern California, between Berkeley and USGS/Menlo Park. These two institutions are joined together in the Northern California Earthquake Management Center (NCEMC). Until now, earthquake processing responsibilities were divided into two components. Responsibility for running the association, location and duration magnitude modules has resided with Menlo Park, while local and moment magnitude, and finite-fault modules run in Berkeley. Redundancy is built into the system by operating two complete systems at all times, the second one as a "hot" backup. Recognizing potential problems associated with the separation of critical system elements across the San Francisco Bay, an effort was launched in 2001 to redesign the Northern California operations. In the new system, which is currently in advanced test mode, two complete systems, which provide processing from detection to location and computation of ground motion parameters and Shakemaps, will operate one in Berkeley and one in Menlo Park. Its implementation is awaiting the retirement of the CUSP real-time earthquake timing system in Menlo Park (see chapter 10). In the past year, CISN funds were also used to complete new broadband stations at Alder Springs, CA (GASB), and at the Marconi Conference Center near Point Reyes (MCCM). FEMA funds made available following the San Simeon earthquake of 2003 are being combined with CISN funds, to purchase equipment for 7 additional new stations that will fill gaps in the present distribution of broadband stations in northern California. This past year the equipment has been ordered and the sites identified among currently operating temporary northern California sites

of the Earthscope/USArray program. BSL staff continue to spend considerable efforts in organizational activities for CISN, notably by participating in the CISN Project Management Group (Neuhauser and Hellweg), which includes weekly 2 hour phone conferences, and the Standards Committee (Neuhauser-chair, Hellweg, Lombard), which strives to define and coordinate software development tasks. Romanowicz and Hellweg serve on the CISN Steering Committee. Doug Neuhauser has also been serving on the CISN Steering Committee in the transition period following Lind Gee's departure in summer 2005. The CISN also represents California as a designated region of ANSS (Advanced National Seismic System) and the BSL is actively involved in planning activities for the ANSS.

The BSL concluded an agreement in June 2004 with IRIS to contribute 19 stations of the BDSN to USArray, while the experiment is deployed in California. This includes 17 existing stations and the two new sites mentioned above: GASB and MCCM. In the past year, BSL has continued to acquire telemetered data from these and other northern California USArray stations and to pay particular attention to the maintenance of those permanent sites which are part of USArray.

The BSL has completed the relocation of the critical operations of data acquisition, processing, archiving and data distribution to 2195 Hearst ("SRB-1"), a recently completed building on Oxford Tract, which was constructed to current seismic codes, with special attention to post-earthquakes operability of the campus computer facility. The computer center contains state-of-the-art seismic bracing, UPS power and air conditioning with generator back-up and extensive security and equipment monitoring. In the past year, BSL has finished moving all of its data acquisition, real-time earthquake processing computers, and data archive and distribution computers to the new facility, including telemetry equipment.

The Parkfield borehole network (HRSN, see chapter 7) undertook an effort to upgrade power modules in early 2005. This has now been completed and has effectively eliminated data drop outs and gaps that had plagued the network during the winter months. The HRSN continues to play a key role in support of the Earthscope SAFOD (San Andreas Fault Observatory at Depth) drilling project, by providing low noise waveforms for events in the vicinity of the target drilling zone. A procedure is underway to refine an automated similar event detection method based on cross-correlation and pattern scanning of the continuous HRSN data, to assist researchers working on repeating micro-earthquakes as well as those working on the target events in the SAFOD drilling zone.

In the past year, infrastructure development for the Northern Hayward Fault Network (NHFN, see chapter 6) has progressed notably. The coverage on the west side of

the Bay has been augmented with the installation of the "Mini-PBO" station MHDL (Marin Headlands), which comprises borehole seismometers and a continuous GPS receiver. It is now part of the NHFN and of the BARD 8 network. Caltrans has provided funding and support for instrumentation of 3 land sites for the NHFN. Station VALB (Vallejo, CA) is operational, whereas PETB (Petaluma River Bridge) is instrumented and awaiting completion of telemetry infrastructure. The third hole has been drilled at St. Mary's College (SMCB) and is nearing completion. On-going network maintenance involves regular inspection of the collected seismic waveform data and spectra for nearby seismic events, and for noise samples, in order to assure that the instruments operate at maximum performance to capture the source spectrum of micro-earthquakes down to negative magnitudes.

The last year has been a transition period for the BARD continuous GPS (C-GPS) network, with the departure of Mark Murray and arrival of Nicolas Houlié. Also, the landscape has been changing in northern California with the construction of the Plate Boundary Observatory (PBO) of Earthscope, which is installing many new C-GPS stations. We are working with PBO to transfer several of our stations to PBO, those that are either not accessible by continuous telemetry or collocated with broadband seismic stations. We are also refocusing BARD on real-time continuous data acquisition at high sampling rates for earthquake hazards applications, responding to a growing interest of our own researchers and of the community. Data from the BARD stations have been traditionally acquired at 15 or 30 s sampling rates, but, for these applications, 1 s or higher sampling rates are needed. Conversion to these higher rates is limited by the telemetry capabilities and nature of receivers at each individual station. We started collecting 1 Hz data at 2 stations in 2003. In the last year, we progressively upgraded nine additional stations to continuous 1 Hz telemetry. These data are made publicly available at the NCEDC, while we develop methods to combine them with seismic data in our real-time earthquake notification system. We have recently acquired 5 new receivers (Ashtech μZ) which will enable us to upgrade several of the sites collocated with BDSN stations.

The NCEDC (see Chapter 9), continues archival and on-line distribution of data from expanding BDSN, NHFN, HRSN, BARD, Mini-PBO, and other networks and data collections in northern California and Nevada, including telemetered continuous data from USArray stations in northern California and vicinity. We are continuing to receive data from the SAFOD pilot hole and main hole, and data from 15 SCSN (southern California) broadband sites as part of the CISN robust "backbone". Previously, only event data were archived from the 1000+ components of the Northern California Seismic Network

(NCSN) operated by USGS/Menlo Park. As a major accomplishment in the past year, we have developed the necessary software and procedures and are now archiving continuous NCSN seismograms at NCEDC. We have developed software and are retroactively working our way to transfer older data from tapes to complete the on-line collection. Having easy access to these continuous data is important, in particular, for scientists working on non-volcanic tremors. It is also of interest to global seismologists working on body waves from large teleseisms. The change from event archiving to continuous archiving has significantly increased the amount of data archived (from 35GB/year to ~ 1750 GB/year). This was accomplished with no additional NCEDC staff, and was made possible by our work to automate the data delivery and archival process, and by the significant decrease in the cost of RAID disk systems.

Finally, with seed funding from the USGS to Prof. Richard Allen, we have started work on the establishment and testing of a prototype earthquake early warning system.

3. BSL staff news

This past year has seen many changes in BSL personnel. Following Eleanor Blair's retirement, Kristen Jensen joined BSL as our new Manager in February 2006. Kristen previously worked as senior analyst in the office of the VCR. We are very fortunate to have her. Jenny Pehl left BSL in July 2006 to follow her husband to a new job in Las Vegas. Nicolas Houlié was hired as a post-doc in February 2006 to take responsibility for our continuous GPS program.

Four graduate students associated with BSL completed their PhD's in the past year: Aimin Cao, Junkee Rhie, David Dolenc and Ingrid Johannson. Ingrid joined the USGS/Menlo Park on a Mendenhall Post-doc, David is in Minnesota (Univ. of Minnesota in Duluth), while Aimin and Junkee are staying on as post-doc's at BSL. Mark Panning, who had stayed as post-doc at BSL after completing his PhD in Fall 2004, left for Princeton in July 2006, where he has a post-doctoral fellowship.

New arrivals have continued through the summer and early Fall of 2006. Kevin Mayeda transferred from LLNL to join BSL research staff in July, while Cyndy Bresloff has been helping with routine processing and data quality control since mid-August. Tina Barber-Riggins joined the business office in September. Alexei Kireev and Mario Aranha joined the programming team in September and October, respectively. They will assist Doug Neuhauser with tasks related to the CISN, the Early Warning Project and the NCEDC.

This year has also been marked by very sad news: Professor Bruce Bolt, who was Director of the Seismographic Stations from 1963 to 1989, passed away after a brief ill-

ness on July 21, 2005, just a few months before the start of the celebrations of the 1906 San Francisco earthquake centennial. A memorial, attended by over 500 people, was held for him at the Faculty Club on July 29, 2005. We include in this report a copy of the obituary (draft version as of 10/17/06) which we have been putting together for UC Berkeley.

4. Acknowledgements

I wish to thank our technical and administrative staff, scientists and students for their efforts throughout the year and their contributions to this Annual Report. Individual contributions to activities and report preparation are mentioned in the corresponding sections, except for the Appendix section, prepared by Kate Conner and Kristen Jensen.

I also wish to specially thank the individuals who have regularly contributed to the smooth operation of the BSL facilities: Rich Clymer, Doug Dreger, John Friday, Jarrett Gardner, Peggy Hellweg, Nicolas Houlié, Bill Karavas, Rick Lelling, Pete Lombard, Rick McKenzie, Mark Murray, Bob Nadeau, Doug Neuhauser, Charley Paffenbarger, Bob Uhrhammer, and Stephane Zuzlewski, and in the administrative office, Kristen Jensen, Kate Conner, Jenny Pehl and Yolanda Andrade. I particularly wish to thank Doug Dreger for serving as Associate Director of the BSL, Peggy Hellweg for taking on responsibilities for CISN and data analysis coordination, Doug Neuhauser for his efforts to build the Earthscope related archival system, and Bill Karavas for organizing an effective test bed for the refurbishment of the STS-1 electronics.

I also wish to thank our undergraduate assistants, Brian Castriota, Chi Sum Chan, Mehershad Dahmubed, Josh Hunt, Kevin Lee, Rose Li, Tomasz Matlak, Rob Porritt, Jake Siegal, Gretchen Sites and Noi Valera for their contributions to our research and operational activities.

I am particularly thankful to Kate Conner and Peggy Hellweg, for their help in putting together this Annual Report.

The Annual Report of the Berkeley Seismological Laboratory is available on the WWW at http://www.seismo.berkeley.edu/seismo/annual_report/.

Barbara Romanowicz
October 15, 2006

Chapter 2

In Memoriam: Bruce Bolt

David Brillinger, Joseph Penzien and Barbara Romanowicz

Bruce Alan Bolt, Professor Emeritus of Seismology at the University of California, Berkeley, died suddenly of pancreatic cancer at Kaiser Permanente Medical Center in Oakland, California on July 21, 2005.

Professor Bolt was born on February 15, 1930 in the small town of Largs, New South Wales, Australia. He attended Largs Public School, Maitland Boys High School, Newcastle Technical College, New England University College, Sydney's Teachers College, and the University of Sydney, all located in New South Wales. Majoring in applied mathematics, he received a B.Sc. degree in 1952 from the New England University College, and M.Sc., Ph.D., and D.Sc. degrees in 1955, 1959, and 1972, respectively, from the University of Sydney. In 1953, he received a Diploma of Education from the Sydney Teachers College.

Having decided upon an academic career, Professor Bolt first taught at Sydney Boys High School in 1953, then progressed through the ranks as Lecturer, 1954-1959, and Senior Lecturer, 1959-1962, in the Department of Applied Mathematics at the University of Sydney. During the period 1963-1993, he served as Professor of Seismology in the Department of Geology and Geophysics at the University of California, Berkeley (UCB) and as Director of UCB's Seismographic Stations. In his early years at UCB, Professor Bolt developed strong research interests with faculty members in structural and geotechnical engineering, which resulted in his serving as Professor of Civil and Environmental Engineering during the period 1983-1993. Upon retiring from UCB in 1993, he received the campus' highest honor, the Berkeley Citation, then became Professor Emeritus of Seismology and Professor in the Graduate School, thus continuing his academic activities until his death.

As a graduate student and lecturer at the University of Sydney, Professor Bolt developed outstanding expertise in the specialty areas of applied mathematics, statistics, and geophysics. As a result, he continued to make valuable contributions to advancing knowledge in these areas throughout his career. His strongest desire was to understand natural phenomena, particularly their mathematical and statistical descriptions. He wrote numerous

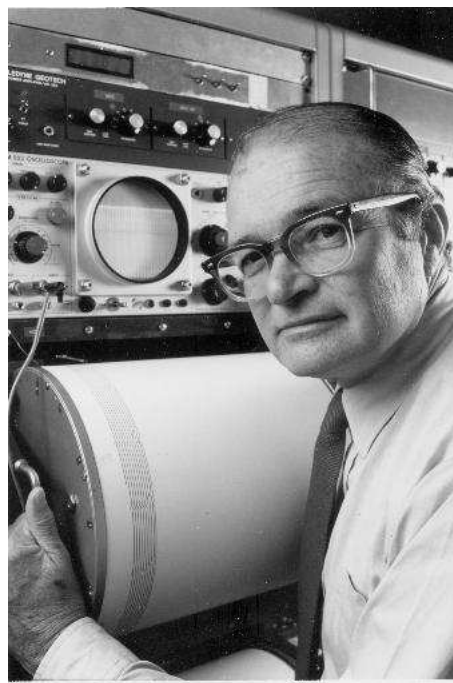


Figure 2.1: Bruce Bolt (1930 - 2005)

novel papers pertaining to the deep earth, dispersion, earthquake engineering, free oscillations, seismology, and statistics. His first published paper was a 1957 note in *Nature*, followed by one in *Geophysical Journal of the Royal Astronomical Society*, on seismic observations of the 1956 atomic explosions in Australia. In 1960, he published a paper with John Butcher on the dispersion of seismic waves, which began his deep involvement with large data sets and digital computing. His creativity in and knowledge of statistical methodologies, with influence from Harold Jeffreys, led to the estimation technique for the revision of earthquake epicenters still in use today (2006). As part of that work, he led statisticians by some ten years in developing the method of robust regression. His many contributions to seismology, including the development of earth models, have involved finite el-

ement methods, elastic wave-propagation theory, broadband and digital recording, strong-motion array development, data collection and interpretation, attenuation relations, and earthquake statistics.

Professor Bolt's numerous publications on topics in seismology include four very popular books: (1) *Earthquakes: A Primer*, 1978, (2) *Inside the Earth: Evidence from Earthquakes*, 1982, (3) *Earthquakes and Geological Discovery*, 1993, and (4) five editions of *Earthquakes*, 5th Edition, 2003. In recognition of his many contributions to seismology, he was elected Fellow of the American Geophysical Union and the Geological Society of America, Associate of the Royal Astronomical Society, and Overseas Fellow of Churchill College, Cambridge. He served as President of the Seismological Society of America in 1974 and editor of its *Bulletin* from 1965 to 1972, President of the International Association of Seismology and Physics of the Earth's Interior from 1980 to 1983, President of the Consortium of Organizations for Strong-Motion Observation Systems (COSMOS), and President of the California Academy of Sciences.

Notably, Professor Bolt was actively involved from the early 1960's through the mid-1980's in the development of reference earth models and towards this goal. contributed many measurements of body wave travel times as well as free oscillation eigenfrequencies and attenuation. He was particularly interested in constraining the average earth structure near two major interfaces: the solid/liquid core mantle boundary (CMB) and the liquid/solid inner core boundary (ICB) and focused many of his studies on the challenging topic of density. He provided some of the first robust measurements of the density jump at the ICB (1970) and also confirmed the density jump at the CMB (1985) and provided insights on the resolution of the density profile throughout the earth's interior (1975). He studied the shear velocity structure near the CMB, and the compressional velocity profile in the outer core, with a continued interest in characterizing resolution and uncertainty, which developed through a fruitful collaboration with Professor David Brillinger in Statistics. He was one of the proponents of the existence of an anomalous layer at the bottom of the outer core. His prominent observations of compressional waves (PKnKP) bouncing multiple times inside the outer core were illustrated in his textbook "Inside the Earth". These observations demonstrated that the CMB must be very spherical.

Many of Dr Bolt's observations were made on records from the Berkeley Seismographic Stations (BSS), which, in the good tradition of previous Directors, he modernized over the years and kept apace of current technology. He introduced broadband recording at Berkeley in 1963 and started replacing paper recording by magnetic tape recording in 1964. Continuing in the innovative vein, under his directorship, the BSS developed a regional

broadband digital network based on inexpensive PC microcomputers, with telemetry to Berkeley over ordinary phone lines, and including three stations equipped with state-of-the-art broadband seismometers at Berkeley, Mt Hamilton and the San Andreas Geophysical Observatory near Hollister. Because of his involvement in the BSS and the related information service on northern California earthquakes, Dr Bolt's research interests gradually shifted towards characterizing ground motions from regional earthquakes in relation to earthquake hazards in the built environment.

In addition to many contributions to seismology, Professor Bolt has made invaluable contributions to the field of earthquake engineering through teaching of basic seismology to graduate students in structural and geotechnical engineering, conducting research characterizing strong ground motions for engineering design purposes, serving as consultant on important engineering projects, and participating as a member of numerous panels, boards, and commissions. He has been an active participant in the UCB Earthquake Engineering Research Center.

Professor Bolt's consulting work focused primarily on setting seismic criteria for new and retrofit designs of important critical structures, such as dams, nuclear power plants, large bridges, underground structures, and pipelines. These structures have included the Aswan Dam, Diablo Canyon Nuclear Power Plant, Golden Gate Bridge, Bay Area Rapid Transit (BART) underground stations, BART transbay tube, and the Alaska Pipeline. His consulting work in 2005 included characterizing the controlling seismic sources and assessing tsunami risk for use in designing the now-planned (2006) suspension bridge crossing the Messina Strait between Italy and Sicily.

His setting of seismic design criteria for critical structures has involved identifying seismic-source zones, guiding the conduct of seismic hazard analyses, generating site-specific response spectra and corresponding free-field ground motions, characterizing the spatial variations of ground motions, and predicting expected future fault offsets. Further, he has participated in evaluating the seismic performance of such structures. His strong background in applied mathematics and mechanics has made it possible for him to effectively communicate with structural and geotechnical engineers on seismic-design and damage-assessment related issues.

The numerous seismic-related panels, boards, and commissions on which Professor Bolt has served include the California Department of Water Resources Consulting Board, California Department of Transportation Seismic Advisory Board, San Francisco Bay Conservation and Development Commission (BCDC) Engineering Criteria Review Board, Metropolitan Transportation Commission (MTC) Engineering and Design Advisory Panel

(EDAP), Golden Gate Bridge Seismic Instrumentation Panel, and the California Seismic Safety Commission (CSSC). As a member of CSSC, he actively participated in the Commission's sponsoring of numerous bills introduced into the legislature which became California law, thus greatly enhancing seismic hazard mitigation in the State.

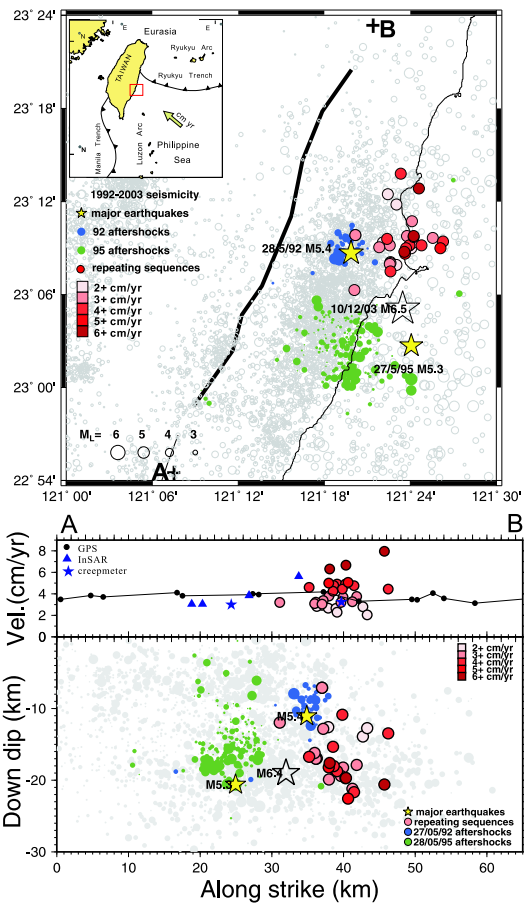
In recognition of Professor Bolt's many valuable contributions to earthquake engineering, he received the Earthquake Engineering Research Institute's 1990 George W. Housner Medal, the California Earthquake Safety Foundation's 1995 Alfred E. Alquist Medal, and was elected to the National Academy of Engineering (NAE) in 1978. His NAE citation reads as follows: "For the application of the principles of seismology and applied mathematics to engineering decisions and public policy."

Having served many years as Chair of the UCB Academic Senate and as President of the Men's Faculty Club, Professor Bolt seemed to know everyone on the Berkeley campus. His close relationship with individuals extended to a myriad of scientists and engineers worldwide. He was sought after as a speaker. Always in meeting one of his many close friends, he would extend a warm greeting with a big smile. His personal character has been admired by all who have had the pleasure of knowing him. He will be greatly missed by his friends, colleagues, students, and all who knew him.

Professor Bolt is survived by his wife Beverley (Bentley) of Berkeley, CA; three daughters, Gillian Bolt Kohli of Wellesley, MA, Helen Bolt Juarez of Fremont, CA, and Margaret Bolt Barber of Rumson, NJ; a son, Robert Bolt of Hillsborough, CA; a sister, Fay Bolt of Sydney, Australia, and fourteen grandchildren.

Chapter 3

Research Studies



1. Is Earthquake Rupture Deterministic?

Richard M Allen and Erik L Olson (University of Wisconsin, Madison)

1.1 Introduction

Understanding the earthquake rupture process is key to our understanding of fault systems and earthquake hazards. Over the past 15 years, multiple hypotheses concerning the nature of fault rupture have been proposed but no unifying theory has emerged. The conceptual hypothesis most commonly cited is the cascade model for fault rupture. In the cascade model, slip initiates on a small fault patch and continues to rupture further across a fault plane as long as the conditions are favorable. Two fundamental implications of this domino-like theory are that small earthquakes begin in the same manner as large earthquakes, and that the rupture process is not deterministic, i.e., the size of the earthquake cannot be determined until the cessation of rupture. Here we show that the frequency content of radiated seismic energy within the first few seconds of rupture scales with the final magnitude of the event. Therefore the magnitude of an earthquake can be estimated before the rupture is complete. This finding implies that the rupture process is to some degree deterministic and has far-reaching implications for the physics of the rupture process.

1.2 τ_p and τ_d observations

The frequency content of P-wave arrivals is measured through the parameter τ_p (Allen and Kanamori, 2003; Olson and Allen, 2005). We calculate τ_p in a recursive fashion from a vertical velocity timeseries to generate τ_p as a function of time, $\tau_p(t)$. Figure 3.1 shows the vertical velocity waveform recorded during a M_L 4.6 earthquake in southern California and the τ_p timeseries derived from it. Figure 3.2 shows a similar example but for the M_w 8.3 Tokachi-oki earthquake. In this case, only acceleration records are available, which have been recursively integrated in a causal fashion to derive the velocity trace from which $\tau_p(t)$ is derived. We define the parameter τ_p^{max} as the maximum $\tau_p(t)$ data point between 0.05 and 4.0 sec after the P-wave trigger as shown in Figures 3.1 and 3.2.

A total of 71 earthquakes producing 1,842 waveforms recorded within 100 km are used in this study. When τ_p^{max} is plotted against M on a log-linear scale, a scaling relation emerges as shown in Figure 3.3a. The τ_p^{max} observations from waveforms at individual stations can exhibit large variability for a single earthquake, which is likely due to measurement error, station and path effects (Lockman and Allen, 2005). Figure 3.3a shows the average τ_p^{max} observation for each earthquake using all

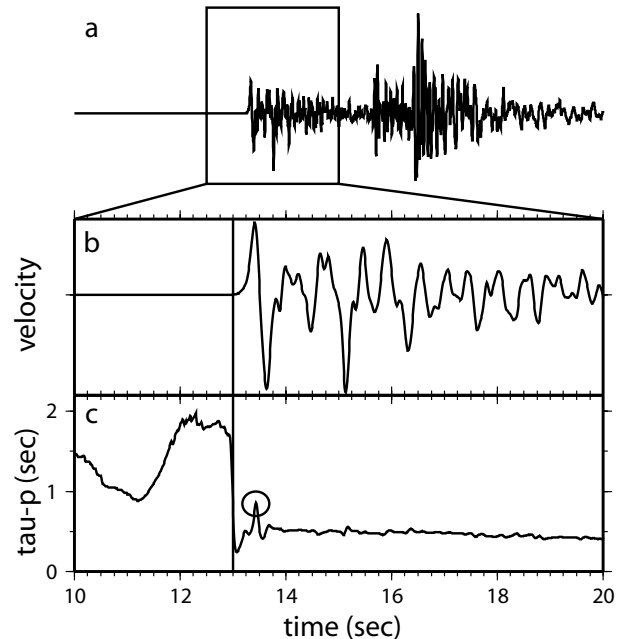


Figure 3.1: Example waveform and τ_p calculation for a M 4.6 earthquake in southern California recorded at station GSC 74 km from the epicenter. a) The raw vertical component waveform recorded by a broadband velocity sensor. b) Ten seconds of the velocity waveform after low-pass filtering at 3 Hz. The P-wave trigger time is shown by the vertical line at 13.01 sec. c) $\tau_p(t)$ trace calculated in a recursive fashion from the waveform in b showing the change in the frequency content from the pre-trigger noise to the post-trigger P-wave. The τ_p^{max} observation is circled (equal to 0.86 sec in this case), τ_d is the delay of τ_p^{max} with respect to the trigger (0.43 sec in this case).

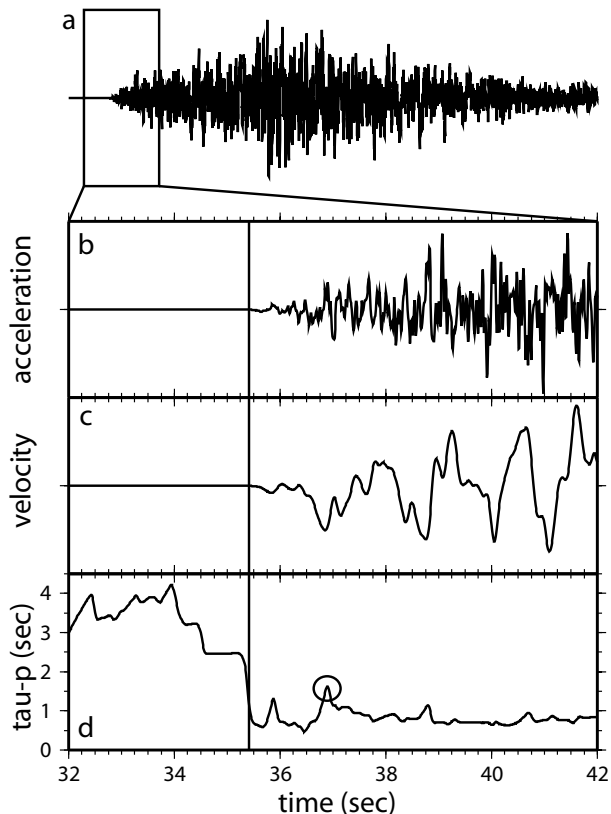


Figure 3.2: Example waveform and τ_p^{max} calculation for the M_w 8.3 Tokachi-oki earthquake recorded at station HKD112 71 km from the epicenter. a) The raw vertical component waveform recorded on an accelerometer. b) Ten seconds of the raw acceleration waveform. The P-wave trigger is shown by the vertical line at 35.41 sec. c) Ten seconds of the velocity waveform determined from the acceleration recording using recursive relations only. It has also been low-pass filtered at 3 Hz. d) $\tau_p(t)$ trace calculated in a recursive fashion from the waveform in c. The τ_p^{max} observation is circled ($\tau_p^{max} = 1.62$ sec, $\tau_d = 1.49$ sec), it has a longer period and is observed later than the example in Figure 3.1c due to the larger magnitude of the earthquake.

available data. The best-fit linear relation to the event averages is $\log \tau_p^{max} = 0.14M - 0.83$, and the average absolute deviation is 0.54 magnitude units. The dataset has a high linear correlation coefficient of 0.9. Although there is variability in τ_p^{max} observations equivalent to ± 1 magnitude unit, a scaling relation is clear, implying that information about the final magnitude of an earthquake is available within the first few seconds of its initiation irrespective of the total rupture duration.

A second parameter, τ_d , is also measured from the τ_p timeseries. τ_d is the delay of the τ_p^{max} observation with respect to the P-wave trigger and is, therefore, in the range of 0.05 to 4 sec (see Figures 3.1 and 3.2). Figure 3.3b plots the event-averaged τ_d observations versus magnitude, which shows a general increase in τ_d with magnitude. Also indicated on Figure 3.3b is the typical rupture duration as a function of magnitude. The relation shown is only approximate as the rupture duration for a given magnitude event can vary by a factor of 2 or 3. Despite the uncertainty in the rupture duration of the specific earthquakes included in this study, it is clear that for earthquakes with $M > 4$ the τ_p^{max} observation is made before the rupture has ceased. While up to 4 sec of data are used to determine τ_p^{max} , the average time window of the P-wave required to determine τ_p^{max} is less than 2 sec for almost all earthquakes in our study.

1.3 Discussion

While there is a 1 magnitude unit scatter in the τ_p^{max} data, the observations show that the rupture process is at least partly deterministic, i.e. the final magnitude of an event is to some degree controlled by processes within the first few seconds (typically < 2 sec) of rupture. The scatter could be due to source processes and/or local site and measurement errors. If the scatter is non-source related, then removal or correction for site and path effects could reduce the scatter in the data points of Figure 3.3a to a single line, implying that the final magnitude of an earthquake is entirely determined within the first few seconds of rupture. Variability in the quality of the τ_p^{max} observations at different stations has already been observed, indicating that site effects do play a role (*Lockman and Allen, 2005*). Nevertheless, it seems unlikely that all the scatter is due only to site effects. Instead, source related processes including rupture behavior, stress heterogeneity and other on-fault variability probably also play a role.

We propose that the final magnitude of an earthquake is partially controlled by the initiation process within the first few seconds of rupture, and partially by the physical state of the surrounding fault plane. The role played by the initiation process can be understood by considering the energy balance of fault rupture. A rupture can only propagate when the available energy is sufficient to supply the necessary fracture energy (*Nielsen and Olsen,*

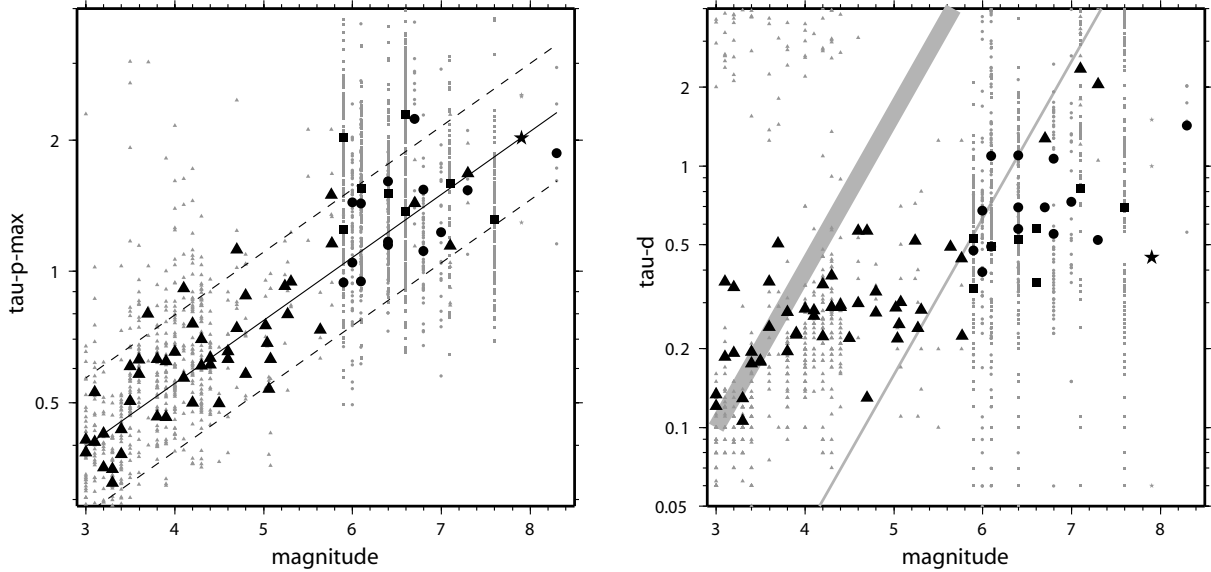


Figure 3.3: The relation between τ_p^{max} , τ_d and magnitude. a) The scaling relation between event averaged τ_p^{max} and magnitude for earthquakes in southern California (triangles), Japan (circles), Taiwan (squares) and Alaska (star). Observations at individual stations can show large scatter for a given event (small grey shapes). The event averaged values are also shown (large black symbols). The best fit line to the averages is also shown (solid). The average absolute deviation of the observations is 0.54 magnitude units; plus and minus two times the average absolute deviation is shown as dashed lines. b) τ_d plotted against magnitude showing the general increase in the time required to make the τ_p^{max} observation with increasing magnitude. The symbols are the same as in a. Grey shapes show individual station observations, black is the event average. The thick grey bar shows the approximate rupture duration as a function of magnitude indicating that the τ_p^{max} observation is made before rupture ceases for all $M > 4$ earthquakes in this study. The thin grey line indicates one tenth the rupture duration and is crossed by the trend of the τ_d data.

2000; *Oglesby and Day*, 2002). When a propagating fracture encounters a patch with a lower stress-drop, the total energy in the system will begin to decrease. Depending on the size of the patch, it may cause the rupture to terminate. The total rupture energy available increases with the amount of slip, so a large-slip rupture will propagate further across a heterogeneous fault plane. Therefore, if the rupture pulse initiates with large slip, it is more likely to evolve into a large earthquake. This explanation is consistent with the observation that large earthquakes do not nucleate at shallow depths, but instead at greater depths where the frictional strength and stress drop are greater (*Das and Scholz*, 1983). A recent study (*Mai et al.*, 2005) also shows that hypocenters are preferentially located within or close to regions of large slip.

1.4 Acknowledgements

We thank Hiroo Kanamori and Stefan Nielsen for helpful discussions, and Yih-Min Wu and Roger Hansen for making waveform data available for the study. Funding for this work was provided by USGS/NEHRP awards 03HQGR0043 and 05HQGR0074.

1.5 References

- Allen, R. M. and H. Kanamori, The potential for earthquake early warning in southern California, *Science*, *300*, 786-789, 2003.
- Das, S. and C. H. Scholz. Why large earthquakes do not nucleate at shallow depths, *Nature*, *305*, 621-623, 1983.
- Lockman, A. and R. M. Allen. Single station earthquake characterization for early warning, *Bull. seism. Soc. Am.*, *95*, 2029-2039, 2005.
- Mai, P. M., P. Spudich and J. Boatwright. Hypocenter locations in finite-source rupture models, *Bull. seism. Soc. Am.*, *95*, 965-980, 2005.
- Nielsen, S. B. and K. B. Olsen. Constraints on stress and friction from dynamic rupture models of the 1994 Northridge, California, earthquake, *Pure And Applied Geophysics*, *157*, 2029-2046, 2000.
- Oglesby, D. D. and S. M. Day, Stochastic fault stress: Implications for fault dynamics and ground motion, *Bull. seism. Soc. Am.*, *92*, 3006-3021, 2002.
- Olson, E. and R. M. Allen, The deterministic nature of earthquake rupture, *Nature*, *438*, 212-215, 2005.

2. Periodic Pulsing of the San Andreas Fault: An Update

Robert M. Nadeau

2.1 Slip Rates from Micro-quakes

A characteristically repeating micro-earthquake sequence (CS) is a sequence of small earthquakes ($M \sim < 3.5$) whose seismograms, locations and magnitudes are nearly identical. Each earthquake in the sequence represents a repeated rupture of the same patch of fault, and the times between the ruptures (i.e., their recurrence intervals) are, in general, inversely proportional to the average tectonic loading rate on the fault (Nadeau and McEvilly, 1999). These unique properties allow CSs to be used to infer slip rates deep within fault zones, and they have been used to particular advantage for this purpose in regions where geodetic measurements are limited in their spatial and temporal coverage.

2.2 Repeating Quake Analysis along the Central SAF

Along much of the 175 km stretch of the San Andreas Fault (SAF) separating the rupture zones of California's two great earthquakes (i.e., the \sim M8 1906 San Francisco and 1857 Fort Tejon events), geodetic measurements have been done relatively infrequently in campaign mode. Along this stretch, however, over 500 CSs have been identified with events occurring between 1984 and 1999 (inclusive), and analysis of these sequences reveal: 1) that the recurrence intervals within any given CS vary significantly through time, 2) that among different CS on a localized fault segment, the recurrence variations are coherent through time, and 3) that in many cases, the coherent variations recurred quasi-periodically (Nadeau and McEvilly, 2004).

Here we report results based on an analysis of the CSs that extend the period studied by (Nadeau and McEvilly, 2004) by an additional 5 years. A primary objective of this extended analysis is to see if systematics in time-varying patterns reported in the 2004 study (i.e., the periodic pulsing of deep slip and its correlation to variations in rates of larger earthquakes) are ongoing phenomena.

2.3 Correlation with Larger Earthquakes

Recurrence variation information for the CSs was used to construct a profile of deep fault slip rate histories along the 175 km study zone for the 1984-2005.25 study period. The profile reveals that along the northwestern-most 80 km segment of the study zone (Figure 3.4), deep fault slip rates commonly vary by over 100% and their variation patterns (i.e., pulse patterns) recur with a periodicity of ~ 3 years. Shown at the right in Figure 3.4 is a com-

parison of this large-scale periodic deep slip pattern with the occurrence times of M3.5 to M7.1 earthquakes (i.e., magnitudes larger than those of the CS events) and with the occurrence times of three known slow slip events in the area (Gwyther *et al.*, 2000). The comparison reveals a significant correlation between the onset periods of the repeating deep slip signals and the occurrence rates of the larger events. Nadeau and McEvilly (2004) observed this pattern for CS data during the period 1984-1999. With the additional 5+ years of CS data, the pattern and correlation observed by Nadeau and McEvilly appears to be continuing (Figure 3.4, right).

Excluding Loma Prieta aftershocks, 66 earthquakes with $M > 3.5$ occurred in region during the 1984-1999 study period, and a general correlation is also observed between the occurrence times of these events and the 1-year onset periods of the pulses (i.e. the time interval where pulse slip velocities transition from low to high values). Forty-two of the 66 events were found to occur during the onset periods, this represents an occurrence rate that is 3.7 times larger than the rate observed during the non-onset periods. When Loma Prieta aftershocks are included into the analysis the onset period rate increased to 4.6 times that of the non-onset period rate.

To the resolution of the characteristic microearthquake slip rate data, the M7.1 Loma Prieta mainshock also occurred coincident with the onset of the P2 timed pulse. The times of the next two largest non-aftershock events in the area and study period (i.e., M5.4 San Juan Bautista mainshock in 1998 and a M4.7 event in 1986) are also coincident with the onset of pulses P5 and P1, respectively, and the P3, P4, and P5 pulse onsets correspond closely to the times of the three slow slip events in the area whose aseismic moment magnitudes were estimated to be $\sim 5M_w$ (Gwyther *et al.*, 2000).

2.4 Implications

Earthquake triggering induced by velocity weakening effects (Dietrich, 1986) associated with increasing fault slip velocities during pulse onsets may provide an explanation for the corresponding rate increases of the larger earthquakes. It is also possible that increased quake rates occur quasi-periodically due to some other mechanism, such as the accelerated rate of loading to failure during onsets of the quasi-periodic deep slip pulses.

Regardless of the causes, the success of predictions of time periods with increased likelihood for larger quakes during the additional 5+ year period, based on the pattern of pulsing that occurred prior to the end of 1999

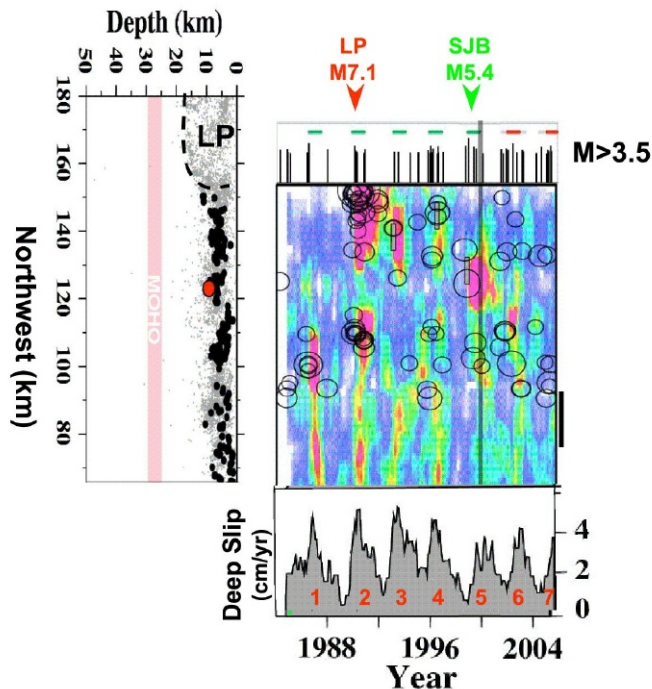


Figure 3.4: (Left) Along fault depth section of background seismicity (gray points) and SAF CS locations (black circles) for an 80 km segment of the central SAF. Rupture zone of the 1989, M7.1 Loma Prieta earthquake is labeled LP. (Right, center) Profile of the 1984-2005.25 deep slip history for the segment from the CS data. Rates (in color) are in percent difference from the 1984-2005.25 average. Color intensity give 95% confidence bounds. Open circles are along fault locations and times of $M > 3.5$ earthquakes. Their sizes are keyed to relative magnitudes, but are significantly larger than their actual rupture dimensions. Vertical gray line is start time of the extended analysis. (Right, bottom) Deep slip rates history for a representative 15 km sub-segment showing the 7 pulses (labeled 1 through 7) observed to date. (Right, top) Occurrence times and magnitudes of the $M > 3.5$ earthquakes in the 80 km zone. Time of Loma Prieta and San Juan Bautista events are labeled at top (LP and SJB, respectively). Horizontal green bars are pulse onset periods before 2000. Horizontal red bars are predicted pulse onset periods based on the green bars. Gray extensions of the red bars are prediction uncertainties.

(Figure 3.4), suggests that significant potential for refinement of time-dependent earthquake forecasts models exists for this area (WGCEP, 1999) on time scales comparable to the average pulse cycle duration of ~ 3 years.

2.5 Acknowledgements

Thanks are given to Roland Bürgmann and Mark H. Murray for stimulating conversations and insightful comments regarding this work. This research was supported by the National Science Foundation through award EAR-0337308.

2.6 References

Dieterich, J.H., A model for the nucleation of earthquake slip, in *Earthquake Source Mechanics*, S. Das, J. Boatwright, and C.H. Scholz (Editors), *American Geophysical Monograph 37*, American Geophysical Union, Washington, D.C., 37-47, 1986.

Gwyther, R.L., C.H. Thurber, M.T. Gladwin, and M. Mee, Seismic and Aseismic Observations of the 12th August 1998 San Juan Bautista, California, M5.3 Earthquake, in *Proceedings of the 3rd Conference on tectonic problems of the San Andreas Fault system*, G. Bokelmann and R. Kovach, Eds., *Stanford California School of Earth Sciences, Stanford University*, 2000.

Nadeau, R.M., and T.V. McEvilly, Fault slip rates at depth from recurrence intervals of repeating microearthquakes. *Science*, 285, 718-721, 1999.

Nadeau, R. M. and T. V. McEvilly, Periodic Pulsing of Characteristic Microearthquakes on the San Andreas Fault, *Science*, 303, 220-222, 2004.

Working Group on California earthquake Probabilities (WGCEP). Earthquake probabilities in the San Francisco Bay Region: 2000 to 2030—a summary of findings, *U.S. Geol. Surv. Open-File Rept. 99-517*, 36 pp., 1999.

3. Monitoring Nonvolcanic Tremor on the San Andreas Fault

Robert M. Nadeau

3.1 Introduction

Nonvolcanic tremor activity (i.e., long-duration seismic signals with no clear P or S waves (Figure 3.5) may provide important clues to the rheology and processes responsible for the nucleation and seismic cycles of large earthquakes. Previously, nonvolcanic tremors had only been observed in subduction zones (i.e., thrust fault plate boundaries) (e.g., *Obara, 2002; Rogers and Dragert, 2003*), where fluids from subduction processes were believed to play an important role in generating these tremors.

3.2 SAF Tremors

Because subduction has not occurred along the central San Andreas Fault (SAF) for several million years, fluids from active subduction are not present, and nonvolcanic tremor activity was not expected along the the central SAF zone.

Recently, however, data from Berkeley's borehole High Resolution Seismic Network (HRSN) at Parkfield, California revealed tremor-like signals originating in the vicinity of Cholame, California (*Nadeau and Dolenc, 2005*). The tremors appear to be confined largely to an 25 km segment of the SAF beneath Cholame at depths of between 20 to 40 km. The depths, frequency content (generally 1 to 10 Hz), S-wave propagation velocity, and waveform character of the SAF tremors were similar to those of the subduction zone tremors; however, the SAF tremors are less frequent, of shorter duration, of smaller amplitude, and of lower seismic energy release.

Our discovery of these nonvolcanic tremors is important for three reasons: 1) they occur along a transform rather than a subduction plate boundary zone, 2) no obvious source for fluid re-charge exists in the Cholame area to aid in tremor genesis, and 3) the highest level of tremor activity in the region occurs beneath the inferred epicentral region of the moment magnitude (M) ~ 7.8 1857 Fort Tejon earthquake, whose rupture zone is currently locked.

The Cholame segment of the SAF has an estimated earthquake recurrence time of 140 years (+93, -69) (*WGCEP, 1995*), and it is now over 140 years since the Fort Tejon event. Because stress changes from ETS events may trigger large earthquakes, future increases in SAF tremor activity may signal periods of increased probability for the next large earthquake on the segment.

An apparent correlation between tremor and local micro-earthquake rates at Cholame (*Nadeau and Dolenc, 2005*) also suggests that deep deformation associ-

ated with the Cholame tremors (i.e., ETS) may also be stressing the shallower seismogenic zone in this area.

Further evidence for stress-coupling between the deep tremor zone and the seismogenic SAF is observed in the correlation between tremor and the 28 September 2004, M6 Parkfield earthquake (~ 10 km NW of Cholame) (Figure 3.6). Between 1 and 3 months before the Parkfield earthquake, tremor activity was extremely low. Then 20 to 22 days prior to the Parkfield quake, tremor activity showed an anomalously large rate of activity (fore-tremor). This is consistent with the observations of *Nadeau and Dolenc (2005)*, which suggest a relationship between the deep tremor and shallower seismogenic zones in which stress changes in one of these zones induces stress changes in the other with a lag time of a few weeks.

Immediately following the Parkfield mainshock an even larger rate increase in tremor activity occurred, and elevated tremor rates persisted for over 500 days. This elevated rate appears now to have subsided and tremor rates are again low. It is too early to say whether or not the low activity rates now being observed are representative of another precursory quiescent period, but given the critical location of the tremors relative to the Fort Tejon locked zone, and the evidence for coupling of tremor rates and earthquake activity seen so far, we are compelled to continue monitoring the tremors for signs of anomalous activity that may signal an increased likelihood for another large event in the area.

3.3 Acknowledgements

This research was supported by U.S. Geological Survey award no. 06HQGR0167.

3.4 References

- Nadeau, R.M. and D. Dolenc, Nonvolcanic Tremors Deep Beneath the San Andreas Fault, *Science*, 307, 389, 2005.
- Obara, K., Nonvolcanic Deep Tremor Associated with Subduction in Southwest Japan, *Science*, 296, 1679-1681, 2002.
- Rogers, G. and H. Dragert, Episodic Tremor and Slip on the Cascadia Subduction Zone: The Chatter of Silent Slip, *Science*, 300, 1942-1943, 2003.
- Working Group on California Earthquake Probabilities (WGCEP), Seismic hazards in southern California: probable earthquakes, 1994 to 2024, *Bull. Seism. Soc. Am.*, 85, 379-439, 1995.

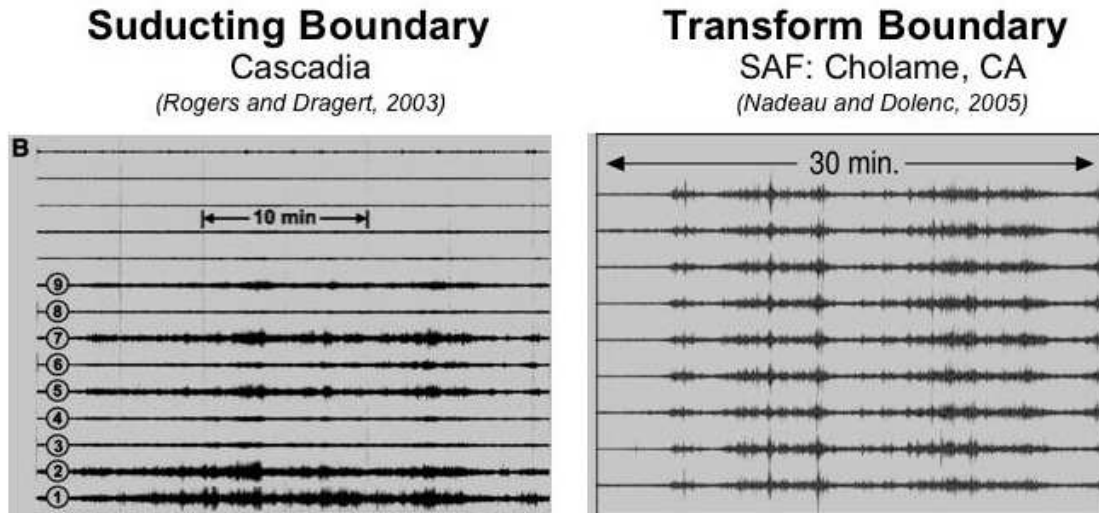


Figure 3.5: Comparison of Cascadia and San Andreas Fault Tremors. In Cascadia, a significant correlation between subduction zone tremor activity and subseismogenic zone (i.e. beneath the upper ~ 15 km of Earth's crust where earthquakes occur) slow slip events (referred to as episodic tremor and slip (ETS, *Rogers and Dragert, 2003*)) has been observed, suggesting that stress changes from ETS events may increase stress and possibly trigger earthquakes in the shallower seismogenic fault zone. No correlation between tremor and deformation changes have yet been observed along the SAF, however, variations in earthquake activity does correlate.

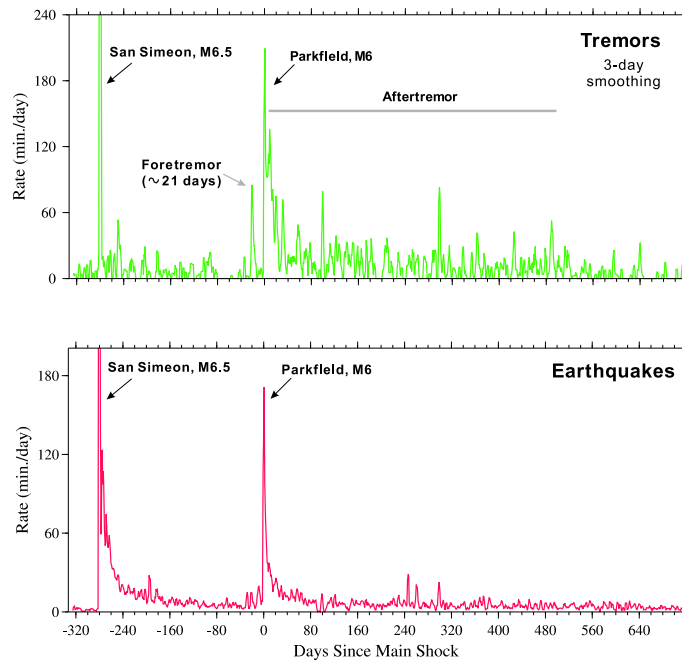


Figure 3.6: Activity rate history of nonvolcanic tremors (green, top) and microearthquakes (red, bottom) detected by the borehole High Resolution Seismic Network (HRSN) at Parkfield, CA. History spans 40 days prior to the San Simeon Earthquake through Sept. 13, 2006 (i.e., 716 days after the Parkfield mainshock). Tremor activity rates were not strongly influenced by the San Simeon event that occurred some 50 km to the west. However, the Parkfield earthquake whose epicenter was about 10 km from the tremor zone had a strong impact. Parkfield aftershocks decayed more rapidly than the tremor activity, suggesting some lag between stress changes in the deep tremor zone relative to that in the seismogenic zone above.

4. Repeating Earthquakes on an Imbricated Thrust Fault in the Arc-Continent Collision Boundary of Eastern Taiwan

Kate H. Chen (National Cheng Kung University), Robert M. Nadeau, and Ruey-Juin Rau (National Cheng Kung University)

4.1 Introduction

The Chihshang fault in eastern Taiwan, characterized by ~ 3 cm of surface slip per year, is one of the most rapidly creeping thrust faults known in the world (*Angelier et al.*, 2000; *Lee et al.*, 2003). Other than a recent ML 6.4 earthquake on the Chihshang fault on 10 December 2003, and a ML 6.0 earthquake in 1951, no significant earthquakes are known to have occurred on this fault. Strike-slip faults that produce both large earthquakes and near surface creep have been studied (i.e., the Hayward fault in central California). They are believed to have zones of locked and creeping fault at depth and only creep near the surface (*Savage and Lisowski*, 1993; *Bürgmann et al.*, 2000). In contrast, the Chihshang fault exhibits mainly by reverse slip and may, therefore, have greater overall strength. However, due to limited geodetic coverage and difficulties in obtaining deformation information from Interferometric Synthetic Aperture Radar (InSAR) in the area (*Hsu and Bürgmann*, 2006), the picture of slip at depth on the Chihshang fault is poorly resolved, and the distribution of locked and creeping fault at depth is, therefore, difficult to determine. A technique for inferring fault slip rate at depth using repeating microearthquakes has recently been developed (*Nadeau and McEvilly*, 1999; *Nadeau and Johnson*, 1998) and has been applied in a variety of tectonic settings. Because the Chihshang fault has many small quakes and is creeping, it may also generate repeating earthquakes. In this study, we search for repeating earthquakes and characterize their behavior in space and time, and use this information to develop a conceptual model of the Chihshang fault.

4.2 Data

We used 3387 earthquakes from the Central Weather Bureau Seismic Network (CWBSN) catalog in our analysis. The events occurred in the Chihshang fault region between 01 January 1991 and 9 December 2003, the day before the 6.4 ML earthquake. The relatively sparse, one-sided coverage of the CWBSN stations in the Chihshang area coupled with poor noise characteristics, complicate the task of defining complete and accurate repeating event sequences in the region. To resolve this problem, we use the threshold criteria in S-P differential time and waveform similarity to identify repeating earthquakes in the Chihshang area.

4.3 Spatial distribution of repeating earthquakes

Using time waveform similarity criteria, we identify 113 repeating events in the Chihshang fault zone, about 3% of the M1.9 to 5.4 earthquakes from the study period. They are organized into 31 repeating sequences with magnitudes ranging from 1.9 to 3.7. Fig. 1 shows examples of the waveforms for one repeating sequence. Locations of the 31 repeating sequences are shown in Fig. 2. All the sequences occur between depths of 7 to 23 km, and tend to concentrate on the northern section of the fault segment.

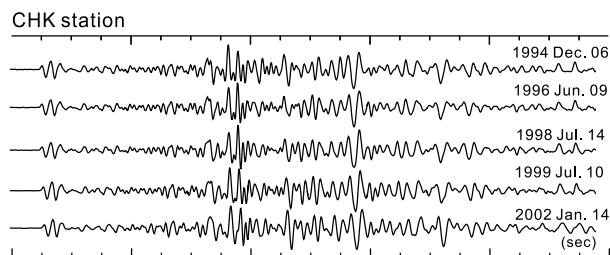


Figure 3.7: Waveforms recorded at station CHK from one of the 31 repeating sequences. Each trace was normalized by its maximum amplitude.

4.4 Deep slip rates

To study the spatial distribution of fault-slip rates, we first compute the sum of slip loads for each sequence site. These sums were then divided by the corresponding sums of recurrence intervals for the sequences, giving the average deep slip rate surrounding each sequence during the study period. The results of deep slip rates are shown in Fig. 2. The slip rate estimates range from 2.0 - 7.9 cm/yr with an average of 4 cm/yr. The coefficient of variation in the slip rates is 0.33. The highest slip rates (above 6 cm/yr) are found on the deep portion of the fault, between 18 and 20 km. Slip rates of less than 3 cm/yr are found above 15 km depth. However, overall slip rates estimates do not reveal a systematic depth-dependent behavior. In the upper panel of Fig. 2, we compare the along-strike variation of deep slip rates with surface observations. The GPS data shown by black dots are a combination of the average uplift rate from 1985-1994 leveling data and horizontal deformation rate from 1992-1999 GPS data (*Liu and Yu*, 1990; *Yu and Kuo*, 2001).

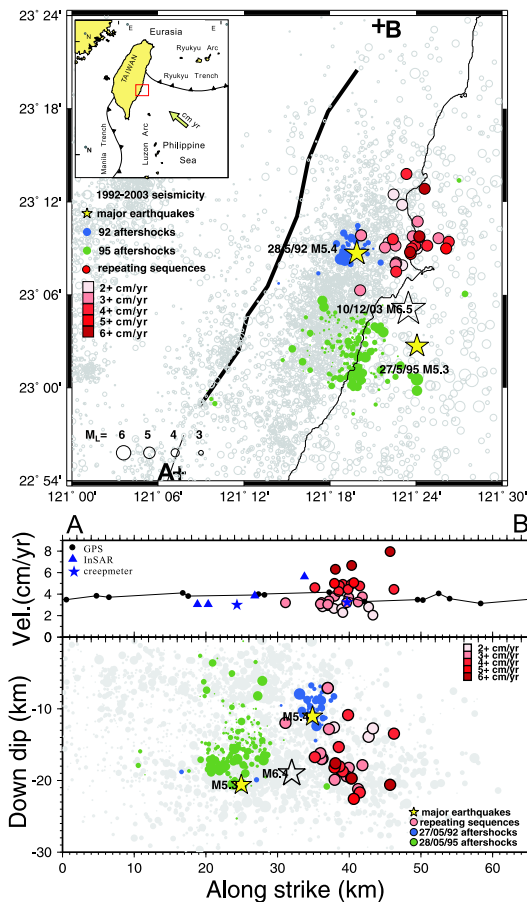


Figure 3.8: The spatial distribution of repeating sequence derived slip rates in mapview (top) and along-strike cross-section (bottom). Filled circles with a black rim represent locations of repeating sequences. Fill colors/shades are keyed to the slip rates. Yellow stars indicate major events occurred during the study time period from 1992 - 2003 December. Open star indicates the event that occurred on 10 December 2003 just after the study period. Background seismicity are shown as gray circles. Aftershock sequences from the 1992 and 1995 M5+ events are shown as blue and green circles without a rim, respectively. (Bottom) Filled circles with a black rim in the upper panel indicate a projection of repeaters on the along-strike distance and their corresponding slip rates. Black dot shows a combined surface slip rates from GPS and leveling data measurement. Blue solid triangles and stars are along-dip projection of InSAR data (Hsu and Bürgmann, 2006) and creepmeter data (Lee et al., 2003), respectively. See color version of figure at front of Research Studies.

The InSAR data (Hsu and Bürgmann, 2006) and creep-meter data (Lee et al., 2003) are projected into along-dip direction assuming a fault dip angle of 60 at near surface. The above surface measurements are consistent with the deep repeating earthquake slip rates (~ 4 cm/yr).

4.5 Conclusion

The Chihshang repeating sequences are concentrated on the northern half of the Chihshang fault zone at 7 - 23 km depth. Their average deep slip rate, 4 cm/yr, are consistent with three types of geodetic measurements at surface. We, therefore, infer the contrasting deep fault slip behavior from north to south on the Chihshang fault. The northern segment is likely creeping and southern segment is likely locked with higher earthquake potential.

(Kate Chen has been a visiting scholar in BSL since March 2006)

4.6 References

- Angelier, J., H. T. Chu, J. C. Lee, and J. C. Hu, Active faulting and earthquake hazard: the case study of the Chihshang Fault, Taiwan, in *J. Geodyn.*, 29, 151 - 185, 2000.
- Bürgmann R., D. Schmidt, R. M. Nadeau, M. d'Alessio, E. Fielding, D. Manaker, T. V. McEvelly, and M. H. Murray, Earthquake potential along the Northern Hayward Fault, California, in *Science*, 289, 1178-1182, 2000.
- Hsu, L and R. Bürgmann, Surface creep along the longitudinal Valley fault, Taiwan from InSAR measurements, in *Geophys. Res. Lett.*, 33, doi:10.1029/2005GL024624, 2006.
- Lee, J. C., J. Angelier, H. T. Chu, J. C. Hu, F. S. Jeng, and R. J. Rau, Active fault creep variations at Chihshang, Taiwan, revealed by creep meter monitoring, 1998-2001, in *J. Geophys. Res.*, 108, doi:10.1029/2003JB002394, 2003.
- Liu, C. C., and Yu, S. B., Vertical crustal deformations in eastern Taiwan and its tectonic implications, in *Tectonophysics*, 183, 111-119, 1990.
- Nadeau, R. M. and L. R. Johnson, Seismological studies at Parkfield VI: moment release rates and estimates of source parameters for small repeating earthquake, in *Bull. Seism. Soc. Am.*, 88, 790 - 814, 1998.
- Nadeau, R. M. and T. V. McEvelly, Fault slip rates at depth from recurrence intervals of repeating microearthquakes, in *Science*, 285, 718-721, 1999.
- Savage, J. C., M. Lisowski, Inferred depth of creep on the Hayward fault, central California, in *J. Geophys. Res.*, 98, 787 - 793, 1993.
- Yu, S. B. and L. C. Kuo, Present-day crustal motion along the Longitudinal Valley Fault, eastern Taiwan, in *Tectonophysics*, 333, 199-217, 2001.

5. Subsurface Creep From Repeating Earthquakes at the Juncture of the San Andreas and Calaveras Faults

Dennise Templeton, Robert Nadeau, and Roland Bürgmann

5.1 Introduction

We investigate fault creep at depth at the juncture of the San Andreas and Calaveras faults using repeating earthquake data from 1984 to 2005. We are interested in studying how creep is partitioned as a fault system transitions from having a single fault accommodate slip to having multiple, sub-parallel fault strands accommodate slip. In the San Francisco Bay Area, the juncture between the San Andreas fault and the Calaveras fault illustrates such a transition. This juncture region is highly complex as the seismically active portions of the Calaveras fault do not illuminate a straight, contiguous fault plane. Additionally, a shorter secondary fault structure, the Quien Sabe fault zone, is more seismically active than the neighboring Calaveras fault. If repeating earthquakes also occur on the Quien Sabe fault zone, this could suggest that this fault is accommodating, at least at depth, some of the total slip associated with the plate boundary.

5.2 Methodology and Results

We identify repeating earthquake sequences by cross-correlating the first 5 seconds of local event waveforms recorded by the Northern California Seismic Network at the surface. Pairs of events which have a cross-correlation coefficient greater than 0.90 are then visually inspected for quality assurance and identified as belonging to the same repeating earthquake sequence. By using this methodology in our study area, we identified 99 repeating earthquake sequences. Repeating sequences were found on all three faults within the study area.

Assuming that these sequences represent a stuck patch in an otherwise creeping fault, we employ the empirical formula of *Nadeau and McEvilly (1999)* to determine the total amount of fault slip at each sequence location by using the number of times a sequence repeats and the average moment magnitude of the repeating sequence as inputs (Figure 3.9). Filled circles indicate the hypoDD location and amount of total slip in centimeters associated with the repeating sequence. Open circles indicate the catalog location of a repeating earthquake sequence not included in the hypoDD relocated dataset. The amount of total slip at a small number of repeating earthquake locations along the southern portion of the Quien Sabe fault zone was greater than 25 cm over the observation period, comparable to total slip amounts along portions of the San Andreas fault. The number of times an earthquake repeats in a sequence depends on a number of factors, including the background loading rate

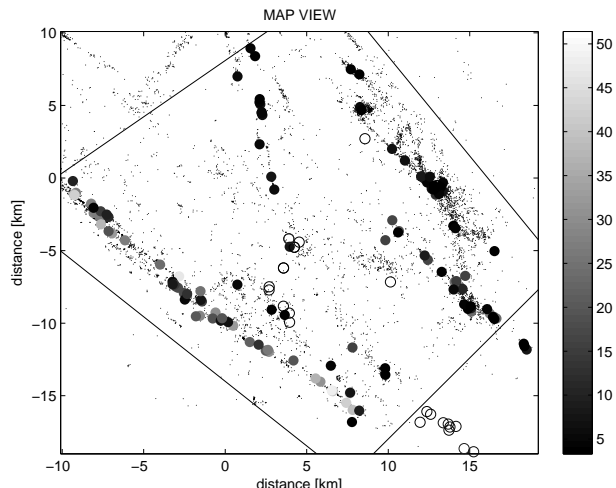


Figure 3.9: Map view of San Andreas fault on the left, Calaveras fault in the middle, and Quien Sabe fault zone on the right. HypoDD relocated background seismicity as small black dots. Filled circles indicate the hypoDD location and amount of total slip in centimeters associated with a repeating earthquake sequence. Open circles indicate the catalog location of a repeating earthquake sequence not included in the hypoDD relocated dataset.

of the fault. This explains why, in general, sequences on the San Andreas fault repeat more often or have greater moment magnitudes, and thus greater amounts of total slip, than sequences on the Calaveras or Quien Sabe fault zone. Preliminary results show that creep is as heterogeneous at depth as it appears on the surface. Locations of repeating earthquake sequences of significantly different total slip amounts can be located close to each other on the fault plane.

5.3 Acknowledgements

Special thank you to USGS-NEHRP for funding this project.

5.4 References

Nadeau, R. M. and T.V. McEvilly, Fault Slip Rates at Depth from Recurrence Intervals of Repeating Microearthquakes, *Science*, 285, 718-721, 1999.

6. Kinematic Modeling of the 2004 Parkfield Earthquake

Ahyi Kim and Douglas Dreger

6.1 Introduction

The September 28, 2004 Mw6.0 Parkfield earthquake (epcenter 35.815N, 129.374W and depth 8.1km) is probably the best recorded moderate sized earthquake to date. The regional broadband geodetic monitoring arrays, InSAR, as well as densely spaced local-distance strong motion instruments provide unprecedented coverage enabling detailed analysis of the kinematic rupture process. In-depth examination of kinematic rupture models, their resolution, and reconciliation with peak ground motion distribution is necessary for better understanding earthquake rupture physics as well as applications of such models for rapid ground motion hazard reporting.

6.2 Data

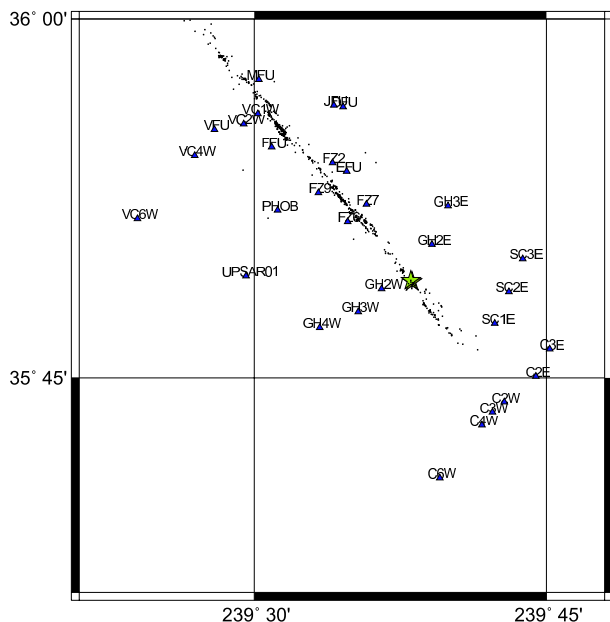


Figure 3.10: Location of the 2004 Parkfield earthquake. The near-fault strong motion stations are plotted as the triangles. Red star indicates the hypocenter and Black dots represents the aftershocks.

To obtain the kinematic model for 2004 Parkfield earthquake, we carried out a joint inversion combining the near-fault strong motion records and geodetic data sets. We used 60 near-fault horizontal-component strong motion records from 30 stations (Figure 1). Each record was integrated to velocity, band-pass filtered using a Butterworth filter with a corner frequency of 0.5 Hz, and re-sampled to 10 samples per second. The distance range

between the fault and the stations is 0.4-7.9km.

Coseismic GPS deformation from 13 sites was obtained from 1 sample per second GPS time histories. To obtain the coseismic deformation, the GPS time histories were averaged from 15 minutes before the event to 2-10 minutes afterward.

The coseismic deformation from ENVISAT InSAR data was obtained from a pre-event scene on 7/3/2003 and post event scene on 9/30/2004. We used the interferogram which was processed by Johanson *et al.* (in press). Johanson *et al.* removed the part of the interferogram affected by non-tectonic effects, especially atmospheric changes.

6.3 Inverse Method

For the inversion, we used the method of Harzell and Heaton (1983), which is a linear, multiple time window approach to invert the data for the spatio-temporal distribution of fault slip, the average rupture velocity and its variation, and the slip rise time. Green's functions for the seismic data were calculated using the FK integration method (Saikia, 1994) for frequencies up to 0.5 Hz with the two 1D velocity models reported in Liu *et al.* (2006), representing the velocity contrast across the SAF.

To generate the Geodetic green's function, we followed the method of Wang *et al.* (2003), assuming the GIL7 layered elastic structure model (Dreger and Romanowicz, 1994).

We assumed the fault plane dimension is 44kmx18km, which is divided into 1kmx1km subfaults. The rise time was allowed to vary from 0.6 sec to 3.6 sec, which is based on the preliminary regional distance results (Dreger *et al.*, 2005). The strike (140°) and dip (89°) were obtained from the aftershock distribution and some trial and error waveform fitting.

6.4 Inversion results

Figure 2a), 2b), and 2c) show slip models obtained from seismic, GPS, and InSAR data sets independently. They show some common features: (1) rupture propagated mainly to northwestward from the hypocenter, and (2) high slip value 10-20km northwest of the hypocenter. In detail, however, these three models are quite different. Basically, the inversion results from the geodetic data are dominated by the shallow slip northwest of hypocenter and some deep slip in southern part of the fault. The kinematic model obtained from the seismic only data shows much more complexity compared to those of geodetic data sets. The results using near-fault strong motion

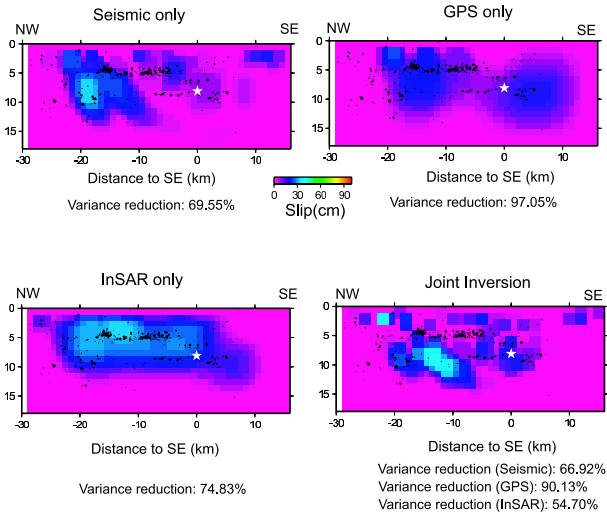


Figure 3.11: Slip models obtained independently from the a) seismic waveforms, b) GPS, and c) InSAR data sets. The model shown in d) compares the result when the three data sets are inverted simultaneously. These models are view NE and the left side is to the NW and the right to SE. The hypocenter is plotted as a white star. In the preferred model most of the slip is around hypocenter and between 10-20km NW of the hypocenter. After shocks are plotted as black dots. The x and y axes show along strike distance and depth in km. The slip located 10km to the SE is needed to fit the large amplitudes observed at the Cholame array.

data show a slip distribution that is consistent with what we obtained previously with the regional seismic waveform and near-fault GPS data in that there is a high slip patch at hypocenter and 10-20km north terminating near Middle Mountain (Dreger *et al.*, 2005). This model also has some low levels of slip to the south that are needed to explain the waveforms and the high peak amplitudes at stations located south of the epicenter. Due to the non-uniqueness of this type of source inversion, it is important to obtain model that simultaneously fit different types of data. The joint inversion results are seen to show similarity with each of the independent inversions and the level of fit to each data set is acceptable.

The joint inversion and preferred model (Figure 2d) indicates a slight bilateral rupture, which is dominated by northward rupture. This model has two primary asperities: one near the hypocenter, and the other 10-20km northward of the hypocenter, which is consistent with our preliminary model with local and regional seismic and GPS data (Dreger *et al.*, 2005). The best rupture velocity was found to be 2.6km/s, and the average rise time was 1.6 sec. The relatively higher slip in the InSAR only model might be due to included postseismic deformation, since the post-event scene is 2 days after the mainshock. In the preferred model, the scalar seis-

mic moment was found to be 1.10×10^{25} dyne-cm (Mw 6.03), while the peak slip was found to be 45.03cm. Slip model from the joint inversion showed us that the use of the geodetic data in the inversion places considerable additional constraint on the slip distribution.

6.5 References

Dreger, D. S., and B. Romanowicz, Source characteristics of events in the San Francisco Bay region, *U. S. Geol. Surv. Open-File Rept.*, 94-176, 301-309, 1994

Dreger, D., L. Gee, P. Lombard, M. Murray, and B. Romanowicz, Rapid Finite-source Analysis and Near-fault Strong Ground Motions: Application to the 2003 Mw 6.5 San Simeon and 2004 Mw 6.0 Parkfield Earthquakes, *Seis. Res. Lett.*, V.76, 40-48 2005

ns: Application to the 2003 Mw 6.5 San Simeon and 2004 Mw 6.0 Parkfield Earthquakes, *Seis. Res. Lett.*, V.76, 40-48 2005 . Dreger D., Murray M., Nadeau R., and Kim A., Kinematic Modeling of the 2004 Parkfield Earthquake, *SSA 2005 annual meetin g abstract* 2005.

Harzell, S. H. and T.H. Heaton, Inversion of strong ground motion and teleseismic waveform data for the fault rupture history of the 1979 imperial Valley, California earthquake, *Bull. Seism. Soc. Am.*, 73, 1553-1583 1983.

Johanson, I., E. Fielding, F. Rolandone, and R. Burgmann, Coseismic and Postseismic Slip of the 2004 Parkfield Earthquake from Space-Geodetic data, *Bull. Seism. Soc. Am.*, (in press)

Liu, P., S. Cautodiodo, and R. J. Archuleta, Kinematic Inversion of the 2004 Mw6.0 Parkfield Earthquake Including site effects, *Bull. Seism. Soc. Am.*, (in press)

Saikia, C. K., Modified frequency-wave-number algorithm for regional seismograms using Filon's quadrature - modeling of L(g) waves in eastern North America, *Geophys. J. Int.*, 118, 142-158, 1994.

Wang, R., F. Martin, and F. Roth, Computation of deformation induced by earthquakes in multi-layered elastic crust - FORTRAN programs EDGRN/EDCMP, *comp. Geosci.*, 29, 195-207 2003.

7. Identifying Isotropic Events Using an Improved Regional Moment Tensor Inversion Technique

Sean R. Ford, Douglas S. Dreger, William R. Walter (Lawrence Livermore National Laboratory)

7.1 Introduction

Identification of events with demonstrably significant non-double-couple components can aid in understanding the source processes of seismic events in volcanic and geothermal areas (e.g. *Dreger et al.*, 2000), and in nuclear event screening and possibly discrimination (*Dreger and Woods*, 2002). We implement the time-domain full regional waveform inversion for the complete moment tensor devised by *Minson and Dreger* (2006) after *Herrman and Hutchensen* (1993) based on the work of *Langston* (1981). The complete moment tensor allows for a characterization of the relative amounts of deviatoric and isotropic source components, the similarity of those components with prior events in the source region, and a constraint on the source depth. This information can aid in the discrimination of events.

7.2 Data and Methods

In general, synthetic seismograms are represented as the linear combination of fundamental Greens functions where the weights on these Greens functions are the individual moment tensor elements. Synthetic displacement seismograms are calculated with a frequency-wavenumber integration method (*Saikia*, 1994) for a one-dimensional (1-D) velocity model of eastern California and western Nevada (*Song et al.*, 1996). The synthetic data is filtered with a 4-pole acausal Butterworth filter between 0.02 and 0.05 Hz. At these frequencies, where the dominant wavelengths are approximately 100 km, we assume a point source for the low-magnitude ($M_W \leq 5.6$) regional events investigated in this study. Data are collected from the TERRAScope network stations, ISA, PAS, and PFO. We remove the instrument response, rotate to the great-circle frame, integrate to obtain displacement, and filter similarly the synthetic seismograms.

We calibrate the algorithm by calculating the full and deviatoric moment tensor for the 1992 Little Skull Mountain event (Figure 3.12a). The deviatoric solution is obtained by constraining the trace of the moment tensor to be zero. Our result fits the data very well and is highly similar to the double-couple solution of *Walter* (1993), the deviatoric solution of *Ichinose et al.* (2003), and the full solution of *Dreger and Woods* (2002), where we assume a source depth of 9 km. The deviatoric component of the full moment tensor is decomposed to a double-couple and compensated linear vector dipole (CLVD) that shares the orientation of the major axis. The 1992

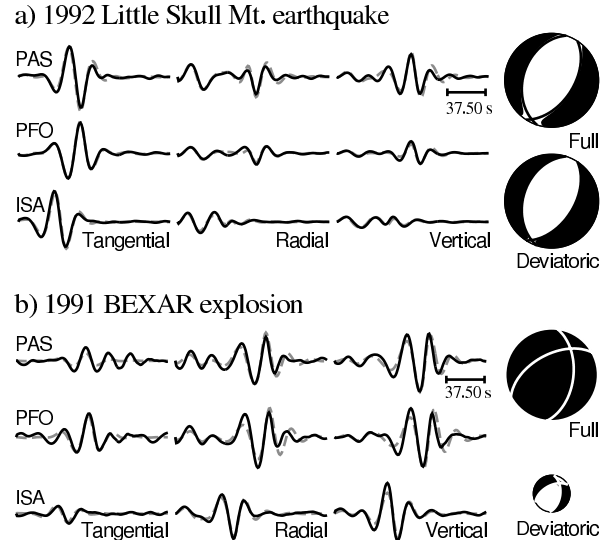


Figure 3.12: Moment tensor analysis of the (a) 1992 Little Skull Mt. earthquake and (b) 1992 BEXAR Nevada Test Site explosion. Data (solid line) and synthetics (dashed grey line) produced by inversion in the 20-50 s passband and resulting full and deviatoric (zero trace) focal spheres with best-fit double-couple planes (black lines), where the radius of the deviatoric sphere is relative to the total scalar moment contribution.

Little Skull Mountain event is almost purely double-couple and there is little change between the full and deviatoric solutions. The best-fit double-couple mechanism produces source parameters of strike 35° and 196° , rake -78° and -104° , and dip 50° and 42° , for the two focal planes, respectively. The total scalar moment (M_0) is 2.92×10^{24} dyne-cm, which results in an M_W of 5.58.

With the same algorithm we calculate the full and deviatoric moment tensor for the 1991 Nevada nuclear test site explosion, BEXAR ($m_b = 5.6$ and $M_S = 4.2$, NEIC; Figure 3.12b). The solution fits the data well and is similar to the full solution of *Minson and Dreger* (2006), where we assume a source depth of 1 km. The moment tensor has a large isotropic component, and the ratio of deviatoric moment (M_{DEV}) to isotropic moment (M_{ISO}) is 0.65, where the M_0 is 4.79×10^{22} dyne-cm (M_W of 4.39). M_{ISO} and M_{DEV} are defined according to *Bowers and Hudson* (1999) and $M_0 = M_{ISO} + M_{DEV}$.

It is difficult to grasp the source-type from the standard focal mechanism plot. Following the source-type

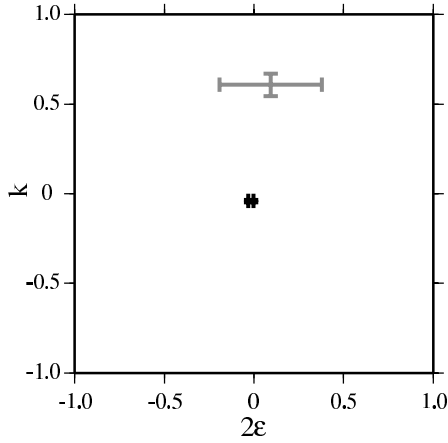


Figure 3.13: Source type plot for the 1992 Little Skull Mt. earthquake (black) and 1991 BEXAR NTS explosion (grey), with standard error (bars).

analysis described in *Hudson et al.* (1989) we calculate 2σ and k , which are given by

$$\sigma = \frac{-m_1}{|m_3|},$$

and

$$k = \frac{M_{ISO}}{|M_{ISO}| + |m_3|},$$

where m_1 and m_3 are the deviatoric principal moments which are ordered $|m_1| \leq |m_2| \leq |m_3|$. σ is a measurement of the departure of the deviatoric component from a pure double-couple mechanism, and is 0 for a pure double-couple and ± 0.5 for a pure CLVD. k is a measure of the volume change, where +1 would be a full explosion and -1 a full implosion. σ and k for the Little Skull Mountain earthquake and NTS explosion, BEXAR are given in Figure 3.13. Error in the values is derived from the standard error in the moment tensor elements given by the estimated covariance matrix obtained in the weighted least-squares inversion. Figure 3.13 shows that the Little Skull Mountain earthquake is within the error of being a perfect double-couple event ($2\sigma = 0$) with no volume change ($k = 0$). The BEXAR test, on the other hand, has a large volume increase with a large variance in the deviatoric source.

Error in the principal axes is analyzed by plotting the best-fit and scatter density of the axes of minimum compression (T), maximum compression (P) and null (N). The scatter density plot is obtained by randomly selecting moment tensor elements assuming a normal distribution for each element described by the standard error (given by the estimated covariance matrix), and diagonalizing the resulting moment tensor to obtain the principal axes. Principal axes plots for the Little Skull Mountain earthquake and NTS explosion, BEXAR are given

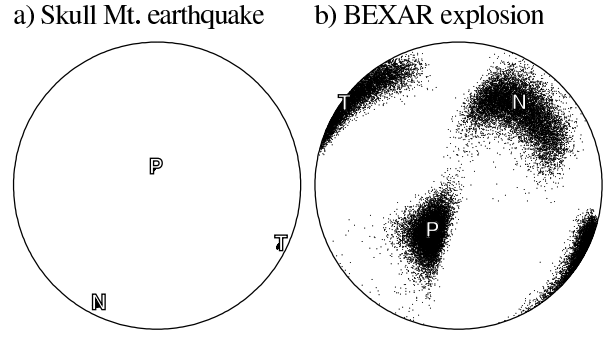


Figure 3.14: Scatter density of principal axes with best fit axes marked by the T, P, and N for the (a) Little Skull Mt. earthquake and (b) BEXAR explosion.

in Figure 3.14. The axes for the Little Skull Mountain event are well constrained, while those for the BEXAR test are more variable. However, the BEXAR test axes do not deviate greatly from the axes of the Little Skull Mountain event, which is likely due to the similar tectonic stresses.

In an effort to better characterize the source significance we adopt the source convention described in *Riedesel and Jordan* (1989). Vectors are defined describing the general,

$$MT = \sum_{i=1}^3 M_i \hat{M}_i,$$

double-couple,

$$DC = \hat{M}_1 - \hat{M}_3,$$

isotropic,

$$ISO = \sum_{i=1}^3 \hat{M}_i,$$

and CLVD sources,

$$CLVD1 = \hat{M}_1 - \frac{\hat{M}_2}{2} - \frac{\hat{M}_3}{2}; \quad CLVD2 = \frac{\hat{M}_1}{2} + \frac{\hat{M}_2}{2} - \hat{M}_3,$$

where \hat{M}_1 , \hat{M}_2 , and \hat{M}_3 are the T, N, and P axes, respectively, and M_1 , M_2 , and M_3 are the principal moments. The T, N, and P axes are chosen as in the double couple case, so that $M_1 \geq M_2 \geq M_3$. The source vectors are subspaces of the space defined by the principle axes of the moment tensor. The vectors are plotted on the focal sphere (similar to the T, N, and P axes) for the Little Skull Mountain earthquake and NTS explosion, BEXAR in Figure 3.15. The general source vector, MT, for the Little Skull Mountain event lies on the great-circle connecting the double-couple and CLVD sources. This great-circle defines the subspace on which MT must lie if the source is purely deviatoric. The MT vector is also collinear with the DC vector, which is to say that

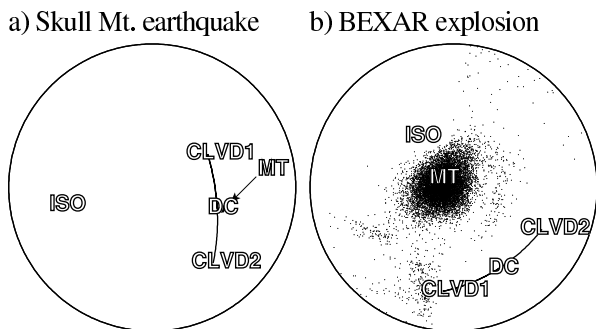


Figure 3.15: Source vector plot with density plot of general source vector, MT, for the (a) Little Skull Mt. earthquake and (b) BEXAR explosion. See text for definition of vectors. The great-circle line connecting the CLVD1, DC, and CLVD2 vectors defines the purely deviatoric solution space.

the source is almost purely double-couple. The MT vector for the BEXAR test lies well off the line defining the deviatoric solution space. The scatter density of possible MT vectors is also plotted and none of them intersect the deviatoric solution space, which is to say that the solution has a significant isotropic component.

Discussion and Conclusions

The 1992 Little Skull Mountain event is a well-constrained, highly double-couple earthquake with an M_W of 5.6. The 1991 NTS nuclear test, BEXAR ($m_b=5.6$ and $M_S=4.2$, NEIC), has a significant positive isotropic component with an M_W of 4.4. The deviatoric components of both events may be responding to the same general Basin and Range stress field of NW-SE extension. Analysis of σ versus k and the source vectors described above allows for an interpretation of the source with error. There are several sources of error in the moment tensor inversion, and the probabilistic method used in this study has the ability to incorporate those sources and produce empirical probability densities of the analyzed parameters (i.e., σ , k , and the source vectors). For example, several velocity models could be used to create the Greens functions for the linear inversion. Each of the moment tensor solutions and their associated scatter density could then be plotted as in Figures 4-6. These types of plots would aid in the understanding of how parameterization choice nonlinearly affects the moment tensor solutions, and help map the solution space of best-fit moment tensors.

The analysis presented here shows that high quality solutions can be obtained for sparsely-recorded events at regional distances, and that these solutions have the potential to discriminate between volume changing (explosions) and double-couple (earthquakes) sources. In the

future, we will test the sensitivity of the inversion to noise and non-ideal station spacing. We will also increase the population of moment tensors for man-made and natural events that deviate from the well recorded, large magnitude, small tectonic release cases presented here. Only an analysis of a wide range of events in different environments will allow for a true comparison of explosion and earthquake moment tensor populations.

7.3 Acknowledgements

Figures were made with Generic Mapping Tools (*Wessel and Smith, 1998*). This research is sponsored by the Department of Energy through the National Nuclear Security Administration, Office of Nonproliferation Research and Development, Office of Defense Nuclear Nonproliferation.

7.4 References

- Bowers, D. and J. A. Hudson, Defining the scalar moment of a seismic source with a general moment tensor, *Bull. Seism. Soc.*, 89(5) 1390-1394, 1999.
- Dreger, D., and B. Woods, Regional distance seismic moment tensors of nuclear explosions, *Tectonophysics*, 356(1-3) 139-156, 2002.
- Dreger, D., H. Tkalic, and M. Johnston, Dilational processes accompanying earthquakes in the Long Valley Caldera, *Science*, 288 122-125, 2000.
- Herrmann, R. B., and K. Hutchensen, Quantification of m_{Lg} for small explosion, *Phillips Laboratory Report PL-TR-93-2070*, 1993.
- Hudson, J. A., R. G. Pearce, and R. M. Rogers, Source type plot for the inversion of the moment tensor, *J. Geophys. Res.*, 94(B1) 765-774, 1989.
- Ichinose, G. A., J. G. Anderson, K. D. Smith, and Y. Zeng, Source parameters of Eastern California and Western Nevada earthquakes from regional moment tensor inversion, *Bull. Seism. Soc.*, 89 XX-XX, 2003.
- Julian, B.R., A. D. Miller, and G. R. Foulger, Non-double-couple earthquakes 1: Theory, *Rev. Geophys.*, 36 525-549, 1998.
- Langston, C. A., Source inversion of seismic waveforms: The Koyna, India, earthquakes of 13 September 1967, *Bull. Seism. Soc. Am.*, 71(1) 1-24, 1981.
- Minson, S. and D. Dreger, Improved seismic moment tensor inversion, to be submitted to *Geophys. J. Int.*, 2006.
- Riedesel, M. A., and T. H. Jordan, Display and assessment of seismic moment tensors, *Bull. Seism. Soc.*, 79(1) 85-100, 1989.
- Saikia, C. K., Modified frequency-wavenumber algorithm for regional seismograms using Filon's quadrature: modelling Lg waves in eastern North America, *Geophys. J. Int.*, 118 142-158, 1994.
- Sileny, J., G. F. Panza, and P. Campus, Waveform inversion for point source moment tensor retrieval with

variable hypocentral depth and structural model, *Geophys. J. Int.*, 109 259-74, 1992.

Song, X. J., D. V. Helmberger, and L Zhao, Broad-band modelling of regional seismograms: The basin and range crustal structure, *Geophys. J. Int.*, 125(1) 15-29, 1996.

Walter, W. R., Source parameters of the June 29, 1992 Little Skull Mountain earthquake from complete regional wave-forms at a single station, *Geophys. Res. Lett.*, 20(5) 403-406, 1993.

Walter, W. R., K. D. Smith, J. L. OBoyle, T. F. Hauk, F. Ryall, S. D. Ruppert, S. C. Myers, R. Abbot, and D. A. Dodge, An assembled western United States dataset for regional seismic analysis, *Lawrence Livermore National Laboratory Report, UCRL-TR-206630*, 2003.

Wessel, P. and W. H. F. Smith, New, improved version of generic mapping tools released, *Eos Trans. AGU*, 79 579 - 579, 1998.

8. 3D Simulations of Ground Motions of the 1989 Loma Prieta Earthquake Using the USGS SF06 Velocity Model

David Dolenc, Doug Dreger, and Shawn Larsen (LLNL)

8.1 Introduction

The United States Geological Survey has recently released an updated 3D velocity model (USGS SF06) of the greater San Francisco Bay Area that will be used to evaluate shaking hazard for possible future events in the region. In this study we used the 3D model and the 3D finite-difference code E3D (Larsen and Schultz, 1995) to simulate ground motions of the 1989 M_w 6.9 Loma Prieta event. Comparison of simulated ground motions with observations served to validate the velocity model for scenario studies of future large earthquakes in the region. This work was done as part of the SF06 Simulation Project Group modeling of the 1906 M_w 7.8 San Francisco earthquake (<http://www.sf06simulation.org>).

8.2 Modeling

The modeling of the great 1906 San Francisco earthquake for the event's 100th anniversary was one of the reasons for the USGS SF06 velocity model release. The model extends to 45 km depth and consists of a detailed model with approximate dimensions of 290×140 km. This detailed model is nested inside an extended model which has approximate dimensions of 650×330 km. The extended model was provided mainly to accommodate the 1906 San Francisco earthquake simulations and as a buffer zone for the simulations with either sources or stations close to the edge of the detailed model. The model's main improvement over the previous model versions is that more realistic material properties were assigned to individual geologic units (Brocher, 2005). Also, the model now includes topography and material properties of water for the Pacific Ocean and the San Francisco Bay.

To use the USGS SF06 model with the finite-difference code, we queried the model to extract values on a grid with a 125-m spacing. For the Loma Prieta earthquake, we employed Wald *et al.* (1991)'s strong motion and strong motion/teleseismic finite-source models. In addition, we used the Beroza (1991) strong motion finite-source model as a comparison. The dimensions of the simulation were $220 \times 135 \times 50$ km and the grid spacing was 125 m. Because of computation limitations, the slowest velocities in the model were increased to a minimum S-wave velocity of 500 m/s, corresponding to a maximum modeled frequency of 0.8 Hz. In our simulations we included water (S-wave velocity 0.0 m/s), but not topography or attenuation. The computations were performed on the BSL Linux cluster. We compared re-

sults obtained with the three different finite-source models to observations. In addition, we compared the recent results to those obtained with the previous version of the USGS (ver. 2) and UCB velocity models (Stidham *et al.*, 1999) that had 250-m grid spacing and 1 km/s minimum S-wave velocity.

8.3 Results

Maximum horizontal velocity maps for the Loma Prieta simulations with the USGS SF06 velocity model and three different finite-source models are shown in Figure 3.16 (top). Results show strong NW directivity of the Wald *et al.* SM/T finite-source model. Amplification of the ground motions over the basins is well observed for all three models.

Recorded and synthetic waveforms at some of the stations that were included in the simulations are compared in Figure 3.16 (bottom). Velocity waveforms were low-pass filtered at 0.8 Hz. The traces from top to bottom are observations (gray), followed by the USGS SF06 velocity model synthetics for the three different finite-source models (Beroza, Wald SM/T, Wald SM). The results showed that the overall agreement between the USGS SF06 model simulations and the observations is very good. Comparison to the results obtained with the previous USGS (ver. 2) model and the UCB model showed that the results obtained with the new USGS SF06 model better matched the observations. Important differences between the results obtained with the three different finite-source models can also be observed. The results obtained for the Loma Prieta event as well as for other smaller events in the region (Dolenc *et al.*, 2006; Rodgers *et al.*, 2006) indicate that the remaining misfit between the simulations and the observations at some stations requires further model refinement.

8.4 References

- Beroza G. C. (1991). Near-source modeling of the Loma Prieta earthquake: Evidence for heterogeneous slip and implications for earthquake hazard, *Bull. Seism. Soc. Am.* 81, 1603-1621.
- Brocher, T. M., Compressional and shear wave velocity versus depth in the San Francisco Bay Area, California: Rules for USGS Bay Area Velocity Model 05.0.0, *U.S. Geol. Surv. Open-File Report 2005-1317*, 2005.
- Dolenc, D., D. Dreger, and S. Larsen, 3D simulations of ground motions in Northern California using USGS SF06 velocity model, *Seism. Res. Lett.*, 77, 300, 2006.

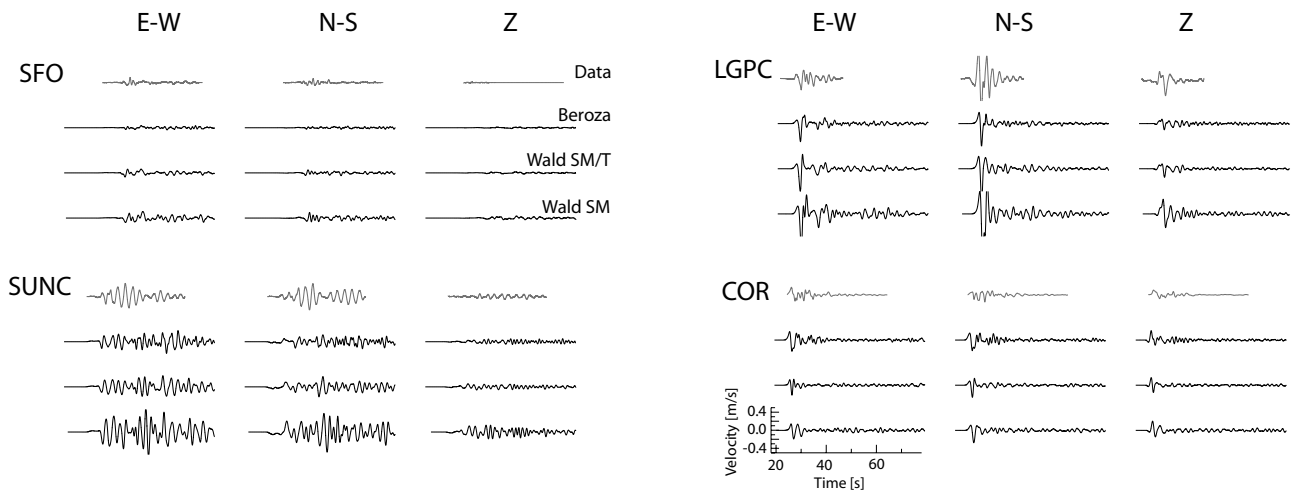
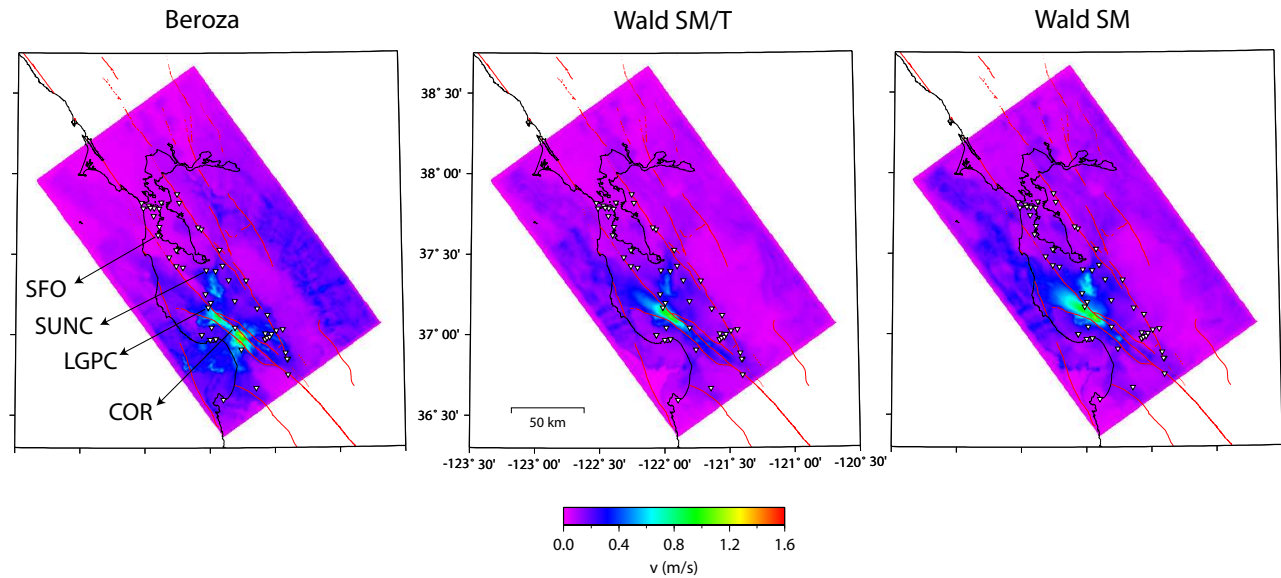


Figure 3.16: *Top*: Maximum horizontal velocity maps for the Loma Prieta simulations with the USGS SF06 velocity model and three different finite-source models. *Left*: Beroza (1991) strong motion model; *Center*: Wald et al. (1991) strong motion/teleseismic model; *Right*: Wald et al. (1991) strong motion model. *Bottom*: Recorded and synthetic waveforms at some of the stations that were included in the simulations. Velocity waveforms were lowpass filtered at 0.8 Hz. The traces from top to bottom are observations (gray), and USGS SF06 velocity model synthetics for the three finite-source models (Beroza, Wald SM/T, Wald SM).

Larsen S. and C. A. Schultz (1995). ELAS3D: 2D/3D elastic finite-difference wave propagation code, *Technical Report No. UCRL-MA-121792*, 19 pp.

Rodgers, A., A. Petersson, S. Nilsson, B. Sjogreen, and K. McCandless, Ground predictions using the USGS seismic velocity model of the San Francisco Bay Area: Evaluating the model and scenario earthquake predictions, *Seism. Res. Lett.*, 77, 281, 2006.

Stidham, C., M. Antolik, D. Dreger, S. Larsen, and B. Romanowicz, Three-dimensional structure influences on the strong-motion wavefield of the 1989 Loma Prieta

earthquake, *Bull. Seism. Soc. Am.*, 89, 1184-1202, 1999.

Wald D. J., D. V. Helmberger, and T. H. Heaton (1991). Rupture model of the 1989 Loma Prieta earthquake from the inversion of strong-motion and broadband teleseismic data, *Bull. Seism. Soc. Am.* 81, 1540-1572.

9. Toward Earthquake Early Warning in Northern California

Gilead Wurman and Richard M. Allen

9.1 Introduction

Although there have been recent advancements in the theory behind Earthquake Early Warning (EEW), there remain several challenges to the implementation of such EEW systems in Northern California. We have been working toward a functional EEW system since August 2005, and as of February 2006 an offline version of ElarmS (Earthquake Alarm System) has been running automatically, in a non-interactive fashion, following every event of $M \geq 3$ in Northern California.

The non-interactive processing of these events has provided us with valuable data regarding the performance of ElarmS in real scenarios, particularly for events in and around the Bay Area. We present the statistical performance of this non-interactive processing, and discuss two specific events which reflect possible major earthquake scenarios.

9.2 Challenges of Northern California

Implementing EEW in Northern California presents specific challenges that have required improvements to the ElarmS methodology used in Southern California. We must integrate data from broadband velocity instruments and strong-motion accelerometers spread across two networks: the Northern California Seismic Network (NCSN) and the Berkeley Digital Seismic Network (BDSN). The disposition of stations in Northern California is shown in Figure 3.17.

The methodology by which ElarmS estimates an earthquake's magnitude relies in part on the measurement of maximum predominant period, τ_p^{max} (Olson and Allen, 2005). However, this method is very susceptible to noise pollution, which is particularly problematic for events smaller than $M \sim 4.5$. To help constrain the magnitudes of small events, we have incorporated a second metric using the peak amplitude of either the displacement (P_d) or velocity (P_v) record following similar work in Taiwan (Wu, *et al.*, 2005). The linear average of the two metrics (P_d and τ_p^{max} or P_v and τ_p^{max}) has proven to significantly improve our magnitude estimates for events of all sizes. The P_d or P_v metric is less susceptible to noise at low magnitudes, but tends to saturate at higher magnitudes. As τ_p^{max} is susceptible to noise but not to saturation, the two metrics complement one another across all magnitudes.

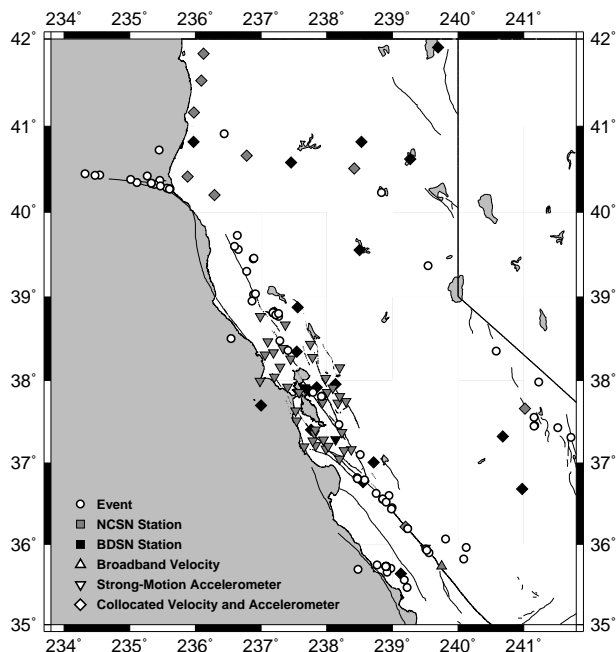


Figure 3.17: Map of Northern California showing NCSN and BDSN stations, and 68 events since February 2006.

9.3 Results of non-interactive processing

Since February of 2006, ElarmS has been running offline, in a non-interactive fashion (meaning with no human input or oversight), after every event in Northern California of $M \geq 3$. The processing is triggered automatically ten minutes after the event notification is received, to allow time for the necessary data to be recorded. Periodically, significant improvements to the ElarmS methodology are incorporated into the non-interactive processing. At that time all the events are reprocessed using the most current version of the code. The reprocessing is done using only the data available at the time of the initial processing, and is still performed non-interactively. Thus, while the reprocessed data does not reflect the fully automated performance of the system, it does reflect how the system would have performed, had the most current version of the code been in place at the time of the events.

As of this writing, a total of 70 instances of non-interactive processing have occurred. Of these, one is a duplicate event, due to the email notification system posting an update to an existing event. One instance was a false event. This was not the result of a false de-

tection by ElarmS, but of an erroneous email notification. The geographic distribution of the remaining 68 events is shown in Figure 3.17. Of these, one event was offshore Mendocino, with no stations within 100 km of the source, and two events suffered system-related processing errors (not resulting from the ElarmS code).

The remaining 65 events range in magnitude from M_d 2.86 to M_L 4.67. The results for these 65 events are presented in Figure 3.18. This figure shows the magnitude errors (with respect to network-based magnitudes, usually M_w or M_L) produced by ElarmS at three different times for each event. The initial magnitude error refers to the magnitude estimation based on only the first second of p-wave data at the first station(s) to detect the event. This is the earliest possible magnitude determination, which can be used to give the maximum warning time. The initial magnitude has a significant scatter ($\sigma \sim 0.8$ magnitude units) due to its reliance often on a single station's data.

The second plot in Figure 3.18 shows the errors at "alarm-time", which we define to be the time at which at least four seconds of p-wave data are available from at least four different channels. This definition is meant to reflect a confidence level in the magnitude which is sufficient to disseminate a public alarm. The magnitude error at this time is considerably less than in the first second ($\sigma \sim 0.5$ magnitude units). Note that there are fewer events represented in this plot (42 events vs. 65 in the other plots), because not all of the events are ever detected in enough channels to meet the alarm criteria. This is primarily due to the weak signal from small ($M \sim 3$) events, and in some cases results from a lack of enough stations within 100 km of the epicenter.

The lowermost plot in Figure 3.18 shows the error in the final magnitude determination for each event, using all available data from stations within 100 km of the source. Note that the scatter has increased over the previous plot ($\sigma \sim 0.6$ magnitude units) due to the incorporation of events which did not meet the alarm criteria.

9.4 Two scenario events

Among the 65 events processed non-interactively by ElarmS, two moderate events represent likely hazardous earthquake scenarios for the Bay Area, and thus provide some insight into what can be expected of ElarmS in a real situation. For these two events we use M_L as a reference, even though M_w values exist for both. This is because M_L is sensitive to the same frequencies (~ 1 -2 Hz) as ElarmS, and because M_L is more directly related to the severity of the event in terms of damage to persons and property.

The first event is a M_L 4.67 event near Gilroy, CA on 15 June, 2006. This event is located near the southern Calaveras fault, close to the likely epicenter of a Calaveras or Southern Hayward fault event. Figure 3.19 shows the

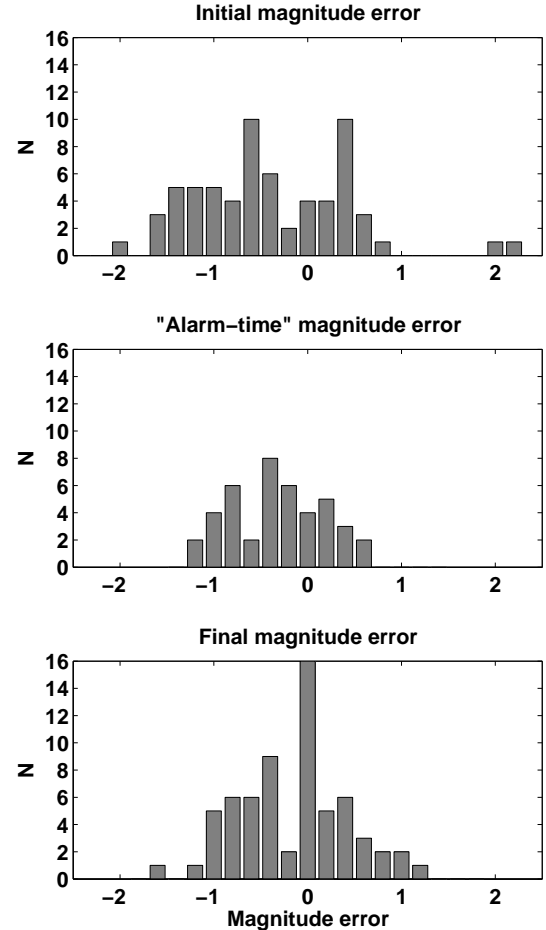


Figure 3.18: Magnitude errors from non-interactive processing. Top: magnitude estimate following first second of p-wave data. Middle: "alarm-time" magnitude error, using at least 4 seconds of p-wave data from 4 channels. Bottom: final magnitude error, using all available stations within 100 km.

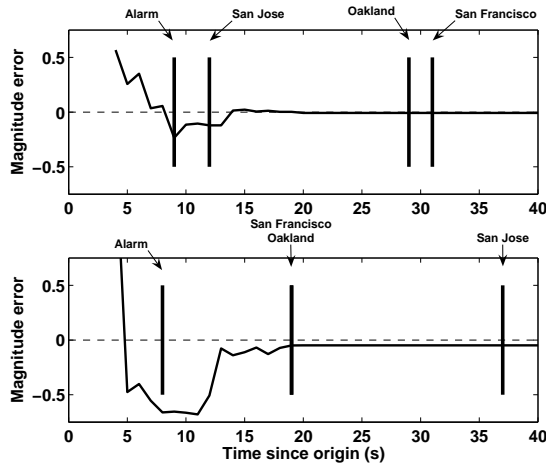


Figure 3.19: Plots of magnitude error vs. time for two representative events. Top: M_L 4.67 Gilroy Earthquake of 15 June, 2006. Bottom: M_L 4.7 Santa Rosa Earthquake of 2 August, 2006. Vertical bars represent (as notated) the “alarm time” for the event, or the time of arrival of severe ground motions at major urban centers in the Bay Area. Arrival times are based on a velocity of 3.55 km/s.

magnitude error vs. time for this event in relation to the arrival time of significant shaking at San Francisco, Oakland and San Jose.

Initial detection of this event by ElarmS occurred 3 seconds after origin, and the initial magnitude estimate was 5.2 one second later. The magnitude estimate came down over the following five seconds due to the incorporation of more data, until the alarm criteria were met at 9 seconds after origin. At that time, the magnitude estimate was 4.44, only 0.23 magnitude units below the actual M_L . The vertical lines on the plot represent the arrival of severe ground shaking at the three major urban centers in the Bay Area, based on a move-out of 3.55 km/s. San Jose experienced peak ground shaking only 12 seconds after event origin, meaning San Jose would have had about 3 seconds warning time in this event, not considering telemetry and dissemination delays. However, Oakland and San Francisco would have had 20 and 22 seconds of warning, respectively for this event. These warning times depend primarily on the disposition of stations around the epicenter, so they would be comparable for a magnitude 7 event.

The second scenario event is a M_L 4.7 event near Santa Rosa on 2 August (local time), 2006. This event is located near the Rodgers Creek fault, near the likely epicenter of a southward-rupturing Rodgers Creek/Hayward fault event. The bottom plot in Figure 3.19 shows the history of this event in the same manner as above.

This event was initially detected 3 seconds after event origin. The initial magnitude, one second later, was rather high, at 6.4. This is a large error, which highlights the utility of waiting for more data to become available rather than issuing the alarm immediately. In the next second, the magnitude dropped to 4.2, and by the time the alarm criteria were met at 8 seconds after origin, the magnitude had dropped further to 4.0. At alarm time, both San Francisco and Oakland had 11 seconds until the arrival of severe ground shaking. However, the magnitude estimate at that time was low, and only rose to about 4.6 at 13 seconds after the origin, leaving only 6 seconds of warning for San Francisco and Oakland. San Jose experienced severe ground motions 37 seconds after origin, so even with the additional 5 second delay for the magnitude estimate to rise, it still had 24 seconds of warning in this instance.

The poor initial estimation of the magnitude of the latter event is primarily because most of the stations to the north of the Bay Area are NCSN strong motion stations, which are susceptible to noise pollution below $M \sim 5$. For large earthquakes this is not a problem, but in smaller events high-gain broadband velocity sensors yield superior data.

9.5 Conclusion

We are now beginning the process of moving ElarmS from the offline development stage to real-time testing at the Berkeley Seismological Laboratory. Based on its performance on 65 events in a non-interactive offline setting, we expect that ElarmS will perform well under real-time testing, without major modification from its present version.

9.6 Acknowledgements

We would like to thank Doug Neuhauser and Bob Uhrhammer for information and discussions related to station equipment and networks. This research was funded by USGS/NEHRP Grant #05HQGR0074.

9.7 References

- Olson, E.L. and R.M. Allen, The deterministic nature of earthquake rupture, *Nature*, 438, doi:10.1038/nature04214, 212-215, 2005.
- Wu, Y.-M., H.-Y. Yen, L. Zhao, B.-S. Huang, and W.-T. Liang, Magnitude determination using initial *P* waves: A single-station approach, *Geophys. Res. Lett.*, 33, doi:10.1029/2005GL025395, 2006.

10. Identifying and Removing Noise from the Monterey Ocean Bottom Broadband Seismic Station (MOBB) Data

David Dolenc, Barbara Romanowicz, Bob Uhrhammer, Paul McGill (MBARI), Doug Neuhauser, and Debra Stakes (MPC)

10.1 Introduction

The Monterey ocean bottom broadband station (MOBB) was installed in April 2002, 40 km offshore in the Monterey Bay, at a water depth of 1000 m, through a collaborative effort between the Monterey Bay Aquarium Research Institute (MBARI) and the Berkeley Seismological Laboratory (BSL; *Romanowicz et al., 2003*). The MOBB includes a 3-component Guralp CMG-1T broadband seismometer, a differential pressure gauge (DPG) and a current meter. Prior to the deployment, the seismometer system was extensively tested and insulated at the BSL to minimize the long-period noise due to the sensitivity of the instrument to air movement within the titanium pressure vessel. During the deployment, further steps were taken to minimize the background noise that could be generated by the flow of water around the pressure vessel housing the seismometers (*Uhrhammer et al., 2002; Dolenc et al., 2006*). The remaining long-period background noise observed at MOBB is primarily due to pressure forcing from the infragravity ocean waves (*Dolenc et al., 2005*). Infragravity waves are ocean surface waves in the frequency band between 0.002 and 0.05 Hz. Results from a previous study (*Dolenc et al., 2005*) showed that the long-period noise data recorded at MOBB can be used to better understand where and when the infragravity waves are generated. But for the study of seismic signals, additional processing is needed to remove the long-period noise from the MOBB data.

10.2 Background noise removal

To remove the long-period background noise from the MOBB data we employed two methods. In the first one we subtracted the simultaneously recorded ocean bottom pressure signal from the vertical seismic acceleration in time domain. The scale factor by which the pressure signal was multiplied was assumed to be frequency independent and was linearly estimated from the data. This method has previously been used to remove atmospheric pressure signal from the vertical seismic data recorded at land stations (*Zürn and Widmer, 1995*). Figure 3.20a,b shows that this method can also be used to remove long-period background noise from the ocean bottom seismic data. The presented results are for a 5.5-hour period for which the pressure signal was removed from the vertical seismic acceleration signal in time domain. The result is shown in frequency domain to illustrate the successful removal of the infragravity “hump”.

In the second approach we combined the pressure observations with measurements of the transfer function between vertical seismic and pressure recordings to predict the vertical component deformation signal. The predicted signal was then removed from the vertical seismic data in either frequency or time domain (*Crawford and Webb, 2000*). The transfer function was calculated from periods without earthquakes. Since it is only a function of structure at the MOBB location, it does not change with time and can be applied to all data from this site. Figure 3.20c-f shows an example of the transfer-function method to remove noise from the earthquake free vertical MOBB data. An example of the long-period background noise removal for a period that included an earthquake is shown in Figure 3.21a-d. The 1-hour period used in the calculation now included the 12/06/2004 M_w 6.8 Hokkaido, Japan event. The same transfer function as described above and shown in Figure 3.20d was used. The result shows that the method successfully recovers the seismic phases that were previously hidden by the long-period background noise and that the result is similar to the waveforms from the nearby land station SAO (Figure 3.21d).

10.3 Signal-generated noise removal

The other type of noise observed at MOBB is the signal-generated noise. It is due to reverberations of seismic waves in the shallow sedimentary layers and may be unavoidable in buried ocean bottom installations. It is particularly strong following the arrival of sharp and strong seismic phases that are characteristic of large deep teleseismic events. We used two methods to remove the signal-generated noise. The first one employs the empirical transfer function constructed from MOBB data and nearby land station data that do not show the signal-generated noise. Results obtained with this method for the Fiji Islands event are presented in Figure 3.21g. Island station FARB was used as a reference land station to obtain the empirical transfer function. To demonstrate that the empirical transfer function from one event can be used to remove signal-generated noise from another event, we used the empirical transfer function obtained from the 11/17/2002 M_w 7.3 Kurile event to “clean” the Fiji Islands event data. The results in Figure 3.21h show that most of the signal-generated noise at MOBB was removed. This suggests that to routinely clean smaller events, we will not need to compute the empirical transfer function every time, but rather use one from a previous

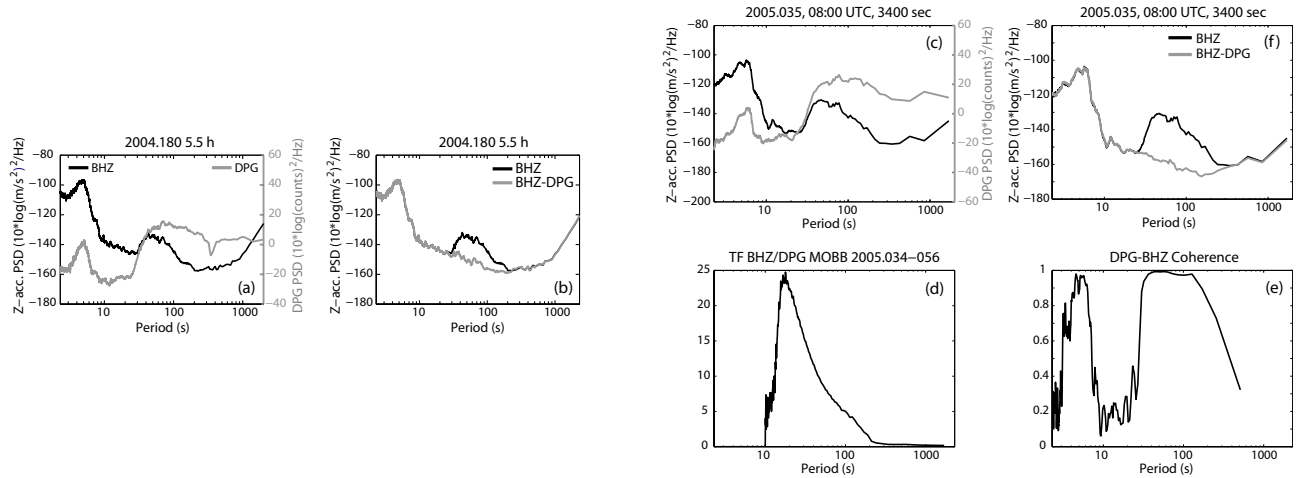


Figure 3.20: *Left*: Example of the time-domain method to remove noise from the earthquake-free vertical data. (a) Power spectral density (PSD) calculated for a 5.5-hour period without earthquakes for the vertical seismic channel (black) and the DPG (gray). At periods longer than 20 s the infragravity “hump” is observed for both datasets. (b) PSD for the vertical seismic channel before (black) and after (gray) the time-domain subtraction of the DPG signal. *Right*: Example of the transfer-function method to remove noise from the earthquake-free vertical data. (c) Power spectral density (PSD) for 1-hour period without earthquakes for the vertical seismic channel (black) and DPG (gray). (d) Transfer function between vertical seismic and DPG signal calculated from 144 1-hour long data windows within 2005.034-056 period. (e) Coherence between the vertical seismic and DPG channel for the selected 1-hour period on day 2005.035. (f) PSD for the vertical seismic channel before (black) and after (gray) the noise removal using the transfer function shown in (d).

strong event.

The second method uses a synthetic transfer function computed by modeling the response of shallow layers at the MOBB location. The response of the sedimentary layers is modeled using the propagator matrix approach (*Kennett and Kerry, 1979*). To obtain the response of the 1-D structure we used a previously published 1-D crustal model for this region (*Begnaud, 2000*) and replaced the top 350 m with a slower sedimentary layer. The synthetic transfer function was obtained by the spectral division of the result obtained with the 1-D model with the additional sedimentary layer and the result obtained with the original 1-D crustal model. The synthetic transfer function was then used to deconvolve the signal-generated noise from the MOBB vertical channel (Figure 3.21i).

Results presented in Figure 3.21e-i show that both methods can successfully remove the signal-generated noise from the MOBB data and that the obtained results are similar to the waveforms observed at the nearby land station (Figure 3.21f).

10.4 Conclusions

The described methods are an important tool to remove noise from the seismic data recorded at the ocean bottom buried broadband installations. Both methods used to remove the long-period background noise require

the locally recorded pressure signal at the seafloor. It is therefore important to have a reliable pressure sensor collocated with the ocean bottom seismometer. It is also important that the sampling rate for the DPG and other environmental data (e.g. temperature, ocean current speed and direction) is high enough so that they can be used in the post-processing for the complete seismic frequency band.

10.5 Acknowledgements

The MOBB instrumentation, deployment, and maintenance were supported by Lucile and David Packard Foundation funds to MBARI, NSF grant OCE9911392, and UC Berkeley funds.

10.6 References

- Begnaud, M. L., K. C. McNally, D. S. Stakes, and V. A. Gallardo, A crustal velocity model for locating earthquakes in Monterey Bay, California, *Bull. Seism. Soc. Am.*, *90*, 1391-1408, 2000.
- Crawford, W. C. and S. C. Webb, Identifying and removing tilt noise from low-frequency (< 0.1 Hz) seafloor vertical seismic data, *Bull. Seism. Soc. Am.*, *90*, 952-963, 2000.
- Dolenc, D., B. Romanowicz, D. Stakes, P. McGill, and D. Neuhauser, Observations of infragravity waves

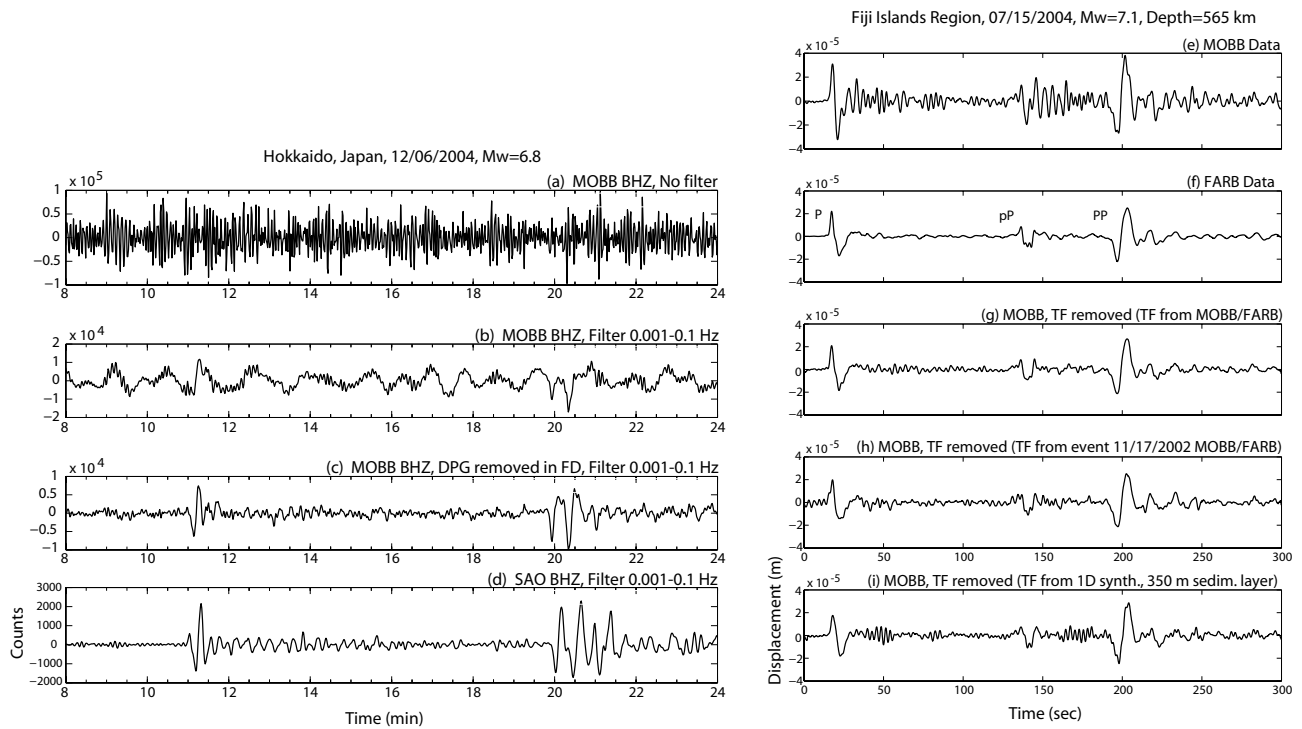


Figure 3.21: *Left*: Example of long-period background noise removal for the 12/06/2004 M_w 6.8 Hokkaido, Japan earthquake using the transfer function shown in Figure 3.20d. (a) Original MOBB vertical data. (b) MOBB data bandpass filtered between 0.001 and 0.1 Hz. (c) MOBB data after removal of the coherent DPG signal and bandpass filtered between 0.001 and 0.1 Hz. (d) Land station SAO data bandpass filtered between 0.001 and 0.1 Hz. *Right*: Three examples of deconvolution of the signal-generated noise at MOBB for the Fiji Islands event. (e) Original MOBB data. (f) Original FARB data. (g) MOBB data after removing empirical transfer function constructed using MOBB and FARB data. (h) Same as (g), only that empirical transfer function obtained from the 11/17/2002 M_w 7.3 Kurile Islands event was used. (i) MOBB data after removing a synthetic transfer function obtained by 1-D modeling of the shallow structure with a 350 m sedimentary layer ($v_p = 0.324\text{km/s}$, $v_s = 0.196\text{km/s}$, and $\rho = 1.3\text{g/cm}^3$).

at the Monterey ocean bottom broadband station (MOBB), *Geochem., Geophys., Geosys.*, 6, (9), 1-13, doi:10.1029/2005GC000988, 2005b.

Dolenc, D., B. Romanowicz, B. Uhrhammer, P. McGill, D. Neuhauser, and D. Stakes, Identifying and removing noise from the Monterey Ocean Bottom Broadband seismic station (MOBB) data, Submitted to *Geochem. Geophys. Geosys.*, 2006.

Kennett, B. L. N., and N. J. Kerry, Seismic waves in a stratified half space, *Geophys. J. R. Astr. Soc.*, 57, 557-583, 1979.

Romanowicz, B., D. Stakes, R. Uhrhammer, P. McGill, D. Neuhauser, T. Ramirez, and D. Dolenc, The MOBB Experiment: A prototype permanent off-shore ocean bottom broadband station, *Eos Trans., AGU*, 84, (34), 325, 331-332, 2003.

Uhrhammer, R., B. Romanowicz, D. Neuhauser, D. Stakes, P. McGill and T. Ramirez, Instrument testing and first results from the MOBB Observatory, *Eos Trans., AGU*, 83, (47), Fall Meet. Suppl., F1008, 2002.

Zürn, W. and R. Widmer, On noise reduction in vertical seismic records below 2 mHz using local barometric pressure, *Geophys. Res. Lett.*, 22, 3537-3540, 1995.

11. The Orinda Earthquake Sequence: Complexity in Small Earthquakes

Margaret Hellweg

11.1 Introduction

How different are large and small earthquakes? In large earthquakes, such as the 2004 Sumatra event, we expect a long lasting rupture process with several episodes of energy release. We usually imagine that earthquakes with magnitudes smaller than 4 are point sources in space and time. The events in sequence of earthquakes which occurred near Orinda, California offers an opportunity to explore this question. On October 19 a M_L 3.5 earthquake (MS) occurred almost directly below Berkeley Seismological Laboratory's station BRIB (37.92 N, 122.15 W). At the surface are a broadband seismometer and an accelerometer. In addition, there is a borehole at the station, with a 3-component geophone and a 3-component accelerometer sampled at 500 sps at a depth of 119 m. The sequence began on 19 Oct 2003 at 14:35:27 UTC, about an hour before the MS with a M_d 2.5 foreshock, and included more than 4000 aftershocks ranging in magnitude from - 2.5 to 3.4 over the course of the next 3 months.

11.2 Event Complexity

The record of the mainshock (15:32:52 UTC on October 19 with M_L 3.53 (Figure 3.22A) is quite simple, as we expect from a point source. However, the slightly smaller aftershock the next day (October 20, 17:50 UTC, M_L 3.4, Figure 3.22B) exhibits a number of P-wave pulses before the arrival of the S-waves. Even smaller events exhibit similar complexity (Figure 3.22C), with several P pulses of similar amplitude arriving before the first S-wave. For each P pulse, there is a corresponding S pulse. Using time-domain polarization analysis to find the azimuth and incidence angles (Plesinger *et al.*, 1986, Abercrombie, 1995), the direction to the source of the waves can be determined. The distance to the source can be derived from the delay between the P- and S-waves from the same source. I performed this analysis for a selection complex events to see if the P-waves came from different locations. Figure 3.23 shows the locations of three P-wave sources for the M_L 3.4 aftershock of October 20 and two for a M_L 0.5. The mainshock location and the locations of the foreshock and a number of other small, simple aftershocks are also shown. Each P-wave pulse from each these events clearly stems from a different location.

11.3 Perspectives

The source of the complexity observed in these two events, as well as in other small events of the Orinda sequence, is as yet undetermined. There are three possible causes for the complexity observed here. The simplest explanation is that several earthquakes of similar size occur with in a very short time of each other, thus that the events are independent. It is also possible that the rupture process of the event is uneven, and P-wave pulses are generated as the rupture propagates through the medium, releasing energy in separate episodes. Finally, the later events may be triggered in the stressed medium by the passing waves of the first event. Further investigations of the timing of the later arrivals may provide insights. However, an important remaining unknown which can influence the interpretation is the velocity structure in the source region.

11.4 References

- Abercrombie, R.E., Earthquake locations using single-station deep borehole recordings: Implications for microseismicity on the San Andreas fault in southern California. *J. Geophys. Res.*, 100, 24003-24014, 1995.
- Plesinger, A., M. Hellweg and D. Seidl, Interactive high-resolution polarization analysis of broad-band seismograms. *J. Geophysics*, 59, 129-139, 1986

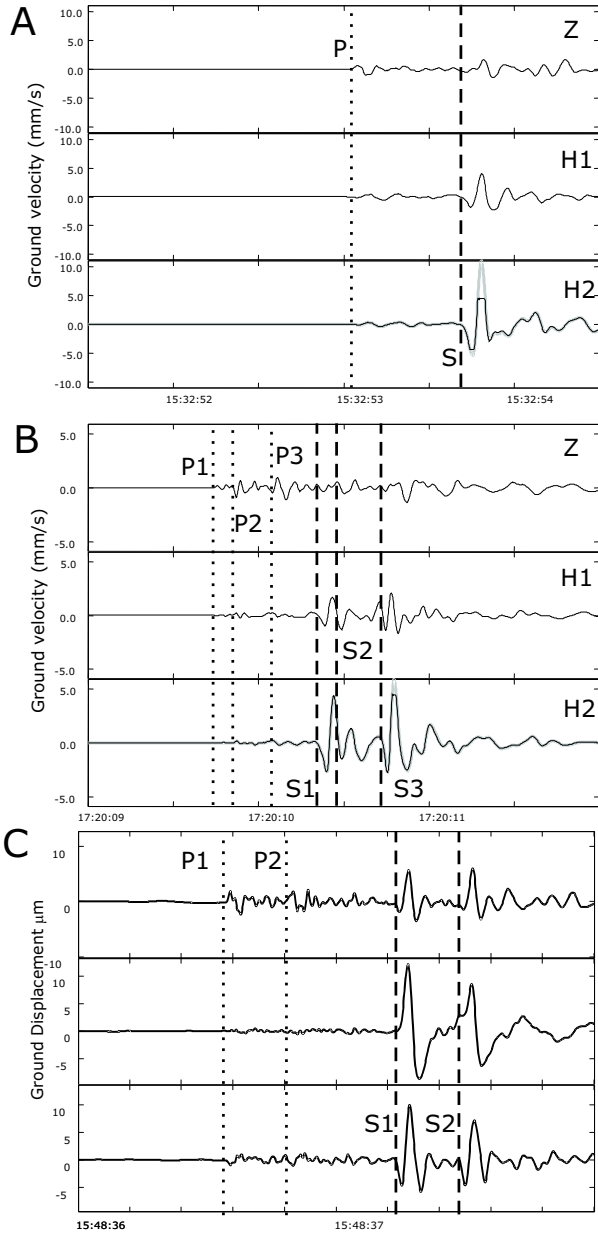


Figure 3.22: Waveforms for the mainshock (A), largest aftershock (B) and a M_L 0.5 aftershock of the Orinda sequence. Note that there are three P-wave pulses in the large aftershock, and at least two in the small one. It may be that these are because several events happen within a short time, or this may be due to rupture propagation.

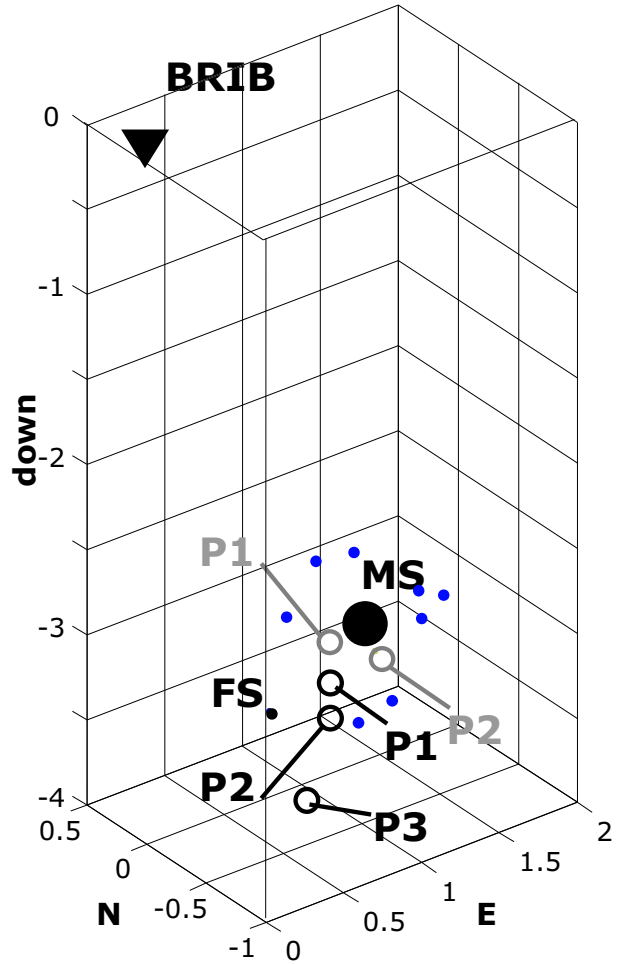


Figure 3.23: Locations of the mainshock (large, solid circle), and a number of small, simple aftershocks (small, solid circles). P-wave locations for the largest aftershock are indicated by the black, open circles (P1, P2, P3). For the small aftershock in Figure 3.22C they are marked by gray, open circles.

12. Northern California Seismicity Project

Robert A. Uhrhammer

12.1 Introduction

The Northern California Seismicity Project (NCSP) is a counterpart to the San Francisco Bay Region (SFBR) - Historical Earthquake Re-analysis Project (HERP), which has been reported upon in previous annual reports. The initial objective of this project, which commenced in August, 2000, is to transcribe the pre-1984 data for $M_L \geq 2.8$ earthquakes, which have occurred in Northern and Central California (NCC) (outside of the SFBR covered by HERP), from the original reading/analysis sheets, kept on store in the Berkeley Seismological Archives, to a computer readable format.

Characterization of the spatial and temporal evolution of NCSP seismicity during the initial part of the earthquake cycle as the region emerges from the stress shadow of the great 1906 San Francisco earthquake is the long term goal. The problem is that the existing BSL seismicity catalog for the SFBR, which spans most of the past century (1910-present), is inherently inhomogeneous because the location and magnitude determination methodologies have changed as seismic instrumentation and computational capabilities have improved over time. As a result, NCC seismicity since 1906 is poorly understood.

Creation of a NCC seismicity catalog that is homogeneous, that spans as many years as possible, and that includes formal estimates of the parameters and their uncertainty is a fundamental prerequisite for probabilistic studies of the NCC seismicity. The existence of the invaluable BSL seismological archive, containing the original seismograms as well as the original reading/analysis sheets, coupled with the recently acquired BSL capability to scan and digitize historical seismograms at high resolution allows the application of modern analytical algorithms towards the problem of determining the source parameters of the historical SFBR earthquakes.

12.2 Background and Motivation

Although the 1910 to present BSL catalog of earthquakes for NCC appears to be a simple list of events, one must remember that it really is a very complex data set. It is easy to misinterpret observed variations in seismicity if we do not understand the limitations of this catalog. The existing 1910 to present BSL catalog of earthquakes for NCC is inhomogeneous in that it suffers from the three types of man-made seismicity changes identified by *Habermann* (1987), namely detection changes, reporting changes, and magnitude shifts. The largest change in the detection capability of the BSL seismic station net-

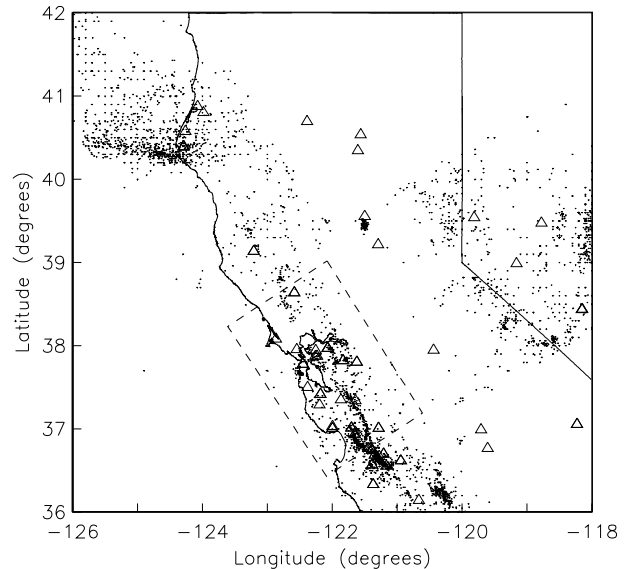


Figure 3.24: Map of the NCC Region showing the 1951-1983 $M_L \geq 2.9$ seismicity (small dots). The triangles are the seismic stations, operated by Berkeley and adjacent networks between 1951 and 1983, for which data are available. Events occurring in the dashed inset box were transcribed and analyzed as a part of the San Francisco Bay Region: Historical Earthquake Re-analysis Project (HERP).

work occurred starting circa 1927 with the installation of the Wood-Anderson and Benioff seismometers at several sites in NCC (see Figure 3.24) and the resulting increase in sensitivity lowered the threshold for detection of NCC earthquakes by about 2 M_L units. The most significant reporting change occurred circa 1942 when the BSL began determining M_L for some earthquakes and by 1948 M_L was routinely determined and reported for all SFBR earthquakes listed in the BSL Bulletin (*Romney and Meeker, 1949*).

The lack of a homogeneous catalog of earthquake for the SFBR that spans most of the past century, the availability of the invaluable BSL seismological archive, the interest in the Working Group on California Earthquake Probabilities (WGCEP, 1999), the funding of an initial effort with support from the USGS-PG&E CRADA, and the purchase and loan of a high-resolution wide-format digitizer by the USGS, combine to provide both an incentive and a unique opportunity to systematically re-process, using modern algorithms, the BSL seismo-

graphic records and data for SFBR earthquakes and to produce a homogeneous catalog of earthquakes for the region.

12.3 Initial Effort

To begin and expedite the transcription process, we first converted all relevant available data from the online NCEDC event catalogs and the in-house phase data to a flat transcription file format for the years 1951 through 1983. We also acquired a copy of the International Data Center (ISC) CDROM which contains events and associated station data published in the ISC Bulletins from January 1964 through December 1977 (Version 1.2). This ISC data set includes event and station data for the subset of Berkeley stations that were contributed to the ISC. The CDROM also contains an algorithm to search the database and extract and translate the ISC coded phase Berkeley data to a readable print format for years 1963 through 1977. This enabled us to start with transcription files that contained approximately half the data that is on the original reading/analysis sheets for the years 1964 through 1983. The primary data from the original reading/analysis sheets that was not included in this process was the Wood-Anderson maximum trace amplitude data that is crucial for the determination of local magnitude.

12.4 Current Effort

During the past year, five students worked on the process of transcribing and verifying the transcription of the data from the original BSL reading/analysis sheets to computer readable form. The verification process had two components: the first step is perform a detailed syntactical check of the transcribed information format using an ad hoc syntactical algorithm, and the second is to obtain an initial location for the event and check for anomalous observations. Syntactical errors were subsequently corrected, and anomalous observations were verified and corrected if necessary. To date, they have transcribed and verified data for over 5200 earthquakes that occurred in NCC between 1951 and 1983. They started by verifying the transcription of the original reading/analysis sheets and locating the earthquakes starting in 1983, and they worked back in time. More detailed felt reports and comments were added when available. Owing largely to the computer readable information that was available from the ISC, processing the 1964 to 1983 files took the least amount of time. Since none of the data on the pre-1964 reading/analysis sheets existed in a computer readable form, all data has to be transcribed, and, consequently, it takes more time to transcribe each event. We have now completed the transcription and verification process for over 5200 NCC ML 2.9+ earthquakes that occurred between 1951 and 1983.

The pre-1951 reading/analysis sheets data do not contain Wood-Anderson maximum trace amplitude data,

which is used in the calculation of local magnitude, so that the original Wood-Anderson seismograms will have to be retrieved from the archive and the amplitudes read. This quite labor intensive component of the project is planned for the coming year.

12.5 Acknowledgements

UC Berkeley students Vicky Chi Sum Chan, Rose Li, Sean Tsai, Noli Valera, and visiting U Pennsylvania student Carmen Rodriguez participated in this project during the past year, and we thank them for their efforts.

This project was partially supported by the USGS funding of the Northern California Earthquake Data Center.

12.6 References

Habermann, R. E., Man-made changes of seismicity rates, *Bull. Seism. Soc. Am.*, 77, 141-159, 1987.

Romney, C. F. and J. E. Meeker, Bulletin of the Seismographic Stations, *University of California Press*, 18, pp. 89, 1949.

13. Seismogram Scanning Project

Robert A. Uhrhammer

13.1 Introduction

This aim of Seismogram Scanning Project (SSP) is to scan selected analog seismograms kept on store in the Berkeley Seismological Laboratory (BSL) Seismogram Archive and generate digital image files for studying microseismic source areas and distribution in relation to wave climate. The Berkeley Seismogram Archive, where approximately 1.2 million analog seismograms dating back to 1910 are stored, contains seismograms recorded at the seismic stations located on the UC Berkeley Campus (BRK and BKS), dating back to 1930, which are crucial for this project. This scanning project is being undertaken in collaboration with Dr. Peter Bromirski of the University of California, San Diego/Scripps Institution of Oceanography on his project funded by the California Department of Boating and Waterways. The corresponding digitization of the scanned seismograms is being done at the Scripps Institution of Oceanography.

13.2 Background and Motivation

The photographic and smoked paper seismograms kept on store in the BSL Seismogram Archive are gradually deteriorating over time, and scanning the seismograms into a computer readable format is essential if they are to be preserved for the future. BSL has a wide format scanner, and whenever the opportunity and funding allows, we make an effort to scan seismograms.

13.3 Initial Effort

The initial effort was to systematically digitize the November-March vertical component Sprengnether seismograms and also the November-March Berkeley vertical component Wilip-Galitzin seismograms for selected "El Nino and La Nina" winters. The seismograms were scanned at a resolution of 400 dots per inch on an Contex Scanning Technology Ideal FSS 18000 DSP Full Scale Scanner using their interactive WIDEimage scanning software package (available via URL: <http://www.contex.com>). The scanned images are stored as Tag Image Format (TIF) bitmap image files. To substantially reduce the storage requirements, a histogram analysis is employed to interactively set an appropriate threshold and the scanned seismograms are stored as 1-bit resolution line-art images. An example of a scanned SPR seismogram is shown in Figure 3.25.

13.4 Current Effort

During the past year we have completed the task of systematically scanning the available November-March Berkeley vertical component Sprengnether seismograms for the winters of 1962 through 1991 and also the available November-March Berkeley vertical component Wilip-Galitzin seismograms for the winters of 1930 through 1964 (a total of approximately 9,300 seismograms). We are also finalizing a paper "Comparison of Wilip-Galitzin, Sprengnether and Streckeisen Seismographic Recordings at Berkeley" to be submitted to the Bulletin of the Seismological Society of America.

13.5 Digitization Procedure

Digitization of the photographic seismograms has two components. The seismograms are first scanned at a resolution of 400 dots per inch on an Contex Scanning Technology Ideal FSS 18000 DSP Full Scale Scanner. The scanned images are stored as Tag Image Format (TIF) bitmap image files. To substantially reduce the storage requirements, a histogram analysis is employed to interactively set an appropriate threshold, and the scanned seismograms are stored as 1-bit resolution line-art images. The traces on the scanned seismogram image are then digitized at nominally 4 samples per second using the SeisDig software package (*Bromirski and Chuang, 2003*) available for download at URL: <http://www.ucsg.edu/~bromirski>. The resulting digitized seismogram has an amplitude resolution of 0.0635 mm (i.e. the pixel resolution and equivalent to a data logger sensitivity of 15748 DU/M) and a time resolution of 0.254 seconds for the SPR seismograms recorded at 15 mm/min and 0.127 seconds for the W-G seismograms recorded at 30 mm/min (also the pixel resolution). The effective dynamic range is approximately 64 dB ($20 \log_{10}(100\text{mm}/0.0635\text{mm})$). An example of a digitized SPR seismogram is shown in Figure 3.25.

13.6 Calibration of Wilip-Galitzin, Sprengnether and Streckeisen Seismographs

As seismic instrumentation has evolved, three different three-component sets of long-period/broadband seismographs have been installed and operated, with overlapping intervals, at Berkeley since the 1930's. Wilip-Galitzin (W-G) seismographs were operated on the northern most seismic piers in the basement of Haviland Hall on the Berkeley Campus (BRK) from August

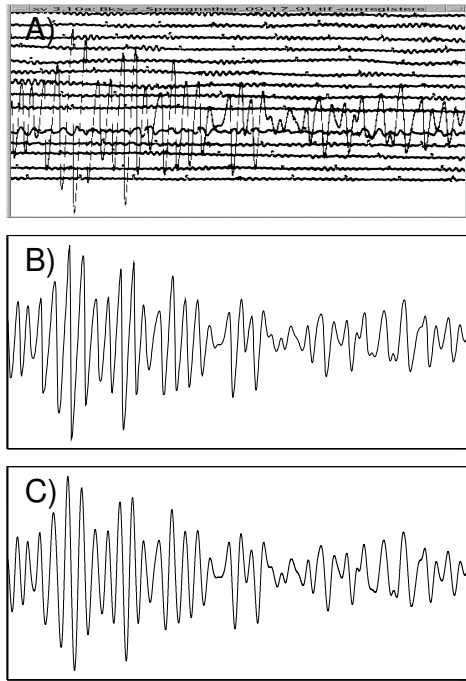


Figure 3.25: A comparison of: A) the scanned BKS Sprengnether Z-component seismogram; B) the corresponding digitized waveform, and; C) the corresponding waveform synthesized from the co-sited Streckeisen STS-1 broadband seismograph. The seismic signal is from a M 5.7 teleseism which occurred 4000 km SE of Berkeley (1991/09/18,09:48:13; 14.65N, 90.99W) in Guatemala. All three plots are at the same scale with the horizontal axis spanning 511.25 seconds and the vertical axis spanning 175 mm. That all three waveforms are highly similar is verification of the accuracy of the digitization procedure and the accuracy of the Sprengnether transfer function.

28, 1930 until February 1, 1965. World Wide Standardized Station (WWSS) Sprengnether (SPR) long-period seismographs were operated in the Byerly Seismic Vault (BKS), located in Strawberry Canyon behind the Botanical Garden, from June 8, 1962 until September 30, 1991. Streckeisen (STS-1) broadband seismographs began recording in the Byerly Seismic Vault (BKS) on May 11, 1987 with a 16-bit PC-based recording system (*Bolt et al.*, 1988) and a 20 second pendulum configuration and by August 8, 1991 they had evolved into the current 24-bit Quanterra Q680 data logger and 360 second very-broadband (VBB) pendulum configuration. The W-G and SPR seismographs operated concurrently, but not co-sited, from June 8, 1962 until February 1, 1965. The SPR

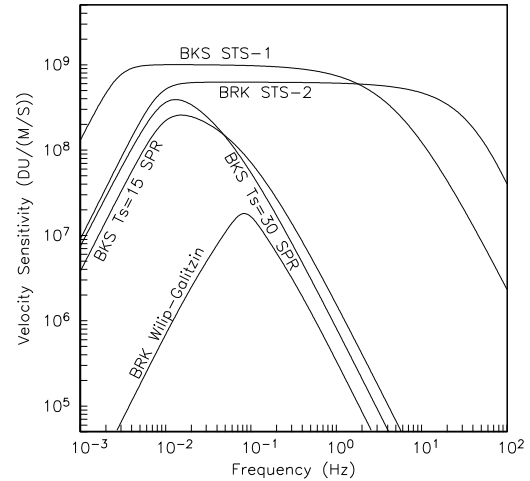


Figure 3.26: A comparison of the velocity responses of the BRK W-G and STS-2 and the BKS SPR and STS-1 seismographs operated at Berkeley. The W-G and SPR instruments recorded galvanometrically on photographic paper, and the paper seismograms are scanned at a resolution of 400 dots per inch. The STS-1 and STS-2 instruments record digitally via a high-resolution data logger. The velocity sensitivity is given in digital units per meter per second (DU/(M/S)). Two responses are given for the SPR because its natural period (T_s) was changed from 30 seconds to 15 seconds on May 12, 1965.

and STS-1 seismographs operated concurrently at BKS from August 8, 1991 until September 30, 1991. Comparison of selected seismograms from these intervals allow us to verify the calibration and response of these seismographs, and to demonstrate that, within appropriate passbands, the earlier instrument seismograms can be reliably synthesized from later instrument seismograms, and that absolute ground motions can be reliably estimated. An example of a SPR seismogram, synthesized from the corresponding STS-1 seismogram, is shown in Figure 3.26. A Streckeisen STS-2 seismograph has operated at BRK since January 1, 1993 and a comparison of selected seismograms from the BKS STS-1 and the BRK STS-2 is used to quantify differences in their site responses. A comparison of the responses of these seismographs is shown in Figure 3.26.

13.7 Acknowledgements

UC Berkeley student Kevin Lee participated in this project during the past year, and we thank him for his efforts.

This project was funded by sub-award of the California Department of Boating and Waterways Contract 03-106-105.

13.8 References

Bolt, B. A., J. E. Friday and R. A. Uhrhammer, A PC-based Broadband Digital Seismograph Network, *Geophysical Journal*, 93, 565-573, 1998.

Bromirski, P. D. and S. Chuang, SeisDig Software to Digitize Scanned Analog Seismogram Images: User's Manual, *Scripps Institution of Oceanography Technical Report*, Scripps Institution of Oceanography, Integrative Oceanography Division, UC San Diego, 28 pp., July 2, 2003.

14. Regional Attenuation Method Comparison for Northern California

Sean R. Ford, Douglas S. Dreger, Kevin Mayeda, William R. Walter (Lawrence Livermore National Laboratory), Luca Malagnini (Istituto Nazionale di Geofisica e Vulcanologia), and William S. Phillips (Los Alamos National Laboratory)

14.1 Introduction

Understanding of regional attenuation (Q^{-1}) can help with structure and tectonic interpretation, and correcting for the effects of attenuation can lead to better discrimination of small nuclear tests. Present threshold algorithms for event identification rely on Q models that are derived differently, and the models can vary greatly for the same region. It is difficult to learn the cause of such discrepancies because the methods and parameterizations change for each analysis. In order to better understand the effects of different methods and parameterizations on Q models, we implement four popular methods and one new method to measure Q of the regional seismic phase, Lg (Q_{Lg}), using a high-quality dataset from the Berkeley Digital Seismic Network (BDSN). With this knowledge, it will be possible to better assess the results of published attenuation studies, and future efforts can benefit from the outlined comprehensive analysis procedure.

14.2 Methods, Comparisons, and Sensitivity Tests

The dataset consists of 158 earthquakes recorded at 16 broadband (20 sps) three-component stations of the BDSN between 1992 and 2004. The wide distribution of data parameters allows for sensitivity testing to a given dataset. We calculate Q_{Lg} by fitting the power-law model, $Q_0 f^\alpha$, in Northern California using five different methods. The first two methods use the seismic coda to correct for the source effect. These methods can produce best-fit power-law parameters for specific stations. The last three methods use the spectral ratio technique to correct for source, and possibly site effects. These methods produce best-fit power-law parameters for specific inter-station paths.

Coda normalization method (CNM)

CNM uses the coda as a proxy for the source and removes it from the Lg spectrum (Aki, 1980; Yoshimoto et al., 1993). The amplitude is then least-squares fit as a function of distance in small frequency bands for each station, where the slope is related to path attenuation, Q^{-1} . Q^{-1} at the center frequency of each band then reveals a power-law Q model for each station.

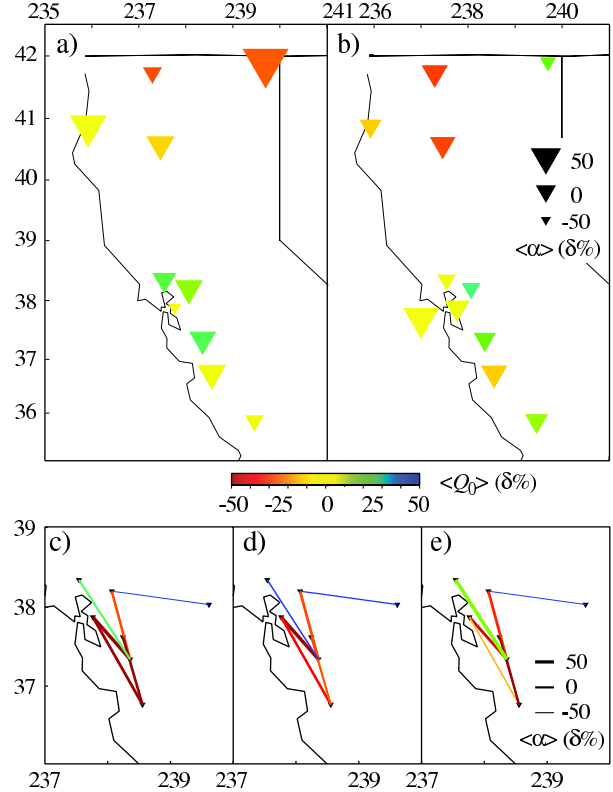


Figure 3.27: Spatial variability in the percent deviation from the method average power-law fit parameters ($Q_0 f^\alpha$) for the (a) coda normalization method, (b) coda-source normalization method, (c) two-station method, (d) reverse two-station method, and (e) source-pair / receiver-pair method. The average models are $104f^{0.61}$, $172f^{0.57}$, $132f^{0.53}$, $121f^{0.52}$, $76f^{0.76}$, respectively

Coda-source normalization method (CSM)

CSM uses the 1-D coda-source spectra previously calculated in the study by Mayeda et al. (2005) and removes it from the Lg spectrum in small frequency bands (Walter et al., 2006). Q^{-1} is calculated for each of these bands for each event-station path. In this application of CSM, all paths to a common station are fit to find a power-law Q model for each station.

Comparison of CSM and CNM

Since both CNM and CSM give a result for each station, we compare these results by finding the percent deviation of each station from the average $Q_0 f^\alpha$ produced

for each method. Comparisons are mapped in Figure 3.27a-b when a solution was calculated for both methods. The average Q_{Lg} model given by the CNM is $104f^{0.61}$, while the CSM produces an average of $172f^{0.57}$. The absolute difference in Q_{Lg} models may be due to the absence of a site correction in the CSM. There is overall relative agreement in the two methods, with low Q in the northern part of the study region and variable Q in the Bay Area. This Bay Area variance may be due to paths crossing different tectonic regimes to reach these stations and forming an average fit. Stations MOD, FARB, and POTR appear to have a strong difference in measured Q_0f^α . However, the fit to a power-law model is poor at frequencies > 2 Hz, and the comparison for a power-law model may be flawed for these stations. Stations BKS and MHC are consistently lesser or greater, respectively, than the average for each method, but there is a large percent deviation for the two stations.

Two-station method (TSM)

TSM takes the spectral ratio of Lg recorded at two different stations along the same narrow path from an event (Xie, 2002; Xie and Mitchell, 1990). We restricted the path to fall in an azimuthal window of 15° . The ratio removes the common source term and the amplitude is fit in the log domain so that the slope is α and the intercept is Q .

Reverse two-station method (RTSM)

RTSM uses two TSM setups where an event is on either side of the station pair in a narrow azimuthal window (Chun et al., 1987; Fan and Lay, 2003). The two ratios are combined to remove the common source and site terms and the amplitude is fit in the log domain so that the slope is α and the intercept is Q .

Source-pair / receiver-pair method (SPRPM)

SPRPM is basically the RTSM with a relaxation on the narrow azimuthal window requirement (Shih et al., 1994).

Comparison of TSM, RTSM, and SPRPM

Since TSM, RTSM, and SPRPM give a result for interstation paths, we compare these results by finding the percent deviation of each interstation path from the average Q_0f^α produced for each method. Comparisons are mapped in Figure 3.27c-e when a solution was calculated for all methods. The average Q_{Lg} model given by the TSM is $132f^{0.53}$, by RTSM is $121f^{0.52}$, and by SPRP is $76f^{0.76}$. Values of Q_0 are fairly uniform with greater than average and lesser than average values consistent across each of the respective methods. A notable exception is the path from MHC to SAO, where the TSM calculates a greater than average Q_0 and the other methods find a

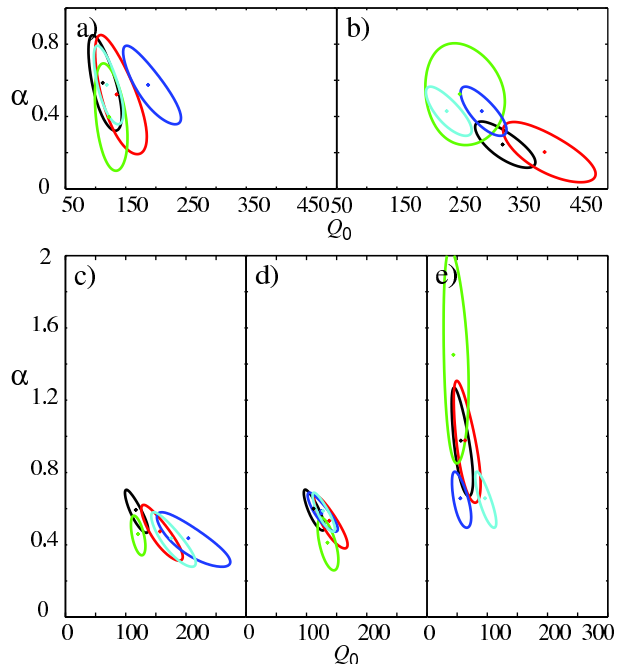


Figure 3.28: 95% confidence ellipses for the power-law model parameters for station PKD calculated by the (a) coda normalization, (b) coda-source normalization, (c) two-station, (d) reverse two-station, and (e) source-pair/receiver-pair methods obtained by the original parameterization (black), and by varying the spreading exponent (red), bandwidth (green), distance (dark blue), and time window (light blue). The small cross is the best-fitting parameter estimate. The coda-based methods are for station PKD, and the spectral ratio-based methods are for the path from MHC to POTR.

less than average Q_0 . The mean value of Q_0 and α for SPRPM are very low for the region, and the power-law exponent, α , varies widely among all methods. This may be due to the variance in the spectral amplitudes, and robust methods of spectrum estimation may reduce the variance.

Sensitivity tests

We investigated how the choice of parameterization affects the results. In each test, only one parameter was varied, and Q_0f^α was calculated with each of the methods. The varied parameters were geometrical spreading dependence ($r^{0.5}$ to $r^{0.83}$), measurement bandwidth (0.25-4 Hz to 0.5-8 Hz), epicentral distance of the data (100-400 km to 100-700 km), and the Lg window (2.6-3.5 km/s to 3.0-3.6 km/s). The range of parameterization was chosen based on the values used in previous studies.

All methods were affected by a change in spreading exponent, where there is a systematic increase in both Q_0 and α as the spreading exponent increases. Also,

when more of the spectrum below 1 Hz is sampled, α can change significantly. The methods that use a maximum Lg amplitude in the time domain to measure Q_{Lg} , CNM and SPRP, are less sensitive to Lg window choice than the other methods. However, CNM is affected by epicentral distance, which may be due to the fixed time that the coda is sampled for all distances. The RTSM is the most robust and resistant to changes in parameterization.

In order to better visualize the sensitivity of the methods to varied parameterization, we produce 1-D power-law Q models for a common station, PKD, for the coda-based methods (Figure 3.28a-b), and a common path, MHC to POTR, for the spectral ratio based methods (Figure 3.28c-e). Error in these 1-D fits is calculated and we produce 95% confidence ellipses for each of the power-law model parameters (Aster *et al.*, 2005).

Estimates of the power-law parameters, Q_0 and α , have a complex relationship with parameterization choice. The greatest variance in Q_0 is given by the CSM (~ 200 -500), while there is a large variance in α calculated with the SPRPM (~ 0.6 -1.8). However, for all methods (with the possible exception of the RTSM) the 95% confidence region is large, and the range of the parameter estimates is greater than is given by previous 1-D Q_{Lg} studies, which often only present one choice of parameterization.

14.3 Conclusions

There is lateral variability in Q_{Lg} at 1 Hz and the power-law dependence on frequency in Northern California. The spatial variability is similar to that found by Mayeda *et al.* (2005), where there is high attenuation in the northern region of the study area and variable attenuation in the Bay Area. Trends in calculated power-law parameters are similar among the methods investigated in this study, though there is large variability in the absolute values for $Q_0 f^\alpha$.

The choice of spreading exponent, distance, and measurement window has a large influence on the best-fit power-law parameter estimates. Unless the parameterization choice can be constrained from a priori information, regional attenuation studies should search the entire solution space in order to report useful power-law Q models.

14.4 Acknowledgements

This research is sponsored by the Department of Energy through the National Nuclear Security Administration, Office of Nonproliferation Research and Development, Office of Defense Nuclear Nonproliferation.

14.5 References

Aki, K., Attenuation of shear-waves in the lithosphere for frequencies from 0.05 to 25 Hz, *Phys. Earth Planet. Inter.*, 21 50-60, 1980.

Aster, R. C., and B. Borchers, and C. H. Thurber, *Parameter Estimation and Inverse Problems*, San Diego: Elsevier Academic Press, 2005.

Chun, K. Y., G. F. West, R. J. Kokoski, and C. Samson, A novel technique for measuring Lg attenuation: Results from eastern Canada between 1-Hz to 10-Hz, *Bull Seism Soc.*, 77 398-419, 1987.

Fan, G. W., and T. Lay, Strong Lg wave attenuation in the Northern and Eastern Tibetan Plateau measured by a two-station/two-event stacking method, *Geophys. Res. Lett.*, 30, 2003.

Mayeda, K., L. Malagnini, W. S. Phillips, W. R. Walter, and D. Dreger, 2-D or not 2-D, that is the question: A northern California test, *Geophys. Res. Lett.*, 32, 2005.

Shih, X. R., K. Y. Chun, and T. Zhu, Attenuation of 1-6 s Lg waves in Eurasia, *J. Geophys. Res.*, 99 23859-23873, 1994.

Walter, W. R., K. Mayeda, L. Malagnini, L. Scognamiglio, Regional body-wave attenuation using a coda source normalization method: application to MEDNET records of earthquake in central Italy, *Seism. Res. Lett.*, 77 260, 2006.

Xie, J. K., LgQ in the eastern Tibetan Plateau, *Bull Seism Soc.*, 92 871-876, 2002.

Xie, J., and B. J. Mitchell, Attenuation of multiphase surface-waves in the Basin and Range Province. 1. Lg and Lg coda, *Geophys. J. Int.*, 102 121-137, 1990.

Yoshimoto, K., H. Sato, and M. Ohtake, Frequency-dependent attenuation of P-wave and S-wave in the Kanto area, Japan based on the coda-normalization method, *Geophys. J. Int.*, 114 165-174, 1993.

15. Geodetically Constraining Indian Plate motion and Implications for Plate Boundary Deformation

Edwin (Trey) Apel, Roland Bürgmann, and Paramesh Banerjee (Wadia Institute of Himalayan Geology)

15.1 Introduction

Traditionally tectonic Indian plate motion has been estimated using closed plate circuit models and summing motions across mid-ocean ridges. More recently *Paul et al.*, (2001), using limited GPS velocity vectors, calculated a pole of rotation that suggested motion slower than that of the rates suggested by sea-floor spreading. *Socquet et al.*, (2006) estimate an India-Eurasia geodetic pole with rates ~ 5 mm/yr slower than *Paul et al.*, (2001). We present new data spanning a larger and more significant portion of the "stable" Indian plate than previous studies. Our preliminary India-Eurasian pole estimates are consistent with *Socquet et al.*, (2006).

In addition to the above mentioned sites, we also include published data from numerous sources. However, many of the sites in this region are on or near plate boundaries (eg. along the Himalayan front or above the Sumatra subduction zone) making it difficult to use them for plate pole parameter determination. We use a block modeling approach to incorporate both rigid block rotation and near-boundary elastic strain accumulation effects in a formal inversion of the GPS velocities. Considered models include scenarios with and without independent microplates and a number of different plate boundary locations and locking depths.

15.2 GPS Velocities

The GPS velocities used in our inversion come from a solution of 164 global stations, including some unpublished campaign style sites from central and north-western India. These data were processed using GAMIT/GLOBK and processed by Paramesh Banerjee from the Wadia Institute of Himalayan Geology. Processing details can be found in (*Banerjee and Bürgmann*, 2002).

In addition to our own analysis, we integrate GPS-station velocities from published work along the Himalayans, throughout China, and southeast Asia (*Bettinelli et al.*, 2006; *Bock et al.*, 2003; *Calais et al.*, 2003; *Shen et al.*, 2005; *Socquet et al.*, 2006; *Zhang et al.*, 2004). We integrated these velocities into the reference frame of our own solutions by estimating translation and/or rotation parameters that minimized the differences in horizontal velocities for common sites. Our combined solution contains ~ 1800 global velocities.

15.3 Plates

We define our plates as rigid blocks on a spherical earth bounded by dislocations in an elastic halfspace and invert for poles and rates of rotation that minimize the misfit to the GPS velocities using an extension of the block modeling code by *Meade and Hager* (2005). The segments that bound the blocks represent uniformly slipping elastic dislocations locked to some specified depth. Because our inversion combines rigid block rotation with elastic strain accumulation effects, the parameterization of the block boundary geometry is critical. Geometry of the block boundaries is based heavily on seismicity and adopted from prior analyses (eg. *Socquet et al.*, 2006, *Reilinger et al.*, 2006, *Meade*, IN PRESS) or adjusted as indicated by the geodetic data.

We invert the horizontal GPS velocities for poles of rotation constrained by the prescribed block geometry defined above. Systematic patterns in the residual velocities (observed minus predicted) are used as an indicator of where and how the model matches the observed surface velocities. Misfit statistics are used to formally evaluate the statistical significance of the plate kinematic scenarios we test.

15.4 Results and Discussion

Our preliminary results constrain a pole of rotation for India with respect to Eurasia to lie at $29.04^\circ \pm 0.7^\circ$ N $16.74^\circ \pm 1.6^\circ$ E with a counterclockwise angular velocity of $0.42^\circ \pm 0.01^\circ$ Myr $^{-1}$. This pole confirms that the NUVEL-1A rate is 20% too fast and the India-Eurasia convergence rates computed along the Himalaya front range from 34 mm/yr to 45 mm/yr between 72° N and 96° N longitude. Residual velocities from our inversion are shown in figure 3.29 and show near zero motion within uncertainties. The geographic distribution of stations within the Indian plate allows us to generate the most robust realization of Indian plate motion to date.

15.5 References

- Banerjee, P., and R. Bürgmann, Convergence across the northwest Himalaya from GPS measurements, *Geophysical Research Letters*, 10.1029/2002GL015184, 2002.
- Bettinelli, P. J. Avouac, M. Flouzat, F. Jouanne, L. Bollinger, P. Willis, G. Chitrakar, Plate motion of India and interseismic strain in the Nepal Himalaya from GPS and DORIS measurements *Journal of Geodynamics*, 10.1007/s00190-006-0030-3, 2006.

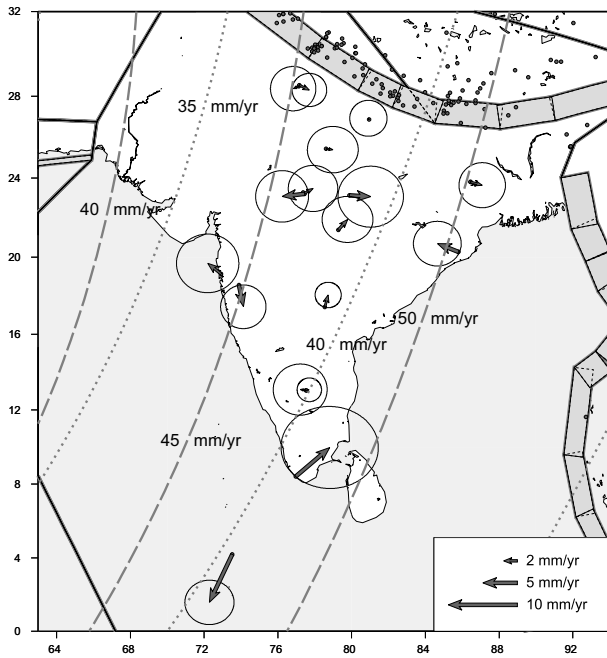


Figure 3.29: Residual velocities on the Indian plate from our robust inversion. Dashed lines show small circle pole traces from the NUVEL-1A IND-EUR pole of rotation, dotted lines are pole traces from this study. Circles show locations of GPS sites along the Himalayan range front however, velocity vectors at these locations have not been shown for the sake of brevity.

Bock, Y., L. Prawirodirdjo, J. F. Genrich, C. W. Stevens, R. McCaffrey, C. Subarya, S. S. O. Puntodewo, and E. Calais, Crustal motion in Indonesia from Global Positioning System measurements, *Journal of Geophysical Research*, 10.1029/2001JB000324, 2003.

Calais, E., M. Vergnolle, V. San'kov, A. Likhnev, A. Miroshnitchenko, S. Amarjargal, and J. Deverchere, GPS measurements of crustal deformation in the Baikal-Mongolia area (1994-2002): Implications for current kinematics of Asia, *Journal of Geophysical Research*, 108(B10), 2003.

Meade, Brendan, Mechanics of the India-Asia Collision Zone, *Geophysical Research Letters*, IN PRESS.

Meade, B. J., and B. H. Hager, Block models of crustal motion in southern California constrained by GPS measurements, *Journal of Geophysical Research*, 110, B03403, 10.1029/2004JB003209, 2005.

Paul, J., Bürgmann, R., Gaur, V. K., Bilham, R. Larson, K. M., Ananda, M. B., Jade, S., Mukal, M., Anupama, T. S., Satyal, G., Kumar, D., The motion and active deformation of India, *Geophysical Research Letters* 28(4), 2001.

Shen, Z.-K., J. Lü, M. Wang, and R. Bürgmann, Contemporary crustal deformation around the southeast borderland of the Tibetan Plateau, *Journal of Geophysical Research*, 10.1029/2004JB003421, 2005.

Socquet, A., Vigny, C., Chamot-Rooke, N., Simons, W., Rangin, C. and Ambrosius, B., India and Sunda plates motion and deformation along their boundary in Myanmar determined by GPS, *Journal of Geophysical Research*, 111, B05406, 10.1029/2005JB003877, 2006.

Zhang, P. Z., Z. Shen, M. Wang, W. J. Gan, R. Bürgmann, and P. Molnar, Continuous deformation of the Tibetan plateau from global positioning system data, *Geology*, 32(9), p. 809, 2004.

16. Large Scale Ground Deformation of Etna Observed by GPS Between 1994 and 2001

Nicolas Houlié, Pierre Briole, Alessandro Bonforte and Giuseppe Puglisi

16.1 Introduction

Etna is the most active volcano in Europe. Several active tectonic structures are located in its eastern part. Some of these structures, such as the Timpe fault system (extensive fault system trending NNW-SSE belonging to the Maltese escarpment) and the NNE-SSW faults (belonging to the Messina-Comiso line) were inherited from its geodynamic setting (Monaco *et al.*, (1997), Laigle, 1998, Nicolich *et al.*, 2000, Jacques *et al.*, 2001). Others, such as the Valle del Bove (Calvari *et al.*, 1998), the Pernicana fault system (Azzaro *et al.*, 1998, 2001a, 2001b), and the rift zones (Tibaldi and Gropelli, 2002), are linked to Mt. Etna's activity.

The Etna volcano GPS network, conceived in the late eighties, improved and maintained by Istituto Nazionale di Geofisica e Vulcanologia (INGV) research team, is composed of two main parts. Firstly, a local reference frame, relatively far from Mt. Etna's influence and assumed stable. Secondly, a monitoring network on the volcano dedicated to the study of the volcano dynamics (Puglisi *et al.*, 2004). Thus, this network is able to detect both volcanic and tectonic deformations of the area.

The last three flank eruptions of Mt. Etna occurred in 1991-1993, in July 2001 and november 2002 (Branca *et al.*, 2004). The time interval of our study was chosen to investigate the deep magma plumbing system of Etna (Patane *et al.*, 2000) while the GPS network remained stable (Puglisi *et al.*, 2004).

16.2 Data and data processing

Between 1994 and early 2001, thirty GPS campaigns were carried out by the INGV research group at twenty-three different benchmarks. All INGV receivers were Trimble 4000 SST/SSI. The various campaigns used in this study were designed for various aims (i.e. monitoring surveys, specific experiment in support to kinematic surveys or photogrammetry). Therefore, they were not homogenous in terms of duration of observations, sampling rates, number of measured benchmarks, number of instruments involved. Typically measurement sessions last two to four hours at 10, 20, or 30 seconds sampling rate. Station 98, located on the roof of the INGV building in Catania, records continuously during the campaigns.

To tie the local network to the European Reference Frame (EUREF), we have processed the available data from permanent sites located in southern Europe with our local dataset using GAMIT software (King and Bock, 1999). All the ambiguities have been fixed for baselines

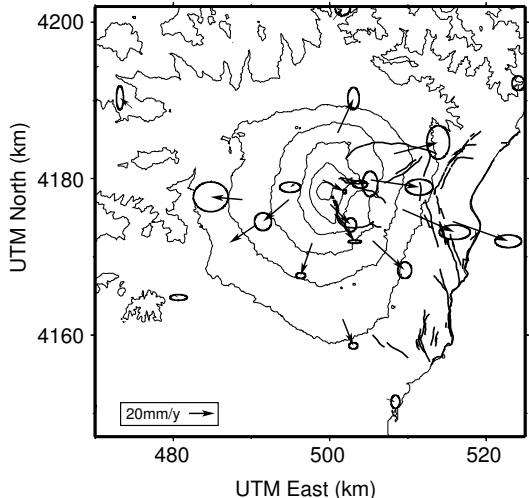


Figure 3.30: Velocities computed from time-series (reference NOTO). The location of the source is symbolized by a black star.

shorter than 500km only. Adjusting the computed baselines for each campaign using the GLOBK software (Herring, 2005), we established a set of coordinates for each campaign for the points measured on Etna as well as for the International GPS Service (IGS) stations.

The velocities are radially distributed (Figure 1) and seem to be organized as the result of a punctual source in a overpressure state located beneath Mt. Etna. As the state of this deep source was already discussed by Patane *et al.*, (2000), we have chosen to model the velocity field associated to the over-pressure of a Mogi point source (Mogi, 1958).

The best-fit solution of the Mogi point is located near the summit of the volcano (East 499.0 km, North 4180.5 km UTM33) located $9.5 \pm 1\text{km}$ beneath the summit assuming a vertical maximal velocity of $80 \pm 5\text{mm/y}$ (Figure 2). The depth of this source is in agreement with the results of several studies carried out by modeling ground deformation data (both GPS and INSAR) (Bonaccorso *et al.*, 1996, Lanari *et al.*, 1998, Puglisi *et al.*, 2001, Bonforte *et al.*, 2003, Lundgren *et al.*, 2003, Lundgren *et al.*, 2004). The vertical accuracy of the GPS velocities were not accurate enough to test the impact of the topography of the volcano on our modelling. However, the numerical simulations of the impact of the topography on the deformation field allow us to estimate that the computed vertical maximal inflation were overestimated of 30 per-

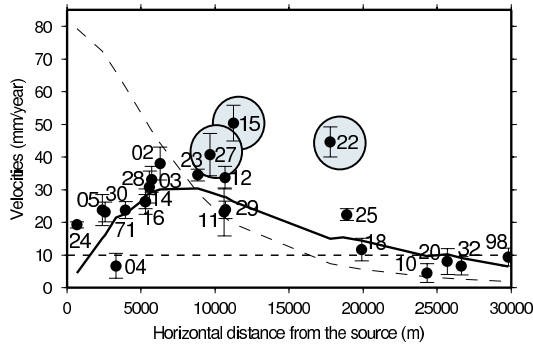


Figure 3.31: Data (black filled circles) and best model (black lines) plotted versus the horizontal distance from the source (Mogi, 1958). The computed horizontal displacements are symbolized by a continuous black line while the vertical one by a dashed one. Three sites dynamics don't fit with the modeled displacements (15, 22 and 27). Those are highlighted by grey filled black circles.

cent near the summit (24mm/yr).

The point source model explains the observations except in the eastern part of the volcano (Sites 15 and 22) and along the Pernicana fault system (Site 27, Figure 3.31). The fact that the model doesn't fit exactly in the eastern part of the network along the Ionian coast is in agreement with the eastward movement of the eastern part of the volcano toward the sea (Rasa et al., 1996, Froger et al., 2001, Puglisi et al., 2003). The magnitude of the site 15's velocity (11mm/y to the East) supports the hypothesis of the existence of a large slough located along the Ionian coast limited by the Pernicana fault to the north, Ionian coast to the East and Timpe fault system to the West. The volume of this slough was estimated from 5 to 50km^3 (Houlié, 2005) while the mechanism driving the dynamic of these units is not clearly identified yet.

16.3 References

Azzaro, R., S. Branca, S. Giammanco, S. Gurrieri, R. Rasà, and M. Valenza (1998), New evidence for the form and extent of the Pernicana fault system (Mt. Etna) from structural and soil-gas surveying, *J. Volcanol. Geotherm. Res.*, *84*, 143–152.

Azzaro, R., S. Barbano, M., R. Rigano, and S. Vinciguerra (2001a), Time seismicity patterns affecting local and regional fault systems in the Etna region; preliminary results for the period 1874–1913, *Journal of the Geological Society of London*, *158*, 561–572.

Azzaro, R., M. Mattia, and G. Puglisi (2001b), Fault creep and kinematics of the eastern segment of the Pernicana fault (Mt. Etna, Italy) derived from geodetic observations and their tectonic significance, *Tectonophysics*, *333*(3–4), 401–415.

Branca, S., and P. Del Carlo (2004), Eruptions of Mt.

Etna During the Past 3,200 Years: A Revised Compilation Integrating the Historical and Stratigraphic Records, in *Mt. Etna: Volcano observatory, Geophysical Monograph Series 143*, pp. 1–27.

Calvari, S., L. H. Tanner, and G. Groppelli (1998), Debris-avalanche deposits of the milo lahar sequence and the opening of the Valle del Bove on Etna volcano (Italy), *J. Volcanol. Geotherm. Res.*, *87*, 193–209.

Jacques, E., C. Monaco, P. Tapponnier, L. Tortorici, and T. Winter (2001), Faulting and earthquake triggering during the 1783 Calabria seismic sequence, *Geophys. J. Int.*, *147*, 499–516.

Herring, T. (2005), *GLOBK: Global Kalman Filter VLBI and GPS Analysis Program, version 10.2*.

Houlié, N. (2005), Mesure et Modélisation de données GPS de volcans. Applications à des études de déformation à diverses échelles et à la tomographie des panaches atmosphériques., Ph.D. thesis, Institut de Physique du Globe de Paris.

King, R., and Y. Bock (1999), *Documentation of the GAMIT software*, MIT/SIO.

Laigle, M., A. Hirn, M. Sapin, J. Lepine, J. Diaz, J. Gallart, and R. Nicolich (2000), Mount etna dense array local earthquake p and s tomography and implications for volcanic plumbing, *J. Geophys. Res.*, *105*, 21.

Mogi, K. (1958), Relations between the eruption of various volcanoes and the deformations of the ground surfaces around them, *Bull. of the Earthquake Research Institute*, *36*, 99–134.

Monaco, C., P. Tapponnier, L. Tortorici, and P. Y. Gillot (1997), Late quaternary slip rates on the acireale-piedimonte normal faults and tectonic origin of mt. etna (sicily), *Earth & Planet. Sc. Lett.*, *147*, 125–139.

Nicolich, R., M. Laigle, A. Hirn, L. Cernobori, and J. Gallart (2000), Crustal structure of the ionian margin of sicily; etna volcano in the frame of regional evolution, *Tectonophysics*, *329*, 121–139.

Patane, D., P. De Gori, C. Chiarabba, and A. Bonaccorso (2003), Magma ascent and the pressurization of mount etna's volcanic system, *Science*, *299*, 2061–2063.

Puglisi, G., P. Briole, M. Coltelli, A. Ferretti, C. Prati, and R. Rocca (2003), ERS SAR PS analysis provides new insights on the long-term evolution of Mt. Etna volcano, *Fringes 2003 proceedings*.

Puglisi, G., P. Briole, and B. A. (2004), Twelve Years of Ground Deformation Studies on Mt. Etna Volcano Based on GPS Surveys, in *Mt. Etna: Volcano observatory, Geophysical Monograph Series 143*.

Tibaldi, A., and G. Groppelli (2002), Volcano-tectonic activity along structures of the unstable NE flank of Mt. Etna (italy) and their possible origin, *J. Volcanol. Geotherm. Res.*, *115*, 277–302.

17. Parkfield-Hollister Electromagnetic Monitoring Array

Karl Kappler, H. Frank Morrison, Gary D. Egbert

17.1 Introduction

The primary objective of the UC Berkeley electromagnetic (EM) monitoring array is to identify EM fields or changes in ground conductivity that might be associated with earthquakes. The array has consisted of up to three sites operating since 1995 at SAO, PKD, and PKD1, each of which measures three orthogonal components of the magnetic field and two orthogonal components of the electric field. Multiple sites are necessary in order to separate the fields of a local source (e.g., an earthquake signal, cultural noise) from the natural regional micropulsations [Gamble 1979]. Our approach has been to determine the transfer function between fields at different sites for periods of normal background EM variations and then use this transfer function to predict fields between sites. Differences between the observed and predicted fields are used to search for anomalous local fields.

17.2 MT Overview

In 1995 we installed two well-characterized electric and magnetic field measuring systems at two sites along the San Andreas Fault which are part of the Berkeley Digital Seismic Network. Since then, magnetotelluric (MT) data have been continuously recorded at 40 Hz and 1 Hz and archived at the NCEDC (references to these data channels can be found in the 2003 BSL Annual Report). At least one set of orthogonal electric dipoles measures the vector horizontal electric field, E , and three orthogonal magnetic sensors measure the vector magnetic field, B . These reference sites, now referred to as electromagnetic (EM) observatories, are co-located with seismographic sites so that the field data share the same time base, data acquisition, telemetry and archiving system as the seismometer outputs.

The MT observatories are located at Parkfield (PKD1, PKD), 300 km south of the San Francisco Bay Area and Hollister (SAO), halfway between San Francisco and Parkfield (Figure 3.32). In 1995, initial sites were established at PKD1 and SAO, separated by a distance of 150 km, and equipped with three induction coils and two 100 m electric dipoles. PKD1 was established as a temporary seismic site, and when a permanent site (PKD) was found, a third MT observatory was installed in 1999 with three induction coils, two 100 m electric dipoles, and two 200 m electric dipoles. PKD and PKD1 ran in parallel for one month in 1999, and then the MT observatory at PKD1 was closed.

Data at the MT sites are fed to Quanterra data loggers, shared with the collocated BDSN stations, synchronized

in time by GPS, and sent to the BSL via dedicated communication links.

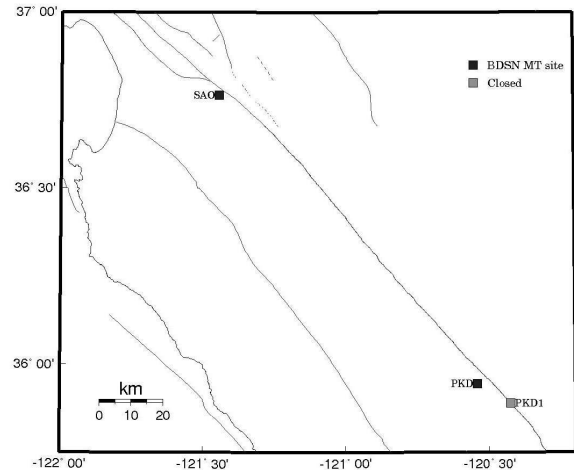


Figure 3.32: Map illustrating the location of operational (filled squares) and closed (grey squares) MT sites in central California.

17.3 2005-2006 Activities

Over the past year, limited maintenance has been performed at Parkfield. Resources have been invested in generating a report regarding array observations near the time of the Sept. 28, 2004 Parkfield Earthquake.

17.4 Data Processing

We have applied a variety of signal processing techniques to the 1sps array data. The 'raw' data stored on the NCEDC is windowed, Fourier transformed, and then band averaged, such that the time series of each data channel is represented by 25 shorter timeseries of band averaged Fourier coefficients (FCs). Details of the transform and band averaging can be found in *Eisel and Egbert (2001)*. The majority of the signal processing applied to date is done using these FC files as the input time series, although some time-domain Weiner Filtering has been applied to the data around the time of the earthquake. An example of the time domain processing is given in the PKD-SAO EM Monitoring Array chapter of the 2003 BSL Annual Report.

The FC time series are first examined in terms of Signal to Noise Ratio (SNR). Robust estimates of SNR

have been calculated daily over the four-year time window [2002-2005] for all 12 channels of data acquisition. The method of outlier downweighting used is called the RMEV estimation process (Robust multivariate errors-in-variables) and is referenced in *Eisel and Egbert (2001)*. These plots show that the electric field SNRs at both sites correlate positively with global geomagnetic activity indices (K_p and A_p), and the Parkfield electric field SNRs correlate negatively with rainfall events.

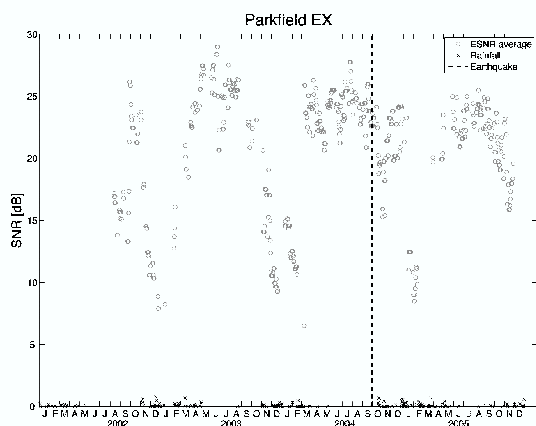


Figure 3.33: The only excessive spikes in the electric field SNR correlate with anomalously high geomagnetic indices. Note the trend towards poor SNR during the rainy season.

The second step of the analysis is the calculation of robust estimates of apparent resistivity curves for Parkfield. These plots showed slight seasonal variation of apparent resistivity on the order of a few percent that also seem to correlate with rainfall. A distortion analysis applied to these curves [*Smith 1995*], where the MT impedance tensor $Z(\omega, t)$ is decomposed into a frequency-dependent and a time-dependent part, shows that the seasonal variation is almost entirely accounted for by a frequency independent distortion tensor, and hence is a near-surface effect. This suggests that if any regional variation in apparent resistivity occurred coincident with the earthquake, that it is small enough to be masked by the seasonal effect. Robust RMEV techniques were applied in this analysis, and are similarly documented in *Eisel and Egbert (2001)*.

The other two lenses through which we have carefully examined the 1Hz data are the use of Principal Components Analysis (PCA) and canonical coherence analysis (CCA), both of which are derived from the data covariance matrices. These techniques rely on rotating the coordinates of the data-space into directions of dominant characteristics. A discussion on the implications of PCA as applied to magnetotelluric data can be found in *Egbert (1989)*. A discussion of the significance of CCA as

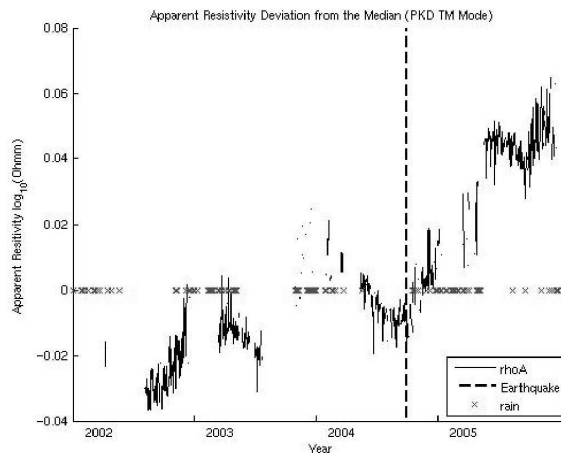


Figure 3.34: Note the offsets in the apparent resistivity which are coincident with times of site maintenance and instrument changes. These offsets are likely responsible for the linear upward trend. A seasonal trend is apparent.

applied to ULF EM data is included in *Kappler et. al. (2006)*.

17.5 Implications and Future Work

The 1Hz data do show several interesting characteristics, such as the seasonal dependence of apparent resistivity and the rainfall correlation. In particular an examination of the apparent resistivity residual TS with the distortion effects removed has not been plotted to date. Also the 3rd and 4th principal components, as well as canonical coherences, are of interest in understanding sources of signal contamination, as these monitor the non-regional signals that the array is detecting. An examination of the 40Hz data in a short time-window around the earthquake (2 months on either side) remains to be done in order to see if any anomalous EM signals were occurring at higher frequencies. A statistical analysis of the time-domain residuals has been started for the 1Hz data, and will need to be summarized, and also performed with the 40Hz data. Though several interesting signals have been detected and isolated from the data, we have not detected any clear evidence for anomalous EM activity preceding earthquakes. Significant EM fields are detected coseismically (during ground shaking) and modeling of these fields has begun as a project for the 2006 SEG annual meeting.

17.6 Acknowledgments

Frank Morrison directs the MT program and collaborates closely with Gary Egbert of Oregon State University. Rich Clymer and Karl Kappler also contribute to the operation of the MT observatories.

17.7 References

Egbert, G.D., Booker, J.R., (1989), Multivariate Analysis of Geomagnetic Array Data 1. The Response Space, *Journal of Geophys. Res.* V94 No.B10 pp14227-14247

Egbert G. D. (1997), Robust multiple-station magnetotelluric data processing, *Geophys. J. Int.* v130 pp475-496

Eisel M., Egbert G.D., (2001), On the stability of magnetotelluric transfer function estimates and the reliability of their variances, *Geophys. J. Int.* v144, pp65-82

Gamble T.D., Goubau W.M., Clarke J. (1979), Magnetotellurics with a remote reference, *Geophysics*, v44, pp53-68

Kappler, K. Egbert, G.D., Morrison, H.F., Long-Term Analysis of ULF electromagnetic fields at Parkfield CA, *in progress*

Smith, J. T., (1995), Understanding Telluric Distortion Matrices, *Geophysical journal International*, v122, 219-226

18. Observation and Analysis of Vertical Electric Fields in the Earth

Karl Kappler, H. Frank Morrison

18.1 Summary

We have been measuring and recording natural horizontal electric and magnetic fields at two sites on the San Andreas Fault near Parkfield and Hollister, California for the past ten years. The objective of the monitoring program was to determine objectively whether anomalies in either of these fields, or in the impedance of the ground, were observed in association with earthquakes on the San Andreas Fault. As part of a more general plan to study the behavior of the natural ULF and ELF fields, we installed a pair of electrodes in a vertical borehole used to deploy a deep three-component seismometer. The vertical dipole was connected to a spare channel of the seismic acquisition system and recorded along with the regular horizontal E and H data in the period from 01 July 2004 to 01 November 2005. The vertical field data displayed a long-term drift over the first few months of operation and a strong diurnal component as well as small variations (micropulsations) typically seen in the horizontal electric fields. We also discovered four striking variations of a few days duration in the recording. These anomalous fields stand out dramatically above the normal micropulsation signals. These signals are significant because: a) There is no counterpart variation in the horizontal electric fields at a station only 1.6 km away; b) No signals like this have been seen on the horizontal electrodes at any time; c) There were no rainfall events immediately prior to any of these anomalous variations; d) No particular pumping or hydrofracture experiments were conducted on the nearby SAFOD deep drilling site at these times. We propose to connect two more vertical dipoles to the network and to acquire two years of observations of this newly discovered phenomena. The horizontal field arrays will be maintained to provide the complimentary data to the three vertical dipoles. In addition we have access to the data from five volumetric strainmeters, at least two tiltmeters, and a long period seismograph all in the vicinity of the vertical electric dipole holes. The objective of the proposal is to study the relationship between vertical electric fields and the other geophysical data to try and determine the cause of the vertical field anomalies. Additionally, through a study of the ionospheric electron content provided by the GPS array, we will investigate whether there is a relationship between the vertical electric fields and ionospheric properties.

18.2 Existing Sites and Instrumentation

The borehole, which is equipped a vertical electric dipole, is labeled as CCRB in Figure 3.35. The site

is between the SAFOD borehole and the PKD electromagnetic observatory. Apart from the orientation of the dipole, the instrumentation and data logging are identical to that described in the Parkfield-Hollister Monitoring Array chapter of this issue.

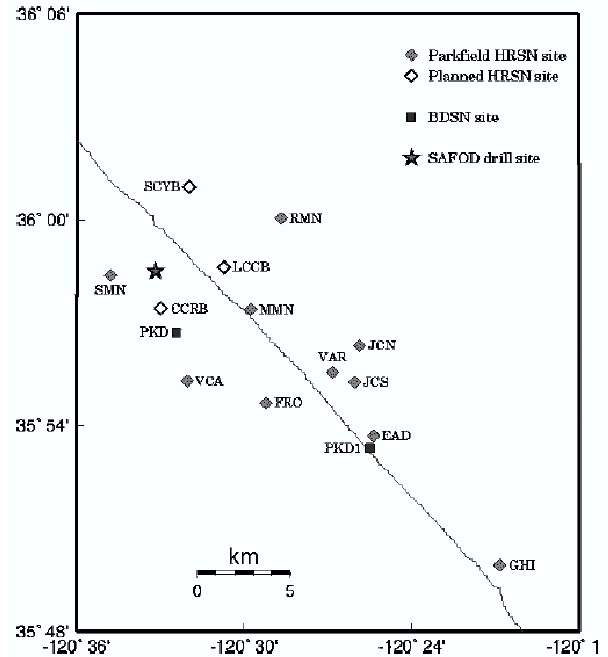


Figure 3.35: Location of borehole network, also showing SAFOD borehole, and PKD ULF observatory, and various other sites with geophysical data acquisition equipment.

18.3 Vertical Electric Dipole Data

The long term timeseries of the vertical electric dipole data is displayed in Figure 3.36. For brevity we include zoom-plots of only the first anomaly labeled as A.

The sharp offset depicted in Figure 3.37 looks suspiciously like an instrument step at this scale, but a closer inspection (Figure 3.38) shows that the onset of the step is in fact smooth.

The sharp corner also shows itself to be smooth in time when the 40Hz data are examined over short time intervals.

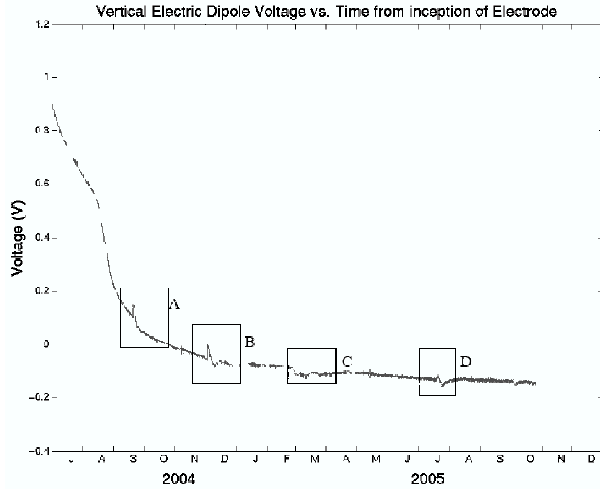


Figure 3.36: The vertical electric field data spanning 16 months of acquisition, mean subtracted. Boxes A-D indicate significant anomalies in the data stream.

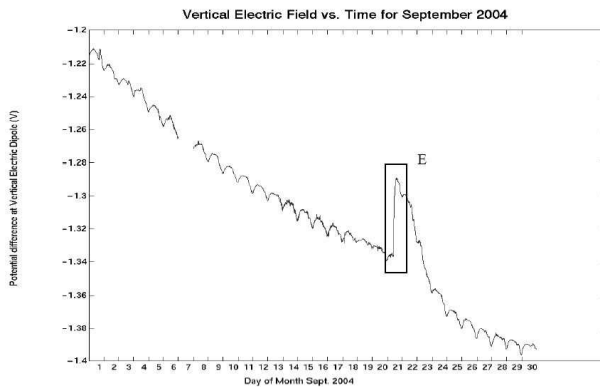


Figure 3.37: A closer look at the first spike in September 2004, shown above in box A.

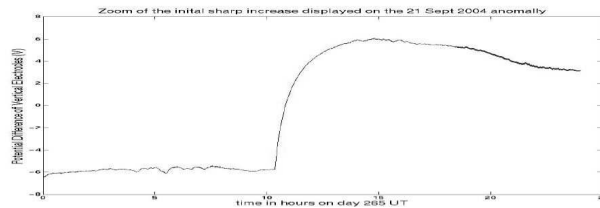


Figure 3.38: Shows the onset of the 21 September 2004 anomaly. The rise-time appears to be on the order of several hours. Once corrected for instrument response the rise is about 10mV.

18.4 Preliminary Analysis

We have found only two previous studies on measurements of vertical electric fields in the ground, at depths below the near-surface soil/unconsolidated materials. *Colangelo et. al.* (2005) report on data from a shallow pair of electrodes. The data is noisy as would be expected when at least one electrode is in a near surface layer where surface moisture and chemistry is highly variable, temperature effects are strong and local streaming potentials are prevalent. *Corwin* (1990) presents a good review of the factors that can cause time variations of tens of millivolts in shallow electrode systems. None of these factors seem relevant for electrodes buried below the water table at depths of 100 or 200 meters. *Antonopoulos et. al.* (1993) report vertical electric fields from two adjacent drill holes on an island in Greece. The electrodes at depth were at 200m, but the upper electrodes were at the surface and, as noted above, subject to variations due to the near surface layer. Nonetheless, both vertical electrodes showed high coherence to a horizontal dipole many miles away, basically showing the same relationship between horizontal and vertical fields that we discussed above for our data. In addition, they claim that anomalous vertical fields were seen, related to distant horizontal fields of similar waveform, that were not related in the same manner as the magnetotelluric fields. These anomalous fields were of 15-20 minute duration and were claimed to be related to distant earthquakes. No anomalies of the type we report were described in their paper.

The anomalous variations seen in Figure 3.36 are well above the background micropulsation variations and are readily identified by eye. It is entirely possible that there are smaller variations down to the level of the micropulsations that are not coherent with the horizontal fields and are indicative of this new vertical field phenomenon. We have developed analysis techniques for the horizontal array studies that can identify such phenomena. In general, *Egbert* (1989) and *Booker and Egbert* (1989), have shown that all the components of electric and magnetic field measured on the surface of the ground that are caused by widespread sources in the ionosphere/magnetosphere are related by simple tensor forms. For example orthogonal electric fields at site A are related to orthogonal electric fields at site B by a simple 2x2 tensor. Over time this transfer function can be determined accurately. It is a function only of the conductivity distribution in the ground and has been found to be generally time invariant. Following similar reasoning the relationship between the vertical field and the orthogonal horizontal fields is described simply by a spectral transfer function of the form:

$$E_z = T_{xz}E_x + T_{yz}E_y \quad (3.1)$$

where E_i represents the i th component of electric field,

and T is a simple 1×2 tensor. The multiple coherence between E_z and the horizontal components provides a measure of the noise in the measurement of the E s. An estimation of this transfer function can be made during a time of good data quality and then used to predict the fields at one site from those at another. The difference between the measured and predicted fields, which we labeled as a residual, becomes a measure of the fields at one site that are not components of the micropulsation source. Of course there is always a residual, which is the noise level of the measurements. So anomalous fields can be assigned a quantitative signal to noise level. *Egbert* (2000, 1997, and 1986) generalized this idea so as to use all the field components measured in two arrays to predict the fields in any one component of either array. This was the basic approach used with the ULF array in an attempt to isolate anomalous electric or magnetic fields that might have been generated by some earthquake related process local to one of the sites. This concept can also be applied in the time domain to yield estimates of electric field as a function of time. In this project we propose to calculate the time domain residuals in the vertical fields using the horizontal components of E and H at site PKD for the reference site. In this way other anomalies of a much smaller scale than the large ones highlighted in Figure 3.36 can be quickly identified.

18.5 Theory

The cause of these vertical field variations is not known. By measuring something that no one seems to have measured before, we may have discovered an interesting process within the earth or a heretofore unexpected coupling between the earth and the ionosphere. At the very low frequencies considered here, conventional wisdom suggests that there are no vertical electric fields at or within a conductor below free space that has an electric charge or field distribution. Within an inhomogeneous half space, there may, of course, be vertical components of the electromagnetically induced telluric currents which, in fact, we do observe.

The simplest explanation is that the observed vertical fields arise from the charge separation that occurs from the streaming potential phenomenon accompanying the development of a vertical pressure gradient. There are two possible sources for such a vertical pressure gradient: a) atmospheric loading leading to the diffusion of a pressure front into the earth or b) a reduction of pressure within the earth due to a dilatational strain. We briefly analyzed the first of these possibilities by plotting the atmospheric pressure variations at station VCA (Figure 3.35), 4.5 km from CCRB in Figure 3.39. In general the vertical field does not track the pressure variations.

Pride (2004) has recently shown that fluid sources or sinks within the ground will only produce vertical electric fields near the surface, not horizontal fields. Local

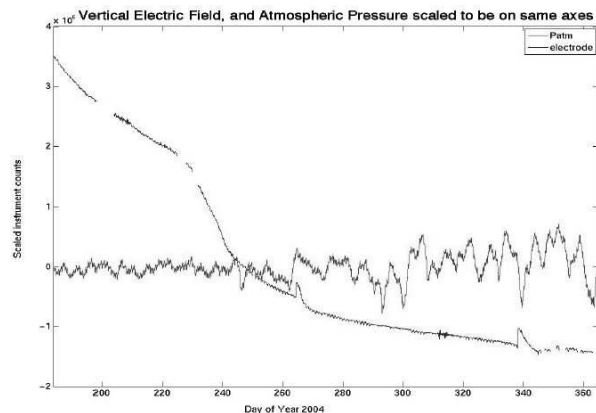


Figure 3.39: Variations of atmospheric pressure plotted together with variations in electric field. No clear correlation between the two signals stands out. The y-axis represents scaled instrument counts, and is only a qualitative measure.

fluid flow transients near the well bore could also cause streaming potentials, but the lack of any correlation with local rainfall and the long time scale of the variations argues against this explanation. *Pride* (2004) also argues that large-scale strain changes after an earthquake should produce long term variations in the streaming potentials with accompanying measurable vertical fields. A cursory examination of the vertical field data after the Parkfield ($M= 6.0$) earthquake on 28 September 2004 (day 272 UT), shows no such trends. A dilatancy strain could certainly produce vertical pressure gradients with associated vertical streaming potentials. We would expect to see some evidence of this in local measurements of strain. We examined the uncorrected strain data from VCA and found, as expected, that the strain tracks the atmospheric pressure changes and the local tidal strain. No anomalous strain associated with the electric field anomalies could be seen in the raw data. We propose to examine the corrected strain data from these sites at the times of the vertical field anomalies. After correction for tidal and atmospheric loading, the noise level for these strainmeters is approximately 0.1 nanostrain [*Malcolm Johnston*, USGS, personal communication, 2006]. These data and the vertical field and ULF array data are directly available from the NCEDC. Another intriguing possibility is that there is some electrical coupling among very low frequency gravity waves, ionospheric properties, local strain and the vertical electric field. *Calais and Minster* (1995) report on the detection of ionospheric perturbations caused by atmospheric-ionospheric-acoustic-gravity waves that were generated by the ground displacement of the 1994 Northridge earthquake. The ionospheric anomalies were found from an analysis of the phase delays on

the two GPS frequencies, which are, in turn, proportional to the electron content of the ionosphere. More subtle transient ground displacements, on the order of 3-5 days, might consequently generate GPS phase delays corresponding to the vertical electric field. As mentioned above it is unlikely that ionospheric fluctuations of such a timescale, essentially electrostatic, could themselves cause the observed fields within the conductive earth.

18.6 Future Analysis

We have submitted an NSF proposal to monitor the vertical electric fields at three sites (LCCB, SCYB, CCRB). We intend to calculate the time domain residuals in the vertical fields using the horizontal components of E and H at site PKD (Figure 3.35) for the reference site. In this way other anomalies of a much smaller scale than the large ones highlighted in Figure 3.38 can be quickly identified. Other geophysical measurements that are available to correlate with the anomalous vertical fields basically break into ground and ionospheric. On the ground we have access to the following measurements in the vicinity of the PKD site:

1) The broadband seismometer co-located with the ULF monitoring sensors at PKD. 2) Tiltmeters located at VAR and GHI on Figure 3.35.

3) Volumetric strainmeters located at FRO and VCA on Figure 3.35., and also at three other sites (DLT, JCN, RHL, not shown) within 40 km.

4) Long period magnetic field observations from Fresno Magnetic observatory

18.7 References

Antonopoulos, G., Kopanas, K., Eftaxias, K., Hadjicostas, V., 1993, On the experimental evidence for SES vertical component, *Tectonophysics*, v224, 47-49

Boyd, O.S., Egbert, G.D., Eisel, M., Morrison, H.F., 1997, A preliminary analysis of EM field monitoring network. *EOS Trans.* 78 AGU, p459

Calais, E., Minster, J.B., 1995, GPS detection of ionospheric perturbations following the January 17, 1994, Northridge earthquake, *Geophysical Research Letters*, v22, no. 9, 1045-1048

Calais, E., Haase, J.S., 2003, Detection of ionospheric perturbations using a dense GPS array in Southern California, *Geophysical Research Letters*

Colangelo, G., Lapenna, V., Telesca, L., 2005, Vertical dipoles to detect self potential signals in a seismic area of southern Italy: Tito station, *Natural Hazards and Earth System Sciences*, v5, 667-671

Corwin, R.F. 1990, The self Potential method for environmental and engineering applications, *Geotechnical and Environmental Geophysics*, v1 SEG Tulsa, OK

Eisel, M., Egbert, G.D., 2001, On the stability of magnetotelluric transfer function estimates and the reliabil-

ity of their variances, *Geophysical Journal International*, v144, 65-82

Egbert, G.D., Booker, J.R., 1986, Robust estimation of geomagnetic transfer functions, *Geophysical Journal of the Royal Astronomical Society*, v87, 173-194

Egbert, G.D., Booker, J.R., Schultz, A., 1992, Very Long Period Magnetotellurics at Tucson Observatory: Estimation of Impedances, *Journal of Geophysical Research*, v97, no. B11, 15113-15128

Egbert, G.D., Booker, J.R., 1989, Multivariate Analysis of Geomagnetic Array Data 1. The Response Space, *Journal of Geophysical Research*, v94, no. B10, 14227-14247

Egbert, G.D., 1989, Multivariate Analysis of Geomagnetic Array Data 2. Random Source Models, *Journal of Geophysical Research*, v94, no. B10, 14249-14265

Egbert, G.D., 1997, Robust multiple-station magnetotelluric data processing: *Geophysical Journal International*, v130, 475-496

Egbert, G.D., Eisel, M., Boyd, O.S., and Morrison, H.F., 2000, DC trains and Pc3s: Source effects in mid-latitude geomagnetic transfer functions, *Geophysical Research Letters*, v27, no. 1, 25-28

Kappler, K.N., Egbert, G.D., Morrison, H.F., 2005, Long Term Monitoring of EM Signals Near Parkfield CA, AGU paper Fall Meeting 2005

Kappler, K.N., Egbert, G.D., Morrison, H.F., 2006, Results of long term EM monitoring at Parkfield CA, (in progress)

Morrison, H.F., 2004, Anomalous em signals and changes in electrical resistivity at parkfield: collaborative research between the universities of California at Berkeley and Riverside and Oregon State University, Final Technical Report to USGS, 01HQGR0060

Morrison, H. F., Fernandez, R., 1986, Temporal Variations in the electrical resistivity of the Earth's Crust, *Journal of Geophysical Research*, v91, no. B11, pp. 11618-11629.

Nichols, E.A., Morrison, H. F., Clarke, J., 1988, Signals and noise in measurement of low-frequency geomagnetic fields: *J.G.R.*, v93, no. B11, pp. 13,743-13,754.

Pride, S.R., 1994, Governing equations for the coupled electromagnetics and acoustics of porous media, *Physical Review B*, v50, no. 21

Pride, S.R., Moreau, F., Gavrilenko, P, 2004, Mechanical and electrical response to fluid pressure equilibration following an earthquake, *Journal of Geophysical Research*, v109, B03302

19. Surface Deformation and Fault Kinematics of the San Francisco Bay Area from PS-InSAR Analysis

Gareth Funning and Roland Bürgmann

19.1 Introduction

The aim of this project is to use high-precision geodetic data to characterize, and subsequently model, the surface deformation field of the San Francisco Bay Area. In so doing we hope to recover information about the fault kinematics of the region, the distribution of creeping and locked areas on the Hayward fault, and also about the sources of nontectonic deformation (such as landsliding, subsidence and aquifer recharge) around the Bay, and thus improve our knowledge of the whereabouts and mechanisms of the principal natural hazards in the region. This study builds upon previous work by members of the Active Tectonics group at the Berkeley Seismological Laboratory (*Schmidt and Bürgmann, 2003, 2005; Hilley et al., 2004; Ferretti et al., 2004; d'Alessio et al., 2005; Bürgmann et al., 2006*).

19.2 PS-InSAR

Permanent Scatterer Interferometric Synthetic Aperture Radar (PS-InSAR) is a sophisticated geodetic technique that can be used to construct spatially dense datasets detailing the rates of surface deformation over wide ($\sim 100 \times 100$ km) areas (*e.g. Ferretti et al., 2004*). The technique differs from conventional InSAR in that it uses information from features on the ground – typically buildings or other man-made structures, but also natural features such as rock outcrops – which can act as permanent reflectors of incident radar radiation. These can be identified even when surrounded by vegetation, allowing a substantial improvement in coverage in areas such as the East Bay Hills which are poorly suited to conventional InSAR. A further benefit of the PS-InSAR technique is the ability to mitigate noise sources using spatial and temporal filtering. By making certain assumptions – that surface deformation is correlated in time but not in space, and that atmospheric signals are correlated over small spatial wavelengths (< 20 km) but not in time – it is possible to decompose the radar signal into deformation and atmospheric components, and thus to eliminate the main source of uncertainty in the measurements.

The PS-InSAR data presented here were processed by our long-standing collaborators at Tele-Rilevamento Europa (TRE), Milan, Italy. One of us (GF) visited Milan in the past year to learn about PS-InSAR methods in detail and to supervise data processing. We are also exploring the possibility of using one of the few freely-available codes (*e.g. Hooper et al., 2004*) in order to have our own in-house processing capability in future.

19.3 Data

We analyse data from two sources – the European Space Agency ERS satellites (49 descending track radar image acquisitions from 1992-2000), and the Canadian Radarsat platform (31 ascending track images from 2001-2004). Both data sets are plotted in Figure 3.40. Each data set provides a dense coverage of surface velocity observations in the line-of-sight direction of the satellite. Given the different viewing geometries of the two data sets, if we assume that the rates of displacement do not vary with time, we can use the two independent measurements to infer the horizontal and vertical deformation rates across the region.

19.4 Creep on the Hayward fault

The Hayward fault is currently considered to pose the greatest threat of a $M \sim 7$ earthquake of the major faults of the San Francisco Bay Area (*Working Group on California Earthquake Probabilities, 2003*). The fault creeps at the surface – this can be seen in both PS-InSAR data sets as an abrupt change in velocity either side of a linear feature (Figure 3.40). Knowledge of the extent and magnitude of creep at depth is important for understanding the future seismic hazard posed by the structure; areas of very low (< 2 mm/yr) or zero creep can be considered locked, and therefore in potential danger of rupture in future.

We model the distribution of creep on the Hayward fault using elastic dislocation modeling (*Okada, 1985*), assuming a vertical fault geometry with a surface trace matching that of the mapped fault, subdivided into 2×2 km patches, and applying Laplacian smoothing. The regional strain gradient is described by placing further, deep, dislocations beneath each of the major faults in the region. The velocity on each fault is inverted for using least squares methods with a positivity constraint to prevent retrograde motion. In addition to the PS-InSAR data, appropriately sub-sampled, we also invert GPS data from 185 sites across the region (*d'Alessio et al., 2005*), and surface creep rates measured at 18 alignment arrays along the trace of the Hayward fault (*Lienkaemper et al., 2001*).

Our model of fault slip is plotted in Figure 3.41a. We find evidence for a patch of very low/zero creep which extends between ~ 20 and 58 km along-strike (measured southeast from Pt Pinole, where the fault trace goes offshore into San Pablo Bay), corresponding to the portion of the fault between south Oakland and Union City. The

overall pattern is similar to that obtained in other studies where characteristic repeating earthquake data are used to constrain creep behavior at depth (e.g. Schmidt et al., 2005). If we assume a long-term slip rate for the Hayward fault of 10 mm/yr, within the uncertainties of geologic estimates (e.g. Lienkaemper and Borchardt, 1996), this implies that this ‘locked’ portion of the fault is accumulating a moment deficit equivalent to a M_w 6.74 event per century. If loading rates have been constant since the last event on the Hayward fault in 1868, the total deficit is equivalent to a M_w 6.9 earthquake; this represents an upper bound of the size of any potential earthquake, as we do not know how much of the total moment deficit would be released aseismically as afterslip or accelerated creep following an earthquake.

This model generally fits the data well, with mean residuals of less than 1 mm/yr (Figure 3.41b). The most prominent residual features are uplift features seen in the Mt Diablo stepover and San Andreas fault restraining bend, which are consistent with the strike-slip fault geometries, but presumably occurring upon structures that we have not modeled in this study. We also see evidence in the Loma Prieta region of the San Andreas fault for continuing residual postseismic subsidence and contraction following the 1989 earthquake in this location. These findings are consistent with other attempts to identify vertical tectonic motions in the San Francisco Bay Area (e.g. Bürgmann et al., 2006).

19.5 Acknowledgements

We would like to thank our collaborators at TRE, especially Alessandro Ferretti, Fabrizio Novali and Chiara Giannico, for their continuing assistance with the PS-InSAR processing and with data acquisition/ordering issues. ERS data are copyrighted by the European Space Agency and supplied through the WInSAR consortium, and under project AOE 750. Radarsat data are copyrighted by the Canadian Space Agency and supplied under an agreement with the Alaska SAR Facility. This project is funded by grants from the National Science Foundation, and the National Earthquake Hazard Reduction Program.

19.6 References

Bürgmann, R., G. Hilley, A. Ferretti, and F. Novali, Resolving vertical tectonics in the San Francisco Bay area from GPS and Permanent Scatterer InSAR analysis, *Geology*, *34*, 221-224, 2006.

d’Alessio, M. A., I. A. Johanson, R. Bürgmann, D. A. Schmidt and M. H. Murray, Slicing up the San Francisco Bay Area: Block kinematics and fault slip rates from GPS-derived surface velocities, *J. Geophys. Res.*, *110*, B06403, doi:10.1029/2004JB003496, 2005.

Ferretti, A., C. Prati and F. Rocca, Permanent Scatterers in SAR Interferometry, *IEEE Trans. Geosci. Remote Sens.*, *39*, 8-20, 2001.

Ferretti, A., F. Novali, R. Bürgmann, G. Hilley and C. Prati, InSAR Permanent Scatterer Analysis Reveals Ups and Downs in San Francisco Bay Area, *EOS Trans. AGU*, *85*, 317, 2004.

Hilley, G. E., R. Bürgmann, A. Ferretti, F. Novali and F. Rocca, Dynamics of slow-moving landslides from permanent scatter analysis, *Science*, *304*, 1952-1955, 2004.

Lienkaemper, J. J. and G. Borchardt, Holocene slip rate on the Hayward fault at Union City, California, *J. Geophys. Res.*, *101*, 6099-6108, 1996.

Lienkaemper, J. J., J. S. Galehouse and R. W. Simpson, Long-term monitoring of creep rate along the Hayward fault and evidence for a lasting creep response to the 1989 Loma Prieta earthquake, *Geophys. Res. Lett.*, *28*, 2265-2268, 2001.

Okada, Y., Surface deformation due to shear and tensile faults in a half-space, *Bull. Seismol. Soc. Am.*, *75*, 1135-1154, 1985.

Schmidt, D. A. and R. Bürgmann, Time-dependent land uplift and subsidence in the Santa Clara valley, California, from a large interferometric synthetic aperture radar data set, *J. Geophys. Res.*, *108*, B9, 2416, doi:10.1029/2002JB002267, 2003.

Schmidt, D. A. and R. Bürgmann, Distribution of aseismic creep rate on the Hayward fault inferred from seismic and geodetic data, *J. Geophys. Res.*, *110*, B08406, doi:10.1029/2004JB003397, 2005.

Working Group on California Earthquake Probabilities, Earthquake probabilities in the San Francisco Bay Region: 2002 to 2031, *U.S. Geol. Surv. Open File Rep.*, *03-214*, 2003.

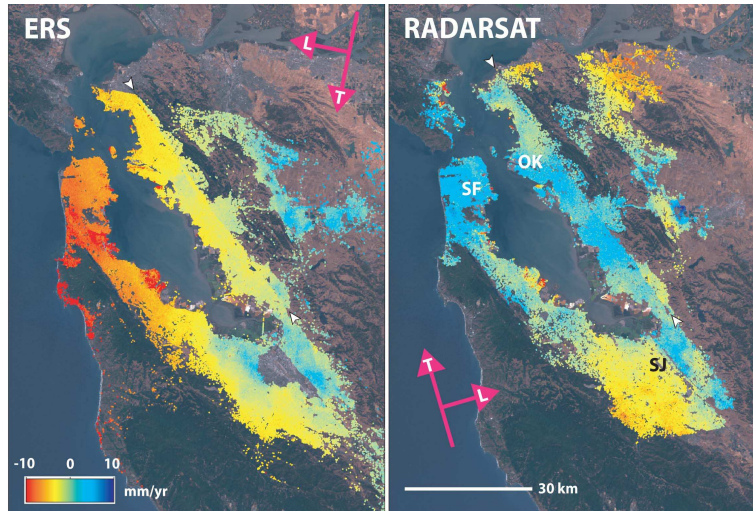


Figure 3.40: PS-InSAR velocities for the San Francisco Bay Area. Red colors indicate motion of the ground away from the satellite, blue colors motion towards. Where a feature has the same color in both datasets, surface deformation is vertical; where colors are opposite, deformation is horizontal. Pink arrows indicate track (T) and line-of-sight (L) directions for each satellite. White arrowheads show the location of the surface trace of the Hayward fault. [SF – San Francisco, OK – Oakland, SJ – San Jose]

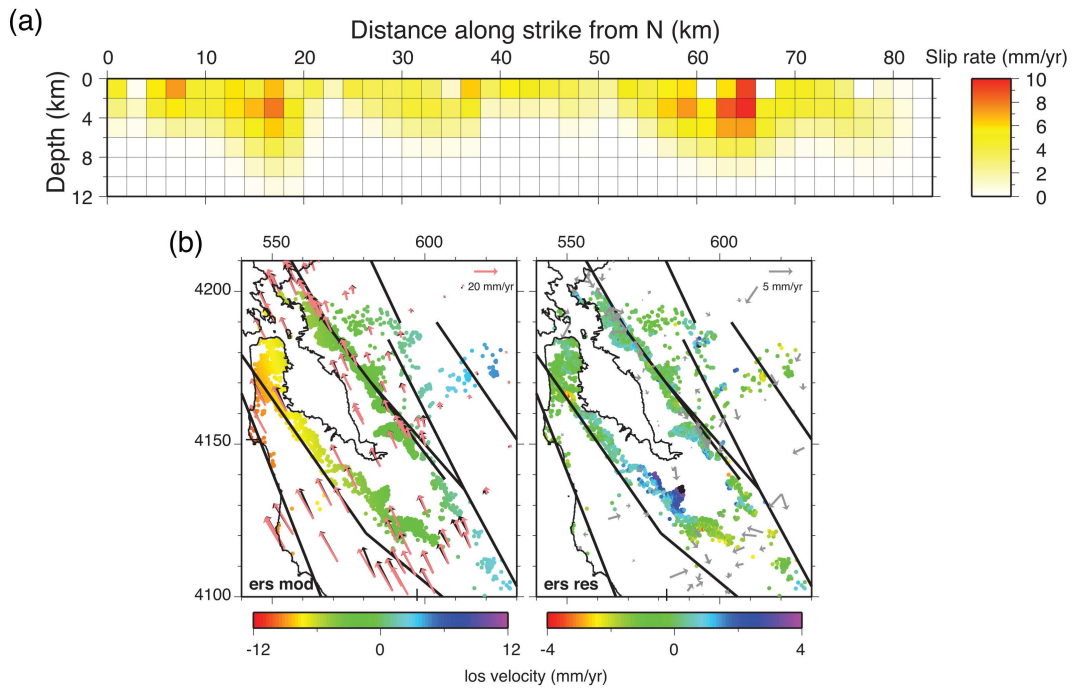


Figure 3.41: (a) Distribution of creep on the Hayward fault. Creep at the surface reaches a maximum of ~ 9 mm/yr at Fremont (~ 66 km). The white area between 20 and 58 km along-strike is the area we believe to be locked. (b) Modeled (left) and residual (right) PS-InSAR and GPS velocities. Only ERS PS velocities are shown here for an example. Black arrows are BAVU GPS velocities, pink arrows show modeled GPS velocities, gray arrows show residual GPS velocities (note change in scale). Solid black lines are faults modeled in the inversion. Most residuals are of the order 1-2 mm/yr; prominent residual uplift features (blue colors) can be seen where there is unmodeled uplift occurring within stepovers and restraining bends of the fault. Coordinate system is UTM km, zone 10.

20. Slip of the 2004 Sumatra-Andaman Earthquake from Joint Inversion of Long Period Global Seismic Waveforms and GPS Static Offsets

Junkee Rhie, Douglas Dreger, Roland Bürgmann, and Barbara Romanowicz

20.1 Introduction

The December 26, 2004 Great Sumatra-Andaman earthquake is an important earthquake in many ways. It is the first great event ($M_w > 9.0$) with sufficient data to allow for a detailed analysis of its complex source rupture process. For the first time, global very broadband seismic and geodetic measurements are available. In this study, we present a slip distribution over the finite fault plane constrained by global long period seismic waves and near-field GPS offsets.

20.2 Data and Inversion Method

We considered all three components of displacement waveforms recorded at 10 IRIS and GEOSCOPE stations within the epicentral range between 43.6° and 65.2° (Figure 3.42). The GPS offset data used for the inversion represent a 38 near-field subset of the 142 coseismic displacement measurements (Banerjee *et al.*, 2006) (Figure 3.42). To account for several weeks of postseismic deformation prior to reoccupation of the GPS stations, we adjusted the offset estimates for near-field campaign-mode GPS sites in this dataset.

To invert data for the slip distribution, we use a widely used least-squares inversion. Here we used normal-mode computed Green's functions for seismic waveforms at teleseismic distances and FORTRAN programs ED-GRN/EDCMB (Wang *et al.*, 2003) for GPS Green's functions for flat layered elastic structures. In both cases, PREM is used for the velocity structure. The seismic data and Green's functions were bandpass filtered between 100 and 500 sec. Since the rise time of each sub-fault is very short compared to the passband, we ignored the detailed variation in slip rise time of each sub-fault. The trigger time of each sub-fault is defined by the passage of circular rupture front with constant rupture velocity. In this study, we choose the rupture velocity of 2.5 km/s as it is consistent with other studies (e.g., Ni *et al.*, 2005). A Laplacian-smoothing operator and slip positivity constraint are applied in all of the inversions and a weighting factor is applied to the GPS data set and Green's functions for optimal slip model explaining both seismic and GPS data sets.

20.3 Results and Discussion

We tested a geometry model, slightly modified from a previous study, constrained by aftershock distribution and the fit to the far-field GPS coseismic offsets (Baner-

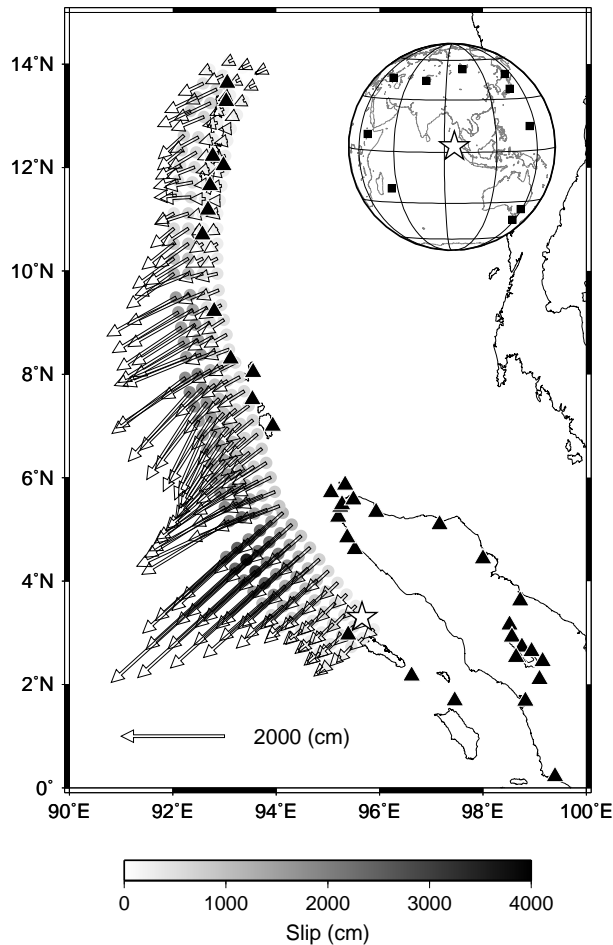


Figure 3.42: The preferred slip distribution model from joint inversion of seismic and GPS static offsets. Color represents total slip and the arrows show the slip vector. Black triangles indicate the locations of the near-field GPS sites and black squares in the small global map on the upper right show 10 selected global seismic stations used in joint inversion. A white star represents the epicenter both in local and global maps.

jee *et al.*, 2005). In this study, we removed the steeper and deeper segments of the fault and made a simple fault geometry model because our data sets are not sensitive to a slight geometry change at deeper depth. The slip model inverted from only seismic waveforms shows large slip patches at around 4° N and a high-slip region with slip larger than 10 m extends only up to 10° N, and

its moment magnitude is 9.12. The joint inversion slip model including near-field GPS static offsets data basically keeps the trend of the slip distribution but increases the level of the slip over nearly the whole fault plane, and its seismic magnitude is determined to be M_w 9.20 (for slip distribution see Figure 3.42).

To constrain key model parameters, we consider sensitivity tests for dip angles and rupture velocity, which are important parameters to understand the source process. Unfortunately our data sets are not very sensitive to these two parameters. While neither of the two parameters are well constrained in this study, distribution of aftershocks and several previous studies support that our dip angles and rupture velocity are reasonable (e.g., *Bilham et al.*, 2005; *Ni et al.*, 2005).

A precise estimate of model error is as important as a detailed slip distribution. An error analysis on our slip model is conducted by a random station selection method. We randomly select 50% of seismic and GPS stations and invert them for slip distribution and then repeat this process 10 times. By doing this, we estimate mean and standard deviation of moment magnitude and also slip at each sub-fault. The mean slip distribution is very similar to the slip distribution inverted from the whole data set. The estimate of mean seismic moment and 1 standard deviation error is $9.19 - 0.02 / + 0.02$.

To confirm our slip distribution model we compare forward GPS static offsets at far-field sites (Figure 3.43). We do not consider stations at > 1000 km because of the large sphericity effect, which we did not consider in our Green's function computation. A forward prediction of GPS vectors at stations on Malaysian Peninsula shows that the slip model inverted using only seismic data significantly underestimates observed GPS offsets but the slip model from the joint inversion can predict observations nearly perfectly.

This indicates that after-slip correction to get coseismic static offsets for near-field campaign GPS offset data is correct and unaccounted post-seismic excess motion is small.

Our slip model from joint inversion is similar to slip models obtained from different data sets in the location of the largest slip patch and the extent of the large slip region (e.g., *Ammon et al.*, 2005). This largest slip patch is consistent with one of the tsunami source regions found by *Fine et al.*, [2005], and the northward extent of significant slip region is consistent with the tsunamigenic region suggested by *Lay et al.*, [2005].

20.4 Acknowledgements

We thank IRIS and GEOSCOPE for providing seismic data. GPS data used in this study were provided by the Survey of India (SOI), BAKO-SURTANAL, the Tectonic Observatory at Caltech, and the Indonesian Institute of Sciences (LIPI).

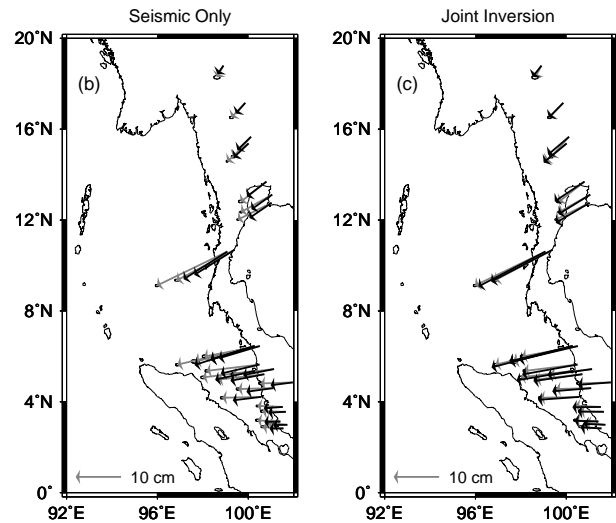


Figure 3.43: Comparison between observed (grey) and synthetic GPS vectors (black) for seismic only and joint inversion models.

20.5 References

- Ammon, C. J., C. Ji, H.-K. Thio, D. Robinsons, S. Ni, V. Hrorleifsdottir, H. Kanamori, T. Lay, S. Das, D. Helmberger, G. Ichinose, J. Polet, and D. Wald, Rupture Process of the 2004 Sumatra-Andaman Earthquake, *Science*, *308*, 1133-1139, 2005.
- Banerjee, P., F. Pollitz, and R. Bürgmann, The size and duration of the Sumatra-Andaman earthquakes from far-field static offsets, *Science*, *308*, 1769-1772, 2005.
- Banerjee, P., F. Pollitz, B. Nagarajan, and R. Bürgmann, Coseismic slip distribution of the 26 December 2005 Sumatra-Andaman and 28 March 2005 Nias earthquakes from GPS static offsets, *Bull. Seism. Soc. Am.*, 2006. (submitted).
- Bilham, R., R. Engdahl, N. Feldi, and S. P. Satyabala, Partial and Complete Rupture of the Indo-Andaman Plate Boundary, *Seismol. Res. Lett.*, *76*, 299-311, 2005.
- Fine, I. V., A. B. Rabinovich, and R. E. Thomson, The dual source region of the 2004 Sumatra tsunami, *Geophys. Res. Lett.*, *32*, L16602, doi:10.1029/2005GL023521, 2005.
- Lay, T., H. Kanamori, C. J. Ammon, M. Nettles, S. N. Ward, R. C. Aster, S. L. Beck, S. L. Bilek, M. R. Brudzinski, R. Butler, H. R. DeShon, G. Ekström, K. Satake, and S. Sipkin,
- Ni, S., H. Kanamori, and D. Helmberger, Energy radiation from the Sumatra earthquake, *Nature*, *434*, 582, 2005.

21. Inversion for the Velocity Structure of the Santa Clara Valley, California

David Dolenc, Doug Dreger, and Shawn Larsen (Lawrence Livermore National Laboratory)

21.1 Introduction

In our previous work, we have found strong correlations between basin depth reported in the USGS 3D seismic velocity model (ver. 2) (*Jachens et al.*, 1997) and different relative measures of ground motion parameters, such as teleseismic arrival delays, P-wave amplitudes, wave energy, local earthquake S-wave amplitudes, and periods of microseism horizontal to vertical spectral ratio peaks (*Dolenc et al.*, 2005; *Dolenc and Dreger*, 2005). The teleseismic, local earthquake, and microseism observations were also found to be strongly correlated with one another. The results suggested that all three datasets are sensitive to the basin structure and could, therefore, be used together to improve the 3D velocity model.

We started to develop a simultaneous inversion of the observations from the three datasets to refine the velocity model within the SCV basins. To reduce the extremely large model space, we invert for the velocity structure within the basins while the basin geometry, as defined in the USGS ver. 2 velocity model, is held fixed. Basin geometry in the USGS model was mainly constrained by the inversion of the gravity data and is one of the better known parameters in the model.

We use the 3D elastic finite-difference code E3D to simulate the teleseismic, local, and microseism wavefields for the models with increasing levels of complexity in the basins. To model the plane wave from the teleseismic events, we used a disc of point sources in the deepest homogeneous layer of the model, representing the upper mantle. To simulate the microseisms, we used a localized source of isotropic Rayleigh waves located offshore.

In the next step, we use the simulated wavefields to do the inversion following the approach developed by *Aoi* [2002]. In his study, *Aoi* [2002] used the inversion scheme to estimate the 3D basin shape from the long-period strong ground motions. In this work we keep the basin geometry fixed and invert for the velocity structure within the basins.

21.2 Results

In the test inversions, we used the synthetic waveforms obtained with a selected target model instead of true observations. This was to test the inversion method while the target 3D velocity structure was known and based on the USGS ver. 2 model. We also used teleseismic data from a set of 38 stations. The structure within the basins was laterally uniform with a single velocity gradient. An example of the test inversion is presented below. The

velocities and density of the target and of the starting model are listed in Figure 3.44. The velocity and density gradients in the SCV basins in the target model were the same as in the USGS model. The velocity and density gradients in the starting model were 50% smaller than the USGS gradients in the SCV basins. The perturbation steps used for all six model parameters (P- and S-wave velocity and density at the surface and their gradients with depth) were 15% of their starting values.

The computations were performed on the BSL Linux cluster. Because of the computational limitations, the slowest velocities in the model were increased to a minimum S-wave velocity of 1 km/s. The slowest P-wave velocity was 1.75 km/s. The computation time for a single forward simulation was ~70 minutes when 16 cluster nodes and 2 processors per node were used. Each forward computation required ~4.5 GB of memory.

Results for a subset of four stations are presented in Figure 3.44. Stations 120 and 238 are located over the basins; station 186 is south of the Cupertino basin, and station PG2 is between the basins. Waveforms for the starting model and for a model from iteration steps 2 and 4 are shown (solid lines) as well as the waveforms obtained with a target model (dotted). Waveforms were bandpass filtered between 0.1 and 0.5 Hz as the waveforms from the recorded teleseisms had most of the energy in this frequency band. Only the first 20 s of the waveforms were used in the inversion. This time period includes the P-wave arrival as well as the P- to S-wave converted arrivals. The waveforms shown in Figure 3.44 include the arrival of the pP-wave that was also modeled, but not included in the inversion, as it arrives after the first 20 s. Results from the test inversions performed so far showed that the method is stable, and that four or less iteration steps were needed to reach the target model (*Dolenc*, 2006).

The presented inversion example used only teleseismic waveforms. Future inversions will use additional parameters obtained from the local earthquake and microseisms data. For the local earthquakes, these parameters will include energy estimates and peak ground velocity values. For the microseisms data, the parameter that will be included in the inversion will be the value of the horizontal to vertical spectral ratio peak. Additional parameters that would characterize the teleseismic waves coda could also be added.

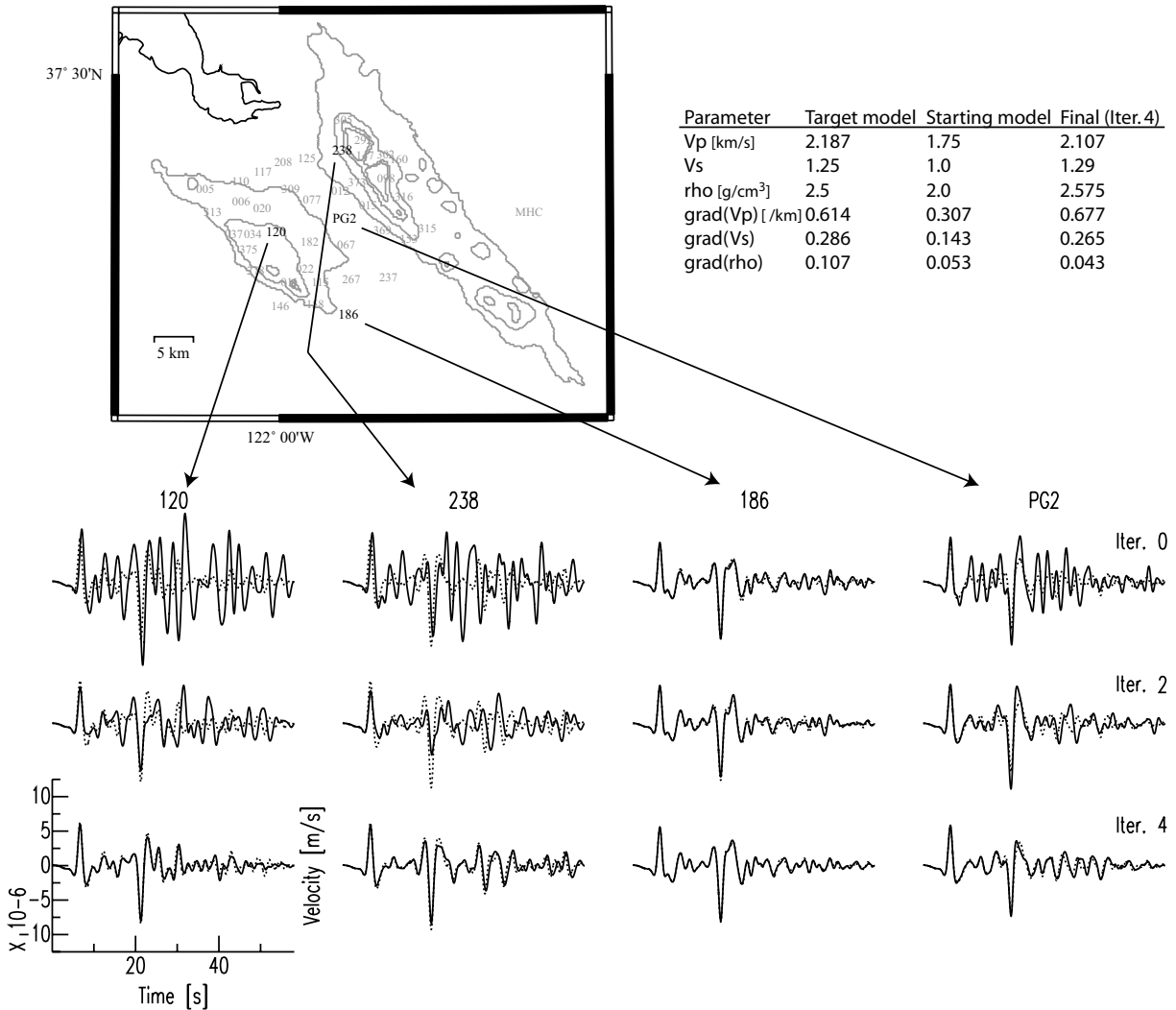


Figure 3.44: *Top left:* Closer look at the SCV region. Contours of the SCV basins from the USGS ver. 2 model at 1 km, 3 km, 5 km, and 6 km are shown in gray. *Top right:* The velocities and density in the SCV basins. *Bottom:* Results from a test inversion. Waveforms for the four SCV station are shown for the starting model (solid, top row) and for a model as it was modified after iteration 2 and 4 (solid, bottom rows). Waveforms obtained with the target model are shown for comparison (dotted).

21.3 Acknowledgements

Part of this work was supported by the USGS grants 99HQGR0057 and 00HQGR0048. The Hellman Faculty Fund is acknowledged for partial support.

21.4 References

Aoi, S., Boundary shape waveform inversion for estimating the depth of three-dimensional basin structures, *Bull. Seism. Soc. Am.*, 92, 2410-2418, 2002.

Dolenc, D., D. Dreger, and S. Larsen, Basin structure influences on the propagation of teleseismic waves in the Santa Clara Valley, California, *Bull. Seism. Soc. Am.*, 95, 1120-1136, 2005a.

Dolenc, D. and D. Dreger, Microseisms observations in the Santa Clara Valley, California, *Bull. Seism. Soc. Am.*, 95, 1137-1149, 2005.

Dolenc, D., Results From Two Studies in Seismology: I. Seismic Observations and Modeling in the Santa Clara Valley, California II. Observations and Removal of the Long-Period Noise at the Monterey Ocean Bottom Broadband Station (MOBB), *Ph.D. Thesis*, University of California, Berkeley, 2006.

Jachens, R. C., R. F. Sikora, E. E. Brabb, C. M. Wentworth, T. M. Brocher, M. S. Marlow, and C. W. Roberts, The basement interface: San Francisco Bay area, California, 3-D seismic velocity model, *EOS Trans. AGU.*, 78, F436, 1997.

22. A Study of the Relation between Ocean Storms and the Earth's Hum

Junkee Rhie and Barbara Romanowicz

22.1 Introduction

It had been shown that long period surface waves, especially Rayleigh wave type, are continuously and primarily radiating from the northern oceans during the northern hemisphere winter and from the southern oceans during the summer (Rhie and Romanowicz, 2004; Nishida and Fukao, 2004; Ekström and Ekström, 2005). In this study, we investigate a four day time window, which is free of large earthquakes but during which the long period seismic amplitude due to the "hum" is unusually high. By doing this, we infer that the "hum" events occur close to the shore rather than the deep ocean and the details of the generation mechanism. We also compare the variation in seismic amplitude at long period and short period bands for three years and show that there is a strong correlation during winter periods. It indicates that the "microseisms" and the "hum" events have a common generation mechanism.

22.2 Earthquake "free" interval 2000.031-034

The time interval between 2000.031 and 2000.034 is important to infer the "hum" mechanism because it is not contaminated by large earthquakes but shows the high level of long period seismic amplitudes. We considered stacks of vertical velocity seismograms recorded at very broadband STS-1 seismometers of two regional arrays in Japan (F-net) and California (BDSN). For each array, we stacked Gaussian filtered seismograms with various center periods according to the dispersion of Rayleigh waves, assuming plane wave propagation from an arbitrary azimuth. We apply a 6 hour running average with a time step of 1 hour to the stacked data at BDSN and F-net respectively. The results of a mean stack amplitude for center period of 150 and 240 s as a function of time and back-azimuth are shown in Figure 3.45. During given time interval, two noise events, probably due to the "hum" of the Earth, are clearly seen on 2000.031 and 2000.033 at both arrays. However, the arrival time of each event at each array is quite different. It is clear that BDSN records the event about 8-10 hours earlier than F-net does. 8-10 hour time difference is too large to be explained by seismic wave propagation, but it can be explained by the propagation speed of "free" infragravity waves at ~ 220 m/s.

We also compare the seismic observation with a direct ocean buoy measurement near the coast of California and Japan. Unfortunately, many buoys near the Japanese

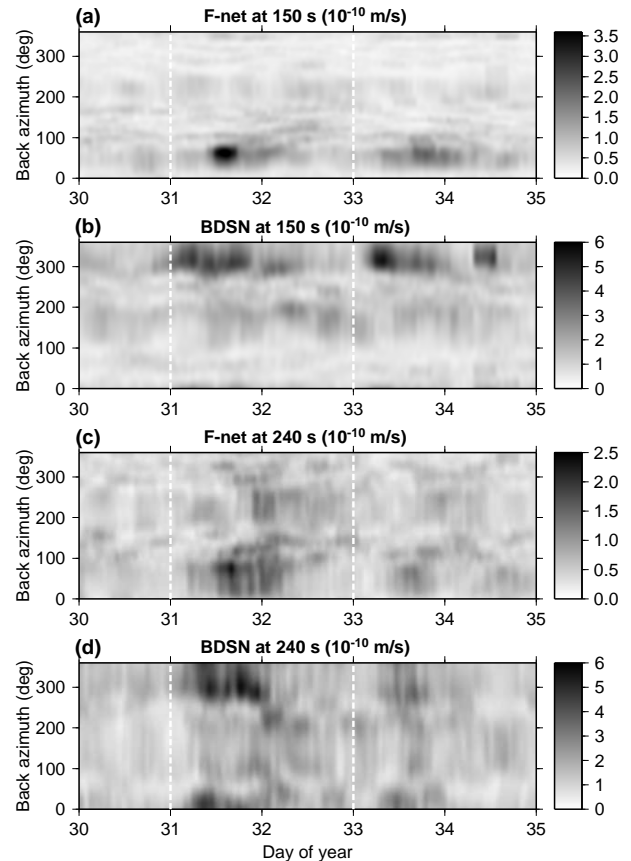


Figure 3.45: (a) Mean stack amplitude (MSA) with 6 hour time window lagged by 1 hour as a function of time and back azimuth for F-net. A Gaussian filter with center period of 150 s was applied before stacking. (b) Same as (a) for BDSN. (c) Same as (a) for center period of 240 s. (d) Same as (c) for BDSN.

eastern coast are not available. However, we can see very strong correlation between the variation in seismic amplitude and significant wave height recorded at buoys near the California coast.

22.3 Comparison with Microseisms

It is well known that non-linear interaction of ocean swells generates microseisms, especially double frequency microseisms, which is dominant seismic noise at short periods (2-25 s, Longuet-Higgins, 1950). We have shown that there is a strong correlation between the variation in

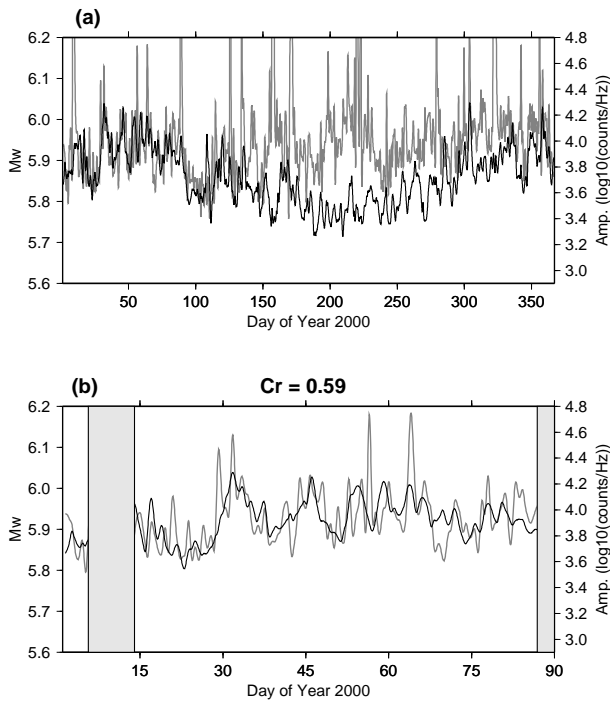


Figure 3.46: (a) A comparison between a processed long period (hum) amplitude (gray) and short period Fourier amplitude (black) for BDSN. (b) Detailed comparison of (a) during first 90 days of year 2000. Time window strongly contaminated by earthquakes are shaded in gray. Corresponding correlation coefficient is shown in the plot.

ocean wave height and long period seismic energy fluctuation. It indicates that both seismic noises at short (microseisms) and long (hum) periods are probably generated from common sources. Therefore, we compared amplitude levels in the two frequency bands for long time interval (e.g., a whole year). To do that, we need to reduce the contamination from the earthquakes. We developed a data processing method that avoids eliminating time windows contaminated by earthquakes (for details see *Rhie and Romanowicz, 2006*).

We compare the processed "hum" and microseism amplitude time series for BDSN over 3 years (e.g., Figure 3.46). The level of low frequency (hum) amplitude does not vary significantly with time (Figure 3.46a). However, there is a seasonal variation in the short period (microseism) amplitude, and it shows a strong correlation with significant wave height at buoys near California. During the winter period, short period amplitudes are maximum and the correlation between long and short period amplitude variations is high (Figure 3.46b).

22.4 Conclusions

By comparison between the variations in long period seismic amplitudes for two regional arrays in Japan and California, we observed that there is a time gap between arrivals of the common "hum" event on both sides of Pacific Ocean. This observation and direct comparison between seismic amplitude and significant wave height measurements at buoys lead us to a detailed scenario of generation of the "hum" comprising three steps: 1) short period ocean waves interact non-linearly to produce infragravity waves as the storm-related swell reaches the coast of North America; 2) infragravity waves interact with the seafloor locally to generate long period Rayleigh waves, which can be followed as they propagate to seismic stations located across North America; 3) some free infragravity wave energy radiates out into the open ocean, propagates across the north Pacific basin, and couples to the seafloor when it reaches distant coasts north-east of Japan, giving rise to the corresponding low frequency seismic excitation observed on the Japanese F-net array.

We have assembled and processed 3 years of microseism data at stations of the BDSN and F-NET arrays, and show a strong correlation of amplitude fluctuations in the microseismic band with that in the "hum" band during the northern hemispheric winter, but not during summer months, suggesting that in the winter, the microseisms and hum have a common "regional" or "local" origin, whereas in the summer, the origin of the hum is indeed distant (southern hemisphere) while the microseisms remain local and have smaller amplitudes

22.5 Acknowledgements

We wish to thank BDSN, F-net, JMA, and NOAA for providing high quality and continuous seismic and ocean buoy data.

22.6 References

- Ekström G., and S. Ekström, Correlation of Earth's long-period background seismic radiation with the height of ocean waves, *Eos Trans. AGU, 86*, Fall Meet. Suppl., Abstract S34B-02, 2005.
- Longuet-Higgins, M. S., A Theory of the origin of microseisms, *Philos. Trans. R. Soc. London, Ser. A, 243*, 1-35, 1950.
- Nishida, K., and Y. Fukao, Spatial variations of excitation amplitudes of Earth's background free oscillations, *Eos Trans. AGU, 84*, Fall Meet. Suppl., Abstract S31B-1068, 2004.
- Rhie, J., and B. Romanowicz, Excitation of Earth's continuous free oscillations by atmosphere-ocean-seafloor coupling, *Nature, 431*, 552-556, 2004.
- Rhie, J., and B. Romanowicz, A Study of the relation between ocean storms and the Earth's hum, *Geochem. Geophys. Geosyst.*, 2006 (in press).

23. Physically Constrained Inversion of Long-Period Seismic Data: Insights on the Nature of the Transition Zone

Fabio Cammarano and Barbara Romanowicz

23.1 Introduction

The thermal state and composition of the Earth's upper mantle and transition zone dictate its dynamics from microscale (e.g., creep mechanisms, earthquakes) to macroscale (e.g., modality of mantle convection, plate tectonics). The knowledge of these fundamental physical parameters and their three-dimensional variations in Earth's deep interior is indirect and relies entirely on the interpretation of geophysical data, based on insights from theoretical and experimental mineral physics. Among these, seismological observations constitute a main source of information. Seismic waves record information about the elastic (and anelastic) structure of the Earth. Long-period seismic data provide the most comprehensive global constraints on upper mantle shear velocity structure. Fundamental-mode surface waves are mostly sensitive to the uppermost mantle structure, while including overtones provide resolution in the transition zone.

Lateral temperature variations in the Earth have been inferred since the first tomography studies began to reconstruct 3-D seismic velocity structure (*Dziewonski et al.*, 1977, *Woodhouse and Dziewonski*, 1984). However, in spite of the ever-improving resolution of seismic velocity models and a general agreement of different models on at least the large-scale structure (e.g. *Ritsema*, 2004, *Su et al.*, 1994, *Li and Romanowicz*, 1995), interpretation is still challenging.

An important issue for seismic interpretation concerns the non-physical nature of any seismic model. Typically, the physical interpretation of a given seismic dataset is performed in two steps. First, a seismic model that fits satisfactorily the data is constructed. Second, the model is interpreted for the physical parameters based on the knowledge of the elastic and anelastic properties of mantle minerals plus constraints on plausible composition and temperature ranges from geochemistry - i.e. the signature of outcropping rocks (orogenic peridotites) and mantle inclusions (xenoliths and xenocrysts) -, heat flow measurements at surface and conditions for melting mantle materials. The second part of the process is commonly regarded as the critical one for the interpretation. Instead, it is often forgotten that the seismic models are already an interpretation of the data. The seismic models are non-unique and depend on the parametrization and distribution, quality and type of data used. More important, it is not ensured that a given best-fit seismic model corresponds to a physical model. For example,

the non-clear physical meaning of the seismic reference models (PREM *Dziewonski and Anderson*, 1981, AK135 *Kennett et al.*, 1995) has been elucidated by the previous work of one of us (*Cammarano et al.*, 2003). The same problems are transferred to 3-D tomography models that are obtained by perturbing the starting average model.

Here we invert long-period seismic waveforms, which are mainly sensitive to shear velocity, with respect to a physical reference model instead than common seismic reference models (e.g., PREM). Velocity variations will thus correspond to thermal (or compositional) variations and a consistent three-dimensional density and V_P structure may be determined. We start assuming purely thermal variations because in the upper mantle composition plays a secondary role. We compare the thermal features constrained by the seismic data against expected thermal variations and estimated geotherms in various tectonic regions. The average velocity model extracted from the physically constrained tomography provides insights on the nature of the transition zone. In order to assess the uncertainties in the thermal model and estimate how well average velocity and velocity gradient with depth in the upper mantle are constrained by long-period seismic data, we perform a series of inversions starting with various models.

23.2 Procedure

We test our inversion by using some of the PREF models from *Cammarano et al.* (2005a,b). These are pyrolytic, adiabatic models that fit global seismic data (i.e. travel times and fundamental modes). We select three PREF models that represent well the differences in seismic and mineral physics properties within the family of PREF models. The use of different starting PREF models, characterized by their own sensitivities of seismic velocities to temperature, will help to assess the effects of the mineral physics uncertainties on the physically-constrained inversion. At the same time, this will test how good is the assumption of non-dependence of the outcome from the starting model. To further investigate this point, we also invert the seismic data starting with a model that has a much smaller jump at 410km and different velocity gradients above and below this discontinuity (Figure 3).

The data used are long-period fundamental and higher-order mode surface waveforms from the existing Berkeley compilation. Events with moment magnitude larger than six and at teleseismic distance (epicentral distance

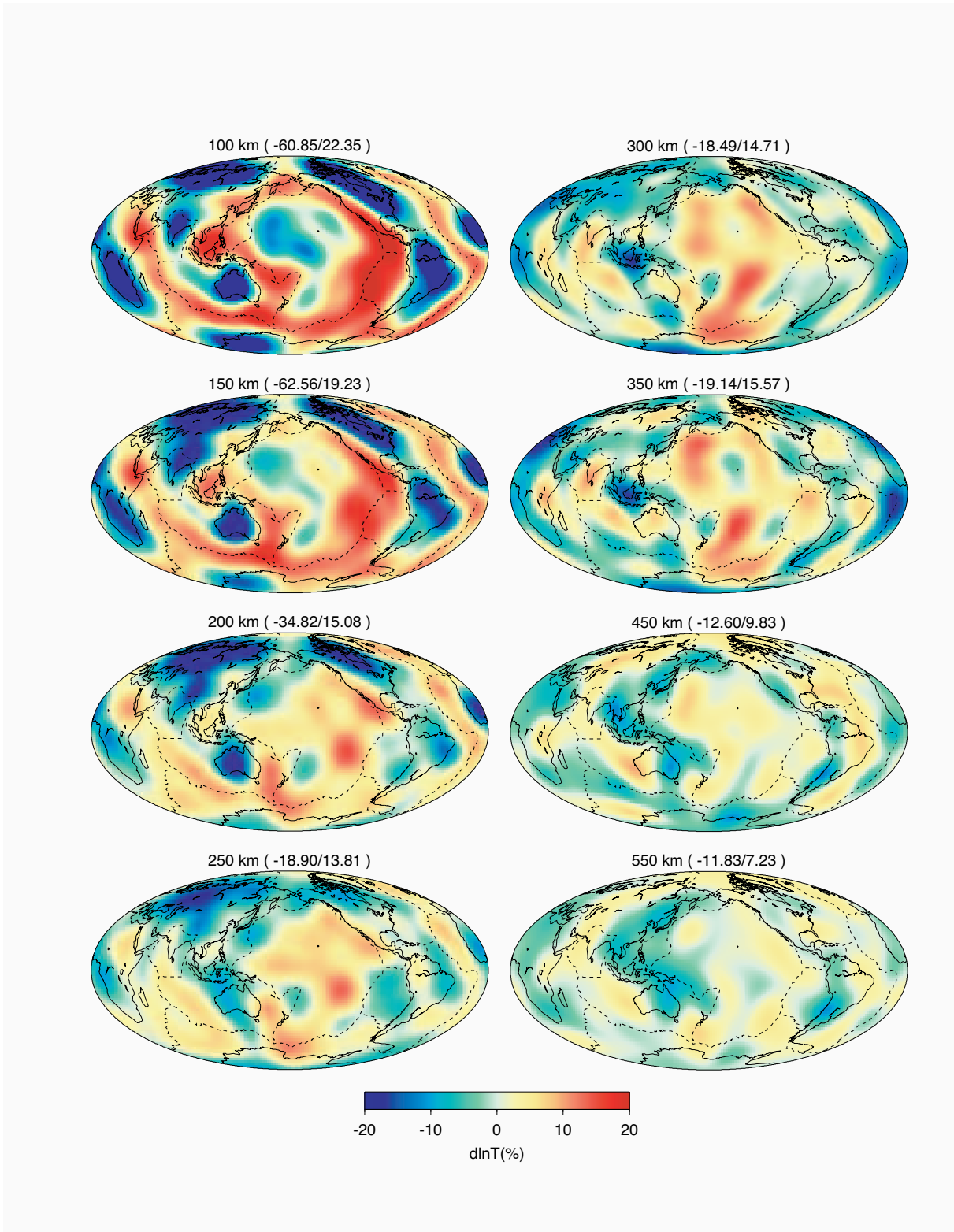


Figure 3.47: Lateral temperature variations inferred from the physically-constrained waveform inversion. In the uppermost mantle, positive anomalies correspond to oceanic ridges, negative to cratonic areas. Negative thermal anomalies related to subduction zones appear below. Minimum and maximum value of anomaly compared to the mean temperature value is given for each depth.

between 15° and 165°) have been selected. The original seismograms have been deconvolved for the instrument response and filtered between 60 s and a variable maximum period, typically between 220 s and one hour, which is chosen according to the event magnitude. Wavepackets for both fundamental and overtones are extracted from the seismograms. The seismic waveform tomographic method is based on the Non-linear Asymptotic Coupling Theory method (NACT, *Li and Romanowicz, 1995*).

We start the inversion with a low-resolution version of a recent anisotropic model (SAW642AN, *Panning and Romanowicz, 2006*), but replacing the background seismic reference model with a physical reference model (i.e., PREF). We invert for the isotropic part down to 1000 km, while we keep fixed the radially anisotropic part of the model, represented by ξ (V_{SH}^2/V_{SV}^2). Radial anisotropy is required to simultaneously fit spheroidal and toroidal fundamental modes. We correct for crustal structure assuming the model CRUST2.0 (*Bassin et al., 2000*). We solve iteratively the inversion procedure following, for each step, the classical least-squares approach.

23.3 The Thermal model

The lateral variations in temperature (Figure 3.47) confirm the primary role of temperature in determining the seismic structure of the upper mantle and transition zone. Thermal variations that explain the seismic data are indeed consistent with the range expected from dynamics modeling. However, the secondary compositional effect clearly emerges when looking at the “too-low” values of temperature obtained in the first 250 km beneath cratons. The lateral thermal variations between inversions with respect to different PREF models are very similar, indicating that the additional uncertainties in the temperature partial derivatives do not affect much the interpretation. Specifically, they affect it much less than regularization schemes required by the inversion process.

The upper-mantle geotherms constrained by long-period seismic data are able to reproduce the range of expected geotherms beneath oceans and cratons (Figure 3.48). We compare the seismic geotherms with geotherms for different oceanic age, based on the plate cooling model (*Turcotte and Schubert, 1982*), and continental geotherms, purely conductive, computed at steady-state and based on surface heat flow and radiogenic heat production in the crust (*Chapman, 1986*). Extremely low temperatures are found, sometimes, in cratons (Figure 3.48), that are likely to be related to the secondary compositional effect.

The capacity of inferring absolute temperatures and thermal gradients depends on how precisely we can determine absolute seismic velocity and gradients. To this end, we should point out that our results rely on assumed crustal and anisotropy structure.

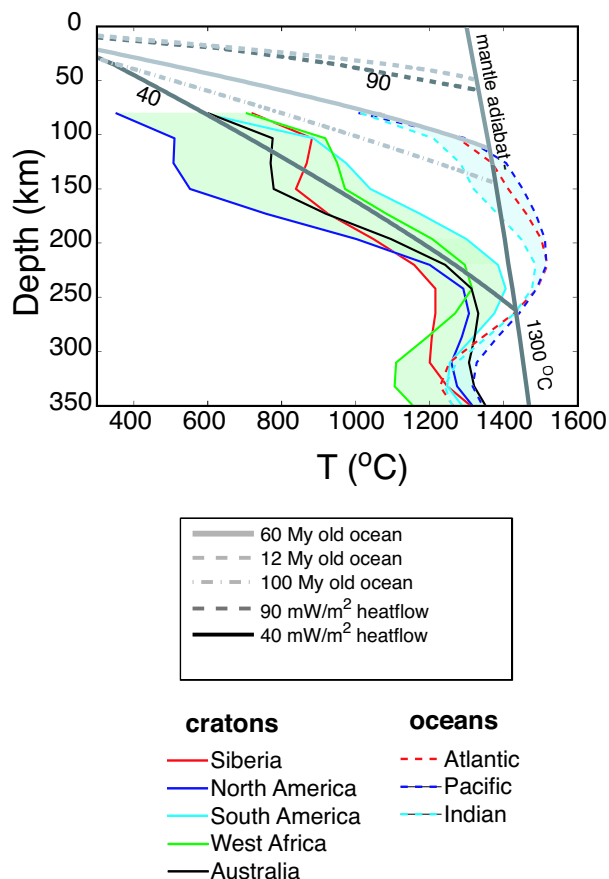


Figure 3.48: Seismic geotherms averaged over oceanic and cratonic regions.

23.4 The average model

In figure 3, we show the inverted average V_S structure obtained by the 3-D tomographic model. Absolute velocities and gradients are well constrained from long period data, except in proximity of the 410 km discontinuity (Figure 3.49). The velocity structure below 300 km is very similar in those different tectonic regions indicating the global character of the inverted average model in the transition zone.

The inverted model tends toward PREM, which is confirmed to be a very good average seismic model. The differences are due to the different starting parametrization. For example, because PREF does not have a 220 km discontinuity as PREM, the final model does not have this feature either. Instead, a higher velocity gradient than the starting model is required by the seismic data around this depth (Figure 3.49). Long-period seismic waveforms are not directly sensitive to the mantle discontinuities, and therefore, the gradients nearby a discontinuity are not well constrained by those data. This can be clearly seen when we compare the gradients nearby the 410 km discontinuity between the PREF inverted model and the

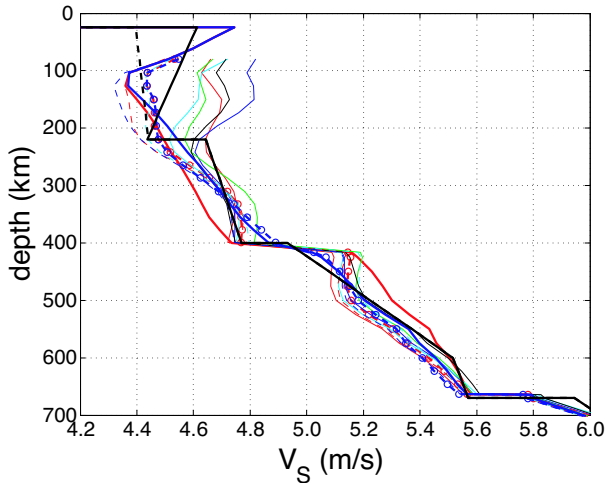


Figure 3.49: Inverted average structures for a PREF model (red) and a model with different gradient and smaller jump at 410km (blue). Solid lines are starting models, dots and dashed lines are inverted models. In background, velocity models beneath oceanic (thin dashed lines) and cratonic (thin solid lines) regions are shown.

model with the small jump at 410 km (see Figure 3.49).

23.5 The nature of the transition zone

The velocity jump imposed in the starting model at the olivine-wadsleyite transition dictates the gradients around it (Figure 3). Pyrolitic models, which have ~60 vol % of olivine, do have a larger jump than seismic reference models for this discontinuity (ΔV_P 6-10%, ΔV_S 6-12% (Cammarano *et al.*, 2005a) vs 2.5% and 3.5%, respectively, for PREM and 3.5% and 4% for AK135). If we assume in our starting model the large jump inferred from mineral physics, long period seismic waveforms require the changes in gradients above and below the 410 km discontinuity shown in Figure 3. A thermal interpretation of this structure is not feasible as we obtain temperatures ~1250 K at 350 km, ~1750 K around 500 km and geodynamically unrealistic thermal gradients throughout the upper mantle. We conclude that dry pyrolite can not be reconciled with seismic data. This conclusion has a global character as the similarity of the velocity profiles below 300 km beneath oceans and cratons show (Figure 3.49).

23.6 References

Bassin C., Laske G. and Masters G., The current limits of resolution for surface-wave tomography in North America, *EOS, Transactions Am. Geophys. Union* 81 F897, 2000

Cammarano F., Goes S., Deuss A. and Giardini D., Is a pyrolitic adiabatic mantle compatible with seismic data? *Earth Planet. Sci. Lett.* 232 227-243, 2005b

Cammarano F., Deuss A., Goes S. and Giardini D. (2005), One-dimensional physical reference models for the upper mantle and transition zone: combining seismic and mineral physics constraints, *J. Geophys. Res.* 110 B01306 doi:10.1029/2004JB003272, 2005a

Cammarano F., Goes S., Giardini D., Vacher P. (2003) *Phys. Earth Planet. Inter.* 138 197-222, 2003

Chapman D.S., Thermal gradients in the continental crust, in *The Nature of the Lower Continental Crust, Geol. Soc. Spec. Publ.*, vol. 24 63-70, 1986

Dziewonski A.M., and Anderson D.L., Preliminary Reference Earth Model, *Phys. Earth Planet. Inter.* 25 297-356, 1981

Dziewonski A.M., Hager B.H. and O'Connell R.J., Large-scale heterogeneities in the lower mantle, *J. Geophys. Res.* 82 239-255, 1977.

Kennett, B.L.N., E.R. Engdahl, and R.P. Buland, Constraints on seismic velocities in the Earth from travel times, *Geophys. J. Int.*, (122, 108-124, 1995.

Li, X.D. and Romanowicz B., Comparison of global waveform inversions with and without considering cross-branch modal coupling, *Geophys. J. Int.* 121 695-709, 1995

Turcotte D.L. and Schubert G. *Geodynamics. Cambridge University Press*, 1982

Ritsema J., van Heijst H.J., and Woodhouse J.H., Global transition zone tomography, *J. Geophys. Res.* 109 B02302, doi:10.1029/2003JB002610, 2004

Su W.J., Woodward R.L., and Dziewonski A.M., Degree 12 model of shear velocity in the mantle, *J. Geophys. Res.* 99 6945-6980, 1994

Woodhouse J.H. and Dziewonski A.M., Mapping the upper mantle: Three-dimensional modeling of the Earth structure by inversion of seismic waveforms, *J. Geophys. Res.* 89 9793-9823, 1994

24. The Fate of the Juan de Fuca Plate

Mei Xue and Richard M. Allen

24.1 Introduction

The Juan de Fuca plate is subducting beneath the northwestern United States and southwestern Canada. While the slab has been imaged to depths of ~ 300 km beneath southern Washington and of at least 200 km beneath southern Oregon, there is little evidence for a slab deeper than ~ 100 km east of High Cascades beneath central Oregon (Bostock, et al., 2002; Harris, et al., 1991; Iyer and Rite, 1981; Michaelson and Weaver, 1986; Rasmussen and Humphreys, 1988; Rondenay, et al., 2001). The apparent absence of the slab east of High Cascades can be interpreted as (1) a low high-velocity contrast making the slab indistinct from the surrounding mantle (Iyer and Stewart, 1977; Michaelson and Weaver, 1986); (2) a more vertical geometry of the slab (Michaelson and Weaver, 1986), or (3) a loss of seismic resolution. To image the slab beneath Oregon, we apply tomography technique using a dataset consisting of our own OATS deployment and all other available data.

24.2 Teleseismic tomography results

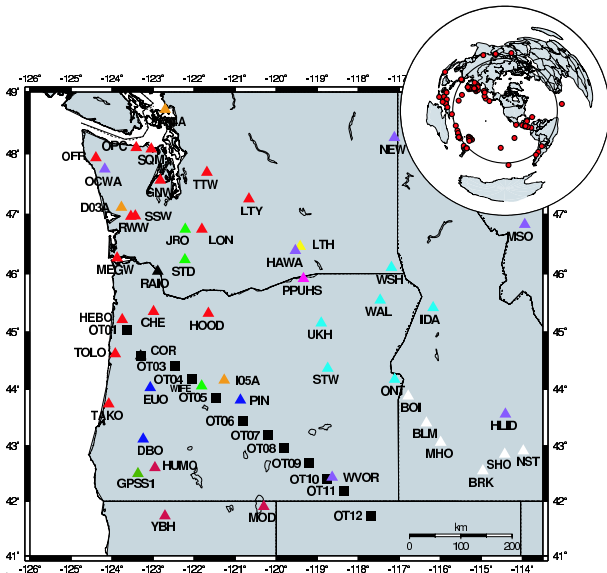


Figure 3.50: Seismic stations used in this study with a total number of 61. Inset shows the distribution of the 95 events used in the inversion for S-wave velocity model.

We have collected data from our own deployment of the Oregon Array for Teleseismic Study (OATS), an array extending northwest-southeast across Oregon from the coast to the McDermitt Caldera (Figure 3.50). We

have also collected data from permanent networks (BK, CC, US, UO, UW, PN, IU, TA, LI), and temporary deployments (XJ, YC, YS) (Figure 3.50). We inspect events with magnitude 6.0 and above from July 19th, 2003 to Nov. 11th, 2004 for a total of 61 stations and follow the same inversion procedure as in (Allen, et al., 2002). For the Vs inversion, a total of 95 events (Figure 3.50) with clear S and SKS phases were recorded at 45 stations, and a total number of 2148 rays were used. For the Vp inversion, a total of 74 events with clear direct P phase were recorded at 46 stations, and a total number of 2043 rays were used.

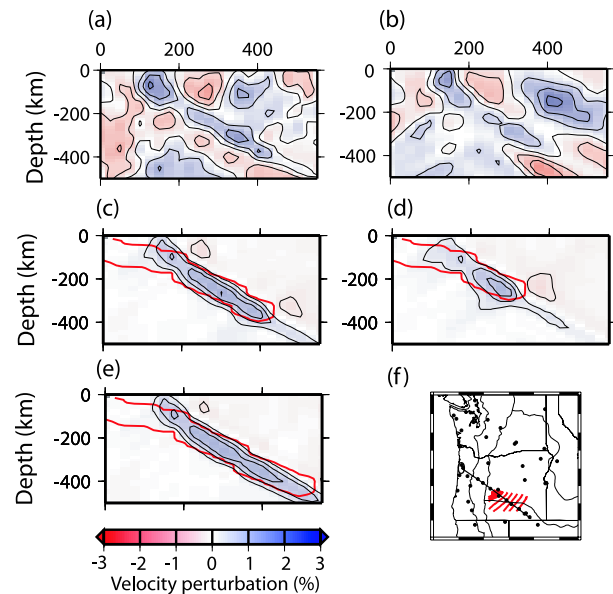


Figure 3.51: Tomographic results showing S- and P-wave velocity structures beneath Oregon and results of inverting synthetic data created from various test slabs. All vertical slices show the same cross section as in (f), along the OATS line, where we have high resolution: (a) the Vs model; (b) the Vp model; resolution tests of S-wave velocity inversion for a slab ending at (c) 400 km depth, (d) 300 km depth, and (e) 500 km depth, and the input anomaly is 3% and dips 50° , outlined by red lines; (f) a map shows the location of the cross-section.

Our tomography results show that the subducted slab extends to a depth of ~ 400 km with a dip of $\sim 44^\circ$ (Figure 3.51, a and b). After correcting the oblique trend of the cross section, the real dip angle is $\sim 50^\circ$. Resolution tests show that structures at shallower depths are better recovered in terms of amplitudes and smearing is less significant. Here, we show three resolution tests for

S-wave velocity models (Figure 3.51, c, d, and e). To test whether the structure we observed between 300 km and 400 km depth is caused by smearing shallow structure or not, we used a synthetic velocity anomaly with a high velocity to 300 km depth only. Figure 2d shows that a slab ending at 300 km depth is not sufficient to produce the observed slab structure between 300 km and 400 km depth. Figure 2c shows a case that the recovered structure resembles what we observed best, where the input slab extends to 400 km and stops there. To test whether the slab stops at 400 km, we conducted the test as shown in Figure 2e where the input slab extends to 500 km depth. Considering the depth range between 400 km to 500 km, the recovered structure differs from the observed structure in three aspects: (1) it has a much stronger velocity anomaly, (2) the transition of velocity anomaly from higher amplitudes to lower amplitudes is smooth, and (3) it didn't lose its width (Figure 3.51e). Thus we speculate that the slab likely stops at ~ 400 km depth and does not extend deeper. The P-wave velocity model also suggests that the slab stops at ~ 400 km (Figure 3.51b). This interpretation can be better tested when USArray data becomes available further east.

24.3 Conclusion

Our tomographic images clearly show the Juan de Fuca plate diving into the mantle beneath Oregon and continues east of the High Cascades with a dip of $\sim 50^\circ$ reaching a depth of ~ 400 km. The slab dips shallower compared with its counterparts to north and south, which have a dip of $\sim 65^\circ$ (Harris, et al., 1991; Rasmussen and Humphreys, 1988). Resolution tests suggest there is little or no velocity anomaly associated with a slab below ~ 400 km.

24.4 Acknowledgements

This work was supported by the NSF (EAR-0539987). We thank Gene Humphreys for allowing us using data from their deployment at Wallowa Mountain. The IRIS DMC provided seismic data. The figures were produced with SAC and GMT (Wessel and Smith, 1995).

24.5 References

Allen, R. M., et al., Imaging the mantle beneath Iceland using integrated seismological techniques, in *Journal of Geophysical Research-Solid Earth*, 107, 2325, doi:2310.1029/2001JB000595, 2002.

Bostock, M. G., et al., An inverted continental Moho and serpentinization of the forearc mantle, in *Nature*, 417, 536-538, 2002.

Harris, R. A., et al., Imaging the Juan Defuca Plate beneath Southern Oregon Using Teleseismic P-Wave Residuals, in *Journal of Geophysical Research-Solid Earth*, 96, 19879-19889, 1991.

Iyer, H. M., and A. Rite, Teleseismic P-wave delays in Oregon Cascades, in *EOS, Trans. Am. geophys. Un.*, 62, 1981.

Iyer, H. M., and R. M. Stewart, Teleseismic technique to locate magma in the crust and upper mantle, in Magma Genesis, in *Proceedings of the AGU Chapman Conference on Partial Melting in the Upper Mantle*, edited by H. J. B. Dick, pp. 281-299, Oreg. Dep. Geol. Min. Ind. Bull, 1977.

Michaelson, C. A., and C. S. Weaver, Upper Mantle Structure from Teleseismic P-Wave Arrivals in Washington and Northern Oregon, in *Journal of Geophysical Research-Solid Earth and Planets*, 91, 2077-2094, 1986.

Rasmussen, J., and E. Humphreys, Tomographic Image of the Juan-Defuca-Plate beneath Washington and Western Oregon Using Teleseismic P-Wave Travel-Times, in *Geophysical Research Letters*, 15, 1417-1420, 1988.

Rondenay, S., et al., Multiparameter two-dimensional inversion of scattered teleseismic body waves 3. Application to the Cascadia 1993 data set, in *Journal of Geophysical Research-Solid Earth*, 106, 30795-30807, 2001.

Wessel, P., and W. H. F. Smith, New version of the Generic Mapping Tools released, EOS, in *Trans. Am. geophys. Un.*, 76, 329, 1995.

25. Applying the Spectral Element Method to Model 3D Attenuation in the Upper Mantle

Vedran Lekic, Barbara Romanowicz and Yann Capdeville (IPGP)

25.1 Introduction

Observations of surface waves and overtones provide a unique opportunity for probing the physical state and dynamics of the upper mantle, due to their global coverage and sensitivity to structure at depths approaching 1000 km. Earth structure affects seismic waveforms through elastic effects of (de)focusing and scattering, as well as anelastic effects that result in amplitude decay and velocity dispersion. Because anelastic processes appear to be thermally activated, temperature has a stronger effect on seismic attenuation than does chemical heterogeneity. This is not the case with seismic velocity, which can strongly depend on both chemical composition and temperature. These differences - combined with a three-dimensional model of both seismic velocity and attenuation - translate into a unique opportunity to separate the effects of temperature variation from those of compositional heterogeneity within the mantle.

25.2 Past Work and Challenges

Normal mode summation methods coupled with approximate first-order perturbation techniques have been successfully applied to modeling of surface waves. Recent high-resolution global tomographic models based on these techniques can resolve regions of fast and slow seismic velocities as small as a few hundred kilometers across (e.g. *Mégnin and Romanowicz, 2000*). Yet, modeling of the 3D distribution of seismic attenuation has lagged behind due to difficulties in separating the effects on seismic waveforms of focusing and scattering of seismic energy in the heterogeneous earth from those due to attenuation intrinsic to the medium. Even when the elastic structure is known perfectly, first-order perturbation techniques are inadequate in modeling wave propagation near the source or receiver, near nodes of the radiation pattern, in locations of strong heterogeneity, and at times long after the source time. Spectral element methods, on the other hand, allow accurate modeling of seismic wave propagation, including the effects of (de)focusing of energy and multiple scattering.

Extracting structural information from seismic waveforms requires calculating the sensitivity kernels of the waveform to parameters like elastic wave velocity and attenuation at each point in the earth. The conventional way of computing sensitivity kernels, called the path average approximation (PAVA), assumes that the wave is only sensitive to structure along the great circle path joining the source with the receiver, and that this sensitivity

is only a function of depth. Higher-order asymptotic approaches, such as non-linear asymptotic coupling theory (NACT: *Li and Romanowicz, 1995*), are capable of more accurately modeling the wave's actual sensitivity within the plane defined by the great circle path. Yet, long period surface waves observed at teleseismic distances are sensitive to structure both along and off the great circle path. While the (de)focusing effects that arise from velocity gradients transverse to the great circle path can be incorporated into the NACT formalism (NACT+F: *Gung and Romanowicz, 2004*), it is also now within reach to use more exact formalisms - such as the full Born approximation - in order to more accurately calculate sensitivity kernels.

25.3 Method

We propose a hybrid approach to tomography, in which we calculate the propagation of seismic waves through an arbitrary 3D medium exactly, using the coupled Spectral Element Method (cSEM: *Capdeville et al., 2003*), and compute the sensitivity kernels approximately, using perturbation theory. This approach allows us to iteratively converge on the correct model as long as the sign of the sensitivity kernels is correct. We apply this approach to 3-component fundamental and overtone waveforms, low-passed at 60 sec, and recorded at more than 100 stations of the IRIS/GSN, GEOSCOPE, GEOFON, and various regional broadband networks. Because of the increased computational costs associated with using cSEM, we at first restrict our focus to ~ 70 events. We ensure excellent global coverage by including major arc surface waves, which provide complimentary sensitivity to minor arc paths. Furthermore, we select deep focus events in all regions where deep seismicity is present. Figure 3.52 shows the events used in our study, color-coded by centroid depth. Resolution tests indicate that our data coverage is sufficient for resolving structures ~ 900 km at the surface, and that vertical smearing is limited.

25.4 Preliminary Results and Future Work

We have modified cSEM to include the effects of ellipticity, topography/bathymetry, radial anisotropy, 3D attenuation, and lateral variations in crustal velocities and depth to the Moho discontinuity. Because their sensitivities are concentrated near the surface, fundamental mode waves are especially strongly affected by 3D Moho topography; in contrast, crustal velocities play a

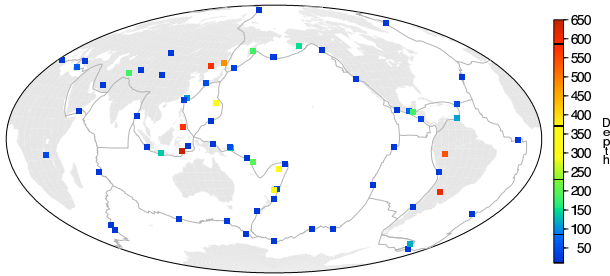


Figure 3.52: Events used in our study color coded by centroid depth.

secondary role. For long continental paths, waveforms corrected for crustal structure display phase delays of 100 sec. Interestingly, first order perturbation theory underpredicts by as much as 50 percent the cSEM phase delays over continents. Along oceanic paths, the differences between cSEM and first order perturbation theory are negligible. Figure 3.53 shows synthetic waveforms calculated by cSEM and NACT for typical long continental and oceanic paths.

We adopt an iterative waveform inversion approach, in which we solve for elastic and anelastic structure in successive steps. As a starting model, we adopt a high-resolution 3D elastic model of Panning and Romanowicz (2006), and a one-dimensional attenuation model constructed from separate upper mantle (QL6: *Durek and Ekstrom, 1996*) and lower mantle (PREM: *Dziewonski and Anderson, 1981*) models. Following our first iteration for elastic structure, which is performed in order to render compatible the starting model with our new dataset, we shall proceed to invert for source parameters. Because rotations of the radiation pattern can result in large amplitude changes - especially near the radiation nodes - inverting for the source mechanism is crucial to developing high resolution models of mantle attenuation.

25.5 Conclusion

We have compiled a waveform dataset of fundamental mode surface waves and overtones with good global lateral and depth coverage. We have modified cSEM to make it capable of accurately modeling wave propagation in an elliptic earth with surface topography / bathymetry, oceans, and 3D crustal structure. We find that first order perturbation theory inadequately predicts the effects of crustal structure on waveforms for long continental paths. Because of the magnitude of this deficiency, we expect our use of cSEM to allow us to model more accurately mantle structure below continents. Furthermore, the use of cSEM will allow us to better model amplitudes of seismic waveforms, and therefore to separate the often elusive signal of attenuation from that due to elastic structure.

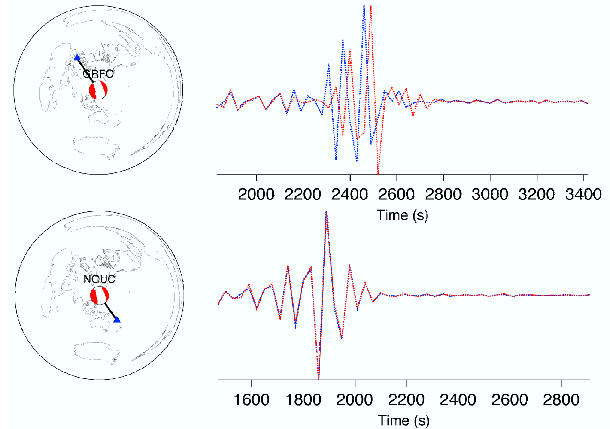


Figure 3.53: Synthetic seismograms from mode summation (blue) and cSEM (red) for a long continental (top) and oceanic (bottom) path.

25.6 Acknowledgements

Support for V. Lekic was provided by the Berkeley Fellowship.

25.7 References

- Capdeville, Y., E. Chaljub, J.P. Vilotte and J.P. Montagner, Coupling the spectral element method with a modal solution for elastic wave propagation in global Earth models. *Geophys. J. Int.*, 152, 34-66, 2003.
- Durek, J.J. and G. Ekström, A radial model of anelasticity consistent with long-period surface-wave attenuation. *BSSA*, 86, 144-158, 1996.
- Dziewonski, A.M. and D.L. Anderson, Preliminary reference Earth model. *Phys. Earth and Planetary Int.*, 25, 297-356, 1981.
- Gung, Y. and B. Romanowicz., Q tomography of the upper mantle using three-component long-period waveforms. *Geophys. J. Int.*, 157, 813-830, 2004.
- Li, X.D. and B. Romanowicz, Comparison of global waveform inversions with and without considering cross-branch modal coupling, *Geophys. J. Int.*, 121, 695-709, 1995.
- Megnin, C. and B. Romanowicz, The three-dimensional shear velocity structure of the mantle from the inversion of body, surface and higher-mode waveforms. *Geophys. J. Int.*, 143, 709-728, 2000.
- Panning, M. and B. Romanowicz, A three-dimensional radially anisotropic model of shear velocity in the mantle. *Geophys. J. Int.*, in press, 2006.

26. Radial and Azimuthal Anisotropic Structure of the North American Upper Mantle From Inversion of Surface Waveform Data

Federica Marone and Barbara Romanowicz

26.1 Introduction

Seismic anisotropy is required for a correct interpretation of the retrieved S -velocity structure in tomographic studies at least in the first 400 km of the upper mantle (Gung *et al.*, 2003). A detailed knowledge of the seismic anisotropic structure of the earth’s mantle also provides insight into paleo and recent deformation processes and therefore mantle dynamics. As a consequence, seismic anisotropy is a very powerful “tool” with the potential to shed light onto debated geophysical issues, such as the nature and strength of the lithosphere/asthenosphere coupling, the depth extent of continental sub-regions and the relation of imaged seismic anisotropy to present-day asthenospheric flow and/or past tectonic events recorded in the lithosphere.

To date, our knowledge of the North American upper mantle anisotropic structure arises mainly from global tomographic models (e.g. Ritsema *et al.*, 1999; Gung *et al.*, 2003) or SKS splitting studies (e.g. Fouch *et al.*, 2000; Savage and Sheehan, 2000), which lack horizontal and vertical resolution respectively, and are limited to either radial or azimuthal anisotropy. It is most probably due to these limitations that to date continental anisotropic models derived from surface and body wave data are not in agreement and cannot be reconciled.

Our goal is a new high resolution model for the North American upper mantle incorporating both radial and azimuthal anisotropy. We aim at unprecedented lateral and depth resolution by improving both data coverage and methodology.

26.2 Dataset

We consider fundamental and overtone surface waveforms selected from 3 component long period seismograms. Surface wave data for paths relevant to the study region have been extracted from the existing compilation used for global tomography in Panning and Romanowicz (2006). This dataset has been further complemented with waveforms from events at teleseismic and far regional distances ($15^\circ < \Delta < 165^\circ$) recorded at permanent and temporary broad band seismic stations in North America. The collected dataset includes data for 657 events from 1990 to 2003, with M_w between 6.0 and 7.0. Each seismogram is filtered (between 60 s and 220 s to 1 hour, according to the event magnitude) and divided into wavepackets containing individual fundamental and higher mode first orbit energy packets. Each wavepacket is weighted so as to equalize the contribution of large and

small amplitude packets in the least-squares inversion. Our final dataset consists of more than 18,000 fundamental mode and 27,000 higher modes high quality surface wave packets, which provides a fairly homogeneous path and azimuthal coverage for North America.

In addition, we compiled station average SKS splitting measurements (delay times dt and fast axis directions ϕ and their uncertainties) from published studies for about 300 North American stations.

26.3 Methodology

We apply a full waveform tomographic method based on the Non-linear Asymptotic Coupling Theory (NACT - Li and Romanowicz (1995)), which permits the inversion of entire long period seismograms in the time domain (including fundamental mode and overtones portions of the record) for 3D elastic structure. NACT is a normal-mode perturbation approach, which takes into account coupling between modes both along and across dispersion branches. The asymptotic calculation of this coupling allows the computation to 2D broad band sensitivity kernels which more rigorously reproduce the sensitivity of body waveforms to structure along and around the ray geometrical path in the vertical plane containing the source and the receiver.

To ensure high quality of the retrieved regional upper mantle structure, accurate crustal corrections are essential. Here, we follow an approach which goes beyond the linear perturbation approximation and split the correction into a linear and non-linear part (Montagner and Jobert, 1988).

We followed an iterative inversion approach. In a first step, we inverted waveform data simultaneously for perturbations in the isotropic S -velocity structure and the anisotropic parameter $\xi = v_{SH}^2/v_{SV}^2$. While keeping this obtained radial anisotropic model fixed, in a second step we inverted the waveform dataset jointly with the compiled SKS splitting measurements for two additional parameters related to the dominant 2Ψ azimuthal dependence of the propagation velocity of surface waves (Montagner *et al.*, 2000; Marone and Romanowicz, 1996a).

26.4 Results

Our 3D radial anisotropic model (Marone *et al.*, 2006b) shares the large scale features of previous regional studies for North America (e.g. Van der Lee and Nolet, 1997; Grand, 2001). We confirm the pronounced difference in the isotropic velocity structure (Figure 3.54a) between

the western active tectonic region and the central/eastern stable shield, as well as the presence of subducted material (Juan de Fuca and Farallon plate) at transition zone depths. Concerning the radial anisotropic signature (Figure 3.54b), we observe a positive ξ anomaly in correspondence of the cratonic areas down to 300 km depth, while a negative ξ anomaly beneath the Appalachians mapped at 250 km depth, where a low velocity feature is also present, supports the hypothesis of mantle upwelling induced by water released during subduction of the Iapetus ocean or related to the subducted Farallon plate (Van der Lee *et al.*, 2005).

Our 3D azimuthal anisotropic model (Figure 3.54c) indicates the presence of two layers of anisotropy with distinct fast axis directions under the stable part of the North American continent: a deeper layer with the fast axis direction aligned with the absolute plate motion direction suggesting lattice preferred orientation of anisotropic minerals in a present day asthenospheric flow and a shallower lithospheric layer likely showing records of past tectonic events. Under the tectonically active western US, where the lithosphere is thin, the direction of tomographically inferred anisotropy is stable with depth and compatible with both absolute plate motion direction and the dominant direction obtained from *SKS* splitting measurements. The combined radial and azimuthal anisotropic 3D structure retrieved in our model, resolved throughout the upper mantle, represents the advancement of this study with respect to previous works. These new results seem to suggest a possible reconciliation between anisotropic models derived from surface and body wave data.

26.5 Acknowledgements

This research was partially supported through a grant from the Stefano Frascini Foundation (Switzerland) and NSF-EAR (Earthscope) grant #0345481. The digital seismograms used in our work have been distributed by the IRIS-DMC, the Geological Survey of Canada and the Northern California Earthquake Data Center (data contributed by the Berkeley Seismological Laboratory, University of California, Berkeley).

26.6 References

Fouch, M.J., K.M. Fischer, E.M. Parmentier, M.E. Wysession and T.J. Clarke, Shear-wave splitting, continental keels, and patterns of mantle flow, *J. Geophys. Res.*, 105, 6255-6275, 2000.

Grand, S.P., Mantle shear structure beneath the Americas and surrounding oceans, *J. Geophys. Res.*, 99, 591-621, 1994.

Gung, Y., M. Panning and B. Romanowicz, Global anisotropy and the thickness of continents, *Nature*, 422, 707-711, 2003.

Li, X.D. and B. Romanowicz, Comparison of global waveform inversions with and without considering cross-branch modal coupling, *Geophys. J. Int.*, 121, 695-709, 1995.

Marone, F. and B. Romanowicz, Non-linear crustal corrections in high resolution regional waveform seismic tomography, *Geophys. J. Int.*, in revision, 2006a.

Marone, F., Y. Gung and B. Romanowicz, 3D radial anisotropic structure of the North American upper mantle from inversion of surface waveform data, *Geophys. J. Int.*, submitted, 2006b.

Montagner, J.-P. and N. Jobert, Vectorial tomography; II. Application to the Indian Ocean, *Geophys. J.*, 94, 309-344, 1988.

Montagner, J.-P., D.-A. Griot-Pommeroy and J. Lavé, How to relate body wave and surface wave anisotropy?, *J. Geophys. Res.*, 105(B5), 19015-19027, 2000.

Panning, M. and B. Romanowicz, A three dimensional radially anisotropic model of shear velocity in the whole mantle, *Geophys. J. Int.*, in press, 2006.

Ritsema, J., H. van Heijst and J. Woodhouse, Complex shear wave velocity structure imaged beneath Africa and Iceland, *Science*, 286, 1925-1928, 1999.

Savage, M.K. and A.F. Sheehan, Seismic anisotropy and mantle flow from the Great Basin to the Great Plains, western United States, *J. Geophys. Res.*, 105, 13715-13734, 2000.

Van der Lee, S. and G. Nolet, Upper mantle *S*-velocity structure of North America, *J. Geophys. Res.*, 102, 22815-22838, 1997.

Van der Lee, S., K. Regenauer-Lieb and D. Yuen, The role of water in connecting past and future episodes of subduction, *Eos Trans., AGU*, 86(52), Fall Meet. Suppl., 2005.

27. Improvements in Waveform Modeling and Application to Eurasian Velocity Structure

Mark Panning (now at Princeton), Federica Marone, Ahyi Kim, Yann Capdeville (IPG Paris), Paul Cupillard (IPG Paris), Yuancheng Gung (National Taiwan University), and Barbara Romanowicz

27.1 Introduction

We introduce several recent improvements to mode-based 3D and asymptotic waveform modeling and examine how to integrate them with numerical approaches for an improved model of upper-mantle structure under eastern Eurasia. There is considerable information on structure in broadband seismograms that is currently not fully utilized. With numerical techniques, such as the Spectral Element Method (SEM), it should be possible to compute the complete predicted wavefield accurately without any restrictions on the strength or spatial extent of heterogeneity. This approach, however, requires considerable computational power.

We have implemented an approach which relies on a cascade of increasingly accurate theoretical approximations for the computation of the seismic wavefield to develop a model of regional structure for the area of Eurasia located between longitudes of 30 and 150 degrees E, and latitudes of -10 to 60 degrees North. The selected area is very heterogeneous, but is well surrounded by earthquakes and a significant number of high quality broadband digital stations, making it an ideal area to test new methods.

27.2 Starting Model

The first step in our modeling approach is to create a large-scale starting model including shear anisotropy using Nonlinear Asymptotic Coupling Theory (NACT; *Li and Romanowicz, 1995*), which models the 2D sensitivity of the waveform to the great-circle path between source and receiver, but neglects the influence of off-path structure. We have recently improved this approach by implementing a new crustal correction scheme, which includes a non-linear correction for the difference between the average structure of several large regions from the global model with further linear corrections to account for the local structure at each point along the path between source and receiver (*Marone and Romanowicz, 2006; Panning and Romanowicz, 2006*).

We inverted a global dataset augmented by additional data collection for paths which cross the region. To use the global dataset, we correct for structure outside the region using a global anisotropic starting model, SAW642AN (*Panning and Romanowicz, 2006*). The model in the region includes isotropic S structure parameterized in level 6 spherical splines, which correspond to a lateral resolution of ~ 200 km (figure 3.55).

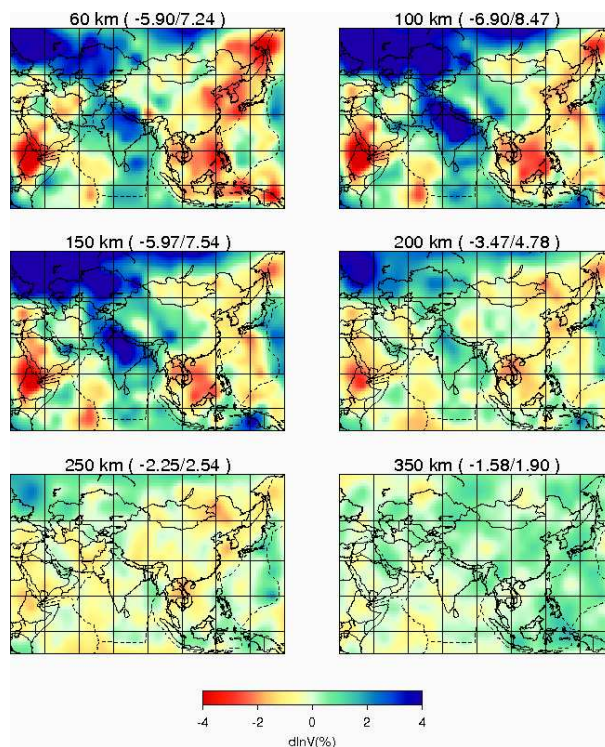


Figure 3.55: Starting isotropic S velocity model for the upper mantle for Eurasia developed using NACT. Values are the percent perturbations in isotropic velocity from PREM. Model is parameterized in radial splines spaced approximately 100 km, and in level 6 spherical splines (spacing ~ 200 km).

It also includes anisotropy through the parameter $\xi = (V_{SH})^2 / (V_{SV})^2$. This is parameterized with a lateral resolution of ~ 400 km (not shown here).

27.3 3D Born approximation

This model is further refined using a 3D implementation of Born scattering (*Capdeville, 2005*). We have made several recent improvements to this method, such as including perturbations to discontinuities. While the approach treats all sensitivity as linear perturbations to the waveform, we have also experimented with a non-linear modification to the approach analogous to that used in development of NACT. This modification allows us to treat large accumulated phase delays determined from a path-average approximation non-linearly, while

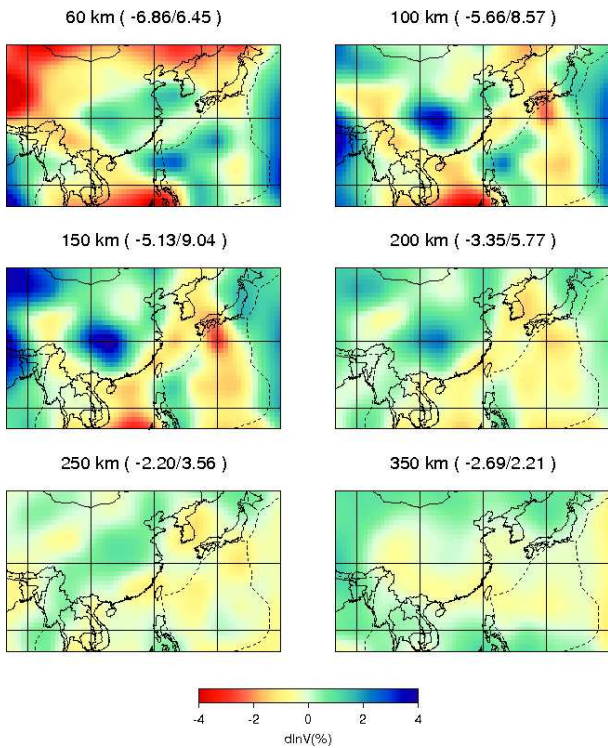


Figure 3.56: Shear velocity model developed using linear Born kernels for 180 events recorded on the vertical component. Values shown are perturbations relative to the isotropic average of the reference model.

still using the full 3D sensitivity of the Born scattering approximation.

We have performed some preliminary modeling of a subregion between longitudes 90 and 145 degrees E, and latitudes 15 and 40 degrees N with a subset of the original dataset consisting of the vertical component data from source-receiver pairs contained within the large region. The preliminary model is a relatively low resolution (~ 400 km) isotropic velocity model. We show the model derived using the Born approximation with (figure 3.56) and without the non-linear correction (figure 3.57). In these preliminary models, it is difficult to determine which model is better able to image the anomalies.

27.4 Numerical approaches

In preparation for the next step in the modeling, we have adapted to the regional case the Spectral Element Method (SEM) code (e.g. *Komatitsch and Vilotte, 1998*). The regionalization is performed by limiting the lateral and radial extent of the volume of interest through the implementation of Perfectly Matched Layers (PML) which effectively eliminate spurious reflections from the boundaries. This code now works for 3D regional models, and will be integrated into the forward modeling of our

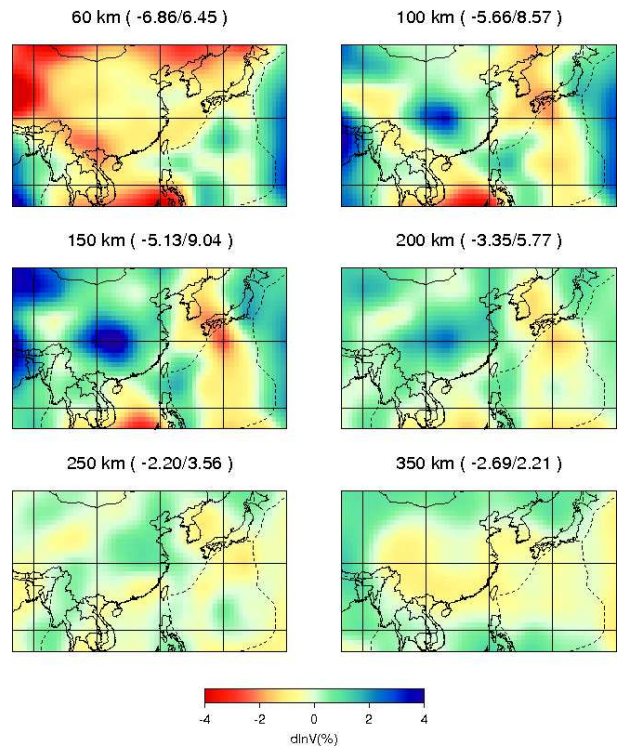


Figure 3.57: Same as figure 3.56 for the model developed using the non-linear Born partial derivatives.

inverse method to further improve our modeling.

27.5 Acknowledgements

This project has been funded through the Dept. of Energy, National Nuclear Security Administration, contract no. DE-FC52-04NA25543

27.6 References

- Capdeville, Y., An efficient Born normal mode method to compute sensitivity kernels and synthetic seismograms in the Earth, submitted to *Geophys. J. Int.*, 2005.
- Komatitsch, D. and J. P. Vilotte, The spectral element method: an effective tool to simulate the seismic response of 2D and 3D geological structures, *Bull. Seism. Soc. Am.*, 88, 368-392, 1998
- Li, X.D. and B. Romanowicz, Comparison of global waveform inversions with and without considering cross-branch modal coupling, *Geophys. J. Int.*, 121, 695-709, 1995.
- Marone, F. and B. Romanowicz, Non-linear crustal corrections in high resolution regional waveform seismic tomography, *Geophys. J. Int.*, in revision, 2006.
- Panning, M.P. and B. Romanowicz, A three-dimensional radially anisotropic model of shear velocity in the whole mantle, *Geophys. J. Int.* online early, doi: 10.1111/j.1365-246X.2006.03100.x, 2006.

28. Toward Constraints on Lateral S Wave Velocity Gradients around the Pacific Superplume

Akiko To, Barbara Romanowicz

28.1 Introduction

Global shear velocity tomographic models show two large-scale low velocity structures in the lower mantle, under southern Africa and under the mid-Pacific. While tomographic models show the shape of the structures, the gradient and amplitude of the anomalies are yet to be constrained. By forward modeling of Sdiffracted phases using the Coupled Spectral Element Method (CSEM, Capdeville *et al.*, 2003), we have previously shown that observed secondary phases following the Sdiff can be explained by interaction of the wavefield with sharp boundaries of the superplumes in the south Indian and south Pacific oceans (To *et al.*, 2005). We search for further constraints on velocity gradients at the border of the Pacific superplume all around the Pacific using a multi-step approach.

28.2 Preliminary Results

We have assembled a large dataset of Sdiff waveforms and travel time throughout the Pacific region. As shown in Fig.3.58, the new dataset has more sampling than the original one especially in the south Pacific. The original dataset was used to construct the original model, SAW24b16 (Méglin and Romanowicz, 2000). We first apply a finite frequency tomographic inversion methodology (NACT, Li and Romanowicz, 1996), which provides a good starting 3D model. In particular, the inversion method allows us to position the fast and slow anomalies and their boundaries quite well, as has been shown previously, but underestimates the gradients and velocity contrasts. The result of the inversion using the newly obtained dataset shows shrinking of the Pacific superplume area in its northern and southern edge (Fig.3.59). Based on this starting model, we will perform forward modeling to search for further constraints on the gradients at the boundary of the Pacific superplume.

28.3 Acknowledgements

The data were downloaded from IRIS DMC and CNSN.

28.4 References

Li, X.D. and B. Romanowicz, Global mantle shear-velocity model developed using nonlinear asymptotic coupling theory, *Geophys. J. R. Astr. Soc.*, 101, 22,245-22,272, 1996.

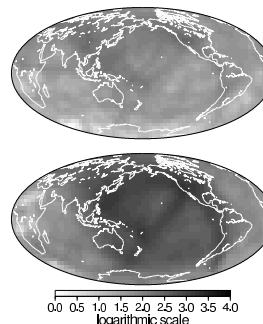


Figure 3.58: Sampling density of the collected Sdiff data. Top: The Sdiff phase raypath distribution of the previously collected dataset. The data is used in the construction of the original model, SAW24B16. Bottom: The raypath distribution of the newly obtained dataset. Compared to the previous dataset, there are more samplings in the south Pacific.

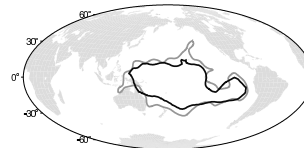


Figure 3.59: Contours of the Pacific superplume. Gray line: Original model, SAW24B16. Black line: New model, obtained from the recently collected dataset. The lines are the contour lines of -0.4% S velocity anomaly at a depth of 2820km. The east sides of the contours overlap each other, whereas the contours are shifted on the north and south side in the new model.

Méglin C. and B. Romanowicz, The three-dimensional shear velocity structure of the mantle from the inversion of body, surface and higher-mode waveforms. *Geophys. J. Int.*, 143, pp. 709-728, 2000

Capdeville, Y., A. To and B. Romanowicz, Coupling spectral elements and modes in a spherical earth: an extension to the "sandwich" case, *Geophys. J. Int.*, 154, 44-57, 2003

To, A., B. Romanowicz, Y. Capdeville and N. Takeuchi, 3D effects of sharp boundaries at the borders of the African and Pacific Superplumes: observation and modeling, *Earth and Planet. Sci. Lett.*, 233, 137-153, 2005

29. Joint Inversion for 3D Velocity Structure of the Broader Africa-Eurasia Collision Region

Suzan van der Lee (Northwestern University), Heather Bedle (Northwestern University), Megan Flanagan (LLNL), Eric Matzel (LLNL), Michael Pasyanos (LLNL), Federica Marone, Barbara Romanowicz, Christian Schmid (ETH Zurich), Arthur Rodgers (LLNL),

29.1 Introduction

The need to monitor broader areas and an increasing number of nations with nascent nuclear weapons programs has led to major challenges to nuclear explosion monitoring research. Agencies must, in fact, be prepared to detect, identify and locate nuclear explosions in wide regions, often aseismic and lacking previous seismic observations. Since the 1980's, the importance of monitoring at regional distances has been well established. However, such monitoring is complicated by the passage of seismic waves through the structurally complex crust and uppermost mantle. As a consequence, traveltimes and amplitudes of regional phases show great variability leading to large uncertainties in event locations and decreased performance of regional discriminants. A major requirement for the accurate modeling of regional seismic data, and therefore improved event locations and regional discriminant performance, are 3D regional velocity models characterized by high resolution from the crust down to the transition zone.

Our aim is a 3D velocity model of the crust and upper mantle for the geographic region extending from the western Mediterranean to Pakistan, including the aseismic region of North Africa. The joint inversion of different types of seismic data with diverse sensitivity to the crust and mantle is essential to achieve a high resolution image of the structure in this tectonically complex area, where six major tectonic plates and several microplates interact with each other. We expect predictions for seismogram characteristics (phase arrival times, amplitudes, dispersion) based on this new model to match most observations and be useful for event discrimination. Simultaneously, the new model will refine our understanding of the structure and tectonics in the study region.

29.2 Technical approach and dataset

Our 3D S -velocity model will be derived from the joint inversion of regional waveform fits, surface wave group velocity measurements, teleseismic arrival times of S and P waves, receiver functions and published results from active source experiments. The strength of jointly using various datasets lies in their redundancy (increase in the results accuracy) and complementarity (resolving power increase and trade-offs reduction).

The fitting of regional fundamental and higher mode Rayleigh waveforms has been accomplished using the Partitioned Waveform Inversion method (Nolet, 1990)

for thousands of paths covering the study area (Figure 3.60). The modeling of both fundamental and higher mode surface waveforms ensures resolution of the entire upper mantle structure down to the transition zone. The inclusion in the inversion of teleseismic arrival times will further boost the resolving power at mid and deep upper mantle levels, while group velocity measurements and constraints on crustal thickness from active-source literature and receiver function analysis will ensure high resolution in the shallow upper mantle.

The seismograms used in this work have been recently recorded by a variety of different stations and networks, both permanent and temporary, operating in the study region: MIDSEA deployment, Kuwait National Seismic Network (KNSN), the United Arab Emirates (UAE) Broadband deployment, the Jordan deployment, the Eastern Turkey Seismic Experiment (ETSE), the Caspian Broadband deployment, the Global Seismic Network (GSN), the International Monitoring System (IMS), MedNet and Geofon. While each of these waveform datasets is valuable on its own, their combination is unique and key to this study.

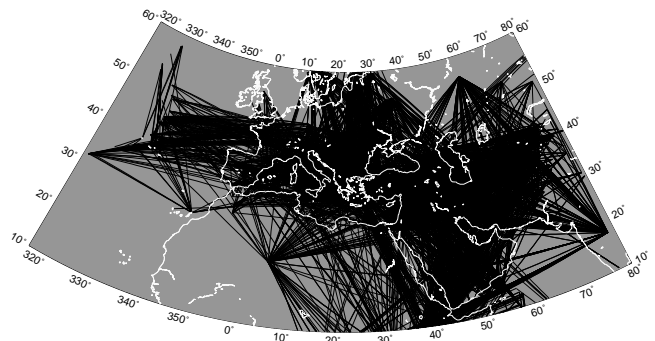


Figure 3.60: Great circle wave paths for the vertical and radial component seismograms used in this study to date.

29.3 Preliminary results

The broad consistency between seismic velocity anomalies inferred from existing and performed measurements of teleseismic arrival times and Rayleigh wave group velocities as well as from regional waveform fits implies that these different types of dataset are at least in part redundant. The consistency further shows that the datasets record the same structural phenomena, despite

differences in size and character between typical sensitivity kernels for each dataset.

The preliminary model (Figure 3.61) obtained by jointly inverting linear constraints provided by the performed waveform fits and collected point constraints on crustal thickness from active-source seismic studies and receiver function analysis shows that the uppermost mantle in the study area is strongly heterogeneous, reflecting the complex tectonics of this region. Particularly low velocities are observed at 100km depth beneath the Mid-Atlantic Ridge, the East African Rift and the western Mediterranean basin. Lower velocities than average are also present deeper (150-200 km) beneath Turkey and western Arabia. High velocity mantle material has been imaged at 100 km depth in correspondence with the Russian Platform and the Ukraine Shield. Linear high velocity features, possibly representing subducted material, are observed in the central Mediterranean basin (Italy and Greece) and beneath the Zagros Mountains Range in Iran (e.g. at 150 km depth).

The observed large scale features of our preliminary model are in agreement with existing regional models (e.g. *Marone et al., 2004; Maggi and Priestley, 2005*).

29.4 Future of the project

Our final 3D S -velocity model will be derived from the joint inversion of regional waveform fits, surface wave group velocity measurements, teleseismic arrival times of S and P waves, receiver functions and published results from active source experiments. This model will be converted to a 3D P -velocity model, using both published data on elastic properties (and their partial derivatives with temperature and pressure) of mantle rocks and empirical information provided by measured arrival times of teleseismic P and Pms waves. This new P -wave model will provide an improved ability to locate seismic events.

The prediction and calibration of regional traveltimes and waveforms depend strongly on the methodology used to compute synthetic traveltimes and waveforms from a 3D velocity model. Our goal is to test the obtained S - and P -wave models' ability to predict regional P and S traveltimes, deflect wave paths and deform waveforms using different approximations (e.g. path average vs. exact numerical approaches). We will assess the effects of 3D heterogeneities first on the studied seismograms (traveltimes and waveforms) and subsequently on the 3D models derived from these data.

29.5 Acknowledgements

This work has been financially supported by the National Nuclear Security Administration, Office of Nonproliferation Research and Engineering and Office of Defense Nuclear Nonproliferation (DE-FC52-04NA25542).

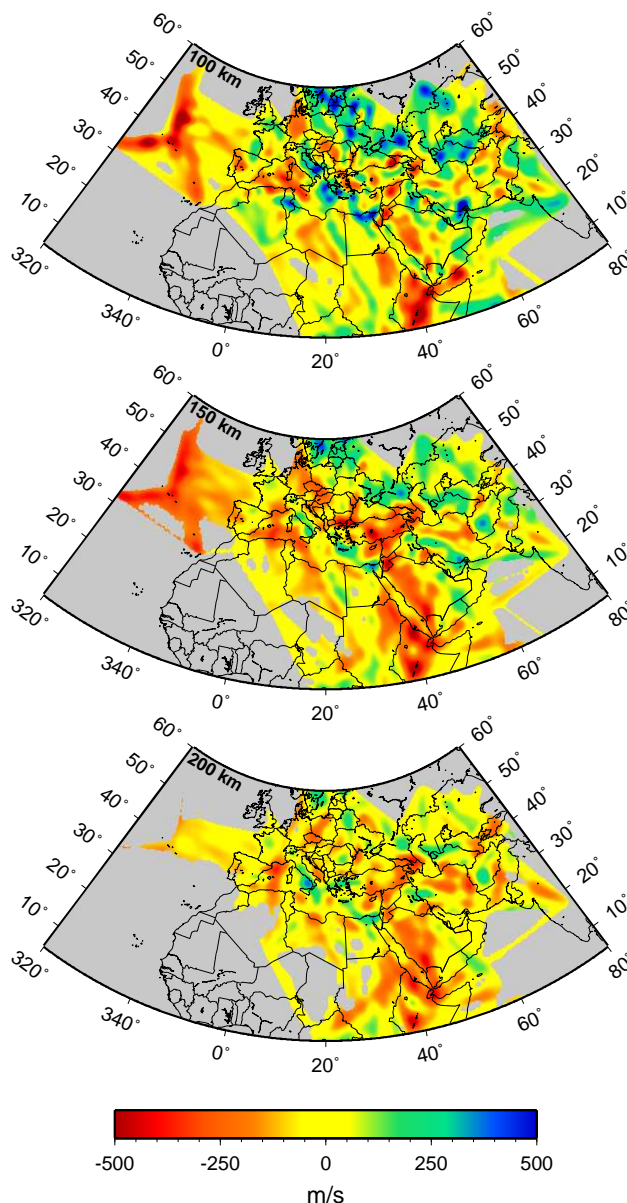


Figure 3.61: Horizontal slices at different depths through our preliminary upper mantle model. Anomalies are relative to a 1D average model for the Mediterranean region.

29.6 References

- Maggi, A. and K. Priestly, Surface waveform tomography of the Turkish-Iranian Plateau, *Geophys. J. Int.*, 160, 1068-1080, 2005.
- Marone, F., S. van der Lee and D. Giardini, 3-D upper mantle S -velocity model for the Eurasia-Africa plate boundary region, *Geophys. J. Int.*, 158, 109-130, 2004.
- Nolet, G., Partitioned waveform inversion and two-dimensional structure under the network of autonomously recording seismographs, *J. Geophys. Res.*, 95, 8499-8512, 1997.

30. A Three Dimensional Radially Anisotropic Model of Shear Velocity in the Whole Mantle

Mark Panning (now at Princeton) and Barbara Romanowicz

30.1 Introduction

The 3D seismic velocity structure of the Earth’s mantle represents a snapshot of its current thermal and chemical state. As tomographic models of the isotropic seismic velocity converge in their main features (*Masters et al., 2000; Mégnin and Romanowicz, 2000; Ritsema and van Heijst, 2000; Gu et al., 2001*), geodynamicists can use them to infer the density structure, and thus the buoyancy contrasts which drive mantle convection. This process, however, is complicated by the difficulty of separating thermal and chemical contrasts, and the lack of direct sensitivity of seismic velocities to the density contrasts which drive the convection.

In many regions of the mantle, analyzing the anisotropy of seismic velocities can give us another constraint on mantle dynamics. Random orientations of the anisotropic minerals which make up the mantle tend to cancel out on the macroscopic scale observable by seismic waves, unless crystals or materials with strongly contrasting elastic properties are aligned through deformation processes. While in the relatively cold regions of the lithosphere these anisotropic signatures can remain frozen in over geologic time-scales (*Silver, 1996*), observed anisotropy at greater depths likely requires dynamic support (*Vinnik et al., 1992*). Thus, the anisotropy observed at sub-lithospheric depths is most likely a function of the current mantle strain field, and these observations can help us map out mantle flow.

30.2 Model results

We have developed a 3D radially anisotropic S velocity model of the whole mantle (SAW642AN; *Panning and Romanowicz, 2006*), obtained using a large three component surface and body waveform dataset and an iterative inversion for structure and source parameters based on Nonlinear Asymptotic Coupling Theory (NACT) (*Li and Romanowicz, 1995*). The model is parameterized in level 4 spherical splines, which have a spacing of ~ 800 km. The model shows a link between mantle flow and anisotropy in a variety of depth ranges.

In the uppermost mantle, we confirm previous observations of regions with $V_{SH} > V_{SV}$ starting at ~ 80 km under oceanic regions and ~ 200 km under stable continental lithosphere (*Gung et al., 2003*), suggesting horizontal flow beneath the lithosphere (figure 3.62). We also observe a $V_{SV} > V_{SH}$ signature at ~ 150 -300 km depth beneath major ridge systems with amplitude correlated with spreading rate for fast-spreading segments. In the transition

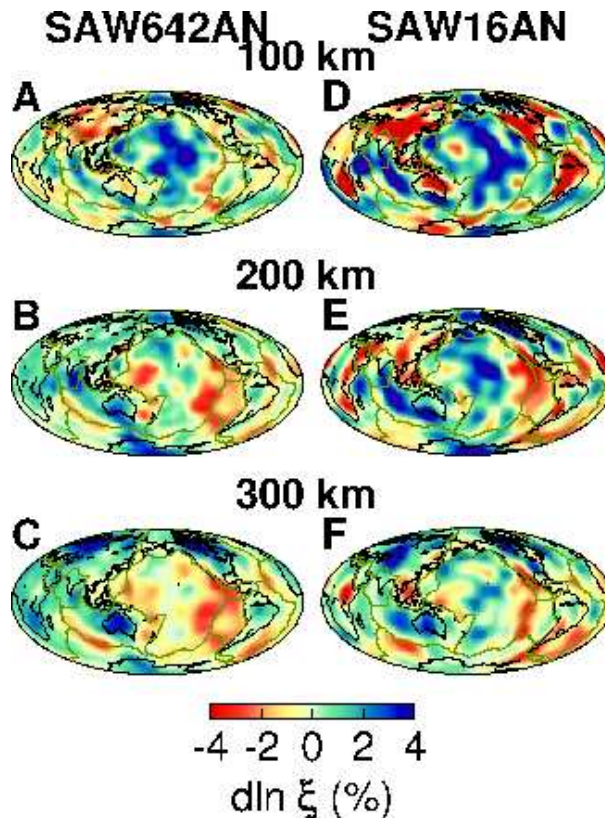


Figure 3.62: Comparison between SAW642AN ξ (A-C) and the upper mantle ξ calculated from SAW16AN (*Gung et al., 2003*) (D-F) at depths of 100 (top), 200 (middle), and 300 km (bottom).

zone (400-700 km depth), regions of subducted slab material are associated with $V_{SV} > V_{SH}$ (figure 3.63), while the ridge signal decreases. We also confirm the observation of radially symmetric $V_{SH} > V_{SV}$ in the lowermost 300 km (*Panning and Romanowicz, 2004*). The 3D deviations from this signature (figure 3.64) are associated with the large-scale low-velocity superplumes under the central Pacific and Africa, suggesting that $V_{SH} > V_{SV}$ is generated in the predominant horizontal flow of a mechanical boundary layer, with a change in signature related to transition to upwelling at the superplumes.

30.3 Acknowledgements

This research was supported by NSF grant EAR-0308750.

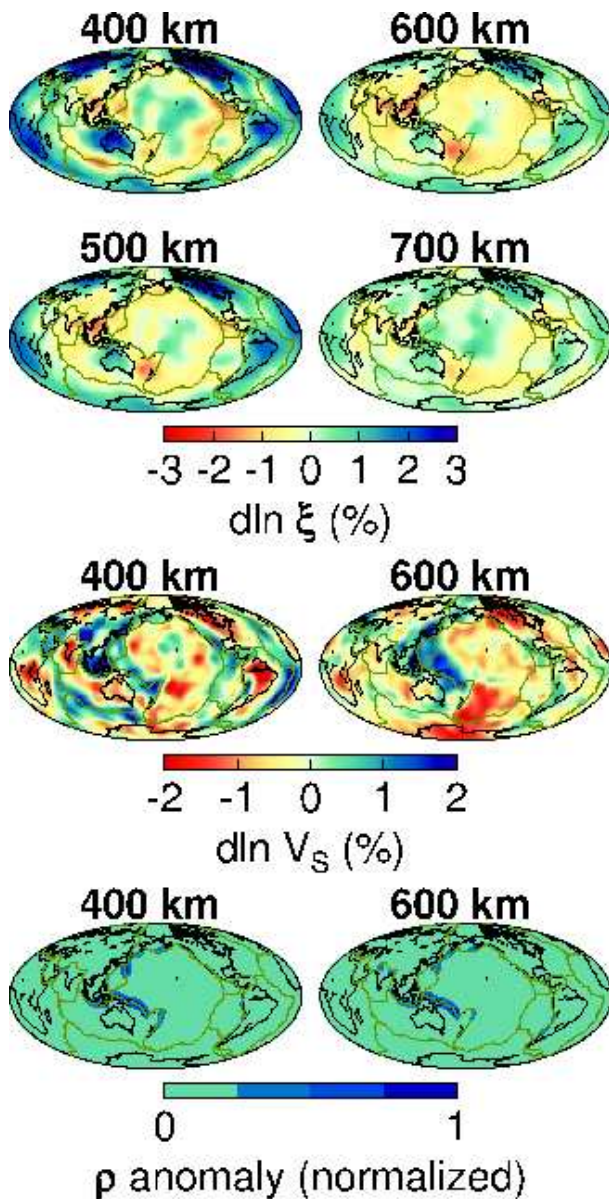


Figure 3.63: ξ structure at depths 400-700 km (top two rows) and V_S at depths of 400 and 600 km (third row). The bottom row shows the density anomalies for layers centered at depths of 362.5 km (left) and 652.5 km (right) for the model of Lithgow-Bertelloni and Richards (1998), normalized to the maximum density anomaly in each depth range.

30.4 References

Gu, Y.J., A.M. Dziewonski, W. Su, and G Ekström, Models of the mantle shear velocity and discontinuities in the pattern of lateral heterogeneities, *J. Geophys. Res.*, **106**, 11,169-11,199, 2001.

Gung, Y., M. Panning and B. Romanowicz, Global anisotropy and the thickness of continents, *Nature*, **422**,

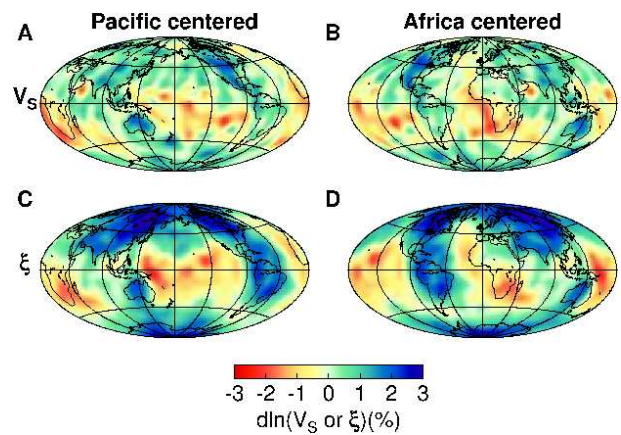


Figure 3.64: V_S (A,B) and ξ structure (C,D) at a depth of 2800 km centered under the central Pacific (A,C) and Africa (B,D)

707-711, 2003.

Li, X.D. and B. Romanowicz, Comparison of global waveform inversions with and without considering cross-branch modal coupling, *Geophys. J. Int.*, **121**, 695-709, 1995.

Lithgow-Bertelloni, C. and M. Richards, The dynamics of Cenozoic and Mesozoic plate motions, *Rev. Geophys.*, **36**, 27-78, 1998.

Masters, G., G. Laske, H. Bolton and A. Dziewonski, The relative behavior of shear velocity, bulk sound speed, and compressional velocity in the mantle: implications for chemical and thermal structure, in *Earth's Deep Interior*, AGU Monograph 117, pp. 63-86, eds. Karato, S., A.M. Forte, R.C. Liebermann, G. Masters and L. Stixrude, Amer. Geophys. Union, Washington, D.C., 2000.

Mégnin, C., and B. Romanowicz, The 3D shear velocity of the mantle from the inversion of body, surface, and higher mode waveforms, *Geophys. J. Int.*, **143**, 709-728, 2000.

Panning, M.P. and B. Romanowicz, A three-dimensional radially anisotropic model of shear velocity in the whole mantle, *Geophys. J. Int.* online early, doi: 10.1111/j.1365-246X.2006.03100.x, 2006.

Ritsema, J. and H.-J. van Heijst, Seismic imaging of structural heterogeneity in Earth's mantle: evidence for large-scale mantle flow, *Science Progress*, **83**, 243-259, 2000.

Silver, P.G., Seismic anisotropy beneath the continents: probing the depths of geology, *Annu. Rev. Earth Planet. Sci.*, **24**, 385-432, 1996.

Vinnik, L.P., L.I. Makeyeva, A. Milev and Y. Usenko, Global patterns of azimuthal anisotropy and deformations in the continental mantle, *Geophys. J. Int.*, **111**, 433-447, 1992.

31. Short Wavelength Topography on the Inner Core Boundary

Aimin Cao, Yder Masson, and Barbara Romanowicz

31.1 Introduction

The ICB separates the liquid outer core from the solid inner core and is the site of important dynamical processes, as the core freezes and light elements are expelled to power convection in the outer core (*Glatzmeier and Roberts, 1995*). Significant long wavelength topography of the ICB is ruled out by dynamical considerations (*Buffett, 1997*). While hemispherical variations in the seismic properties at the top of the inner core have been documented, seismological investigations indicate that the ICB is, to a good approximation, quite spherical. However, the observation of significant PKiKP coda, likely due to multiple scattering (*Poupinet and Kennett, 2004*), indicates that the structure of the ICB is more complex at short wavelengths. There is also evidence for significant scattering near the top of the inner core (*Vidale and Earle, 2000*). Recently, in a study of amplitudes of ICB reflected phases (PKiKP), *Krasnoshchekov et al. (2005)* have proposed that the ICB is “patchy” in its reflective properties at scales of 10-200km laterally. Because their data were obtained at sub-critical distances, these authors could not constrain the precise nature of the variability in the measured PKiKP amplitudes.

In their efforts to constrain the rate of differential rotation of the inner core previously estimated using PKP(DF-BC) differential travel times on paths to Alaska stations in the epicentral distance range $147-155^\circ$, *Zhang et al. (2005)* found several high quality earthquake doublets in the South-Sandwich region, separated in time by a decade or more. The high waveform similarity at many stations indicates that the two sources are located within a wavelength for compressional waves. One of the earthquake doublets reported in the *Zhang et al.* study is of exceptional quality (Dec 1, 1993/ Sep 6, 2003). Highly similar waveforms for both events were recorded at 102 stations with a broad coverage of epicentral distances and azimuths, and the hypocenter separation of the two events was inferred to be 100 m vertically and less than 1.0 km horizontally.

31.2 Data, Method, and Results

We found that this doublet was also well recorded on the short-period Yellowknife Seismograph Array (YK) in northern Canada, which is located in an optimal position for the study of mantle phases PP as well as both refracted (PKIKP) and post-critically reflected (PKiKP) core phases. Indeed, these phases are emitted near the maximum in the lobe of the doublet’s radiation pattern (Figure 3.65), at an epicentral distance of 137.8° , where

the two core phases are well separated and where the PKiKP undergoes total reflection. High signal-to-noise seismic waveforms were recorded for both events at eighteen of the nineteen YK stations. In a 50-second time window around the PP phases of the doublet, unfiltered waveforms are very highly similar at all stations of the array, with cross-correlation coefficients larger than 0.97. The amplitudes of PP for both events differ only by a factor of 1.05. This provides strong additional confirmation of the high quality of this doublet. We therefore expect the waveforms of other phases to be very similar in shape and amplitude for this special doublet.

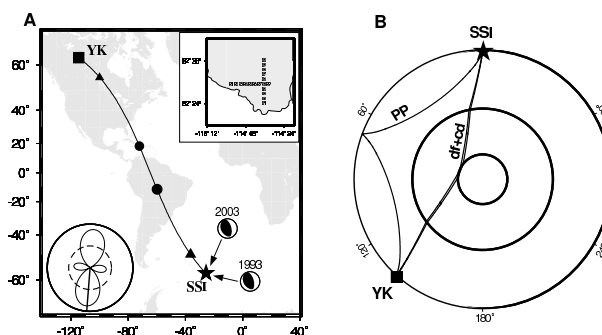


Figure 3.65: (A) Yellowknife Seismic Array (YK) and the doublet. The 19 stations of the array form two arms, one along a lake (shore indicated) and one orthogonal to it. Its aperture is 25 km with a station interval of 2.5 km (upper-right inset). The doublet consists of two South Sandwich Islands (SSI) events at an epicentral distance of 137.8° : Dec 1, 1993, $m_b=5.5$, depth=33 km according to the PDE catalog; and Sept. 6, 2003, $m_b=5.6$, depth=33 km according to the PDE catalog. According to Harvard CMT (<http://www.seismology.harvard.edu>), scalar moments and depths are ($M_o=3.53 \times 10^{24}$ dyne-cm, $h=45$ km) and ($M_o=4.02 \times 10^{24}$ dyne-cm, $h=44$ km), respectively. The lower-left inset is the P-wave radiation pattern of the doublet based Harvard CMT moment tensors. Black triangles and dots are entry (exit) points of PKIKP at the ICB and the CMB, respectively. (B) Ray paths of PP, PKIKP(df), and PKiKP(cd) phases used in this study.

However, the first two arrivals (PKIKP and PKiKP) in the individual unfiltered YK seismograms, which are well separated for both events, have significantly different waveforms (Figure 3.66A). For the 2003 event, the waveforms of PKiKP are simply reversed in polarity with respect to those of PKIKP as theoretically predicted

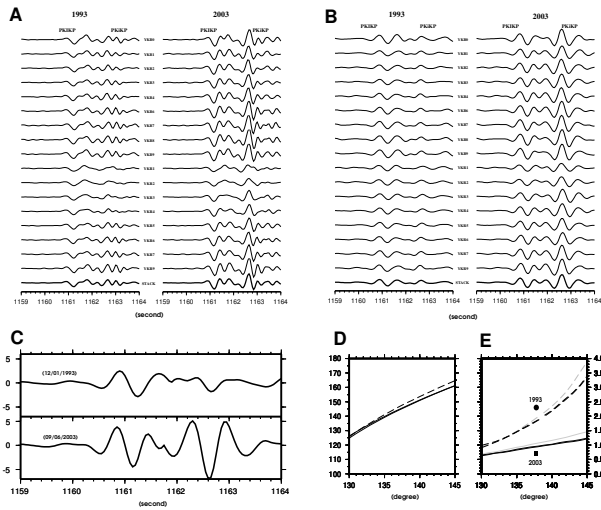


Figure 3.66: (A) Original waveform profile of PKIKP and PKiKP phases. For each event, waveforms are highly similar at most of stations except YKR1, YKR2, and YKR3 stations. These three stations are close to the lake, and they have a common feature for both events: site-related filtering of higher frequencies. (B) Bandpass filtered waveform profile of PKIKP and PKiKP phases (from 1.0 to 2.0 Hz). In this frequency range, waveforms of PKIKP and PKiKP are highly similar at all stations (including YKR1, YKR2, and YKR3) for each event. Also, waveform shapes of PKIKP and PKiKP for the 1993 event are more similar to those of the 2003 event. In this profile, it is obvious that phase shifts between PKiKP and PKIKP are close to 180° as predicted theoretically. (C) Linearly stacked waveforms of PKIKP and the reversed PKiKP phases after bandpass filtering (1-2Hz) showing the similarity of shape. Vertical broken line indicates place where the PKiKP waveform has been cut and reversed. The amplitude of PKIKP for 2003 event is 1.5 times larger than that for 1993 event; the amplitude of PKiKP for 2003 event is 7.2 times larger than that for 1993 event. Amplitude ratios of PKIKP to PKiKP are 2.3 (1993) and 0.7 (2003) event. (D) Theoretical phase shifts of PKiKP with respect to PKIKP based on PREM, IASPEI91, and AK135 reference models. In this study, the phase shift is $\sim 145^\circ$. (E) Theoretical amplitude ratios of PKIKP to PKiKP. Dashed lines are assuming that the inner core $Q_\alpha = \infty$ (i.e., no seismic attenuation in the inner core) based on the above three reference models. Solid lines are using $Q_\alpha = 445$ provided in PREM model. The black dot and square are observed amplitude ratios of PKIKP to PKiKP for the 1993 and 2003 events, respectively.

for post-critical reflections (Figure 3.66D). For the 1993 event, the amplitudes of PKiKP are much reduced (by a factor of 3.0). The later part of the PKiKP waveform also shows some change. In the frequency range 1-2 Hz, PKIKP and PKiKP waveforms of both events are simpler (Figure 3.66B), so that reversed waveforms of PKiKP are similar to those of PKIKP for both events (Figure 3.66B,C). In this frequency range, where the amplitude ratios can be determined more robustly, the amplitudes of PKiKP for 2003 and 1993 events differ by a factor of 7.2. Given the striking similarity of the PP waveforms and their coda, and the other evidence for the quality of the doublet, we infer that both phases (especially the PKiKP phase) have undergone temporal changes within 10 years.

This observation, complemented by data from several other doublets, indicates the presence of topography at the inner-core boundary, with a horizontal wavelength of about 10 km. Such topography could be sustained by small scale convection at the top of the inner core, and is compatible with a rate of super-rotation of the inner core of ~ 0.1 - 0.15 deg/year. In the absence of inner core rotation, decadal scale temporal changes in the ICB topography would provide an upper bound on the viscosity at the top of the inner core.

31.3 Acknowledgements

We thank the operators of Yellowknife Seismic Array and Canadian National Seismograph Network. This work was partially supported by the NSF.

31.4 References

Glatzmeier, G.A., P. H. Roberts, A three-dimensional self-consistent computer simulation of a geomagnetic field reversal, *Nature*, 377, 203, 1995.

Buffett, B.A., Geodynamic estimates of the viscosity of the earth's inner core, *Nature*, 388, 571, 1997.

G. Poupinet, B.L.N. Kennett, On the observation of high frequency PKiKP and its coda in Australia, *Phys. Earth Planet. Inter.*, 146, 497, 2004.

J.E. Vidale, P.S. Earle, Slow differential rotation of the Earth's inner core indicated by temporal changes in scattering, *Nature*, 404, 273, 2000.

D.N. Krasnoshechekov, P.B. Kaazik, V.M. Ovtchinnikov, Seismological evidence for mosaic structure of the surface of the Earth's inner core, *Nature*, 435, 483, 2005.

Zhang, J., et al., Inner core differential rotation confirmed by earthquake waveform doublets. *Science*, 309, 1357 2005.

32. Long Period Seismology on Europa

Fabio Cammarano, Mark Panning, Ved Lekic, Michael Manga, Barbara Romanowicz

32.1 Introduction

Seismological observations provide unparalleled capability for studying planetary interiors. While seismological studies of the Earth and, to a lesser extent, the Earth's Moon have placed strong constraints on the internal structure and dynamics of these bodies, the absence of seismic measurements on other planetary bodies has stymied analysis of their detailed structures. There are a wide variety of internal compositions and structures hinted at by recent exploration of the Jovian and Saturnian systems. In order to inform future mission design, it is important to determine what observations hold potential for answering outstanding questions concerning planetary interiors.

Physically consistent models of planetary bodies, constrained by moment of inertia measurements and by well-characterized elastic and anelastic properties of relevant minerals, make possible the study of the seismic response of planetary bodies, even when seismic measurements are not yet available.

Here, we summarize the main results of such interdisciplinary approach for the Jupiter's moon Europa. We develop a menagerie of physically consistent models of Europa (Cammarano *et al.*, 2006) which allows us to explore which seismic measurements on Europa have the potential to answer the many outstanding questions about its structure and current thermal state (Panning *et al.*, 2006).

32.2 Physically consistent interior models

We calculate a range of thermodynamically consistent models for the physical structure of Europa, as constrained by the satellite's mass and moment of inertia. We start with either a pyrolitic or a chondritic mantle composition and a core of either pure iron or iron plus 20% sulfur. The models completely characterize the radial seismic structure, i.e. elastic and anelastic properties, and they can be used to compute the seismic response of the planet.

The coupling between the thermal state of the ice shell and its viscosity dictates the ice-shell thickness and its seismic properties. It is likely that attenuation could be very high within the "warm", convective part of the ice shell. Due to the feedback between radiogenic and tidal heating, two extreme thermal profiles are possible in the mantle (see Figure 1). Strong dispersion and dissipation are expected in the hot convective mantle, while anelasticity effects will be much weaker in the case of the cold

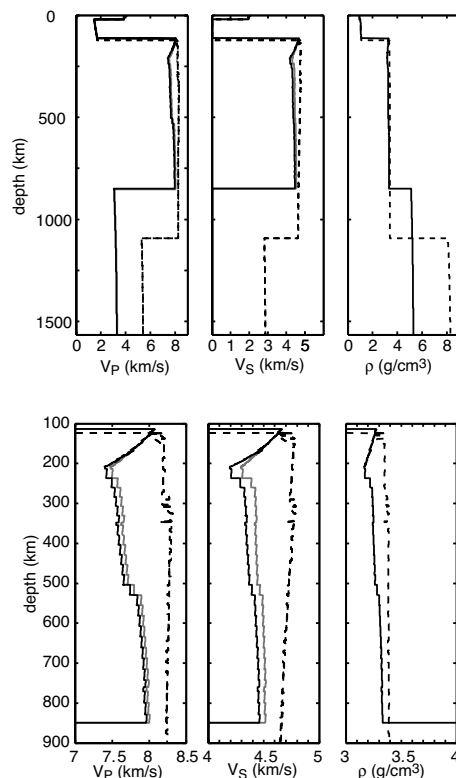


Figure 3.67: Physically consistent models for hot (solid lines) and cold (dashed) thermal structures with a pyrolitic mantle. Purely elastic models without dissipative effects are shown in light gray. The bottom panel shows a mantle close-up of the same models.

mantle. There is a strong relationship between different thermal structures and compositions. The "hot" mantle may well keep temperatures high enough to be consistent with a liquid core made of iron plus light elements. In the case of the "cold scenarios", the possibility of a solid iron core cannot be excluded and it may even be favored. The depth of the ocean and of the core-mantle boundary are determined with high precision once we assume a composition and thermal structure. Furthermore, the depth of the ocean is not very sensitive to the core composition used.

32.3 Predicted Seismic Response

The normal modes for the determined seismic radial structures of Europa are computed with the MINOS code (Woodhouse, 1988). Seismograms for any proposed

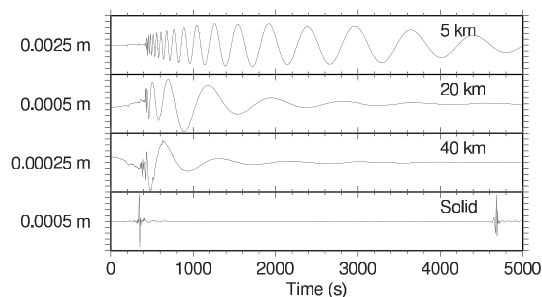


Figure 3.68: Synthetic displacement seismograms at a distance of 25° (680 km) from the $M_W = 5$ normal event. Seismograms are calculated for the low-attenuation cold chondritic model with ice shell thicknesses (from top) of 5, 20, 40, and a solid 137 km thick ice layer model. The maximum amplitude for each panel is shown to the left of the panel.

source and receiver configuration can then be modeled using normal mode summation, which models the complete broadband seismic wavefield. Given the normal mode catalogs and a predicted seismic source process, we can compute synthetic seismograms at any distance from the source. The seismograms presented here assume a $M_W = 5$ (seismic moment of 3.94×10^{16} Nm) normal faulting source, as proposed in *Nimmo and Schenk (2006)*. For simplicity, we used a dip-slip event with a 45° dip and 90° rake. We computed all modes up to 0.1 Hz, and then bandpass filtered the seismograms with corner frequencies at 12 and 800 seconds period, and cut-off frequencies at 10 and 1000 seconds period. We send to *Panning et al. (2006)* for a detailed discussion about measurement requirements and potential for answering questions on Europa's interior. Compared to high frequency signals, that require a surface installation, long-period measurements can be acquired potentially by an orbiter. Unless an orbiter is at the correct altitude for geosynchronous orbit, the seismic measurements will be made at a moving point on the surface. This presents additional challenges, but may provide us with interesting methods for determining surface wave velocities from a single measurement. To test this, we adapted the mode summation code to synthesize seismograms at a moving observation point. Seismic displacement from an event that occurs near the trajectory of the orbiter recorded on an observation point moving away from the source location produces a seismogram at sufficient time after the event with a resonant frequency (Figure 3). This resonance is caused by a wavepacket of a given frequency having a group velocity which closely matches the velocity of the observation point. Because the frequency at which the group velocity will match a given orbital velocity depends on the ice shell model, an observation of this resonance phenomenon may be diagnostic.

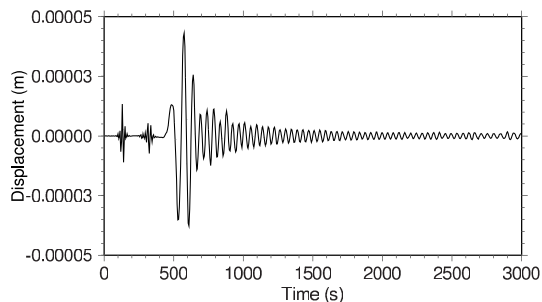


Figure 3.69: 3000 seconds of seismic displacement (in m) for an observation point that starts 15° (410km) east of the source at the event origin time, and moves north with an apparent surface velocity of 1.4 km/s calculated in the low attenuation 5 km thick ice shell model. The arrivals at about 120 s and 350 s are the P and S waves respectively.

32.4 Conclusions

Long-period seismic observations on Europa have potential to greatly expand our knowledge of the satellite. Long-period displacement measurements with millimeter accuracy may be able to determine the current tectonic activity of Europa's surface, the presence of a liquid ocean, and the thickness of the ice shell. These observations hold considerable promise relative to shorter period acceleration and velocity measurements, as the peak amplitudes occur at frequencies that minimize the complications from unknown 3D heterogeneity and finite source dimension and duration. Such displacement measurements may be possible from orbit, but many instrument design and data processing details need to be carefully considered. Determination of deeper structure with seismic measurements is much more difficult in the presence of a global liquid subsurface ocean, which acts to decouple deeper seismic energy from the surface.

32.5 References

- Cammarano, F., Lekic, V., Manga, M., Panning, M., Romanowicz, B. (2006) Long-period seismology on Europa: I. Physically consistent models, *J. Geophys. Res. - Planets*, in press.
- Nimmo, F., Schenk, P. (2006), Normal faulting on Europa: implications for ice shell properties, *J. Struct. Geol.*, in press.
- Panning, M., Lekic, V., Manga, M., Cammarano, F., Romanowicz, B. (2006) Long-period seismology on Europa: II. Predicted Seismic Response *J. Geophys. Res. - Planets*, in press.
- Woodhouse, J.H., (1988) The calculation of eigenfrequencies and eigenfunctions of the free oscillations of the Earth and the Sun, *Seismological Algorithms*, 321-370, ed. Doornbos, D.J.

33. Tidal Excitation of Free Oscillations of Icy Satellites

Vedran Lekic and Michael Manga

33.1 Motivation

Small bodies, lacking both significant heat of accretion and possessing large surface to volume ratios, were thought to lack significant internal sources of heat, and therefore to be geologically dead. However, exploration of Jovian and Saturnian systems by the Voyager spacecraft revealed that the surfaces of a number of satellites were actively modified by volcanic and tectonic processes. Europa, Jupiter’s third-largest satellite, is marked by many fractures, yet few craters, indicative of a geologically young, active surface. Subsequent study by the Galileo probe confirmed the existence of an ocean beneath its icy shell (*Kivelson et al.*, 2000). Images of Enceladus, a smallish moon of Saturn, revealed a highly reflective surface marked by large tectonic features. Recently, the Cassini probe found anomalously high temperatures at ice fractures near Enceladus’ south pole (*Spencer et al.*, 2006), and a diffuse plume of water molecules reaching hundreds of kilometers above the surface (*Hansen et al.*, 2006).

Tidal dissipation appears to be an important source of heat for the Galilean satellites, which are locked in orbital resonances which force orbital eccentricities. Eccentric orbits allow transfer of orbital/rotational energy to internal heat even for synchronously rotating satellites. The efficiency of this transfer is related to the anelasticity of the moon in question, which causes a phase lag between the tidal forcing and the resulting deformation, and is on the order of 10^{-4} (*Hussman and Spohn*, 2004). Tidal excitation of free oscillations may be a more efficient mechanism of tidal heating, but has heretofore been neglected, due to the assumption that frequencies of free oscillations are incompatible with those of tidal forcing.

Europa’s subsurface ocean is a potential habitat for life (e.g. *Marion et al.*, 2003). Orbital modeling that includes the effects of thermal dissipation indicates that heat dissipation within Europa has varied through time, causing the thickness of the liquid ocean to oscillate (e.g. *Hussmann and Spohn*, 2004). In order to ascertain the potential for life in the European ocean, it is important to identify possible tidal dissipation feedback mechanisms that would work to stabilize the ocean on geological timescales. We propose to study the effects of tidal excitation of free oscillations for a variety of ice-shell/ocean models of Europa, and to quantify the resulting heat deposition.

Widespread fracturing and heating of water ice on Enceladus cannot be explained by heat dissipation through tidal deformation (e.g. *Poirier et al.*, 1983;

Porco et al., 2006). Furthermore, tidal forcing on Enceladus is comparable to that experienced by other moons that, despite their larger size and radioactive heat budget, do not exhibit signs of geological activity. We propose to investigate the possibility of tidal excitation of free oscillations on Enceladus as a more efficient means of orbital-to-heat energy transfer.

33.2 Method

We adopt the approach of *Press and Teukolsky* (1977), in which the tidal potential is projected onto the normal modes, and the amount of tidal normal mode coupling is quantified in terms of an overlap integral

$$A_n(\omega) = \int_V \xi_n \cdot \nabla \tilde{U}(\omega) dv, \quad (3.2)$$

where the subscript n is the mode identifier, ξ_n is the eigenfunction in question, $\nabla \tilde{U}(\omega)$ is the gradient of the potential in the frequency domain, ω is the relevant frequency of oscillation, and integration is carried out over the perturbed body. The energy deposited into the mode is then simply

$$\Delta E_n = 2\pi^2 |A_n(\omega)|^2. \quad (3.3)$$

We can see that tidal excitation of free oscillations requires that the tidal forces overlap with a given mode both spatially and in the frequency domain. Studies of tidal excitation of stellar oscillations (*Wu and Murray*, 2003) demonstrate that spatial overlap falls rapidly with increasing radial order of the mode under consideration.

Quantifying frequency overlap requires both calculating the frequency spectrum of tidal forcing and the frequencies of the body’s free oscillations. For Europa, we consider the tidal effects of Jupiter, Io, and Ganymede, and plot the dominant frequencies of forcing from these bodies in Figure 1. We expect Saturn, Dione and Rhea to contribute significantly to tidal forces acting on Enceladus, and we plot the relevant dominant frequencies in Figure 2. Next, we proceed to calculate a range of possible frequencies for the ${}_0S_2$ mode of oscillation (“the football mode”) by considering a set of 1D models of elastic velocity and density for Enceladus and Europa. In order to calculate the frequencies and functions describing the free oscillations of a spherically symmetric body, we employ the MINOS code (*Woodhouse*, 1988). At present, we neglect effects of viscosity.

33.3 Preliminary Results

Figure 3.70 shows that the frequency of ${}_0S_2$ on Europa decreases with decreasing thickness of its subsurface ocean. We use the physical model developed by Cammarano et al (2006) for a chondritic mantle topped by a 137 km thick ice/water layer. Note that tidal forces due to Io excite Europa's ${}_0S_2$ when the ocean is several kilometers thick, Ganymede's effect becomes relevant when the ocean is a few kilometers thick, and frequency overlap with the dynamical tide due to Jupiter occurs when the ocean is a mere 100 m thick.

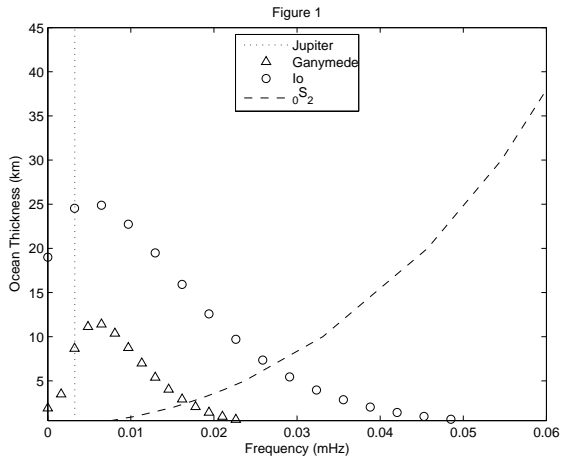


Figure 3.70: The dashed line shows the frequency of ${}_0S_2$ as a function of ocean thickness. Frequencies and amplitudes (in arbitrary units) of tidal forcing due to Ganymede (triangles) and Io (circles) are also shown. The dominant frequency of Jupiter forcing is indicated by the vertical dotted line.

In Figure 3.71, we show the frequency of ${}_0S_2$ on Enceladus as a function of the thickness of a hypothetical subsurface ocean. We consider a physical structure of Enceladus which fits the density and shape constraints (Porco et al., 2006). Our model consists of a core with a density of $\rho = 1700 \text{ kgm}^{-3}$ overlain by a ocean/ice layer that is 10 km thick. The low density of the rocky core is consistent with a 2:3 rock-to-water mixture. We use the upper bounds on seismic velocities in the mantle derived by computing the Voigt average of the rock and water moduli (Watt et al., 1976). We consider a fully differentiated Enceladus – with a non-porous chondritic interior and a $\sim 50 \text{ km}$ thick ocean/ice layer – to be unlikely, given the paucity of accretionary and radiogenic heating, and inconsistency with the observed shape (Porco et al., 2006). Note that tidal forces due to Dione and Rhea excite ${}_0S_2$ when the thickness of the hypothetical subsurface ocean $\leq 1 \text{ km}$.

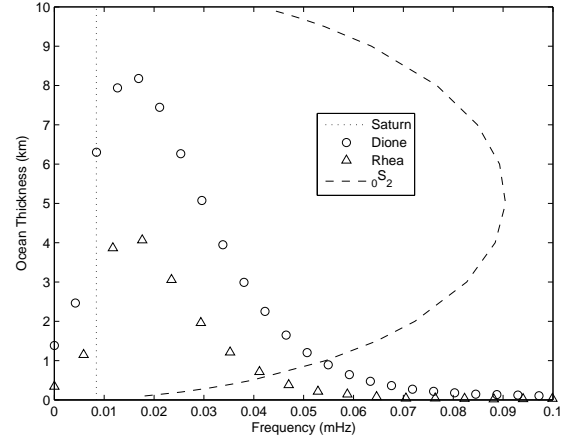


Figure 3.71: The dashed line shows the frequency of ${}_0S_2$ as a function of ocean thickness. Frequencies and amplitudes (in arbitrary units) of tidal forcing due to Rhea (triangles) and Dione (circles) are also shown. The dominant frequency of Saturn forcing is indicated by the vertical dotted line.

33.4 Implications and Future Work

Having identified the interactions that may give rise to tidal excitation of free oscillations, we shall proceed to quantify the effect, and determine whether it is, or may have been, an important source of heat for Europa and Enceladus. Since ${}_0S_2$ frequencies for very thin ice shells are of the same order as the Maxwell relaxation time, we must modify our purely elastic treatment of the problem to include effects of viscosity.

Recent modeling of Ceres by McCord and Sotin (2005) suggests that it may have a subsurface ocean layer, which would result in very low frequency for ${}_0S_2$. We will explore the implications that tidal excitation of free oscillations has for Ceres and other bodies suspected of harboring subsurface oceans (e.g. Callisto, Ganymede, etc.). Furthermore, the transfer of angular momentum into heat through excitation of free oscillations – even if insufficient to drastically raise the temperature within the affected body – may significantly affect orbital evolution within the Jovian and Saturnian systems, or perhaps even the asteroid belt.

33.5 References

- Cammarano, F., V. Lekic, M. Manga, et al., Long period seismology on Europa: I. Physically consistent interior models. submitted to *J. Geophys. Res.*
- Hansen, C.J., L. Esposito, A.I.F. Stewart, et al., Enceladus' water vapor plume. *Science*, 311, 1422-1425. 2006.
- Hussmann, H and T. Spohn, Thermal-orbital evolution

of Europa. *Icarus*, 171, 391-410, 2004.

Kivelson, M.G., K.K. Khurana, C.T. Russell, et al., Galileo magnetometer measurements: A stronger case for a subsurface ocean at Europa. *Science*, 289, 1340-1343, 2000.

Marion, G.M., C.H. Fritsen, H. Eicken, et al., The search for life on Europa: Limiting environmental factors, potential habitats, and earth analogues. *Astrobiology*, 3:4, 785-811, 2003.

McCord, T.B. and C. Sotin, Ceres: Evolution and current state. *J. Geophys. Res.*, 110, doi:10.1029/2004JE002244, 2005.

Poirier, J.P., L. Boloh, and P. Chambon, Tidal dissipation in small viscoelastic ice moons: The case of Enceladus. *Icarus*, 55, 218-230, 1983.

Porco, C.C., P. Helfenstein, P.C. Thomas, et al., Cassini observes the active south pole of Enceladus. *Science*, 311, 1393-1401. 2006.

Press, W.H. and S.A. Teukolsky. On formation of close binaries by two-body tidal capture. *Astrophys. J.*, 213, 183-192, 1977.

Spencer, J.R., J.C. Pearl, M. Segura, et al., Cassini encounters Enceladus: Background and the discovery of a south polar hot spot. *Science*, 311, 1401-1405, 2006.

Watt, J.P., G.F. Davies and R.J. O'Connell, The elastic properties of composite materials. *Rev. of Geophys. and Space Phys.*, 14:4, 541-563, 1976.

Woodhouse, J.H., The calculation of eigenfrequencies and eigenfunctions of the free oscillations of the Earth and the Sun. *Seismological Algorithms*, ed. Doornbos, D.J., 321-370, 1988.

Wu, Y. and N. Murray, Planet migration and binary companions: The case of HD 80606b. *Astrophys. J.*, 589, 605-614, 2003.

34. A Comparison of Standard Inversion, Neural Networks and Support Vector Machines

Karl Kappler, Heidi Kuzma, James W. Rector

34.1 Summary

The object of geophysical inversion is to recover earth parameters from measured data. If the relationship between an earth model and the data is linear, then three different methods of data interpretation, linear inversion, Neural Networks and Support Vector Machines, arrive at the same model from different paradigms. Linear inversion finds a model by minimizing a least squares objective function to which there is a closed form solution. NNs and SVMs use training data to approximate a functional inverse. If the relationship between models and data is non-linear, there is no longer a closed form solution to the inversion objective function, and a model is found by iterative guessing, or by applying a linear approximation to the non-linear physics governing the problem in conjunction with standard linear inversion. An NN finds non-linear relationships by adopting an architecture tuned to a user-designed search algorithm. A SVM is rendered non-linear by changing a single parameter. All three approaches can be used independently or in combination. We are actively developing a tutorial which explains the differences and relationships between these methods.

34.2 Introduction

Geophysical relationships can be written

$$d = G(m) \tag{3.4}$$

d is a vector of measured data, m is a vector of model parameters that describe the earth, and G is a function derived from physics and geometry. The goal of geophysical inversion is to find m , given G and d .

Linear Inversion

If the relationship between data and models is linear, then G can be written as a matrix of coefficients:

$$d = Gm \tag{3.5}$$

Least squares linear inversion is done by minimizing an objective function:

$$m_{inv} = \underset{m}{\operatorname{argmin}} ((d - Gm)^T (d - Gm)) \tag{3.6}$$

which has the well known closed form solution

$$m_{inv} = (G^T G)^{-1} G^T d \tag{3.7}$$

Notice that any vector of data can be inverted once the matrix $(G^T G)^{-1} G^T$ has been computed.

Inversion via Machine Learning

In the machine learning paradigm, it is assumed that examples of m and d are available, and G does not necessarily have to be known. The goal of inversion via machine learning, either with a Neural Network or a Support Vector Machine, is to find a function S such that

$$m_{ML} = S(d) \approx SVD(d) \approx NN(d) \tag{3.8}$$

In geophysics, usually G is known, and it is possible to select a series of example models and use G to compute a corresponding set of training data. The goal of a linear machine learning problem is to find S such that

$$M = DS \tag{3.9}$$

M is now a matrix of example or 'training models' and D is a matrix in which each row is the corresponding 'training data'.

Linear Neural Network

Another frame of reference in which to cast information processing is that of a network of interlinked, adaptive data structures, broadly known as neural networks. The neural net format is inspired by the neuron model. The neuron is composed of three main parts. There are the input channels (dendrites), a cell which performs a function on the inputs (the neuron body), and an output channel to conduct the function result away from the body (axon).

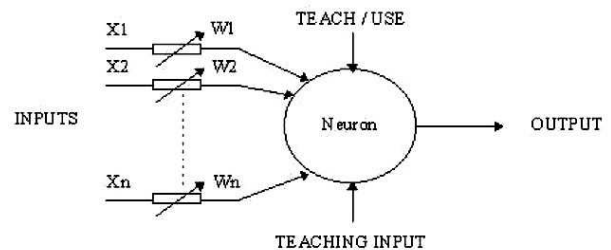


Figure 3.72: Schematic of a single Neuron

In a simple, linear neural net, the inputs are subjected to a weighting scheme which seeks to optimize the output of the network. The method of steepest ascent is the most common method of selecting weights for the input

Inversion, NN and SVM channels. In the case of a linear weighting scheme applied to a single set of inputs, the steepest ascent reduces to the method of ordinary least squares, or linear inversion. Neural Network approaches to computing partition the coding into nodal structures like the neuron and interlink the nodes with axon/dendrites. Using the NN paradigm when designing software is helpful in making the design modular.

Linear SVM

Least Squares SVMs (LS-SVM) are derived starting from equation 6 by minimizing an objective function of the form.

$$S_{SVM} = \underset{S}{\operatorname{argmin}} (C(DS - M)T(DS - M) - STS) \quad (3.10)$$

If the scalar C (picked by the user) is very large, then the solution to equation (7) reduces to

$$S_{SVM} = (G^T G)^{-1} G^T \quad (3.11)$$

Instead of solving equation 7 directly, an LS-SVM is derived from an equivalent, dual form of the minimization (Kuzma, 2003). The solution is formed in terms of inner-products, or Kernel functions. In the simplest case the kernel function is just the standard dot-product. A LS-SVM does not find S directly, but instead finds a set of coefficients α such that

$$\alpha = (DD^T + \frac{1}{2C})^{-1} M \quad (3.12)$$

To then use the SVM to find a model from new data, the following is computed

$$m = SVM(d) = \sum_{\text{training data}} \alpha_i (d_i^T d) \quad (3.13)$$

In essence the SVM is approximating the model which fits the field data by 'projecting' the field data onto a basis of training data vectors (the support vectors). Thus a weighted linear combination of training models forms the solution. This is described in more detail in the tutorial we are preparing.

Non-Linear Inversion

If the relationship between models and data is not linear, then it is no longer possible to invert G directly. Nonlinear iterative inversions rely on numerical methods to minimize objective functions similar to that in equation 3. Non-linear inversion follows a sequence of steps:

1. Make an initial guess for m
2. Compute data (or gradients) via equation 1
3. Update the guess for m
4. Repeat steps 2 and 3 until a solution is established

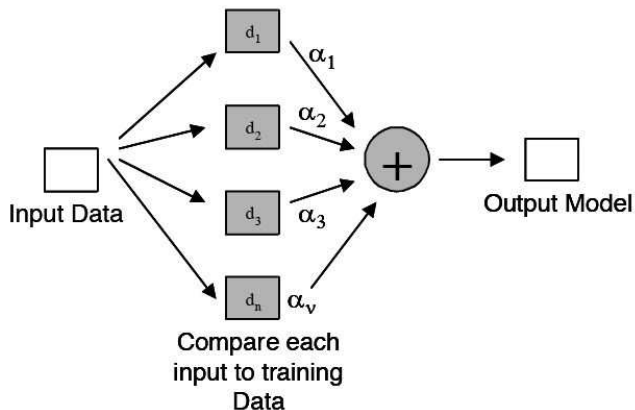


Figure 3.73: Given proper training data, the models found from a linear LS-SVM are equivalent to those found by linear inversion

In practice, many different algorithms may be used for nonlinear inversion. Constraints, regularization and limits on step size may be used to force the solution toward desired models. In our tutorial we treat the following common numerical methods by outlining them conceptually, and citing formulae:

Newton's Method

Gradient : Steepest Ascent/Descent

Conjugate Gradient

Monte Carlo methods: Genetic and Simulated Annealing

Occam's Constraint

Some of the pitfalls of each method, such as slow convergence or choice of a good starting model are discussed, as well as tricks to avoid these pitfalls. For example using a simple SVM to select a good starting model and a decaying step size applied to a subsequent gradient search.

Non-linear NN

A linear NN refers to the linear relationship between neurons. Each node itself can be working in a non-linear fashion, as in the case of a network of switching nodes in which node potentials decay exponentially when node is off, and increase linear when it is on (Kappler et al. 2002). The linearity is in the connection between nodes. The state or potential of a given node depends on a linear function of the state and the potentials of its input nodes. The NN offers the advantage of being adaptable, and can respond to a changing data set on the fly, where as a linear inversion needs to be recomputed whenever a data set changes. The SVM and NN share this property, that once trained they can interpret new data for free.

A more complicated neural net often uses connectivity as a strength for optimizing a solution. Once the data are

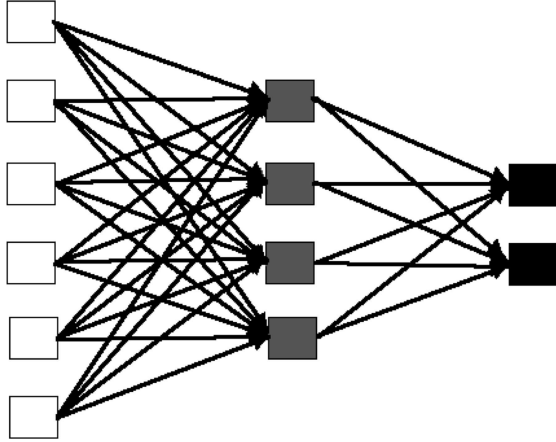


Figure 3.74: Diagram of a neural net with a single hidden layer, comprised of four nodes

input, a series of hidden layers are used to analyze different aspects of data. The connection strengths between nodes can be varied. A NN could incorporate a group of parallel SVMs, each optimizing different functions, and weighting the inversion from each SVM into a resulting output.

A description of a NN which emulates an SVM and the supporting mathematics can be found in *Haykin* CH7. In the NN paradigm, SVMs are known as radial basis function networks.

Non-Linear SVMs

The architecture of a non-linear SVM is the same as the architecture of a linear SVM except that dot products are replaced by kernel function. To capture non-linear relationships in an LS-SVM, equations 11 and 12 are replaced by

$$\alpha = \left(\Gamma + \frac{1}{2C}\right)^{-1}M \quad (3.14)$$

$$\Gamma_{i,j} = K(d_i, d_j) \quad (3.15)$$

$$m = \sum_{\text{trainingdata}} \alpha_i K(d_i^T d) \quad (3.16)$$

The kernel function $K(d_i, d_j)$ can be any function such that the Gram matrix, G , is positive definite (has no negative eigenvalues). In practice, K is picked by trial and error out of a small library of kernels. Training the SVM means finding the s , which still only requires inverting a well conditioned matrix that is the size of the number of training examples.

34.3 Implications and Future Work

The ordinary method of linear inversion can be recovered from simple assumptions applied to Neural Networks and SVMs. The NN and SVM approach however offer several advantages such as adaptability, expanding training sets without restarting the inversion, and nonlinear methods. The framework of a NN is also intuitive in the sense that the neural clusters can be set up so that each set of nodes is working on a specific user defined question.

34.4 Acknowledgments

The DCI Postdoctoral Fellowship Program partially supported this work.

34.5 References

- Haykin, S., 1994, *Neural Networks*, A comprehensive Foundation, Macmillan
- Kappler et al., 2002 *Dynamics in High Dimensional Networks*, *Signal Processing, Elsevier*
- Kuzma, H. A., Rector, J.W., (2004), *Non-linear AVO inversion using support vector machines: 74th annual International Meeting of Soc. Expl. Geophysics* Scholkopf, B. and Smola, A., 2002, *Learning with Kernels, Support Vector Machines, Regularization, Optimization, and Beyond: The MIT Press.*

BSL Operations

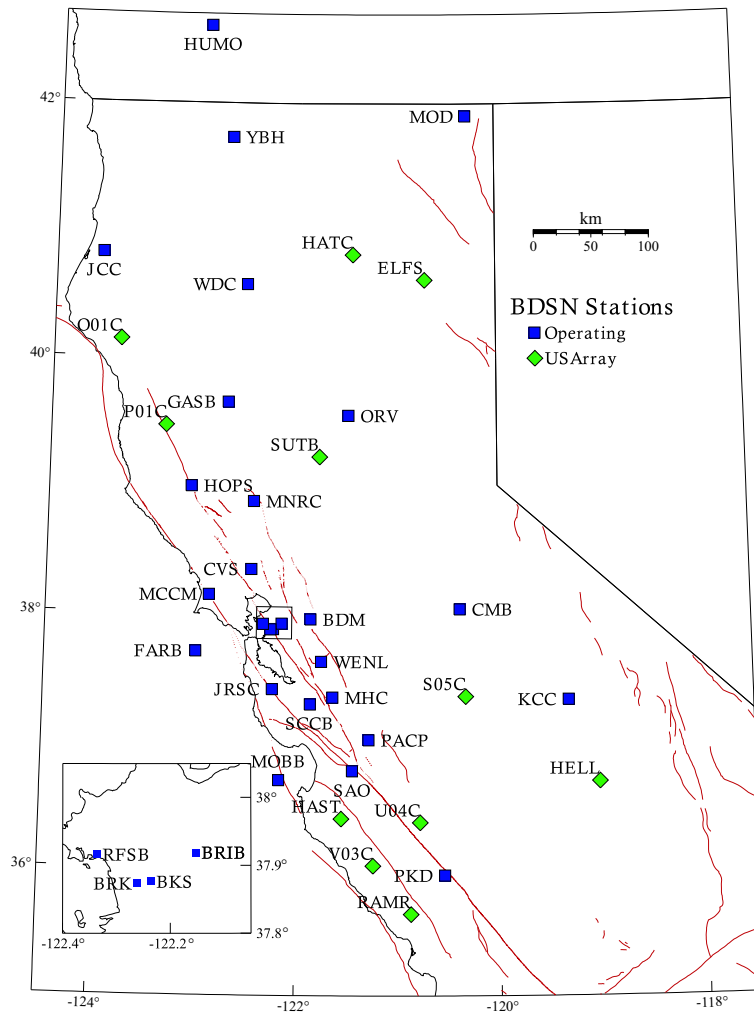


Figure 3.75: Map illustrating the distribution of BDSN stations (squares) in northern and central California. The diamonds indicate sites currently operated by USArray which we are monitoring as perspective future stations.

Chapter 4

Berkeley Digital Seismic Network

1. Introduction

The Berkeley Digital Seismic Network (BDSN) is a regional network of very broadband and strong motion seismic stations spanning northern California and linked to UC Berkeley through continuous telemetry (Figure 3.75 and Table 4.1). The network is designed to monitor regional seismic activity at the magnitude 3+ level as well as to provide high quality data for research projects in regional and global broadband seismology.

Since 1991 the BDSN has grown from the original 3 broadband stations installed in 1986-87 (BKS, SAO, MHC) to comprise 27 stations, including an autonomous ocean-bottom seismometer in Monterey Bay (MOBB). We take particular pride in high quality installations, which often involve lengthy searches for appropriate sites away from sources of low-frequency noise, as well as continuous improvements in installation procedures and careful monitoring of noise conditions and problems. Thus, although three new stations were completed, the focus of this year's technical efforts evolved to maintenance and repair, because of aging instruments, the desire for higher data rates, corrosion and outright equipment failure.

Further expansion of our network, one of BSL's long term goals, is contingent on the availability of funding and coordination with other institutions for the development of a denser state-of-the-art strong motion/broadband seismic network and joint earthquake notification system in this seismically hazardous region.

Equally important, data quality and the integrity of the established network must be preserved and remain assured despite expansion. The first generation of broadband seismometers installed by BSL have been operating for almost 25 years. At the same time, the first generation of broadband dataloggers are entering their 16th year of service. These will both require continued vigilance and greater time commitment to repairs in the future.

2. BDSN Overview

Twenty-four of the BDSN sites are equipped with 3 component broadband seismometers and strong-motion accelerometers, and a 24-bit digital data acquisition system or datalogger. Two additional sites (RFSB and SCCB) consist of a strong-motion accelerometer and a 24-bit digital datalogger. The ocean-bottom station MOBB is equipped with a 3 component broadband seismometer. Data from all BDSN stations, except MOBB, are transmitted to UC Berkeley using continuous telemetry. In order to insure against data loss during utility disruptions, each site has a 3-day supply of battery power and is accessible via a dialup phone line. The combination of high-dynamic range sensors and digital dataloggers ensures that the BDSN has the capability to record the full range of earthquake motion for source and structure studies. Table 4.2 lists the instrumentation at each site.

Most BDSN stations have Streckeisen STS-1 or STS-2 three-component broadband sensors (*Wielandt and Streckeisen, 1982; Wielandt and Steim, 1986*). A Guralp CMG-3T downhole broadband sensor contributed by LLNL is deployed in a post-hole installation at BRIB. A Guralp CMG1-T is deployed at MOBB. The strong-motion instruments are Kinematics FBA-23 or FBA-ES-T with ± 2 g dynamic range. The recording systems at all sites are either Q330, Q680, Q730, or Q4120 Quanterra dataloggers, with 3, 6, 8, or 9 channel systems. The Quanterra dataloggers employ FIR filters to extract data streams at a variety of sampling rates. In general, the BDSN stations record continuous data at .01, 0.1, 1.0, 20.0 or 40.0, and 80 or 100 samples per second, although some sites send triggered data at the highest sampling rate using the Murdock, Hutt, and Halbert event detection algorithm (*Murdock and Hutt, 1983*) (Table 4.3). In addition to the 6-channels of seismic data, signals from thermometers and barometers are recorded at nearly every site (Figure 4.1).

In parallel with the upgrade of the broadband network, a grant from the CalREN Foundation (California Research and Education Network) in 1994 enabled

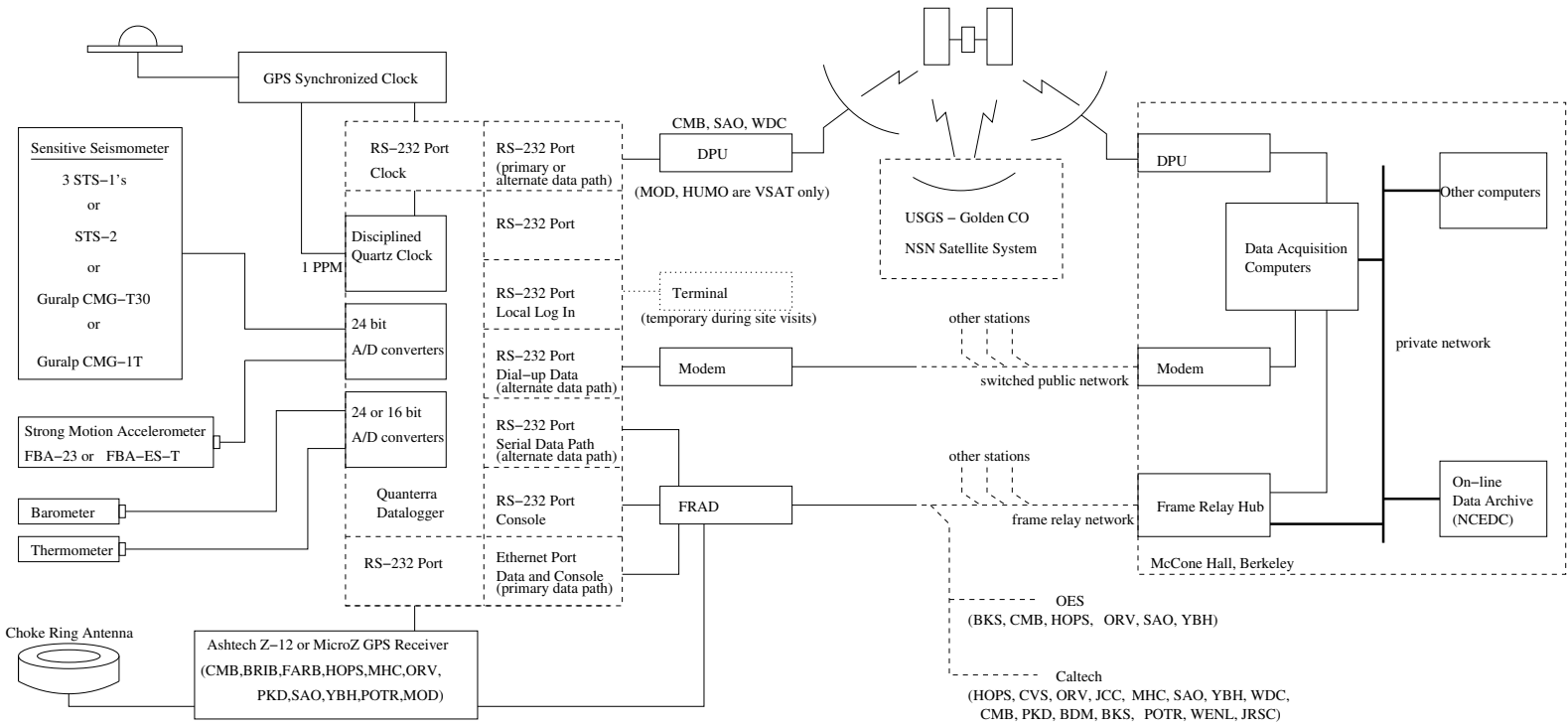


Figure 4.1: Schematic diagram showing the flow of data from the sensors through the dataloggers to the central acquisition facilities of the BSL.

the BSL to convert data telemetry from analog leased lines to digital frame-relay connections. The frame-relay network uses digital phone circuits that can support 56 Kbit/s to 1.5 Mbit/s throughput. Since frame-relay is a packet-switched network, a site may use a single physical circuit to communicate with multiple remote sites through the use of “permanent virtual circuits”. Frame Relay Access Devices (FRADs), which replace modems in a frame-relay network, can simultaneously support multiple interfaces such as RS-232 async ports, synchronous V.35 ports, and ethernet connections. In practical terms, the upgrade to frame relay communication provides faster data telemetry between the remote sites and the BSL, remote console control of the dataloggers, additional services such as FTP and telnet to the dataloggers, data transmission to multiple sites, and the ability to communicate and transmit data from multiple instruments such as GPS receivers and/or multiple dataloggers at a single site. Today, 23 of the BDSN sites use frame-relay telemetry for all or part of their communications system.

As described in Chapter 10, data from the BDSN are acquired centrally at the BSL. These data are used for rapid earthquake reporting as well as for routine earthquake analysis (Chapters 5 and 11). As part of routine quality control (Chapter 10), power spectral density (PSD) analyses are performed weekly. Figure 4.2 shows a summary of the results for 2005-2006.

The occurrence of a significant teleseism also provides the opportunity to review station health and calibration. Figure 4.3 displays BDSN waveforms for a M_w 7.6 deep focus earthquake in the Banda Sea region on January 27, 2006.

BDSN data are archived at the Northern California Earthquake Data Center. This is described in detail in Chapter 9.

2.1 Electromagnetic Observatories

In 1995, in collaboration with Dr. Frank Morrison, the BSL installed two well-characterized electric and magnetic field measuring systems at two sites along the San Andreas Fault which are part of the Berkeley Digital Seismic Network. Since then, magnetotelluric (MT) data have been continuously recorded at 40 Hz and 1 Hz and archived at the NCEDC (Table 4.4). At least one set of orthogonal electric dipoles measures the vector horizontal electric field, E , and three orthogonal magnetic sensors measure the vector magnetic field, B . These reference sites, now referred to as electromagnetic (EM) observatories, are co-located with seismographic sites so that the field data share the same time base, data acquisition, telemetry and archiving system as the seismometer outputs.

The MT observatories are located at Parkfield (PKD1, PKD) 300 km south of the San Francisco Bay Area, and Hollister (SAO), halfway between San Francisco and

Sensor	Channel	Rate (sps)	Mode	FIR
Broadband	UH?	0.01	C	Ac
Broadband	VH?	0.1	C	Ac
Broadband	LH?	1	C	Ac
Broadband	BH?	20/40	C	Ac
Broadband	HH?	80/100	C	Ac/Ca
SM	LL?	1	C	Ac
SM	BL?	20/40	C	Ac
SM	HL?	80/100	C	Ac/Ca
Thermometer	LKS	1	C	Ac
Barometer	LDS	1	C	Ac

Table 4.3: Typical data streams acquired at BDSN stations, with channel name, sampling rate, sampling mode, and the FIR filter type. SM indicates strong-motion; C continuous; T triggered; Ac acausal; Ca causal. The LL and BL strong-motion channels are not transmitted over the continuous telemetry but are available on the Quanterra disk system if needed. The HH channels are recorded at two different rates, depending on the datalogger type. Q4120s provide 100 sps and causal filtering; Q680/980s provide 80 sps and acausal filtering.

Sensor	Channel	Rate (sps)	Mode	FIR
Magnetic	VT?	0.1	C	Ac
Magnetic	LT?	1	C	Ac
Magnetic	BT?	40	C	Ac
Electric	VQ?	0.1	C	Ac
Electric	LQ?	1	C	Ac
Electric	BQ?	40	C	Ac

Table 4.4: Typical MT data streams acquired at SAO and PKD, with channel name, sampling rate, sampling mode, and FIR filter type. C indicates continuous; T triggered; Ac acausal.

BDSN PSD Low Noise Synopsis (2005–2006)

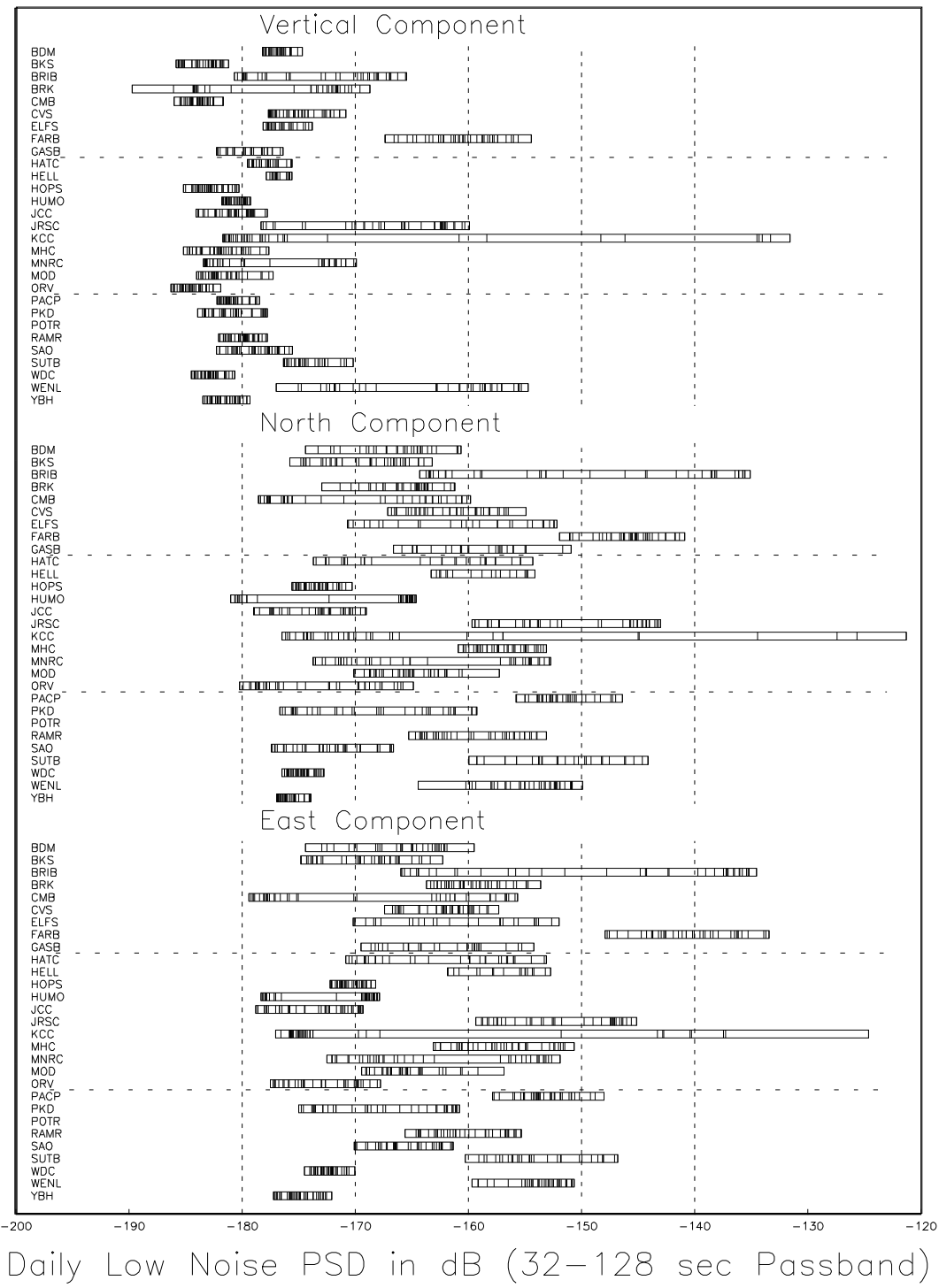


Figure 4.2: PSD noise analysis for BDSN stations, by channel, in the period range from 32-128 sec from 7/1/2005-6/30/2006. BRIB (situation in a shallow vault that is prone to tilting) and FARB (located on the Farallon Islands) stand out as sites with high noise levels. HUMO (located in an abandoned mine) stands out as an exceptionally quiet site.

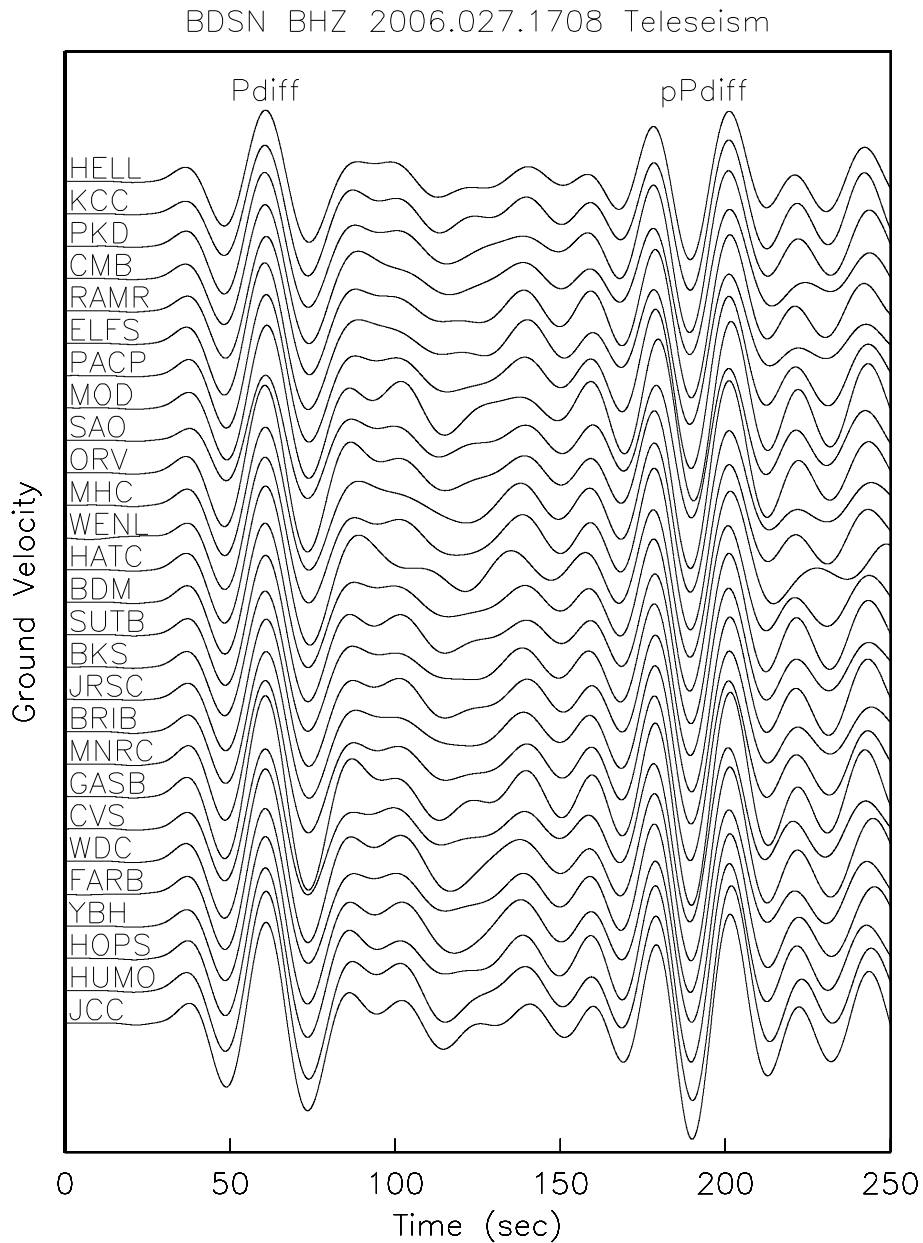


Figure 4.3: P_{diff} and pP_{diff} vertical component broadband waveforms recorded across BDSN from a deep focus (397 km) M_w 7.6 teleseism which occurred on January 27, 2006, in the Banda Sea at 5.482° S, 128.093° E, at a distance of 108.8° from Berkeley, and at an azimuth of N82W. The traces are deconvolved to ground motion, scaled absolutely, and ordered by distance from the epicenter. They are aligned on the first trough of P_{diff} . The pP_{diff} waveform, arriving 100 seconds later, is an inverted image of P_{diff} due to the polarity inversion that occurs when the P wave reflects from the free surface near the source. The highly similar waveforms recorded across the BDSN provide evidence that the broadband sensors are operating within their nominal specifications.

Code	Net	Latitude	Longitude	Elev (m)	Over (m)	Date	Location
BDM	BK	37.9540	-121.8655	219.8	34.7	1998/11 -	Black Diamond Mines, Antioch
BKS	BK	37.8762	-122.2356	243.9	25.6	1988/01 -	Byerly Vault, Berkeley
BRIB	BK	37.9189	-122.1518	219.7	2.5	1995/06 -	Briones Reservation, Orinda
BRK	BK	37.8735	-122.2610	49.4	2.7	1994/03 -	Haviland Hall, Berkeley
CMB	BK	38.0346	-120.3865	697.0	2	1986/10 -	Columbia College, Columbia
CVS	BK	38.3453	-122.4584	295.1	23.2	1997/10 -	Carmenet Vineyard, Sonoma
FARB	BK	37.6978	-123.0011	-18.5	0	1997/03 -	Farallon Island
GASB	BK	39.6547	-122.716	1354.8	2	2005/09 -	Alder Springs
HOPS	BK	38.9935	-123.0723	299.1	3	1994/10 -	Hopland Field Stat., Hopland
HUMO	BK	42.6071	-122.9567	554.9	50	2002/06 -	Hull Mountain, Oregon
JCC	BK	40.8175	-124.0296	27.2	0	2001/04 -	Jacoby Creek
JRSC	BK	37.4037	-122.2387	70.5	0	1994/07 -	Jasper Ridge, Stanford
KCC	BK	37.3236	-119.3187	888.1	87.3	1995/11 -	Kaiser Creek
MCCM	BK	38.1448	-122.8802	-7.7	2	2006/02 -	Marconi Conference Center, Marshall
MHC	BK	37.3416	-121.6426	1250.4	0	1987/10 -	Lick Obs., Mt. Hamilton
MNRC	BK	38.8787	-122.4428	704.8	3	2003/06 -	McLaughlin Mine, Lower Lake
MOBB	BK	36.6907	-122.1660	-1036.5	1	2002/04 -	Monterey Bay
MOD	BK	41.9025	-120.3029	1554.5	5	1999/10 -	Modoc Plateau
ORV	BK	39.5545	-121.5004	334.7	0	1992/07 -	Oroville
PACP	BK	37.0080	-121.2870	844	0	2003/06 -	Pacheco Peak
PKD	BK	35.9452	-120.5416	583.0	3	1996/08 -	Bear Valley Ranch, Parkfield
RFSB	BK	37.9161	-122.3361	-26.7	0	2001/02 -	RFS, Richmond
SAO	BK	36.7640	-121.4472	317.2	3	1988/01 -	San Andreas Obs., Hollister
SCCB	BK	37.2874	-121.8642	98	0	2000/04 -	SCC Comm., Santa Clara
WDC	BK	40.5799	-122.5411	268.3	75	1992/07 -	Whiskeytown
WENL	BK	37.6221	-121.7570	138.9	30.3	1997/06 -	Wente Vineyards, Livermore
YBH	BK	41.7320	-122.7104	1059.7	60.4	1993/07 -	Yreka Blue Horn Mine, Yreka

Table 4.1: Currently operating stations of the Berkeley Digital Seismic Network. Each BDSN station is listed with its station code, network id, location, operational dates, and site description. The latitude and longitude (in degrees) are given in the WGS84 reference frame and the elevation (in meters) is relative to the WGS84 reference ellipsoid. The elevation is either the elevation of the pier (for stations sited on the surface or in mining drifts) or the elevation of the well head (for stations sited in boreholes). The overburden is given in meters. The date indicates either the upgrade or installation time.

Parkfield (Figure 3.75). In 1995, initial sites were established at PKD1 and SAO, separated by a distance of 150 km, and equipped with three induction coils and two 100 m electric dipoles. PKD1 was established as a temporary seismic site, and when a permanent site (PKD) was found, a third MT observatory was installed in 1999 with three induction coils, two 100 m electric dipoles, and two 200 m electric dipoles. PKD and PKD1 ran in parallel for one month in 1999, and then the MT observatory at PKD1 was closed.

Data at the MT sites are fed to Quanterra dataloggers, shared with the collocated BDSN stations, synchronized in time by GPS and sent to the BSL via dedicated communication links.

3. 2005-2006 Activities

3.1 USArray

The BSL concluded an agreement with IRIS during 2003-2004 to contribute 19 stations of the BDSN to US-Array while the experiment is deployed in California. This included 17 existing stations: CMB, CVS, FARB, HOPS, HUMO, JCC, JRSC, KCC, MNRC, MOD, ORV, PACP, PKD, POTR, WDC, WENL, and YBH as well as the two new sites: GASB and MCCM.

The 19 BDSN sites provided USArray with a running start in northern California. In June of 2004, the BSL set up the software necessary to exchange data with USArray and made modifications to the dataloggers to change the BH sampling rate from 20 Hz to 40 Hz. In this third year of USArray, the BDSN has continued to use the 40 Hz sampling rate for the BH channels.

During the station installation phase for northern and

Code	Broadband	Strong-motion	datalogger	T/B	GPS	Other	Telemetry	Dial-up
BDM	STS-2	FBA-23	Q4120	X			FR	
BKS	STS-1	FBA-23	Q980	X		Baseplates	FR	X
BRIB	CMG-3T	FBA-23	Q980		X	Vol. Strain	FR	X
BRK	STS-2	FBA-23	Q680				POTS	
CMB	STS-1	FBA-23	Q980	X	X	Baseplates	FR	X
CVS	STS-2	FBA-23	Q4120	X			FR	
FARB	CMG-3T	FBA-23	Q4120	X	X		R-FR/R	
GASB	STS-2	FBA-ES-T	Q4120	X			R-FR	
HOPS	STS-1	FBA-23	Q980	X	X	Baseplates	FR	X
HUMO	STS-2	FBA-ES-T	Q4120	X			VSAT	X
JCC	STS-2	FBA-23	Q980	X			FR	X
JRSC	STS-2	FBA-23	Q680				FR	X
KCC	STS-1	FBA-23	Q980	X		Baseplates	R-Mi-FR	X
MCCM	STS-2	FBA-ES-T	Q4120				VSAT	
MHC	STS-1	FBA-23	Q980	X	X		FR	X
MNRC	STS-2	FBA-ES-T	Q4120	X			None	X
MOBB	CMG-1T		GEOSense			Current meter, DPG	None	
MOD	STS-1	FBA-ES-T	Q980	X	X	Baseplates	VSAT	X
ORV	STS-1	FBA-23	Q980	X	X	Baseplates	FR	X
PACP	STS-2	FBA-ES-T	Q4120	X			Mi/FR	
PKD	STS-2	FBA-23	Q980	X	X	EM	R-FR	X
RFSB		FBA-ES-T	Q730				FR	
SAO	STS-1	FBA-23	Q980	X	X	Baseplates, EM	FR	X
SCCB		FBA-ES-T	Q730		X		FR	
WDC	STS-2	FBA-23	Q980	X			FR	X
WENL	STS-2	FBA-23	Q4120	X			FR	
YBH	STS-1 & STS-2	FBA-23	Q980	X	X	Baseplates	FR	X

Table 4.2: Instrumentation of the BDSN as of 06/30/2006. Except for PKD1, RFSB, SCCB and MOBB, each BDSN station consists of collocated broadband and strong-motion sensors, with a 24-bit Quanterra datalogger and GPS timing. The stations PKD1, RFSB and SCCB are strong-motion only, while MOBB has only a broadband sensor. Additional columns indicate the installation of a thermometer/barometer package (T/B), collocated GPS receiver as part of the BARD network (GPS), and additional equipment (Other) such as warpless baseplates or electromagnetic sensors (EM). The obs station MOBB also has a current meter and differential pressure gauge (DPG). The main and alternate telemetry paths are summarized for each station. FR - frame relay circuit, R - radio, Mi - microwave, POTS - plain old telephone line, VSAT - USGS ANSS satellite link, None - no telemetry at this time. An entry like R-Mi-FR indicates telemetry over several links, in this case, radio to microwave to frame relay.

central California, the BSL collaborated with USArray to identify and permit sites that might be suitable as BDSN stations, several at UC reserves and field stations. The stations currently operating at Sutter Buttes, Hat Creek Radio Observatory, Eagle Lake Biological Field Station, Kirkwood Ski Area, Ben Lomond Conservation Camp, and at the summer home of a BSL staff member (M. Hellweg) in the Sierra Nevada foothills were established with support from BSL staff. Data from these sites (Figure 3.75) are being sent directly to the BSL as well as to the Array Network Facility. In addition, the BSL is monitoring data from several other USArray stations to evaluate their performance as possible future BDSN stations when USArray moves on across the country. In particular, noise comparisons are being conducted in different

frequency bands for all BDSN and USArray stations in northern California (see Chapter 10 for further details).

3.2 Station Upgrades, Maintenance and Repairs

Given the remoteness of the off-campus stations, BDSN data acquisition equipment and systems are designed, configured, and installed so that they are both cost effective and reliable. As a result, the need for regular station visits has been reduced. Most station visits are necessitated by some catastrophic failure. The 2005-2006 fiscal year was no exception.

NSN VSAT modifications

In a collaborative effort with USGS/NEIC (US-NSN program), satellite dishes (VSAT's) were installed 10 years ago at stations SAO, CMB and WDC. The satellite connections allow us to contribute data to the NSN, while at the same time providing a redundant telemetry path to BSL. A VSAT was also installed in 1999 at MOD, where this was the only available means of telemetry. In 2002, station HUMO was installed as a collaboration between BSL, NEIC and the IRIS/GSN and VSAT telemetry installed as the only telecommunications link. A VSAT down-link is also provided at the BSL data center. Due to a change in satellite vendors, hardware at all installations was changed and the satellite dishes repointed in 03/04. This effort was coordinated to minimize the interruption to the data flow. In early 2006, a third site at the Marconi Center (MCCM) was added to the partnership with NEIC and the IRIS/GSN. The NEIC also provided VSAT equipment for MCCM and is described elsewhere in this report.

KCC Telemetry Upgrade

Since 1996, telemetry links for all the BSL stations have been upgraded to 56 kbaud digital circuits with the exception of KCC, which is located in a hydropower facility operated by Edison International within the Sierra Nevada range. Due to the remoteness of the site, access to the area is limited after the first snowfall. Planning for the upgrade of KCC began in early 2001, when BSL engineers began discussions with Edison engineers. The terrorist events of September 11, 2001 required Edison to re-evaluate their network and site security, relegating BSL's telemetry upgrade at the KCC site to the back burner until the summer of 2005.

BSL and Edison upgraded the data link from the site over a two day period in October of 2005. Ethernet connectivity over a continuous 56k baud circuit was achieved to the site.

Also at that time, BSL engineers reinstalled the external reference clock. At KCC, the datalogger is located nearly 400 meters inside a granite tunnel. Satellite clock reception at the datalogger is impossible. During the original installation in 1996, the clock was placed at the entrance of the tunnel and digital clock output signals relayed to the datalogger via solid state short haul modems. Periodically, clock quality would suffer under this arrangement.

This year, BSL engineers moved the external reference clock to the back of the tunnel (near the datalogger) and installed a high gain antenna outside the tunnel. The connection between the clock and the antenna is via a super low loss coaxial cable. The printed circuit board which provides internal/external clock functions within the Quanterra datalogger was also replaced due to age related failure.

Temporary Removal of Seismometers from WENL

The BSL broadband installation at Wente Brothers Vineyards (WENL) was initially installed in 1997 at the rear of an adit that is used for the aging and storage of wine. The winter of 2005-2006 brought record rainfall to northern California. During the rains, the output from both the STS-2 and FBA-EST strong motion instruments were observed to be peculiar. Engineers from BSL found that ground water had risen and was touching the bottom of the seismometers. The cooling effect of the water had altered their responses. In order to prevent damage to the instruments in the event that the water should continue to rise, the instruments were immediately removed and returned to Berkeley. After inspection and verification of their response, the instruments were reinstalled at WENL six weeks later when the water had subsided.

Vandalism at MNRC

By design, stations of the BDSN are located in remote locations. This remoteness assures minimization of the cultural noise while providing a measure of security. Occasionally, the remoteness provides opportunity for mischief. In early 2006, such mischief occurred at the MNRC site. Vandals broke the lock off the line power meter box and switched the power off. The system continued to operate off of battery back up power until battery voltage fell critically low. BSL engineers restored the site operation with a station visit in which they turned the line power back on and installed a new lock. These simple tasks however, required five hours of round trip driving from Berkeley.

Electromagnetic Instruments at JRSC

BSL has jointly operated and maintained seismic instruments with Stanford University at the Jasper Ridge site (JRSC) since June of 1994. During the past year, BSL engineers endeavored on several days to reduce offsets and long period noise at the site. Largely these efforts involved altering grounding schemes and changing power connections with varying success. Backup batteries at the site were also changed and the FBA-23 strong motion instrument was changed to accommodate 2G full scale. Concurrent to these efforts, BSL engineers worked several days at Stanford installing and troubleshooting to support a joint USGS, Stanford Bay Area ULF-EM monitoring project. BSL has a subcontract award grant for assistance in installation, telemetry and data archiving for this project. BSL engineers troubleshoot cabling, connection, power and polarity issues. Additionally, a method for injection EM and magnetic signals into the ground was developed in order to verify system operation.

Upgrade and Repair of Dataloggers

As a result of aging, a number of BDSN dataloggers required repairs in 2005-2006. The dataloggers at BKS, BRK, and KCC experienced large drifts in their internal clocks as the crystal oscillators aged. These instruments were initially purchased during the network upgrades in the early 1990's. Replacement oscillators were available from the manufacturer. In each case, a backup datalogger was rotated in to replace the original unit, which was sent for service.

Support for Earthscope Transportable Array at SUTB, RAMR and HAST

BSL has supported the Earthscope Transportable Array (TA) within northern California by helping to permit sites, visiting them to maintain equipment, and by providing telemetry.

During 2005-2006, the TA installed a temporary broadband station near Sutter Buttes. Located within the flat central valley of California, the Sutter Buttes are the remnant of an ancient volcano. They rise steeply 700 meters above the valley floor, and their highest point holds a cluster of commercial radio towers and support facilities. Due to the remoteness and topology of the area, the planned telemetry via the cell phone network was found to be unreliable, and no commercial telephone service is available.

Since 1997, BSL has operated a BARD GPS station by special arrangement with the radio site operator. For this station, BSL engineers installed a digital radio link to the BSL site at ORV approximately 30 kilometers away. There, the data are consolidated with that of the seismic and GPS installations at ORV, and fed via a single 56k telco circuit to Berkeley. To support the US Traveling Array, the radio hardware at Sutter Buttes was changed in 2005 to enable the radio there to act as both a repeater for the USArray seismic data and a radio transmitter for the BARD GPS data from Sutter Buttes. Correspondingly, the radio equipment at the ORV end was changed. At present, the single digital telco circuit between ORV and Berkeley thus carries data from the ORV seismic instruments and GPS, the GPS instruments at Sutter Buttes, and the USArray seismic installation.

BSL engineers made multiple site visits to both the Sutter Buttes radio installation and the US Array seismic site in order to achieve the desired network connectivity.

The Hasting Reservation is a research and natural history facility operated by the University of California system in Monterey County California. The BSL provided permitting and logistic support during placement of the USArray instrument as well a strong motion instrumentation for the site. BSL engineers visited the site to replace the failed accelerometer in early 2006.

3.3 New Installations

Two new BDSN stations, Alder Springs (GASB) and Marconi Conference Center (MCCM) were completed and brought on line in 2005/2006. Both stations provide broadband and strong motion data with continuous data telemetry. No existing buildings or structures were available at these locations. BSL engineers constructed the necessary infrastructure.

Alder Springs (GASB)

The Alder Springs (GASB) site is located approximately 35 kilometers west of the central valley town of Willows. Local geology is mostly serpentine and Franciscan. In the past, a short period observatory has been operated at the Alder Springs site by the California Department of Water Resources. The GASB site is being developed in cooperation with the CREST (Consolidated Reporting of EarthquakeS and Tsunamis) network, and closes a gap in the BDSN network between stations MNRC and WDC.

In June 2004, construction began on a steel and concrete seismographic vault similar to those at JCC, PKD, HOPS, and MNRC. On-site excavation was contracted. Inmates from the CDF Valley View Conservation Camp provided labor for the concrete pour and back filling of the excavation. BSL engineers built the forms and framing for the concrete, as well as all electrical wiring at the site. The permit for this site was provided by the US Forest Service, Mendocino National Forest.

Although, physical work at the site temporarily stopped in September 2004, a frame-relay circuit was installed at the CDF camp in early January of 2005. Local loop connectivity to the vault was achieved via wireless Ethernet bridge (radio). Installation of the seismic instruments at GASB was completed in September 2005, and broadband data acquisition began.

Marconi Conference Center (MCCM)

In November 2004, BSL and the University of California signed a License Agreement to construct a seismic vault and install instruments at the Marconi Conference Center near Marshall, CA. Located along the Tomales Bay, the surface trace of the San Andreas Fault, the conference center is part of the California State Park system. The site for the station was selected for its proximity to existing utilities and to minimize the disturbances to the historical and visual elements of the park. This site was constructed with combined funding from BSL, USGS/NEIC and the IRIS/GSN and is part of the ANSS backbone network.

Following the success of the seismic vaults at HOPS, PKD, and MNRC, the vault at MCCM was constructed using a recycled, ocean going, steel shipping container. The design is advantageous in locations where exist-

ing facilities or mine adits do not exist. Construction began in February 2005, with excavation and concrete pours. However, the installation of the instrumentation was delayed until after December 2005, when the electrical power was connected. Telemetry from the site is achieved via a NEIC VSAT. The satellite installation was completed by joint efforts of BSL and NEIC engineers in February 2006.

The station has been recording data since early February 2006, and VSAT telemetry has been operating since late February. The MCCM site features a Q4120 datalogger, a STS-2 seismometer, and a FBA ES-T strong motion instrument with 2 G limit. BSL engineers are presently pursuing a permit to augment the site telemetry via digital radio repeater. This permit is expected sometime in the next year.

3.4 The Monterey Bay Ocean Bottom Seismic Observatory (MOBB)

The Monterey Ocean Bottom Broadband observatory (MOBB) is a collaborative project between the Monterey Bay Aquarium Research Institute (MBARI) and the BSL. Supported by funds from the Packard Foundation to MBARI, NSF/OCE funds and UC Berkeley funds to BSL, its goal has been to install and operate a long-term seafloor broadband station as a first step towards extending the on-shore broadband seismic network in northern California, to the seaside of the North-America/Pacific plate boundary, providing better azimuthal coverage for regional earthquake and structure studies. It also serves the important goal of evaluating background noise in near-shore buried ocean floor seismic systems, such as may be installed as part of temporary deployments of “leap-frogging” arrays (e.g. Ocean Mantle Dynamics Workshop, September 2002).

BSL staff put significant effort in the development of procedures to minimize instrumental noise caused by air circulation inside the seismometer package casing (see 2001-2002 and 2002-2003 BSL Annual Reports). These procedures were later applied to the preparation of 3 similar packages destined for installation on the Juan de Fuca plate in the framework of University of Washington’s Keck project.

This project follows the 1997 MOISE experiment, in which a three component broadband system was deployed for a period of 3 months, 40 km off shore in Monterey Bay, with the help of MBARI’s “Point Lobos” ship and ROV “Ventana” (Figure 4.4). MOISE was a cooperative program sponsored by MBARI, UC Berkeley and the INSU, Paris, France (*Stakes et al.*, 1998; *Romanowicz et al.*, 1999; *Stutzmann et al.*, 2001). During the MOISE experiment, valuable experience was gained on the technological aspects of such deployments, which contributed to the success of the present MOBB installation.

The successful MOBB deployment took place April 9-

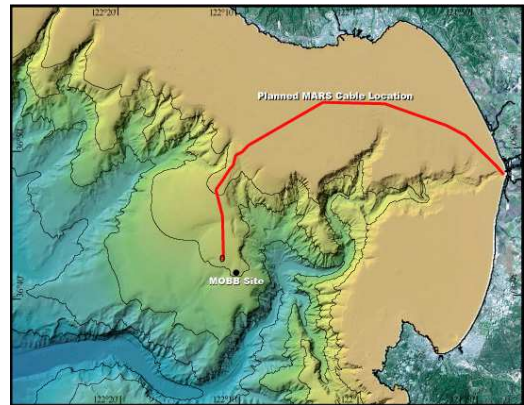


Figure 4.4: Location of the MOBB station in Monterey Bay, California, against seafloor and land topography. The projected path of the MARS cable is indicated by the solid line.

11, 2002 and the station is currently recording data autonomously (e.g. *Romanowicz et al.*, 2003). It comprises a 3 component very broadband CMG-1T seismometer system, a differential pressure gauge (DPG, *Cox et al.*, 1984) and a current meter. Data from the DPG are acquired with a sampling rate of 1 sps, and are crucial for the development and implementation of a posteriori noise deconvolution procedures to help counteract the large contribution of infragravity wave noise in the period range 20-200 sec. Procedures for removal of infragravity wave noise as well as signal generated noise have been developed (see chapter 10.).

Seventeen “dives” involving the MBARI ship “Point Lobos” and ROV “Ventana” have so far taken place to exchange dataloggers and battery packages during the time period 04/10/02 to 06/15/06. In February 2004, the N/S component seismometer failed. It was temporarily replaced, from 05/19/04 to 07/09/04 by one of the Keck seismometer packages which was conveniently available at that time. The original seismometer was sent back to Guralp Inc. for repair and successfully reinstalled on 07/09/04.

The data collection from the broadband seismic system is fairly complete. However, there have been recurring DPG sensor as well as DPG data storage problems in the first two years of the MOBB operation. Well recorded DPG data are available since 03/18/2004.

The MOBB station is located close to the projected path of the MARS cable (Figure 4.4) which is scheduled to be deployed in the Fall of 2006. The connection of MOBB to the MARS cable will allow continuous, real-time data acquisition from this site. Developing the interface for the connection to MARS is the object of a proposal to NSF submitted in the summer of 2006.

4. Acknowledgements

Under Barbara Romanowicz's general supervision, Peggy Hellweg and Doug Neuhauser oversee the BDSN data acquisition operations and Bill Karavas heads the engineering team. John Friday, Jarrett Gardner, Rick Lellinger and Bob Uhrhammer contribute to the operation of the BDSN. Karl Kappler has been responsible for the operation of the EM observatories. Bill Karavas, Bob Uhrhammer, and Peggy Hellweg contributed to the preparation of this chapter.

The California Governor's Office of Emergency Services provided funding toward the development of sites MCCM and GASB as part of the CISN. The Incorporated Research Institutions in Seismology provided matching funds for the installation of MCCM. The CREST project provided a datalogger for GASB. Earthscope (USArray) provided funds towards telemetry of northern California TA stations through BSL and operation of joint BDSN/USArray stations.

MOBB is a collaboration between the BSL and MBARI, involving Barbara Romanowicz, Bob Uhrhammer, Doug Neuhauser and David Dolenc from the BSL, and Debra Stakes and Paul McGill from MBARI. The MBARI team also includes Steve Etchemendy (Director of Marine Operations), Jon Erickson, John Ferreira, Tony Ramirez and Craig Dawe. The MOBB effort at the BSL is supported by UC Berkeley funds. MBARI supports the dives and data recovery. The MOBB seismometer package was funded by NSF/OCE grant #9911392.

The Earthscope Transportable Array provides support for telemetry and maintenance of the 19 BDSN stations from which the BSL supplies data to the USArray efforts.

5. References

Cox, C., T. Deaton and S. Webb, A deep-sea differential pressure gauge, *J. Atm. Ocean. Tech.*, 1, 237-245, 1984.

Crawford W. C., and S. C. Webb, Identifying and removing tilt noise from low-frequency (≤ 0.1 Hz) seafloor vertical seismic data, *Bull. Seis. Soc. Am.*, 90, 952-963, 2000.

Murdock, J., and C. Hutt, A new event detector designed for the Seismic Research Observatories, *USGS Open-File-Report 83-0785*, 39 pp., 1983.

Romanowicz, B., D. Stakes, J. P. Montagner, P. Tarits, R. Uhrhammer, M. Begnaud, E. Stutzmann, M. Pasyanos, J.F. Karczewski, S. Etchemendy, MOISE: A pilot experiment towards long term sea-floor geophysical observatories, *Earth Planets Space*, 50, 927-937, 1999.

Romanowicz, B., D. Stakes, R. Uhrhammer, P. McGill, D. Neuhauser, T. Ramirez and D. Dolenc, The MOBB experiment: a prototype permanent off-shore ocean bottom broadband station, *EOS Trans. AGU*, Aug 28 issue, 2003.

Stakes, D., B. Romanowicz, J.P. Montagner, P. Tarits, J.F. Karczewski, S. Etchemendy, D. Neuhauser, P. McGill, J-C. Koenig, J.Savary, M. Begnaud and M. Pasyanos, MOISE: Monterey Bay Ocean Bottom International Seismic Experiment, *EOS Trans. AGU*, 79, 301-309, 1998.

Stutzmann, E., J.P. Montagner et al., MOISE: a prototype multiparameter ocean-bottom station, *Bull. Seism. Soc. Am.*, 81, 885-902, 2001.

Wielandt, E., and J. Steim, A digital very broad band seismograph, *Ann. Geophys.*, 4, 227-232, 1986.

Wielandt, E., and G. Streckeisen, The leaf spring seismometer: design and performance, *Bull. Seis. Soc. Am.*, 72, 2349-2367, 1982.

Zürn, W., and R. Widmer, On noise reduction in vertical seismic records below 2 mHz using local barometric pressure, *Geophys. Res. Lett.*, 22, 3537-3540, 1995.

Chapter 5

California Integrated Seismic Network

1. Introduction

Advances in technology have made it possible to integrate separate earthquake monitoring networks into a single seismic system as well as to unify earthquake monitoring instrumentation. In California, this effort began in the south with the TriNet Project. There Caltech, the California Division of Mines and Geology, now called the California Geological Survey (CGS), and the USGS combined their efforts to create a unified seismic system for southern California. With major funding provided by the Federal Emergency Management Agency (FEMA), the California Governor's Office of Emergency Services (OES), and the USGS, the TriNet project provided the opportunity to upgrade and expand the monitoring infrastructure, combining resources in a federal, state and university partnership. More recently, the integration effort has been expanded to the entire State in a cooperation between the California Geological Survey, Caltech, UC Berkeley, USGS Menlo Park, and the USGS Pasadena called the California Integrated Seismic Network (CISN).

The initial efforts to create this collaboration are described in the 2000-2001 Annual Report. The CISN is now in the sixth year of collaboration and its fifth year of funding from the OES.

2. CISN Background

2.1 Organization

The organizational goals, products, management, and responsibilities of the CISN member organizations are described in the founding MOU and in the strategic and implementation plans. To facilitate coordination of activities among institutions, the CISN has formed three management centers:

- Southern California Management Center: Caltech/USGS Pasadena
- Northern California Earthquake Management Center: UC Berkeley/USGS Menlo Park

- Engineering Strong Motion Data Center: California Geological Survey/USGS National Strong Motion Program

One important goal of the CISN is for the Northern and Southern California Management Centers to operate as twin statewide earthquake processing centers while the Engineering Strong Motion Data Center has the responsibility for producing engineering data products and distributing them to the engineering community.

The Steering Committee oversees CISN projects and comprises two representatives from each core institution and a representative from OES. The position of chair rotates among the institutions; Woody Savage is currently the chair of the Steering Committee.

An external Advisory Committee, representing the interests of structural engineers, seismologists, emergency managers, industry, government, and utilities, has been formed for review and oversight. The Advisory Committee is chaired by Stu Nishenko of Pacific Gas and Electric Company. The Advisory Committee last met in October 2005. The agendas from previous meetings and the resulting reports may be accessed through the CISN Web site (<http://www.cisn.org/advisory>). The next meeting is planned for August 2006.

The Steering Committee has formed other committees, including a Program Management Group to address planning and coordination, a Strong Motion Working Group to focus on issues related to strong-motion data, and a Standards Committee to resolve technical design and implementation issues.

In addition to the core members, several organizations contribute data that enhances the capabilities of the CISN. Contributing members of the CISN include: University of California, Santa Barbara; University of California, San Diego; University of Nevada, Reno; University of Washington; California Department of Water Resources; Lawrence Livermore National Lab; and Pacific Gas and Electric.

2.2 CISN and ANSS

The USGS Advanced National Seismic System (ANSS) is being developed along a regionalized model. Eight regions have been organized, with the CISN representing California. David Oppenheimer of the USGS serves as the CISN representative to the ANSS National Implementation Committee (NIC).

Over the past 7 years, ANSS funding in California has been directed primarily to the USGS Menlo Park to expand the strong-motion instrumentation in the San Francisco Bay Area. As a result, more than 100 sites have been installed or upgraded, significantly improving the data available for ShakeMaps.

As the ANSS moves forward, committees and working groups are being established to address issues of interest. BSL faculty and staff have been involved in several working groups of the Technical Integration Committee, including Doug Dreger, Pete Lombard, Doug Neuhauser, Bob Uhrhammer, and Stephane Zuzlewski.

2.3 CISN and OES

The California Governor's Office of Emergency Services has had a long-term interest in coordinated earthquake monitoring. The historical separation between northern and southern California and between strong-motion and weak-motion networks resulted in a complicated situation for earthquake response.

OES has been an advocate of increased coordination and collaboration in California earthquake monitoring and encouraged the development of the CISN Strategic and Implementation Plans. In FY01/02, Governor Gray Davis requested support for the CISN, to be administered through OES. Funding for the California Geological Survey, Caltech and UC Berkeley was made available in spring 2002, officially launching the statewide coordination efforts.

Following the first year of funding, OES support led to the establishment of 3-year contracts to the UC Berkeley, Caltech, and the California Geological Survey for CISN activities. The first multi-year award covered activities in 2002-2005. The first year of the current, three-year contract has just been completed.

2.4 Statewide Communications

One of the major accomplishments in FY01/02 was the design and initial implementation of a CISN "backbone" communications infrastructure. Doug Neuhauser of the BSL took the lead in investigating options and the CISN partners decided to establish a "ring" of T1 communication links (Figure 5.1) with redundant routers at each site. The CISN backbone will gracefully revert to routing traffic through encrypted tunnels over the Internet should the T1 circuits fail at a site.

The CISN backbone has been operating since FY03/04. It is being used to transmit seismic waveform data and parametric data, including strong motion parameters, between the management centers and to distribute ShakeMaps to OES. It is also used to support mirroring of the CISN Web server.

All of the routers, with the exception of those at OES, have Internet connections for backup tunnels over the Internet if the T1 circuits fail. However, if the CISN T1 circuits were to go down at OES, OES would be completely isolated from the CISN network and all CISN partners. This continues to be an issue of major concern.

3. 2005-2006 Activities

The CISN funding from OES facilitated a number of activities at the BSL during the past year.

3.1 FEMA Hazard Grant Mitigation Program Funds

The San Simeon and Parkfield earthquakes highlighted the sparseness of high quality instrumentation in northern California, outside of the Bay Area. In both cases, the initial ShakeMaps were not well constrained, due to the lack of digital instrumentation with real-time communications. One major difference between these two events is that the Parkfield area is very densely instrumented, particularly with accelerometers deployed by the California Geological Survey. However, since these instruments were primarily analog, the data were not available until several days after the event.

As a result of the San Simeon earthquake and other disasters, FEMA has made funds available to OES under the Hazard Grant Mitigation Program (HGMP). The BSL, Caltech, and CGS submitted joint applications for funds to two of the HGMP programs, which were funded in August 2005 and May 2006. Funds to BSL from the first grant have been used to purchase equipment for one broadband station, and to relocate the data acquisition and processing systems from McCone Hall to 2195 Hearst (described in Chapter 10). The seismic equipment will be installed at the USArray station RAMR near the epicenter of the San Simeon event. The second grant will be used to purchase equipment for three further broadband stations, which will be installed in sparsely instrumented areas. One will also be in central California at HAST. The two other new stations will be located along the northern California coast, another seismically active region with few stations.

3.2 Expanded Instrumentation

In the past year, the BSL completed the installation broadband stations at two sites, Alder Springs, California, and the Marconi Conference Center, near Pt. Reyes,

California (GASB and MCCM, Figure 3.75). The station at GASB has been under discussion for a number of years, initially as part of the National Tsunami Hazards Program. It has been transmitting data since November, 2005. MCCM has been partially funded by IRIS, as a permanent component of USArray, and by USGS and OES. The first data were recorded in early February, 2006, with the installation of power, and telemetry commenced later in the month, when the ANSS VSAT system was installed.

With the completion of GASB and MCCM, the BSL has installed 4 of the 5 sets of site equipment purchased in the first year of the CISON. The efforts at GASB and MCCM are more fully described in Chapter 4.

3.3 Network Operations

With funding from the CISON project, the BSL purchased upgrade kits for 23 Q4120 data loggers to improve remote diagnostic capabilities. Three types of kits were purchased – power board only, calibration board only, and combined power and calibration boards – so that each Q4120 has a power board and that each 8-channel Q4120 also has a calibration board. The power boards allow battery voltage to be monitored, so staff can discriminate between power and telemetry problems remotely. The calibration boards provide the capability to monitor mass position and allow remote calibration of the seismic sensors. Both boards also record data logger temperature. To upgrade the dataloggers they must be returned to the lab, where the boards are installed and the lattices on the CPU board replaced. New cables must be prepared to transmit the mass position signals. When the upgrade is complete, the datalogger is redeployed to the field. The 3 remaining upgrades were completed this year, with cables or lattices being replaced where necessary.

3.4 Collaboration with USArray

In late 2003, the CISON concluded a memorandum of agreement with the Incorporated Research Institutions in Seismology (IRIS) covering the duration of the USArray project in California. As a result 19 stations operated by the BSL and 41 stations operated by Caltech are part of USArray during its California deployment. Both Caltech and the BSL modified some station operations in order to meet the USArray specifications. In particular, USArray requires BH data to be sampled at 40 sps, rather than the 20 sps as was standard in California. The surface broadband stations of BDSN were converted to 40 sps over June 15-16th, 2004. The BSL has also provided accelerometers for use at USArray sites which may be of interest as future BDSN stations. We continue to monitor the data from these stations in real time, and use the data in ShakeMaps and moment tensors. The collaboration

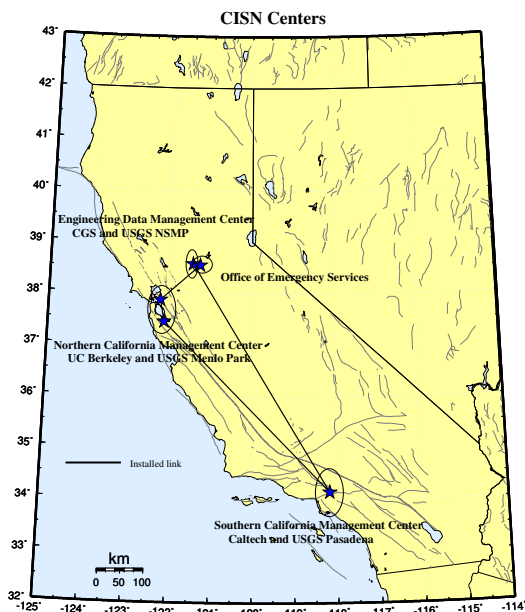


Figure 5.1: Map showing the geographical distribution of the CISON partners and centers. The communications “ring” is shown schematically with installed links (solid lines).

between the BSL and USArray is discussed more fully in Chapters 4 and 10, including the telemetry the BSL provides for the two USArray stations RAMR and SUTB.

3.5 Northern California Earthquake Management Center

As part of their effort within the CISON, the BSL and the USGS Menlo Park have begun to implement the next generation of the northern California joint notification system. Chapter 11 describes the operations of the existing Management Center and reports on design discussions.

Communications Infrastructure

In order to move ahead with plans for restructuring the northern California earthquake monitoring system, the USGS Menlo Park and BSL have been working to improve their communications infrastructure.

At present, the BSL and the USGS Menlo Park are connected by two dedicated T1 circuits. One circuit is a component of the CISON ring, while the second circuit was installed in 2004-2005 (Figure 5.3) to support dedicated traffic between Berkeley and Menlo Park above and beyond that associated with the CISON.

The installation of the second dedicated T1 between Berkeley and Menlo Park freed up a frame-relay connection deployed by the BSL as part of the CalREN project

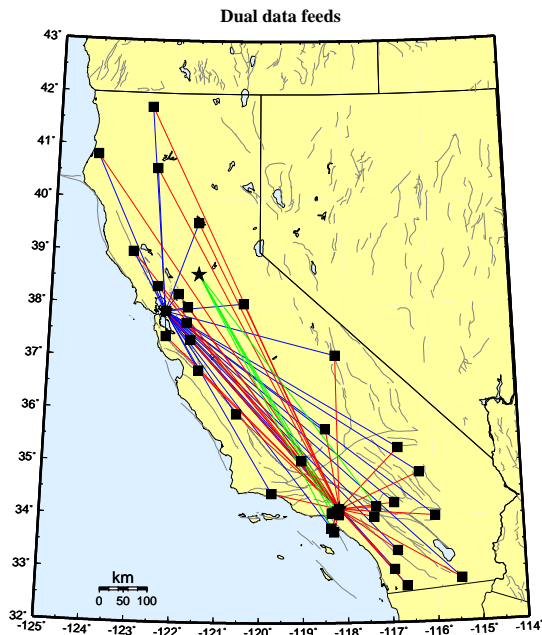


Figure 5.2: Map showing the 30 stations selected to send data directly to the Northern and Southern California processing centers, and the 5 stations that send data directly to the Engineering Data Center and the Southern California processing center.

in mid-1990s. The BSL has reconfigured this frame-relay circuit to serve as a second data acquisition link. The plan is to distribute the BDSN data acquisition between the two frame-relay T1 circuits, eliminating what had been a single point of failure. A second component of the plan is to establish an additional Permanent Virtual Circuit (PVC) at each BDSN site so that each station has connections to both T1s.

The acquisition of seismic data is now distributed between the two T1s and a second PVC is established at each frame-relay site. This effort has improved the robustness of data acquisition at the BSL by providing redundancy in the incoming circuit.

In the long term, the BSL and USGS Menlo Park hope to be connected by high-bandwidth microwave or satellite service. Unfortunately, we have not been able to obtain funding for this additional communication link at this time.

4. Statewide Integration

BSL staff are involved in many elements of the statewide integration effort. The Standards Committee continues to define and prioritize projects necessary to develop a prototype system and establish working groups to address them (see minutes from meetings and conference calls at <http://www.cisn.org/standards/meetings.html>).

Dual Station Feeds

One of the major accomplishments in the first few years has been the establishment of “dual station feeds” at 30 stations (15 in northern California and 15 in southern California) (Figure 5.2). To achieve this, the BSL and Caltech both ordered the DLCIs (data link connection identifier) that allow the 2nd center to establish a PVC to each station using the frame-relay network.

The Northern California Earthquake Management Center (NCEMC) is using data from the Southern California stations to estimate magnitudes on a routine basis. A subset of these stations are being used for the moment tensor inversions, a computation that is sensitive to the background noise level.

Data Exchange

Pick exchange was initiated between the NCEMC and its Southern California counterpart in 2001-2002. The software CISN has developed to produce and exchange the reduced amplitude timeseries has been completed. Currently, these timeseries are being exchanged at the NCEMC, but not yet statewide.

Using a common format, the CISN partners continue to exchange observations of peak ground motion with one another following an event or a trigger. This step increases the robustness of generating products such as ShakeMap, since all CISN partners now exchange data directly with one another. This also improves the quality of ShakeMaps for events on the boundary between northern and southern California, such as the San Simeon earthquake, by allowing all data to be combined in a single map. Finally, this is a necessary step toward the goal of generating statewide ShakeMaps.

Software Calibration & Standardization

The CISN partners are working together on the problem of software calibration, particularly as it pertains to automated earthquake processing. Currently, the software implemented in the NCEMC and in Southern California Management Center is very different. Initially, the CISN focused on the issue of calibration although the last year has seen an increased focus on standardization.

In 2002-2003, effort was focused on phase pickers (*pick-ew*), the association algorithm (*binder*), the location algorithm (*hypoinverse*), and magnitude estimation (various). Since then, magnitude estimation continues to be a significant area of focus, as well as ShakeMap configuration, metadata exchange, and database standardization.

At this point, the issues of a statewide detection and location system are largely addressed. Configuration files have been standardized and a statewide system has been running in Menlo Park for more than a year. It performed well during the December 2003 San Simeon sequence and

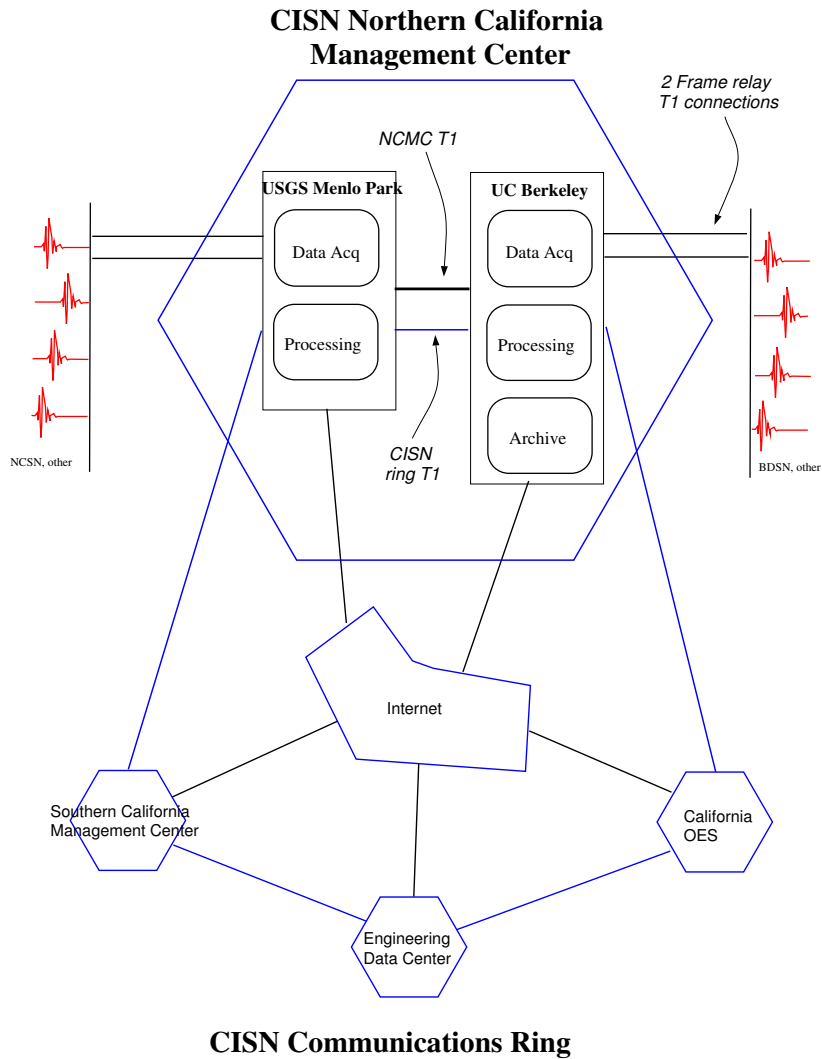


Figure 5.3: Schematic diagram illustrating the connectivity between the real-time processing systems at the USGS Menlo Park and UC Berkeley, forming the northern California Management Center, and with other elements of the CISN.

the 2004 Parkfield earthquake. A number of outstanding issues still remain to be addressed.

Magnitude: Calibrating magnitude estimates has proven to be more difficult than the CISN originally anticipated. As described in 2003-2004, three lines of evidence indicate that there is a bias between the northern and southern California magnitude estimates. First, a comparison of nearly 500 earthquakes over a 20 year period in central California recorded by both networks shows a bias of 0.14 magnitude units, with NC magnitudes higher than SC magnitudes. Second, efforts to in-

vert Wood Anderson amplitudes using a differential approach, a constraint that the BKS and PAS adjustments sum to zero, and fixing the attenuation relationship to one determined by *Kanamori* (1993), indicates a bias of 0.14. Finally, an independent inversion of a different dataset (absolute approach, a different set of station constraints, and simultaneous inversion for attenuation) suggests a bias of 0.20.

Efforts to understand this issue have been hampered by the lack of a good statewide dataset. In 2005-2006, Bob Uhrhammer selected data from 180 earthquakes dis-

tributed throughout the state and comprising recordings from 976 horizontal components from the AZ, BK, CI and NC networks. He has begun to assess station-specific corrections for M_L by determining the difference for each station-component pair. State-wide, the average difference is -0.039. The primary advantage of using this differencing method is that the results are independent of a reference station.

A final component of the magnitude efforts is the designation of a magnitude reporting hierarchy. After many discussions, there is general agreement that, at least for the near future, each region will continue to use its own preferences for magnitude reporting.

ShakeMap: In addition to the efforts in standardizing earthquake locations and magnitudes, a CISN working group has been addressing issues related to ShakeMaps. At present, ShakeMaps are generated on 5 systems within the CISN. Two systems in Pasadena generate “SoCal” Shakemaps; 2 systems in the Bay area generate “No-Cal” Shakemaps; and 1 system in Sacramento generates ShakeMaps for all of California. The Sacramento system uses QDDS to provide the authoritative event information for northern and southern California.

During the past year, the Working Group has continued to address standardization issues for ShakeMap. Initially efforts focused on the look and feel of the maps (topography, geology, faults, road, lake outlines, cities, and fonts). The Working Group reviewed a comprehensive compilation of the differences in configuration among the 3 implementations. Efforts continue to address the remaining differences between the centers, which range from the small (URL used in the “addon” message) to the significant (use of regressions, linear versus log amplitude weighting). Resolving these differences will move the CISN forward toward having fully standardized ShakeMaps.

The lack of stations in the near source region of the 2003 San Simeon earthquake raised the issues of how to measure the quality of a ShakeMap and to quantify the uncertainty. A subset of the Working Group has been working on this issue, based on the work of *Hok and Wald* (2003). *Lin et al* (2006) presented progress toward quantifying ShakeMap uncertainty. When the method is validated, we can use this information to determine a grade.

Toward the goal of improving access to ShakeMap, the working group has put together an outline of how to create a unified set of Web pages. With general agreement about what to do, small progress has been made on actual implementation. The primary difficulty has been time, since creating unified Web pages requires a separation between product generation and Web page generation.

A second goal of this effort was to improve the robustness of ShakeMap generation and delivery by taking advantage of the fact that ShakeMaps are generated in the

Bay Area, Pasadena, and Sacramento. Renewed efforts in this direction will likely be based on the new USGS ShakeMap webpages at the National Earthquake Information Center. Work in this direction continues in the coming year.

Location Codes: The CISN adopted a standard for the use of “location” codes (part of the Standard for the Exchange of Earthquake Data (SEED) nomenclature to describe a timeseries based on network-station-channel-location) in the late fall of 2003. USGS and UC Berkeley developers have modified the Earthworm software to support the use of location codes. The migration to their use is awaiting the transition at USGS Menlo Park away from the CUSP analysis system.

Metadata Exchange: The availability and exchange of metadata is vital to CISN activities, as correct metadata are required to insure valid interpretation of data. CISN is also working on issues related to the reliable and timely exchange of these data.

Several years ago, the Metadata Working Group compiled a list of metadata necessary for data processing and developed a model for exchanging metadata. In this model, each CISN member is responsible for the metadata for its stations and for other stations that enter into CISN processing through it. For example, Menlo Park is responsible for the NSMP, Tremor, and PG&E stations, while Caltech is responsible for the Anza data.

Initially, the exchange of metadata was to be accomplished through database replication. In the past two years, individual developments at the various CISN partners have made this an unwieldy solution. At the present time, dataless SEED volumes are being used to exchange metadata between the NCEMC and the SCMC, while the Metadata Working Group develops a better and more robust means of exchange. In the long term, it will be important to develop a vehicle for the exchange of a more comprehensive set of metadata than is permitted in dataless SEED volumes. They cannot encompass, for example, all the parameters which must be included in V0 formatted data.

In parallel, the Working Group has developed a plan for importing metadata from CGS. Their metadata is not currently stored in a database and is maintained in simple files. Their policy is to distribute the metadata as part of a waveform package using the especially developed V0 format. The Working Group developed the concept of a “dataless” V0 format (analogous to the dataless SEED files) which is used to distribute the metadata. The CGS now provides dataless V0 files containing current metadata for ShakeMap quality stations (i.e., with channels meeting CISN Reference Station or better standards) in the CGS network. They are being distributed and are also placed at the CGS FTP site. As agreed, the comment field in the V0 header defines the valid time period for the metadata. Each dataless V0 file contains the 3

channels of the reference sensor at the site. The Working Group plan includes the ability to handle corrections, as well as updates as stations are serviced.

In order to make use of the dataless V0 file, tools have been developed to parse the file and write an XML file containing the information (an expansion of capabilities of the v02ms program). The NCEMC has taken advantage of previously existing tools to create a system where the XML is converted into a spreadsheet format and then imported into the database. This plan will be further tested as CGS generates more dataless V0 files and the database is populated.

As part of this process, the issue of mapping the sensor orientation into the SEED channel nomenclature has come up. The v02ms program now uses the same algorithm for generating channel names as used by CGS.

Standardization The CISON's focus on standardization, rather than calibration of software continues. For example, the BSL and the USGS Menlo Park are adapting the software running at the SCMC for use at the NCEMC and are currently testing its various elements. Examples of collaboration include the development of the CISON Messaging Service - software designed to replace the commercial **SmartSockets** package used in the initial development of TriNet, implementation of the **RequestCardGenerator** and **Jiggle** in northern California, and ongoing efforts to develop specifications for a magnitude coordinator.

4.1 CISON Display

CISON Display is an integrated Web enabled earthquake notification system, designed to provide earthquake information for emergency response at 24/7 operations centers. First-responders, organizations with critical lifelines and infrastructure, and emergency responders are invited to register for an account at <http://www.cisn.org/software/cisndisplay.htm>.

The application provides users with maps of real-time seismicity, and automatically provides access to Web-related earthquake products such as ShakeMaps. CISON Display also offers an open source GIS mapping tool that allows users to plot freely available layers of public highways, roads and bridges, as well as private layers of organizational-specific infrastructure and facilities information. The current version of CISON Display is 1.31.

4.2 Earthquake Information Distribution

The USGS hosted a workshop in October 2004 to develop plans for the installation and use of the EIDS software. Doug Neuhauser and Pete Lombard participated in this workshop, which resulted in a document outlining the steps necessary for the installation and migration of the earthquake notification system from the current Quake Data Distribution Services (QDDS) to EIDS.

4.3 Outreach

There has been progress at www.cisn.org in FY05/06. The CISON Web site is now supported by two servers located at Berkeley and Caltech. The Web servers are set up so that the load can be distributed between them, providing improved access during times of high demand. With the increased robustness provided by the new servers, the CISON has begun to provide access to certain earthquake products directly from www.cisn.org. For example, ShakeMaps are now served directly from the CISON Web site, in addition to being available from several USGS Web servers and the CGS.

The design and content of <http://www.cisn.org> continues to evolve. The Web site is an important tool for CISON outreach as well as for communication and documentation among the CISON partners.

The CISON continues to support the dedicated Web site for emergency managers. Following a suggestion from the Advisory Committee, we have designed a Web site to provide personalized access to earthquake information. Known as "myCISON," the Web site is available at eoc.cisn.org. Access to the Web site is limited to registered users in order to provide highly reliable access. At present, "myCISON" is a single Web server located at UC Berkeley. However, modifications to the database are underway to allow for multiple servers in the future. A second computer, already purchased, will either be installed in Sacramento or in southern California.

As part of the CISON, the BSL also contributed to efforts to raise awareness during 1906 centennial activities. In particular, we co-hosted the *1906 Earthquake Conference* contributed to the preparation of the CISON booth at the meeting (see Chapter ??)

5. Acknowledgements

CISON activities at the BSL are supported by funding from the Governor's Office of Emergency Services.

Barbara Romanowicz and Peggy Hellweg are members of the CISON Steering Committee. Peggy Hellweg is a member of the CISON Program Management Group and she leads the CISON project at the BSL, with support from Doug Neuhauser during the transition. . Doug Neuhauser is chair of the CISON Standards Committee, which includes Peggy Hellweg and Pete Lombard as members.

Because of the breadth of the CISON project, many BSL staff have been involved including: John Friday, Peggy Hellweg, Bill Karavas, Pete Lombard, Doug Neuhauser, Charley Paffenbarger, Bob Uhrhammer and Stephane Zuzlewski. Peggy Hellweg contributed to this chapter. Additional information about the CISON is available through reports from the Program Management Committee.

6. References

Ad Hoc Panel on Earthquake Information Distribution (L. Gee and D. Oppenheimer, chairs), Requirements for an Earthquake Information Distribution System, http://www.cisn.org/ahpeid/ahpeid_final.pdf, 2003.

Gee, L., D. Dreger, G. Wurman, Y. Gung, B. Uhrhammer, and B. Romanowicz, A Decade of Regional Moment Tensor Analysis at UC Berkeley, *EOS Trans. AGU*, 84(46), Fall Meet. Suppl., Abstract S52C-0148, 2003.

Gee, L., D. Oppenheimer, T. Shakal, D. Given, and E. Hauksson, Performance of the CISN during the 2003 San Simeon Earthquake, http://www.cisn.org/docs/CISN_SanSimeon.pdf, 2004a.

Gee, L., J. Polet, R. Uhrhammer, and K. Hutton, Earthquake Magnitudes in California, *Seism. Res. Lett.*, 75(2), 272, 2004b.

Hauksson, E., L. Gee, D. Given, D. Oppenheimer, and T. Shakal, Report to the CISN Advisory and Steering Committees, #5, <http://www.cisn.org/oes/2003.05.30.pdf>, 2003.

Hok, S., and D. J. Wald, Spatial Variability of Peak Strong Ground Motions: Implications for ShakeMap Interpolations, *EOS. Trans. AGU*, 84(46), F1121, 2003.

Kanamori, H., J. Mori, E. Hauksson, T. Heaton, L. Hutton, and L. Jones, Determination of earthquake energy release and M_L using TERRASCOPE, *Bull. Seis. Soc. Am.*, 83, 330-346, 1993.

Lin, K-W., D. Wald, B. Worden and A.F. Shakal, Progress toward quantifying CISN ShakeMap uncertainty, *Eighth National Conference on Earthquake Engineering, San Francisco, California, April 18-21, 2006*.

Chapter 6

Northern Hayward Fault Network

1. Introduction

Complementary to the regional broadband network, a deployment of borehole-installed, wide-dynamic range seismographic stations is being established along the Hayward Fault and throughout the San Francisco Bay toll bridges network. This network is a cooperative development of the BSL and the USGS, with support from USGS, Caltrans, EPRI, the University of California Campus/Laboratory Collaboration (CLC) program, LLNL, and LBNL (Figure 6.1 and Table 6.1). Efforts at ongoing development of the network have also recently been enhanced through coordinated efforts with the Mini-PBO project which is partially funded by NSF and by the member institutions of that project.

The purpose of the network is threefold: 1) to lower substantially the threshold of microearthquake detection, 2) to increase the recorded bandwidth for events along the Hayward fault, and 3) to obtain bedrock ground motion signals at the bridges from small earthquakes for investigating bridge responses to stronger ground motions. A lower detection threshold increases the resolution of the fault-zone seismic structure; allows seismologists to monitor the spatial and temporal evolution of seismicity at magnitudes down to $M \sim -1.0$, where earthquake rates are many times higher than those captured by surface sites; allows researchers to look for pathologies in seismicity patterns that may be indicative of the nucleation of large damaging earthquakes; and allows scientists to investigate fault and earthquake scaling, physics and processes in the San Francisco Bay Area. This new data collection will also contribute to improved working models for the Hayward fault. The bedrock ground motion recordings are also being used to provide input for estimating the likely responses of the bridges to large, potentially damaging earthquakes. Combined with the improved Hayward fault models, source-specific response calculations can be made as well.

The Hayward Fault Network (HFN) consists of two parts. The Northern Hayward Fault Network (NHFN) is operated by the BSL and currently consists of 28 stations with various operational status, including those located

on Bay Area bridges and at borehole sites of the Mini-PBO (MPBO) project. This network is considered part of the BDSN and uses the network code BK. The Southern Hayward Fault Network (SHFN) is operated by the USGS and currently consists of 5 stations. This network is considered part of the NCSN and uses the network code NC. This chapter is primarily focused on the NHFN and activities associated with the BSL operations.

2. NHFN Overview

The five MPBO sites have 3-component borehole geophone packages. All the remaining HFN sites have six-component borehole sensor packages. The packages were designed and fabricated at LBNL's Geophysical Measurement Facility by Don Lippert and Ray Solbau, with the exception of site SFAB. For the HFN sites, three channels of acceleration are provided by Wilcoxon 731A piezoelectric accelerometers, and three channels of velocity are provided by Oyo HS-1 4.5 Hz geophones. Velocity measurements for the MPBO sites are provided by Mark Products L-22 2 Hz geophones (Table 6.2). The 0.1-400 Hz Wilcoxon accelerometers have lower self-noise than the geophones above about 25-30 Hz, and remain on scale and linear to 0.5 g. In tests performed in the Byerly vault at UC Berkeley, the Wilcoxon is considerably quieter than the FBA-23 at all periods, and is almost as quiet as the STS-2 between 1 and 50 Hz.

Sensors are generally installed at depths of about 100 m, but several sites have sensors emplaced at depths of over 200 m, and the Dumbarton bridge sites have sensors at multiple depths (Table 6.1). During initial stages of the project, the NHFN sensors provided signals to on-site Quanterra Q730 and RefTek 72A-07 dataloggers.

Today, 14 of the NHFN sites have Quanterra dataloggers with continuous telemetry to the BSL. Similar to BDSN sites, these stations are capable of on-site recording and local storage of all data for more than one day and have batteries to provide backup power. Signals from these stations are digitized at a variety of data rates up to 500 Hz at 24-bit resolution (Table 6.3).

The NHFN dataloggers employ casual FIR filters at

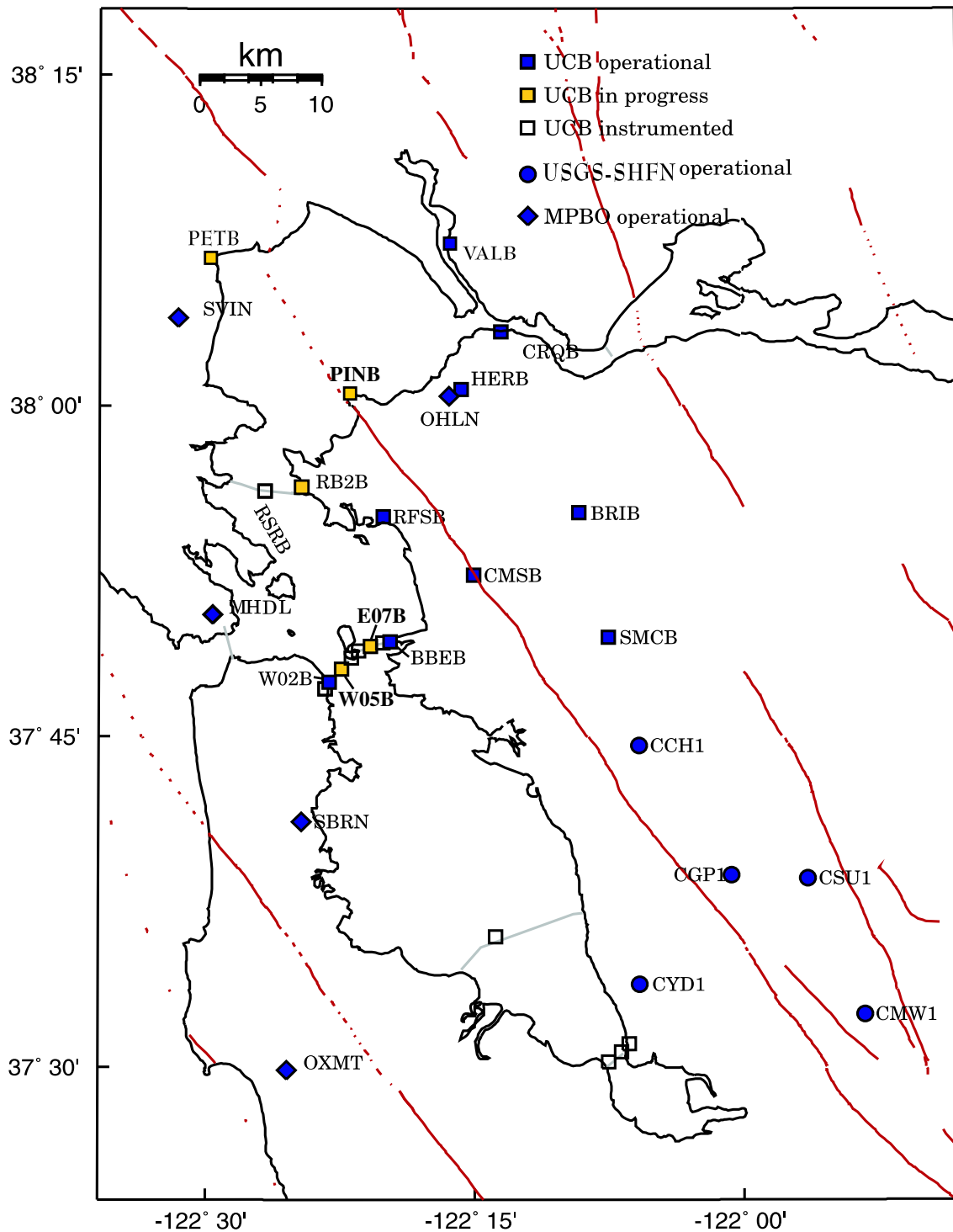


Figure 6.1: Map showing the locations of the HFN stations operated by the BSL (NHFN - squares) and the USGS (SHFN - circles) and Mini-PBO stations (diamonds) in the San Francisco Bay Area. Operational sites are filled blue/black, while sites in progress are yellow/grey. Other instrumented boreholes are indicated as open symbols.

high data rates and acausal FIR filters at lower data rates. Because of limitations in telemetry bandwidth and disk storage, 9 of these sites transmit one channel of 500 sps continuous data and 90 sec., 500 sps triggered data snippets for the remaining channels. The Murdock, Hutt, and Halbert (MHH) event detection algorithm (*Murdock and Hutt, 1983*) is operated independently at each station on 500 sps data for trigger determinations. Continuous data for all channels at reduced rates (20 and 1 sps) are also transmitted to and archived at the BSL. The five MPBO sites transmit continuous 100, 20 and 1 sps 3 component data streams that are also archived at BSL.

The remaining 14 sites of the NHFN have in the past recorded data using RefTek dataloggers. These sites do not have continuous telemetry for acquisition and in the past required visits from BSL staff for data recovery. Collection of data from these sites has been discontinued, but efforts are underway to upgrade them with Quanterra Q4120, Q730 or Q330 dataloggers and continuous telemetry.

Signals from the 5 SHFN stations are digitized by Nanometrics data loggers at 100 sps and transmit continuous data to Menlo Park by radio. These digital data streams are processed by the Earthworm system with the NCSN data and waveforms are saved when the Earthworm detects an event.

Data from both the NHFN and SHFN are archived at the NCEDC (Northern California Earthquake Data Center). At this time, the tools are not in place to archive the Hayward fault data together. The NHFN data are archived with the BDSN data, while the SHFN are archived with the NCSN data.

2.1 Station Maintenance

Ongoing network maintenance involves regular inspection of the collected seismic waveform data and spectra for nearby seismic events, and also from noise samples. Other common problems include changes to background noise levels due to ground loops, failing preamps, as well as power and telemetry issues. Troubleshooting and remediation of problems often require a coordinated effort with a technician at the BSL to examine seismic waveforms and spectra as the field technicians are still on site. BSL technicians regularly review data and assist in troubleshooting.

NHFN Station Maintenance Synopsis

The NHFN station hardware has proven to be relatively reliable. Nonetheless, numerous maintenance and performance enhancement measures are still required. Below is a synopsis of maintenance efforts performed recently for several NHFN stations that serves to illustrate some of the ongoing maintenance and enhancement measures that are typically performed.

BEB: Ran radio tests on Wilan link to Space Sciences Lab at 18 dBm and at maximum power (23 dBm) to ascertain effect on dropped packets. At 24 dBm power, the throughput was 6 times higher than at 18 dBm power and the number of dropped packets reduced from 4.6

BRIB: Numerous frame relay telemetry problems were encountered during August and September, and the station was visited several times to troubleshoot and correct the problem.

CMSB: Quanterra hung after 8/17 reboot. The power was manually recycled, and the Quanterra came back up.

CRQB: Quanterra hung after 8/17 reboot. The power was manually recycled, and the Quanterra came back up and was functioning normally.

HERB: Velocity channel was found in September to not be responsive to events. The problem was traced to a blown fuse in the power system, although it is unclear as to how that problem effected the responsiveness of the velocity channel.

RFSB: Visited station several times to repair frame relay and power supply problems.

SMCB: Quanterra hung after 8/17 reboot. The power was manually recycled, and the Quanterra came back up.

W02B: Telemetry link went down in October and again in December due to an antenna problem.

Quality Control

A commonly used check on the calibration of the borehole installed network, is to compare the bandpass filtered (0.3-2 Hz) ground velocity data recorded at NHFN and MPBO stations for large teleseismic earthquakes. As an example, a M 7.5 intermediate focus teleseism that occurred in Peru at a depth of 115 km is shown in Figure 6.3.

Another practise for quality control is the assessment of power spectral density (PSD) distributions for the network stations. Shown in Figure 6.2 are power spectral density distributions of background noise for a sample of 13 NHFN land and bridge site stations. In general, background noise levels of the borehole HFN stations is more variable and generally higher than that of the Parkfield HRSN borehole stations (see Parkfield Borehole Network chapter). This is due in large part to the significantly greater level of cultural noise in the Bay Area, and to the fact that noise reduction efforts on the much more recently installed NHFN stations are still underway. For example the two noisiest stations (i.e. BEB and W02B) are located on the Bay Bridge, which is currently undergoing earthquake retrofit and east span reconstruction. These stations have also only recently come back on-line with upgraded infrastructure and instrumentation, so the full complement of noise reduction modifications have not yet been implemented.

On average the MPBO component of the NHFN sites is more consistent and somewhat quieter. This is due in

Code	Net	Latitude	Longitude	Elev (m)	Over (m)	Date	Location
VALB	BK	38.1215	-122.2753	-24	155.8	2005/11 - current	Napa River Bridge
PETB	BK	38.1189	-122.5011	-30	113	in progress	Petaluma River Bridge
CRQB	BK	38.05578	-122.22487	-25	38.4	1996/07 - current	CB
HERB	BK	38.01250	-122.26222	-25	217.9	2000/05 - current	Hercules
PINB*	BK	38.0113	-122.3653	tbd	tbd	in progress	Point Pinole
BRIB	BK	37.91886	-122.15179	219.7	108.8	1995/06 - current	BR, Orinda
RFSB	BK	37.91608	-122.33610	-27.3	91.4	1996/01 - current	RFS, Richmond
CMSB	BK	37.87195	-122.25168	94.7	167.6	1994/12 - current	CMS, Berkeley
SMCB	BK	37.83881	-122.11159	180.9	151	1997/12 - current	SMC, Moraga
SVIN	BK	38.03325	-122.52638	-21	158.7	2003/08 - current	MPBO, St. Vincent's school
OHLN	BK	38.00742	-122.27371	-0	196.7	2001/07 - current	MPBO, Ohlone Park
MHDL	BK	37.84227	-122.49374	94	160.6	2006/05 - current	MPBO, Marin Headlands
SBRN	BK	37.68562	-122.41127	4	157.5	2001/08 - current	MPBO, San Bruno Mtn.
OXMT	BK	37.4994	-122.4243	209	194.2	2003/12 - current	MPBO, Ox Mtn.
BBEB	BK	37.82167	-122.32867	-31	150.0	2002/05 - current	BB, Pier E23
E17B	BK	37.82086	-122.33534		160.0	1995/08 - current *	BB, Pier E17
E07B	BK	37.81847	-122.34688	tbd	134.0	1996/02 - current *	BB, Pier E7
YBIB	BK	37.81420	-122.35923	-27.0	61.0	1997/12 - current *	BB, Pier E2
YBAB	BK	37.80940	-122.36450		3.0	1998/06 - current *	BB, YB Anchorage
W05B	BK	37.80100	-122.37370	tbd	36.3	1997/10 - current *	BB, Pier W5
W02B	BK	37.79120	-122.38525	-45	57.6	2003/06 - current	BB, Pier W2
SFAB	BK	37.78610	-122.3893		0.0	1998/06 - current *	BB, SF Anchorage
RSRB	BK	37.93575	-122.44648	-48.0	109.0	1997/06 - current *	RSRB, Pier 34
RB2B	BK	37.93	-122.41	tbd	133.8	2003/07 - current *	RSRB, Pier 58
SM1B	BK	37.59403	-122.23242		298.0	not recorded	SMB, Pier 343
DB3B	BK	37.51295	-122.10857		1.5	1994/09 - 1994/11	DB, Pier 44
					62.5	1994/09 - 1994/09	
					157.9	1994/07 - current *	
DB2B	BK	37.50687	-122.11566			1994/07 - current *	DB, Pier 27
					189.2	1992/07 - 1992/11	
DB1B	BK	37.49947	-122.12755		0.0	1994/07 - 1994/09	DB, Pier 1
					1.5	1994/09 - 1994/09	
					71.6	1994/09 - 1994/09	
					228.0	1993/08 - current *	
CCH1	NC	37.7432	-122.0967	226		1995/05 - current	Chabot
CGP1	NC	37.6454	-122.0114	340		1995/03 - current	Garin Park
CSU1	NC	37.6430	-121.9402	499		1995/10 - current	Sunol
CYD1	NC	37.5629	-122.0967	-23		2002/09 - current	Coyote
CMW1	NC	37.5403	-121.8876	343		1995/06 - current	Mill Creek

Table 6.1: Stations of the Hayward Fault Network. Each HFN station is listed with its station code, network id, location, operational dates, and site description. The latitude and longitude (in degrees) are given in the WGS84 reference frame. The elevation of the well head (in meters) is relative to the WGS84 reference ellipsoid. The overburden is given in meters. The start dates indicate either the upgrade or installation time. The abbreviations are: BB - Bay Bridge; BR - Briones Reserve; CMS - Cal Memorial Stadium; CB - Carquinez Bridge; DB - Dumbarton Bridge; MPBO - mini-Plate Boundary Observatory; RFS - Richmond Field Station; RSRB - Richmond-San Rafael Bridge; SF - San Francisco; SMB - San Mateo Bridge; SMC - St. Mary's College; and, YB - Yerba Buena. The * for station PINB indicates that this station name has been requested but has not yet been approved and may change. The * in the Date column indicates that the stations have recorded data from an earlier period of manually retrieved tapes, but that are currently off-line.

large part to the greater depth of the MPBO sensors, the locations of MPBO stations in regions of generally less

industrial and other cultural noise sources, and possibly to the absence of powered sensors (i.e. accelerometers)

Site	Geophone	Accelerometer	Z	H1	h2	datalogger	Notes	Telem.
VALB	Oyo HS-1	Wilcoxon 731A	TBD	TBD	TBD	Q330		FR
PETB	Oyo HS-1	Wilcoxon 731A	TBD	TBD	TBD	TBD		TBD
CRQB	Oyo HS-1	Wilcoxon 731A	-90	251	341	Q4120		FR
HERB	Oyo HS-1	Wilcoxon 731A	-90	TBD	TBD	Q4120		FR
PINB	Oyo HS-1	Wilcoxon 731A	TBD	TBD	TBD	TBD		TBD
BRIB	Oyo HS-1	Wilcoxon 731A	-90	79	349	Q4120	Acc. failed, Dilat.	FR
RFSB	Oyo HS-1	Wilcoxon 731A	-90	256	346	Q4120		FR
CMSB	Oyo HS-1	Wilcoxon 731A	-90	19	109	Q4120		FR
SMCB	Oyo HS-1	Wilcoxon 731A	-90	76	166	Q4120	Initially Posthole	FR
SVIN	Mark L-22		-90	298	28	Q4120	Tensor.	FR/Rad.
OHLN	Mark L-22		-90	313	43	Q4120	Tensor.	FR
MHDL	Mark L-22		-90	TBD	TBD	Q4120	Tensor.	FR
SBRN	Mark L-22		-90	347	77	Q4120	Tensor.	FR
OXMT	Mark L-22		-90	163	253	Q4120	Tensor.	FR
BBEB	Oyo HS-1	Wilcoxon 731A	-90	TBD	TBD	Q4120	Acc. failed	Radio
E17B	Oyo HS-1	Wilcoxon 731A	-90	TBD	TBD	None at present		
E07B	Oyo HS-1	Wilcoxon 731A	-90	TBD	TBD	None at present		
YBIB	Oyo HS-1	Wilcoxon 731A	-90	257	347	None at present	Z geop. failed	FR/Rad.
YBAB	Oyo HS-1	Wilcoxon 731A	-90	TBD	TBD	None at present		
W05B	Oyo HS-1	Wilcoxon 731A	-90	TBD	TBD	None at present		
W02B	Oyo HS-1	Wilcoxon 731A	-90	TBD	TBD	Q4120		Radio
SFAB	None	LLNL S-6000	TBD	TBD	TBD	None at present	Posthole	
RSRB	Oyo HS-1	Wilcoxon 731A	-90	50	140	None at present	2 acc. failed	FR
RB2B	Oyo HS-1	Wilcoxon 731A	-90	TBD	TBD	None at present	1 acc. failed	
SM1B	Oyo HS-1	Wilcoxon 731A	-90	TBD	TBD	None at present		
DB3B	Oyo HS-1	Wilcoxon 731A	-90	TBD	TBD	None at present	Acc. failed	
DB2B	Oyo HS-1	Wilcoxon 731A	-90	TBD	TBD	None at present		
DB1B	Oyo HS-1	Wilcoxon 731A	-90	TBD	TBD	None at present	Acc. failed	
CCH1	Oyo HS-1	Wilcoxon 731A	-90	TBD	TBD	Nanometrics HRD24	Dilat.	Radio
CGP1	Oyo HS-1	Wilcoxon 731A	-90	TBD	TBD	Nanometrics HRD24	Dilat.	Radio
CSU1	Oyo HS-1	Wilcoxon 731A	-90	TBD	TBD	Nanometrics HRD24	Dilat.	Radio
CYD1	Oyo HS-1	Wilcoxon 731A	-90	TBD	TBD	Nanometrics HRD24	Dilat.	Radio
CMW1	Oyo HS-1	Wilcoxon 731A	-90	TBD	TBD	Nanometrics HRD24	Dilat.	Radio

Table 6.2: Instrumentation of the HFN as of 06/30/2006. Every HFN downhole package consists of co-located 3-component geophones and accelerometers, with the exception of MPBO sites which have only 3-component geophones and are also collecting tensor strainmeter data. Six HFN sites (5 of the SHFN and 1 of the NHFN) also have dilatometers (Dilat.). Currently, 14 NHFN sites have Quanterra dataloggers with continuous telemetry to the BSL. The remaining sites are either still being developed with support from Caltrans or are being upgraded to Quanterra dataloggers. The 5 SHFN sites have Nanometrics dataloggers with radio telemetry to the USGS. The orientation of the sensors (vertical - Z, horizontals - H1 and H2) are indicated where known or identified as "to be determined" (TBD).

in their borehole sensor packages.

One of the most pervasive problems at NHFN stations equipped with the Q4120 dataloggers is power line noise (60 Hz and its harmonics at 120, 180, and 240 Hz). This noise reduces the sensitivity of the MHH detectors. Whenever a NHFN station is visited, the engineer at the site and a seismologist at the BSL work together to expedite the testing process, especially when attempting to identify and correct ground-loop faults which generally

induce significant 60, 120, 180, and 240 Hz seismic signal contamination due to stray power line signal pickup, generally inductively coupled and aggravated by the presence of ground loops.

Geophone Calibration Test Equipment

Comparisons of the inferred ground accelerations generated by local earthquakes from co-sited NHFN geophone and accelerometer pairs show that the waveforms

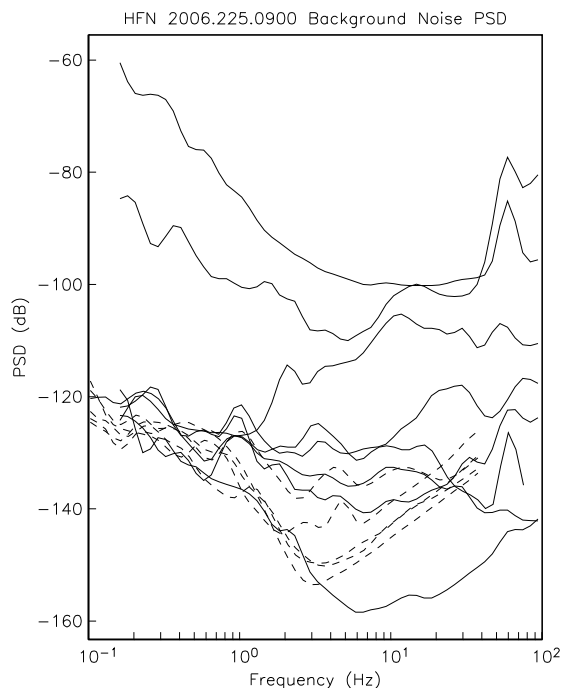


Figure 6.2: Plot showing typically observed background noise PSD for the NHFN borehole stations (including the MPBO in dashed lines) as a function of frequency. The data are from 2 am Local time on a Sunday morning. Note that there is considerable variation in the general level and structure of the individual station background noise PSD estimates. Of all the HFN stations, BRIB, the quietest borehole emplaced station, is also the farthest from local cultural noise sources. The signals from three of the stations (BBEB, SMCB and W02B) have 60 Hz noise, which is due to the presence of ground loops. The four noisiest stations (BBEB, CRQB, VALB and W02B) are near bridge anchorages. The PSD ranking of the stations of the stations at 4.6 Hz (near minimum PSD for most of the stations) is:

BRIB.BK.DP1 -156.46204
 CMSB.BK.DP1 -151.96701
 OXMT.BK.EP1 -151.28152
 MHDL.BK.EP1 -149.33257
 SVIN.BK.EP1 -148.51234
 SBRN.BK.EP1 -138.45128
 RFSB.BK.DP1 -137.71815
 OHLN.BK.EP1 -132.80258
 SMCB.BK.DP1 -131.35008
 VALB.BK.EP1 -128.44617
 CRQB.BK.DP1 -114.13147
 BBEB.BK.DP1 -109.71306
 W02B.BK.DP1 -98.61494

generally are quite coherent in frequency and phase response, but that their inferred ground accelerations differ significantly. At times, the amplitudes differ by up to a factor of 2 while the times of the peak amplitudes are identical. This implies that the free period and damping of the geophones are well characterized. However, it also indicates that the generator constant is not accurate (assuming that the corresponding ground accelerations inferred from the accelerometers are accurate).

Generally speaking, the accelerometers, being an active device, are more accurate and also more stable than the geophones, so it is reasonable to assume that the most likely reason for the difference is that the assumed generator constants for the geophones are inaccurate. *Rodgers et al.* (1995) describe a way to absolutely calibrate the geophones in situ and to determine their generator constant, free period and fraction of critical damping. The only external parameter that is required is the value of the geophones inertial mass.

We have built a calibration test box which allows us to routinely perform the testing described by *Rodgers et al.* whenever site visits are made. The box drives the signal coil with a known current step and rapidly switches the signal coil between the current source and the datalogger input. From this information, expected and actual sensor response characteristics can be compared and corrections applied. Also, changes in the sensor response over time can be evaluated so that adjustments can be made, and pathologies arising in the sensors due to age can be identified. Once a geophone is absolutely calibrated, we can also check the response of the corresponding accelerometer.

We are still performing the initial calibration tests and response adjustments for all NHFN stations as sites are visited for routine maintenance. We also plan to schedule routine re-tests of all sites to monitor for sensor responses changes through time.

3. 2005-2006 Activities

In addition to routine maintenance, operations and data collection, activities of the NHFN project over the past year have also included numerous efforts at network expansion, quality control and data analysis.

3.1 New Installations

As originally conceived, the Hayward Fault Network was to consist of 24 to 30 stations, 12-15 each north and south of San Leandro, managed respectively by UCB and USGS. Due to funding limitations, however, progress has been slow and the original plan has been significantly modified. Fortunately and with additional Caltrans support continued development of the NHFN component of the project has been possible and is ongoing. This important contribution to the Hayward Fault Network has

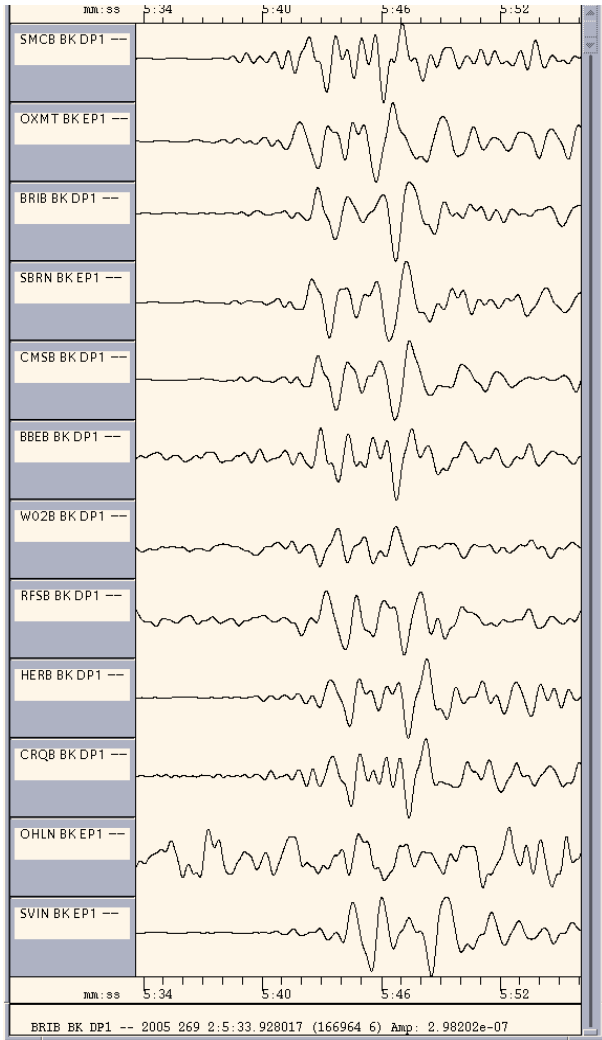


Figure 6.3: Plot of P-wave seismograms, recorded by 12 NHFN/MPBO borehole stations operating at the time of a major intermediate focus earthquake occurring this past year (2005/09/26; 01:55:38 UT; 115 km deep; M_w 7.5; 60.8 deg. S55E of Berkeley, CA). Here vertical component geophone data have been deconvolved to ground acceleration, 0.3-2 Hz 6-pole, BP filtered and ordered by increasing distance (top to bottom). Of the 12 HFN, BB and MPBO vertical geophones that recorded the event, all the P waveforms are highly similar except for OHLN, which is noisy and not responding nominally to ground motion, and W02B, which has a low amplitude and distorted signal.

more than doubled the number of sites with instrumentation that would otherwise not have existed. Caltrans continues to provide holes of opportunity (e.g., recently SMCB, PETB, VALB), so we have plans for additional stations that will bring the network geometry to a more effective state for imaging and real-time monitoring of the

Sensor	Channel	Rate (sps)	Mode	FIR
Accelerometer	CL?	500.0	T	Ca
Accelerometer	BL?	20.0	C	Ac
Accelerometer	LL?	1.0	C	Ac
Geophone	DP?	500.0	T,C	Ca
Geophone	EP?	200.0	C	Ca
Geophone	BP?	20.0	C	Ac
Geophone	LP?	1.0	C	Ac

Table 6.3: Typical data streams acquired at each NHFN site, with channel name, sampling rate, sampling mode and FIR filter type. C indicates continuous, T triggered, Ca causal, and Ac acausal. Typically the DP1 continuous channel is archived and the remaining high sample rate data (i.e., CL and DP channels) are archived as triggered snippets. Prior to Sept. 2004, however, only triggered data was archived for all high sample rate channels.

Hayward fault. Below are short summaries of activities over the past year related to the preparation, installation and activation of new NHFN stations.

San Francisco Bay and Richmond-San Rafael Bridges

Current support is allowing 4 Bay-Bridge stations to be included in the compliment of NHFN stations and two of these stations are already on-line (i.e., BBEB and W02B). Telemetry issues dictate that these two site also serve as rely sites for data coming from the remaining two sites (i.e., W05B and E07B). Because of their critical roles as data relay sites, robust telemetry from these sites is needed. This year various adjustments have been made to optimize telemetry performance of these two stations including their upgrade to Wilan radio telemetry. The infrastructure of the W05B and E07B sites has been upgraded with the installation of weatherproof boxes, power, and telemetry in anticipation of installing Q4120 dataloggers and telemetering their data back to Berkeley.

These and continuing efforts to bring W05B and E07B on-line have been significantly hampered by ongoing Bay-Bridge retrofit work. As a particularly poignant example of this occurred in the Spring of 2006 when retrofit work crews severed the sensor cable to the mid-western span station W05B, losing the cabling into deep bay waters. Fortunately, with Caltrans assistance, a deep diving crew was dispatched and the sensor cable was recovered in good condition.

On the Richmond-San Rafael Bridge, similar problems associated with Bridge retrofit work have been encountered. In addition to the complete loss of mid-span station RSRB a few years ago, our toll plaza site RB2B has had to be relocated. Drilling and installation of the sensors down hole for the site was finished last year and this

year installation of the new site infrastructure and electronics has been largely completed. Coordination with Caltrans for power and telephone hook-ups are currently underway.

Land Sites

Agreements with Caltrans and St. Mary's College have been made to replace the post hole installation at St. Mary's College (SMCB) with a deep borehole installation. This year the hole was drilled by Caltrans as a hole of opportunity (i.e., when the schedule of a Caltrans drilling crew had an opening). The site has been reviewed by UCB, Caltrans and St. Mary's College personnel, and with assistance from Caltrans and St. Mary's College grounds crew personnel, the site infrastructure is nearly complete, and data acquisition and telemetry to UCB is expected to begin shortly.

Caltrans has also provided funding and support for drilling and sensor installation at 2 other land sites (VALB and PETB). The Napa River Bridge site in Vallejo, CA (VALB) is now operating and has been on-line since November of 2005. The PETB (Petaluma River Bridge) site has been drilled and instrumented. Infrastructure construction on the site continues and should be completed within weeks. Routine data flow and archival at the NCEDC is expected after telemetry and power hook-ups are completed.

Currently we are also considering three other sites (in Pt. Pinole regional Park, Mt. Diablo Regional Park and at Wildcat Mtn.) as candidates for two additional holes-of-opportunity in the North//East Bay. We are in the process of obtaining permission from the East Bay Regional Park District (EBRPD) to site the Pt. Pinole station at the Point Isabel Regional Shoreline and have completed field inspection of the two other sites which appear to be suitable.

Mini-PBO

The stations of the Mini-PBO project are equipped with 3-component borehole seismometers and tensor strainmeters. As these stations have become operational, they augment well the HFN's coverage of the Bay Area (Figure 6.1). In the last year, MHDL (Marine Headlands) has come on-line and is now adding much needed coverage on the west side of the Bay.

3.2 Quality control and Data Analysis

In order to monitor and capture the source spectrum of moderate down to micro-scale earthquakes, it is essential that the NHFN instruments operate at high precision and in an extremely low noise environment. Therefore, the stations record at high sample rate and their sensors are emplaced in deep boreholes to reduce noise contamination originating in the near surface weathered zone and

from cultural noise sources. In addition, the reduction of noise at these stations through vigilant monitoring of actual seismic events plays a central part of our quality control effort.

The Aug. 3, 2006 Glen Ellen Earthquake

In Figure 6.4, we show a profile of the NHFN stations for the recent (August 3, 2006) M_L 4.6 earthquake located at Glen Ellen, California, about 60 km NW of Berkeley. Figures such as this are helpful for evaluating network health, and analysis of the waveforms and spectra assist in troubleshooting problems. As Figure 6.4 shows the network is performing very well, but there are some stations exhibiting problems. For example, the Bay Bridge site W02B shows high frequency noise, and OLNH and OXMT show sensitivity and dropout problems.

Microseismicity

As mentioned, a key aspect of quality control of the NHFN data is the analysis of actual seismic events. Seismic events of larger magnitude are relatively rare and generally provide more energy at lower frequencies. Hence in order to provide more frequent real events and quality control in the higher frequency band of the NHFN stations, analysis of recordings from the much more frequent microearthquakes are needed. Because real event analyses are relatively labor intensive and because of inadequate insufficient funding, traditional methods of event analysis have proven financially infeasible. To help circumvent these problems, efforts to develop new and improved analysis techniques are ongoing. We have developed and are currently testing some promising techniques that are particularly well suited to the analysis of similar and repeating microearthquakes. The advantages of similar and repeating event analyses for both quality control and scientific purposes are numerous, and the nature of the seismograms from these types of events make automated, rapid and robust analysis possible.

Towards this end, we are currently testing three new algorithms which we have developed: 1) a phase onset time detector with sub-sample timing resolution for improved absolute pick time accuracy, 2) a pattern scanning recognition scheme to detect, pick, locate and determine magnitudes for small and very small similar events recorded either continuously or from among large volumes of noisy triggered data snippets, and 3) a phase coherency method for identification of characteristically repeating events sequences from among groups of similar event multiplets.

Phase Onset Time Detection: The phase onset time detector makes use of the concept that the complex spectral phase data over the bandwidth of interest (i.e., where the SNR is sufficiently high) will sum to

a minimum at the onset of an impulsive P-wave. The algorithm searches for the minimum phase time via phase shifting in the complex frequency domain over the bandwidth where the SNR is above 30 dB to identify the onset time of the seismic phase. The algorithm requires that the recorded waveforms be deconvolved to absolute ground displacement. This implicitly requires that any acausality in the anti-aliasing filtration chain, such as the FIR filters used in the BDSN Quanterra dataloggers, be removed. The algorithm typically resolves P-wave onset times to one-fiftieth of the sample interval or better.

Pattern Scanning Recognition: The Murdock-Hutt detection algorithms used by MultiSHEAR, which basically flags an event whenever the short-term average exceeds a longer-term average by some threshold ratio, is neither appropriate for nor capable of detecting the smallest seismic events where signal to noise levels approach those of spurious cultural and earth noise signals. This is because the increased sensitivity parameters needed for small event detection also result in a large fraction of false event triggers. The use of multiple station association filters to reduce the false trigger rates are also of limited value since many of the smaller events are only recorded with enough signal to noise to trigger at a few stations and noise triggers at high sensitivity also often appear to associate temporally at several stations. Added to this is this the exponential increase in the frequency of events with decreasing magnitude, which quickly makes analyst time requirements for comprehensive review and processing of the smallest events financially infeasible.

The approach we have been working on this year to help overcome these problems has been to enhance the effective signal to noise and to focus on identification and processing of some of the more scientifically significant events through the use of a cross-correlation based scanning approach, which scans known waveform patterns through either continuous or collections triggered event snippets (regardless of the triggered event noise levels). With this approach continuous or triggered waveform data that does not match selected patterns are ignored while waveforms that approximately match selected reference event patterns are flagged as newly identified earthquakes.

This approach is less comprehensive in that it only detects events that are somewhat similar in waveform character to the reference patterns. However, it can be generalized significantly by increasing the number of event patterns scanned or by using fairly low maximum cross-correlation thresholds for event flagging. Preliminary tests of our scanning code show that scans of 100 distinct event patterns can be scanned through a days worth of waveform data in 75 minutes on one 900Mhz SPARC cpu when continuous seismic data is used. Scanning through collections of all triggered snippets is sub-

stantially faster, in proportion to the inverse fraction of total time spanned by the snippet data.

The approach also provides automated cross-correlation pick alignments that can be used for high precision relative locations and for automated low-frequency spectral ratio determinations for magnitude estimates. Clearly the method has potential for automatically cataloging a large fraction of the more numerous microearthquakes, and in conjunction with the special attributes of similar event groups, updates of the catalogs in an automated monitoring mode can provide near-real-time microearthquake information that can be a powerful tool for monitoring network performance of real event data. Future plans include development and implementation of an automated similar event scanning and cataloging scheme that will provide real-event data from similar small magnitude events for assessment of network health on a much more frequent basis (every few days).

Perhaps more significantly, the approach can also capture and rapidly catalog some of the most scientifically relevant events (e.g. repeats of characteristically repeating microearthquakes used for deep slip rate monitoring and swarms of similar events typically associated with foreshocks and aftershocks). The approach is also surprisingly good at detecting events over a wide magnitude range. Hence there is clear potential for using patterns from larger aftershocks (e.g. flagged by REDI) to rapidly and automatically develop a high-resolution picture of foreshock and aftershock activity associated with large mainshocks. Tests so far using waveform patterns from an aftershock from the Parkfield magnitude 6 event (2.2MI) have been able to detect and fully process similar events as low as MI - 1.2 (a range of 3.4 magnitude units). Testing in this regard is continuing, but clearly the 3.4 magnitude range is a lower bound on the potential magnitude range attainable.

Phase Coherency: A spectral phase coherency algorithm was developed to facilitate high resolution quantification of the similarities and differences between highly similar Hayward fault events that occur months to years apart. The resolution of the complex spectral phase coherency methodology is an order of magnitude better than the cross correlation method, which is commonly used to identify highly similar events with resolution of order of a few 10's of meters. This method, originally developed using NHFN borehole data, is now also being tested and refined using data from another borehole network (the HRSN). The goal of the testing and refinement is ultimately to develop a scheme for rapid and objective discrimination and identification of characteristically repeating microearthquakes sequences down to the lowest magnitude possible (where recurrence times are short and hence temporal resolutions are higher) at both Parkfield,

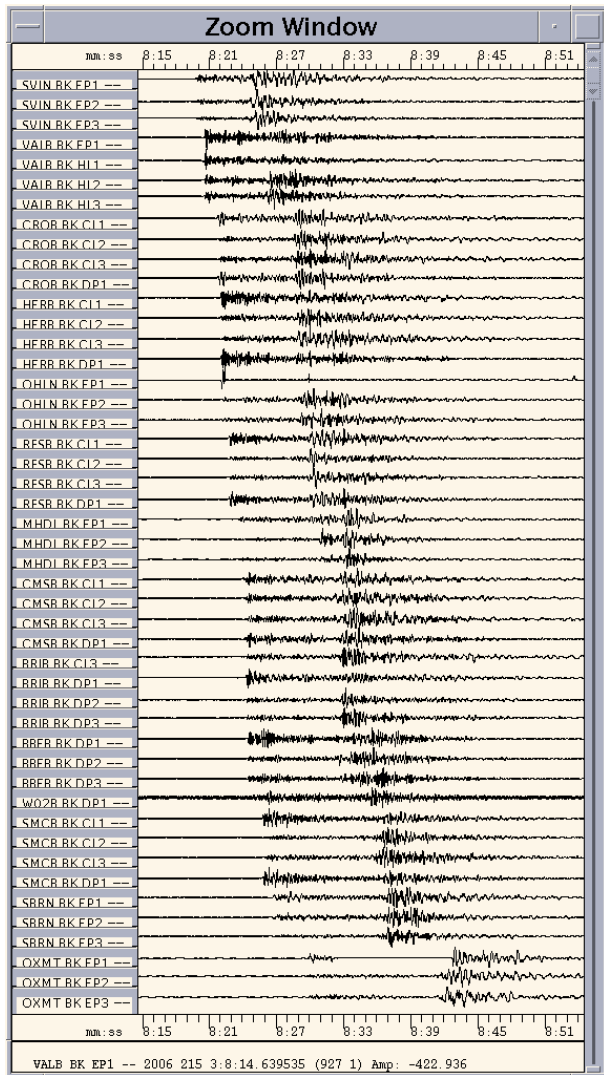


Figure 6.4: Record section of NHFN data for the 03 August 2006, MI 4.6 Glen Ellen, California earthquake located about 60 km northwest of Berkeley. These raw waveform data are ordered by epicentral distance and are relatively scaled.

and in the Bay Area of California.

4. Acknowledgments

Thomas V. McEvelly, who passed away in February 2002, was instrumental in developing the Hayward Fault Network, and without his dedication and hard work the creation and continued operation of the NHFN would not have been possible.

Under Bob Nadeau's, Bob Uhrhammer's and Doug Dreger's general supervision, Rich Clymer, Doug Neuhauser, Bill Karavas, John Friday, and Rick Lellingner all contribute to the operation of the NHFN. Bob Nadeau

and Bob Uhrhammer contributed to the preparation of this chapter.

Partial support for the NHFN is provided by the USGS through the NEHRP external grant program (grant no. 04HQGR0104). Expansion of the NHFN has been made possible through generous funding from Caltrans (grant no. 59A0245), with the assistance of Pat Hipley. Larry Hutchings and William Foxall of LLNL have also been important collaborators on the project in years past.

5. References

Rogers, P.W., A.J. Martin, M.C. Robertson, M.M. Hsu, and D.B. Harris, Signal-Coil Calibration of Electromagnetic Seismometers, *Bull. Seism. Soc. Am.*, 85(3), 845-850, 1995.

Murdock, J., and C. Hutt, A new event detector designed for the Seismic Research Observatories, *USGS Open-File-Report 83-0785*, 39 pp., 1983.

Chapter 7

Parkfield Borehole Network (HRSN)

1. Introduction

The operation of the High Resolution Seismic Network (HRSN) at Parkfield, California began in 1987, as part of the United States Geological Survey (USGS) initiative known as the Parkfield Prediction Experiment (PPE) (*Bakun and Lindh, 1985*).

Figure 7.1 shows the location of the network, its relationship to the San Andreas fault, sites of significance from previous and ongoing research using the HRSN, double-difference relocated earthquake locations from 1987-1998, routine locations of seismicity from August 2002 to July 2003, nonvolcanic tremor locations from January 2001 through April 2005, and the epicenter of the 1966 and 2004 M6 earthquakes that motivated much of the research. The HRSN records exceptionally high-quality data, owing to its 13 closely spaced three-component borehole sensors (generally emplaced in the extremely low attenuation and background noise environment at 200 to 300 m depth (Table 7.1), its high-frequency wide bandwidth recordings (0-100 Hz; 250 sps), and its low magnitude detection threshold (below magnitude 0.0 Ml).

Several aspects of the Parkfield region make it ideal for the study of small earthquakes and nonvolcanic tremors and their relationship to tectonic processes and large earthquakes. These include the fact that the network spans the SAFOD (San Andreas Fault Observatory at Depth) experimental zone, the nucleation region of earlier repeating magnitude 6 events and a significant portion of the transition from locked to creeping behavior on the San Andreas fault, the availability of three-dimensional P and S velocity models (*Michelini and McEvilly, 1991*), the existing long-term HRSN seismicity catalogue that is complete to very low magnitudes and that includes at least half of the M6 seismic cycle, a well-defined and simple fault segment, the existence of deep nonvolcanic tremor (NVT) activity, and a homogeneous mode of seismic energy release as indicated by the earthquake source mechanisms (over 90% right-lateral strike-slip).

In a series of journal articles and Ph.D. theses, we have presented the cumulative, often unex-

pected, results of UC Berkeley's HRSN research efforts (see: http://www.seismo.berkeley.edu/seismo/faq/parkfield_bib.html). They trace the evolution of a new and exciting picture of the San Andreas fault zone responding to its plate-boundary loading, and they are forcing new thinking on the dynamic processes and conditions within the fault zone at the sites of recurring small earthquakes and deep nonvolcanic tremors (*Nadeau and Dolenc, 2005*).

The Parkfield area has also become an area of focus of the EarthScope Project (<http://www.earthscope.org>) through the SAFOD experiment (<http://www.icdp-online.de/sites/sanandreas/news/news1.html>), and the HRSN is playing a vital role in this endeavor. SAFOD is a comprehensive project to drill into the hypocentral zone of repeating $M \sim 2$ earthquakes on the San Andreas Fault at a depth of about 3 km. The goals of SAFOD are to establish a multi-stage geophysical observatory in close proximity to these repeating earthquakes, to carry out a comprehensive suite of down-hole measurements in order to study the physical and chemical conditions under which earthquakes occur, and to monitor and exhume rock, fluid, and gas samples for extensive laboratory studies (*Hickman et al., 2004*).

2. HRSN Overview

2.1 1986 - 1998

Installation of the HRSN deep (200-300m) borehole sensors initiated in 1986, and recording of triggered 500 sps earthquake data began in 1987. The HRSN sensors are 3-component geophones in a mutually orthogonal gimbaled package. This ensures that the sensor corresponding to channel DP1 is aligned vertically and that the others are aligned horizontally. In November 1987, the Varian well vertical array was installed and the first VSP survey was conducted, revealing clear S-wave anisotropy in the fault zone (*Daley and McEvilly, 1990*). During 1988, the original 10 station network was completed, which included a deep (572 m) sensor from the Varian well string. Data from network stations was

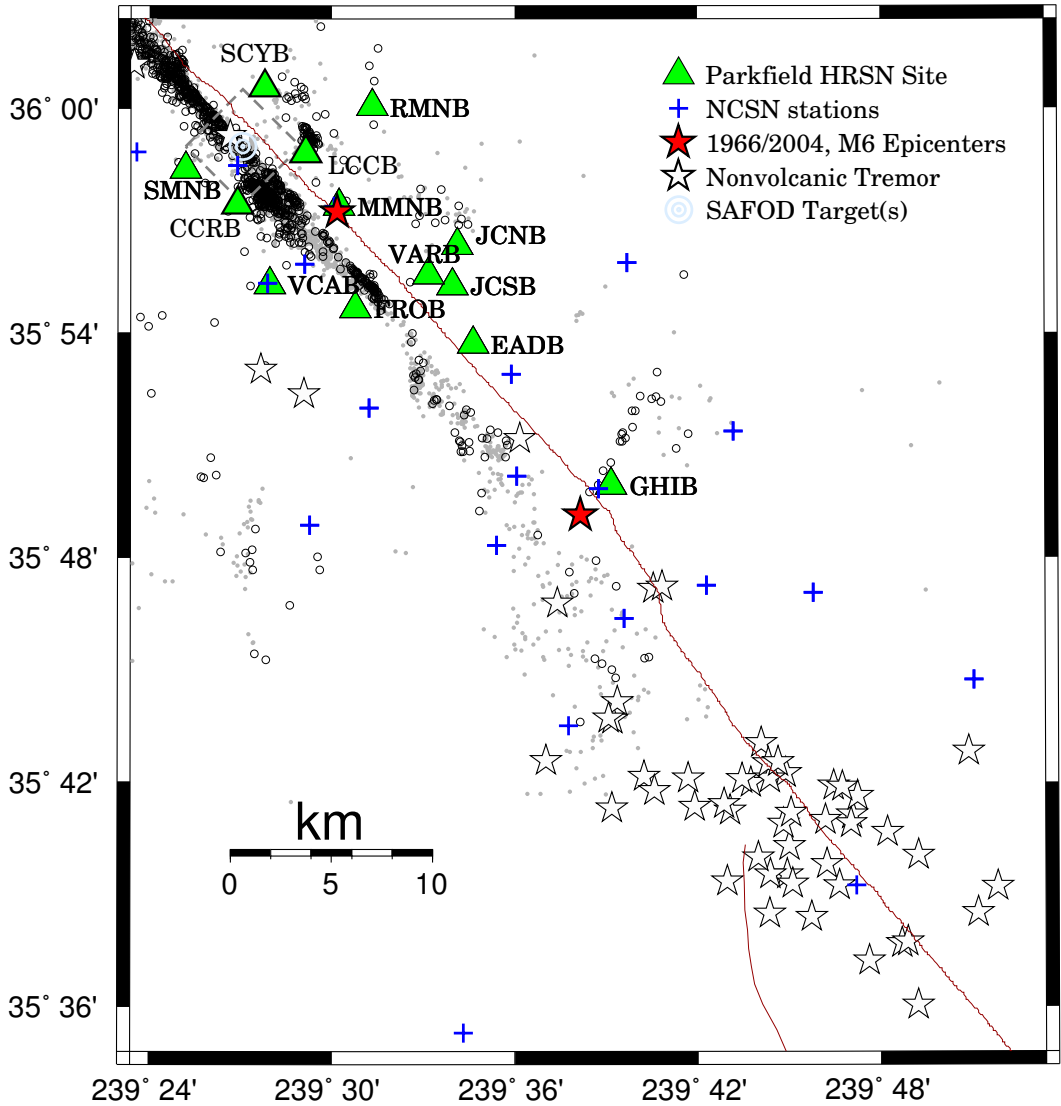


Figure 7.1: Map showing the San Andreas Fault trace and locations of the 13 Parkfield HRSN stations, the repeating M2 SAFOD targets (a 4 km by 4 km dashed box surrounds the SAFOD zone), and the epicenters of the 1966 and 2004 M6 Parkfield main shocks. Also shown are locations of the recently discovered nonvolcanic tremors, routine locations of earthquakes recorded by the expanded and upgraded 13 station HRSN (small open circles) and locations of events recorded by the earlier vintage 10 station HRSN relocated using an advanced 3-D double-differencing algorithm (gray points) applied to a cubic splines interpolated 3-D velocity model (*Michelini and McEvilly, 1991*).

telemetered into a central detection/recording system operating in triggered mode. Also in 1988, the Varian string system was slaved for about two years to the Vibroseis control signals, allowing simultaneous recording of vibrator signals on both systems. For several years beginning in 1991, low-gain event recorders (from PASSCAL) were installed at several of the sites to extend the dynamic range upward from about M_L 1.5 to about M_L 4.5.

The data acquisition system operated quite reliably until late 1996, when periods of unacceptably high down time developed. During this period, as many as 7 of the remote, solar-powered telemetered stations were occasionally down simultaneously due to marginal solar generation capacity and old batteries, and recording system outages of a week or more were not uncommon. In July 1998, the original data acquisition system failed permanently. This system was a modified VSP recorder acquired from LBNL, based on a 1980- vintage LSI-11 cpu and a 5 MByte removable Bernoulli system disk with a 9-track tape drive, configured to record both triggered microearthquake and Vibroseis data (Vibroseis discontinued in 1994, *Karageorgi et al.*, 1997). The system was remote and completely autonomous, and data tapes were mailed about once a month to Berkeley for processing and analysis. The old system also had a one-sample timing uncertainty and a record length limitation because the tape write system recovery after event detection was longer than the length of the record, leaving the system off-line after record termination and until write recovery was completed.

2.2 1998 - 1999

In December 1998, the original HRSN acquisition system was replaced by 10 stand-alone PASSCAL RefTek systems with continuous recording. To process these data, development of a major data handling procedure will be required in order to identify the microearthquakes below $M_L = 0.0$, since continuous telemetry to the Berkeley Seismological Laboratory (BSL) and application of a central site detection scheme was not an option at that time.

In July 1999, the network was reduced, due to limited instrument availability, to four RefTeks at critical sites that would ensure continuity in monitoring at low magnitudes and the archive of characteristic events for studying the evolution of their recurrence intervals. Properties of the 10 original sites are summarized in Table 7.2.

2.3 2001 Upgrade and SAFOD Expansion

Thanks to emergency funding from the USGS NEHRP, we replaced the original 10-station system with a modern 24-bit acquisition system (Quanterra 730 4-channel digitizers, advanced software using flash disk technol-

Sensor	Channel	Rate (sps)	Mode	FIR
Geophone	DP?	250.0	T and C	Ca
Geophone	BP?	20.0	C	Ac

Table 7.3: Data streams currently being acquired at each HRSN site. Sensor type, channel name, sampling rate, sampling mode, and type of FIR filter are given. C indicates continuous; T triggered; Ac acausal; Ca causal. “?” indicates orthogonal vertical and 2 horizontal components.

ogy, spread-spectrum telemetry, Sun Ultra 10/440 central processor at the in-field collection point, with 56K frame-relay connectivity to Berkeley) in 2001. The new system is now online and recording data continuously at a central site located on California Department of Forestry (CDF) fire station property in Parkfield.

We have also added three new borehole stations, with NSF support, at the NW end of the network as part of the SAFOD project to improve resolution of the structure, kinematics and monitoring capabilities in the SAFOD drill-path and target zones. Figure 7.1 illustrates the location of the drill site, the new borehole sites, and locations of earthquakes recorded by the initial and upgraded/expanded HRSN.

The three new SAFOD stations have a similar configuration as the original upgraded 10 station network and include an additional channel for electrical signals. Station descriptions and instrument properties are summarized in Tables 7.1 and 7.2. All HRSN Q730 dataloggers employ FIR filters to extract data at 250 and 20 Hz (Table 7.3).

The remoteness of the drill site and new stations required an installation of an intermediate data collection point at Gastro Peak, with a microwave link to the CDF facility. The HRSN stations use SLIP to transmit TCP and UDP data packets over bidirectional spread-spectrum radio links between the on-site data acquisition systems and the central recording system at the CDF. Six of the sites transmit directly to a router at the central recording site. The other seven sites transmit to a router at Gastro Peak, where the data are aggregated and transmitted to the central site over a 4 MBit/second digital 5.4 GHz microwave link. All HRSN data are recorded to disk at the CDF site.

The upgraded and expanded system is compatible with the data flow and archiving common to all the elements of the BDSN/NHFN and the NCEDC (Northern California Earthquake Data Center), and is providing remote access and control of the system. It has also provided triggered data with better timing accuracy and longer records, which are to eventually flow seamlessly into NCEDC. The new system also helps minimize the problems of timing resolution, dynamic range, and missed detections, in ad-

Site	Net	Latitude	Longitude	Surf. (m)	Depth (m)	Date	Location
EADB	BP	35.89525	-120.42286	466	245	01/1988 -	Eade Ranch
FROB	BP	35.91078	-120.48722	509	284	01/1988 -	Froelich Ranch
GHIB	BP	35.83236	-120.34774	400	63	01/1988 -	Gold Hill
JCNB	BP	35.93911	-120.43083	527	224	01/1988 -	Joaquin Canyon North
JCSB	BP	35.92120	-120.43408	455	155	01/1988 -	Joaquin Canyon South
MMNB	BP	35.95654	-120.49586	698	221	01/1988 -	Middle Mountain
RMNB	BP	36.00086	-120.47772	1165	73	01/1988 -	Gastro Peak
SMNB	BP	35.97292	-120.58009	699	282	01/1988 -	Stockdale Mountain
VARB	BP	35.92614	-120.44707	478	572	01/1988 - 08/19/2003	Varian Well
VARB	BP	35.92614	-120.44707	478	298	08/25/2003 -	Varian Well
VCAB	BP	35.92177	-120.53424	758	200	01/1988 -	Vineyard Canyon
CCRB	BP	35.95718	-120.55158	595	251	05/2001 -	Cholame Creek
LCCB	BP	35.98005	-120.51424	640	252	08/2001 -	Little Cholame Creek
SCYB	BP	36.00938	-120.53660	945	252	08/2001 -	Stone Canyon

Table 7.1: Stations of the Parkfield HRSN. Each HRSN station is listed with its station code, network id, location, date of initial operation, and site description. The latitude and longitude (in degrees) are given in the WGS84 reference frame, the surface elevation (in meters) is relative to mean sea level, and the depth to the sensor (in meters) below the surface. Coordinates and station names for the 3 new SAFOD sites are given at the bottom.

Site	Sensor	Z	H1	H2	RefTek 24	RefTek 72-06	Quanterra 730
EADB	Mark Products L22	-90	170	260	01/1988 - 12/1998	12/1998 - 07/1999	03/2001 -
FROB	Mark Products L22	-90	338	248	01/1988 - 12/1998	12/1998 - 07/1999	03/2001 -
GHIB	Mark Products L22	90	failed	unk	01/1988 - 12/1998	12/1998 - 07/1999	03/2001 -
JCNB	Mark Products L22	-90	0	270	01/1988 - 12/1998	12/1998 - 06/2001	03/2001 -
JCSB	Geospace HS1	90	300	210	01/1988 - 12/1998	12/1998 - 07/1999	03/2001 -
MMNB	Mark Products L22	-90	175	265	01/1988 - 12/1998	12/1998 - 06/2001	03/2001 -
RMNB	Mark Products L22	-90	310	40	01/1988 - 12/1998	12/1998 - 07/1999	03/2001 -
SMNB	Mark Products L22	-90	120	210	01/1988 - 12/1998	12/1998 - 06/2001	03/2001 -
VARB	Litton 1023	90	15	285	01/1988 - 12/1998	12/1998 - 07/1999	03/2001 -
VCAB	Mark Products L22	-90	200	290	01/1988 - 12/1998	12/1998 - 06/2001	03/2001 -
CCRB	Mark Products L22	-90	N45W	N45E	-	-	05/2001 -
LCCB	Mark Products L22	-90	N45W	N45E	-	-	08/2001 -
SCYB	Mark Products L22	-90	N45W	N45E	-	-	08/2001 -

Table 7.2: Instrumentation of the Parkfield HRSN. Most HRSN sites have L22 sensors and were originally digitized with a RefTek 24 system. After the failure of the WESCOMP recording system, PASSCAL RefTek recorders were installed. In July of 1999, 6 of the PASSCAL systems were returned to IRIS and 4 were left at critical sites. The upgraded network uses a Quanterra 730 4-channel system. For the three new stations (bottom) horizontal orientations are approximate (N45W and N45E) and will be determined more accurately as available field time permits.

dition to providing the added advantage of conventional data flow (the old system recorded SEG-Y format).

2.4 Present Status

Because of limitations in telemetry bandwidth, however, not all continuous waveform data are currently transmitted to BSL. Instead, all continuous data are archived on DLT tapes which are brought to BSL every several weeks and uploaded to the NCEDC. A modified version of the REDI system (this report) was used to detect events in the HRSN data, extract waveform triggers, and transmit the waveform segments to the BSL in near-real-time. The December 22, 2003 San Simeon earthquake and its aftershocks, however, sent the HRSN into a nearly continuous triggering state. As a result, BSL staff had to disabled the transmission of triggered data.

At present, all 38 continuous 20 sps data streams are telemetered to the BSL. All continuous 250 sps data are migrated periodically from HRSN computer in Parkfield to DLT tape. These tapes are then mailed periodically to the BSL and are then processed and archived at the NCEDC. Seven vertical 250 sps channels are also telemetered to the NCEDC for purposes of quality control and SAFOD related activities. These data are archive temporarily (for 10 days) and then removed. Copies of the data are later restored for permanent archiving during uploading of the 38 250 sps continuous data streams from the DLT tapes.

A feature of the new system that has been particularly useful both for routine maintenance and for pathology identification has been the Internet connectivity of the central site processing computer and the station dataloggers with the computer network at BSL. Through this connection, select data channels and on-site warning messages from the central site processor are sent directly to BSL for evaluation by project personnel. If, upon these evaluations, more detailed information on the HRSN's performance is required, additional information can also be remotely accessed from the central site processing computer at Parkfield. Analysis of this remotely acquired information has been extremely useful for trouble shooting by allowing field personnel to schedule and plan the details of maintenance visits to Parkfield. The connectivity also allows certain data acquisition parameters to be modified remotely when needed, and commands can be sent to the central site computer and dataloggers to modify or restart processes when necessary.

The network connectivity also allows remote monitoring of the background noise levels being recorded by the HRSN stations. For example, shown in Figure 7.3 are power spectral density plots of background noise for vertical components of the 7 HRSN stations that are most critical for monitoring seismicity in the region containing SAFOD. The PSD analysis gives a rapid assessment of

the HRSN seismometer responses across their wide bandwidth. By routinely generating these plots with data telemetered from Parkfield, changes in the seismometer responses, often indicating problems with the acquisition system, can be easily identified, and corrective measures can then be planned and executed on a relatively short time-frame.

2.5 Data Flow

Initial Processing Scheme. Continuous data streams on all 38 HRSN components are recorded at 20 and 250 sps on disk on the local HRSN computer at the CDF facility. The 20 sps data are transmitted continuously to the Berkeley Seismological Laboratory (BSL) over a frame-relay link and then archived at the NCEDC. In addition, the vertical component channels for the 7 stations critical to resolving seismicity in the SAFOD area are also being transmitted continuously at 250sps over a frame-relay circuit to the USGS and have been integrated into their NCSN (Norther California Seismic Network) trigger detection scheme to increase the sensitivity of the NCSN in the SAFOD area. The 7-channel 250 sps data is also being transmitted to the BSL for purposes of quality control and fine tuning the triggering algorithm for the detection of the smallest possible events around SAFOD. These telemetered 250 sps data are archived on disk for only about 1 week at the BSL and are then deleted. When the local HRSN computer disk space is full, the continuous 250 sps data on the HRSN local computer are migrated onto DLT tape, and the tapes sent to Berkeley for long-term storage and for upload to disc into the NCEDC archive. Efforts are currently underway to transmit all 38 HRSN channels to the USGS and BSL over a T1 line to enhance NCSN detection further and to make the data web-available in near-real-time.

Shortly after being recorded to disk on the central site HRSN computer, event triggers for the individual station data are determined, and a multi-station trigger association routine then processes the station triggers and identifies potential earthquakes. For each potential earthquake that is detected, a unique event identification number (compatible with the NCEDC classification scheme) is assigned. Prior to San Simeon earthquake of December 22, 2003, 30 second waveform segments were then collected for all stations and components and saved to local disk as an event gather, and event gathers were then periodically telemetered to BSL and included directly into the NCEDC earthquake database (dbms) for analysis and processing.

Because of its mandate to detect and record very low magnitude events in the Parkfield area, the HRSN is extremely sensitive to changes in very low amplitude seismic signals. As a consequence, in addition to detecting very small local earthquakes at Parkfield, the HRSN also detects numerous regional events. For example spot

checks of aftershocks following the M6.5 San Simeon earthquake of December 22, 2003 using continuous data and HRSN event detection listings have revealed that the overwhelming majority of HRSN detections following San Simeon resulted from seismic signals generated by San Simeon's aftershocks despite the HRSN's ~ 50 km distance from the events. Data from the California Integrated Seismic Network (CISN) show that there were $\sim 1,150$ San Simeon aftershocks with magnitudes > 1.8 in the week following San Simeon, and during this same period, the number of HRSN event detections was $\sim 10,500$ (compared to an average weekly rate before San Simeon of 115 detections) This suggests that despite the ~ 50 km distance the HRSN is detecting San Simeon aftershocks well below magnitude 1.

Since the beginning of the network's data collection in 1987 and up until recently, the local and regional events were discriminated based on analyst assessment of S-P times, and only local events with S-P times less than ~ 2.5 sec at the first arriving station were picked and located as part of the HRSN routine catalog. However, because of the large swarms of aftershocks from the San Simeon and M6 Parkfield earthquake of September 2004 and because of declining funding levels, this approach has had to be abandoned.

Current Processing. Subsequent to the M6.5 San Simeon earthquake on December 22, of 2003, our long-standing data handling procedure was no longer viable due to the enormous rate of San Simeon aftershock detections (Figures 7.2) In the first 5 months following the San Simeon mainshock, over 70,000 event detections were made by the HRSN system (compared to an average 5 month detection rate of 2500 prior to San Simeon). In the first month following the 28 September 2004 Parkfield M6 quake, over 40,000 detections were also made. Numerous additional (false) detections have also been occurring as a result of drilling activities associated with SAFOD drilling.

The dramatic increase in event detections vastly exceed the HRSN's capacity to process both the continuous and triggered event waveform data. To prevent the loss of seismic waveform coverage, processing of the triggered waveform data has been suspended to allow archiving of the 250 sps continuous data to tape to continue uninterrupted. Cataloging of the event detection times from the modified REDI real-time system algorithm is also continuing, and the continuous 250 sps waveform data is currently being periodically uploaded from the DLT tape archive onto the NCEDC for access to the research research community.

Funding to generate catalogs of local events from the 10's of thousands of aftershock detections has not been forthcoming, and as a consequence major changes in our approach to cataloging events have had to be implemented, which involves integration of HRSN data into

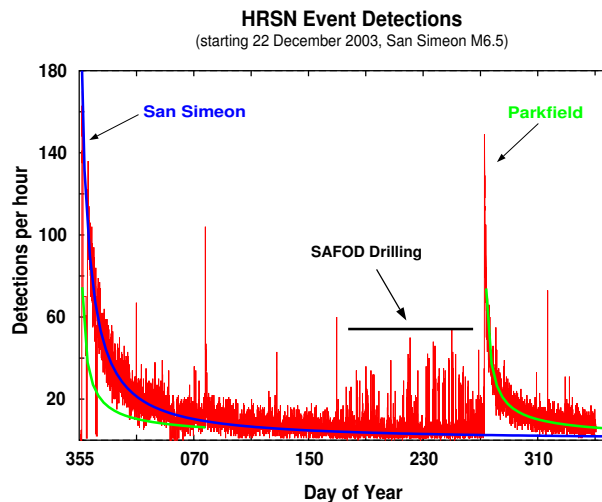


Figure 7.2: Shown are the number of HRSN triggers per hour for a period beginning with the San Simeon earthquake and continuing through several months after the Parkfield earthquake. For comparison, before these two large events, the average number of hourly HRSN triggers was less than 0.5 (i.e., about 10 per day). “Eyeball” fits of the decay curves for both events are also shown. The cumulative number of HRSN triggers in the first 5 months following San Simeon exceeded 70,000, and trigger levels continued to be over 150 triggers per day through the Parkfield quake. In the first month following the Parkfield quake nearly 20,000 triggers were recorded. Extrapolation of the decay curve indicates that daily trigger levels will not return to near pre-San Simeon levels until well into 2007. At the same time, funding to support analyst's time for routine processing and cataloging of the events has virtually dried-up, requiring the development and implementation of a new scheme for cataloging events.

NCSN automated event detection and cataloging (with no analyst review) combined with a high resolution procedure now being developed to automatically detect, pick, locate and determine magnitudes for similar and repeating events down to very low magnitudes (i.e., below magnitude -1.0Ml). These new schemes are discussed in more detail in the activities section below.

3. 2005-2006 Activities

In addition to the routine operations and maintenance of the HRSN (California's first and longest operating borehole seismic network), research into: 1) How to process the enormously increased rate of network detections 2) similar and repeating aftershocks from the 28 September 2004 Parkfield M6 earthquake, 3) ongoing non-volcanic tremors in the Parkfield-Cholame area and 4) SAFOD related activities have been the primary driving forces behind most of the HRSN project's activities this year.

3.1 Operations and Maintenance

Routine maintenance tasks required this year to keep the HRSN in operation, include cleaning and replacement of corroded electrical connections, grounding adjustments, cleaning of solar panels, re-seating, resoldering and replacement of faulty pre-amp circuit cards, the testing and replacement of failing batteries, and insulation and painting of battery and datalogger housings to address problems with low power during cold weather.

Remote monitoring of the networks health using the Berkeley Seismological Laboratory's SeisNetWatch software are also performed to identify both problems that can be resolved over the Internet (e.g. rebooting of data acquisition systems due to clock lockups) and more serious problems requiring field visits.

Over the years, such efforts have paid off handsomely by providing exceptionally low noise recordings (Figure 7.3) of very low amplitude seismic signals produced by microearthquakes (below magnitude 0.0Ml) and nonvolcanic tremors (*Nadeau and Dolenc, 2005*).

3.2 Enhancing HRSN Performance

Detection, monitoring, and high-resolution recording of low-amplitude seismic signals (e.g., nonvolcanic tremors and earthquakes down to the smallest possible magnitude) with the highest possible signal-to-noise (especially in the region of SAFOD drilling) are major objectives of the HRSN data collection effort. The minimization of data loss due to station outages and data-dropouts is also critical to these objectives.

Over the previous several years, we have had a serious decline in the robustness of the power system components (primarily the aging solar panels and batteries that have

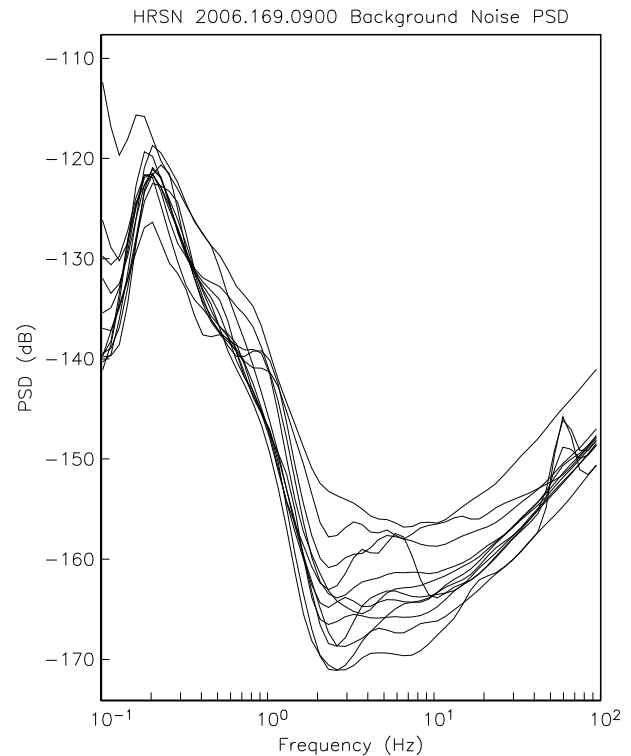


Figure 7.3: Typical background noise PSD for the 250 sps vertical component channels of the HRSN borehole stations as a function of frequency. The data are from 2 AM Local time on 6/18/2006 (Sunday morning). Note the relatively low PSD levels and the overall consistency for all the HRSN stations. The 2 Hz minimum for the sensors occurs because of the 2 Hz sensors used at these sites. Below 2 Hz, noise levels rise rapidly and the peak at 3 sec (.3 Hz) is characteristic of teleseismic noise observed throughout California. EADB, GHIB and SCYB have a 60 Hz noise peak in the PSD, which is indicative of a ground loop problem. The PSD (dB) ranking of the stations of the stations at 2.9 Hz (near minimum PSD for most of the stations) is:

- SCYB.BP.DP1 -171.05231
- LCCB.BP.DP1 -170.58481
- MMNB.BP.DP1 -168.70798
- JCNB.BP.DP1 -167.85416
- EADB.BP.DP1 -165.73283
- SMNB.BP.DP1 -164.71182
- FROB.BP.DP1 -163.79599
- CCRB.BP.DP1 -163.56433
- GHIB.BP.DP1 -161.44427
- VCAB.BP.DP1 -159.84996
- RMNB.BP.DP1 -156.86127
- VARB.BP.DP1 -154.02579

been in use since initiation of the network in 1987) of the network. Simultaneous outages at multiple stations are now becoming an all too frequent occurrence and are seriously affecting efforts to monitor tremor and micro-repeating earthquake activity in the Parkfield area.

For example, during the winter of late 2004/early 2005, monitoring for nonvolcanic tremor activity using a standard detection set of 8 HRSN channels revealed significant (and sometimes catastrophic) gaps in the data. Figure 7.4 illustrates the seriousness of the problem with an example from tremor monitoring during periods of overcast weather. During the 7 day period shown, all 8 stations used for monitoring tremor activity were out simultaneously for over 50% of the time. The remaining 50% of the time, outages occurred for at least some of these 8 stations, resulting in significantly degraded capability for unambiguous detection of the low-amplitude tremor activity.

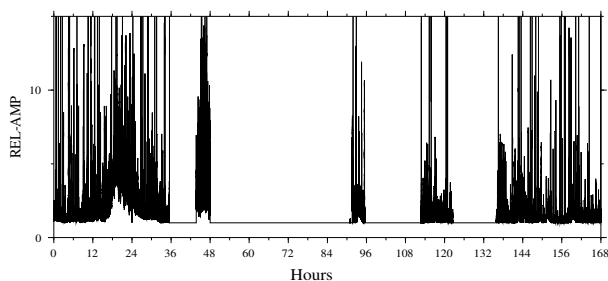


Figure 7.4: Stacked root-mean-square seismograms for the 8 stations of the HRSN used in monitoring tremor activity. Shown are 7 days of data starting at Hour 00 (UTC) of day 7 of 2005. Times when relative RMS amplitudes (REL-AMP) are 1.0 indicate periods when all 8 stations were out simultaneously.

As suspected, further investigation, both remotely and on site, showed that these gaps occurred due to insufficient battery re-charge at many of the network's stations, which are remote solar powered installations. In previous years, similar but less severe data gaps have occurred during the winter months and have been attributed to overcast skies during the rainy season. In the winter of 2005 exceptionally heavy rainy season exacerbated the outage problem to an intolerable level, and to avoid a potential repeat of the situation, efforts were undertaken to refurbish and upgrade the solar power systems.

Specifically, the following steps were and continue to be taken:

- 1) replacement of the oldest batteries and switching of the remaining old batteries to the less power consuming pre-amplifiers;
- 2) improvement of the wiring scheme along the lines suggested by the solar power representative;
- 3) upgrade/replacement of solar panels. (Solar panels

degrade at $\sim 1\%$ per year, and newer versions have improved output. Since the installation of the HRSN over 18 years ago, the same size/format panel has gone from 40 watts to 55). This is a relatively easy field task, and should gain us 20-30% capacity at each site.

Among the three newer sites (CCRB, SCYB, LCCB), both the batteries and solar panels are relatively new. Nonetheless, stations CCRB and LCCB both had some outages last winter, which is most likely explained by the limited sunlight in these areas due to hilly terrain. We have, therefore, added one more solar panel at each of these sites to enhance their power system robustness.

The table shown in figure 7.4 summarizes the tasks of the power system upgrade effort, and shows the state of completion of the tasks as of the end of 2005. To date all tasks have now been completed.

3.3 Tremor Monitoring

The HRSN data played an essential role in the discovery of nonvolcanic tremors along the San Andreas Fault (SAF) below Cholame, CA (*Nadeau and Dolenc, 2005*). This location occupies a critical location between the smaller Parkfield ($\sim M6$) and much larger Ft. Tejon ($\sim M8$) rupture zones of the SAF. Because the time-varying nature of tremor activity is believed to reflect time-varying deep deformation and presumably episodes of accelerated stressing of faults, and because an anomalous increase in the rate of Cholame tremor activity preceded the 2004 Parkfield M6 by ~ 21 days, we are continuing to monitor the tremor activity observable by the HRSN to look for anomalous rate changes that may signal an increased likelihood for another large SAF event to the SE. Results of monitoring effort are described further in the "Research" section of this report.

3.4 High Resolution Similar Event Catalog

As described in the "Data Flow" section above, circumstances relating to the dramatic increase in HRSN event detections spawned by larger earthquakes and by SAFOD drilling activity have required new thinking on how to catalog microearthquakes detected by the HRSN. One action taken to help address this problem has been to integrate HRSN data streams into the NCSN event detection and automated cataloging process (described below).

This approach has been successful at discriminating small events in the local Parkfield area from other types of event detections and for providing automated locations of a significantly increased number of small events in the local area (approx. double that of the NCSN network alone). However, the rate of local events from the HRSN sensitized NCSN catalog is still only catching about 1/2 the number of local events previously cataloged

HRSN POWER UPGRADES														
Fall, 2005														
Site	Data Logger Batteries (3/site)			Preamp Battery (1/site)		Data Logger Controller		Data Logger Solar Panels		Preamp Solar Panel		Q730 Serial Port		Site
	Age	Action	Rewiring	Age	Action	Type	Action	Status	Action	Status	Action	TD Output	Action	
JCSB	OLD	replaced w/ new	done	OLD	replaced w/ used	Prostar	good	All around M30	REPLACE w/ old	M75	REPLACE	4.6V	repaired	JCSB
RMNB	OLD	replaced w/ new	done	OLD	replaced w/ used	Prostar	good	5 M75 panels	good	M75	none	?	Repair	RMNB
VCAB	Recent	keep	done	Recent	keep	Flexcharge	replaced	Needs more panel	replaced w/ bigger	M40	replaced	4.2V	Repair	VCAB
SMNB	OLD	replaced w/ new	done	OLD	replaced w/ used	Flexcharge	replaced	Needs more panel	replaced w/ bigger	SM50-H	none	6.1V	Marginal	SMNB
CCRB	4-YR OLD	replaced w/ new	done	4-yr old	keep	Flexcharge	replaced	Needs more panel	replaced w/ bigger	two 10-watt	none	7.9V	good	CCRB
JCNB	Recent	keep	done	OLD	replaced w/ used	Prostar	good	Needs more panel	replaced w/ bigger	good	none	4.2V	repaired	JCNB
GHIB	OLD	replaced w/ new	done	*New Jan '99*	replaced w/ used	Prostar	good	1 M40, 3 M75	M40 replaced w/ M75	M40	replaced	failed	repaired	GHIB
MMNB	OLD	replaced w/ new	done	OLD	replaced w/ used	Flexcharge	replaced	5 M75 panels	good	M75	none	1.1V	repaired	MMNB
VARB	OLD	replaced w/ new	done	OLD	replaced w/ used	Prostar	good	4 M65**	replaced w/ 4 M75s	M65**	replaced	3.4V	repaired	VARB
EADB	OLD	replaced w/ new	done	OLD	replaced w/ used	Prostar	good	1 M55, 3 M75	M55 replaced w/ M75	M40	replaced	4.4V	repaired	EADB
FROB	Recent	keep	done	OLD	replaced w/ used	Prostar	good	1 modul M40	done	M75 (2)	none	failed	repaired	FROB
LCCB	4-YR OLD	replaced w/ new	done	4-yr old	keep	Flexcharge	replaced	5 SM50-H	good	SM50-H	none	3.2V***	good (?)	LCCB
SCYB	4-YR OLD	replaced w/ new	done	4-yr old	keep	Flexcharge	replaced	5 SM50-H	good	SM50-H	none	7.6V	good	SCYB
GAS PK	4-YR OLD	replaced w/ new	done	NA	none	2 Prostar-30s	good	12 SP75	none	NA	none	NA	NA	GAS PK

NOTES:

*Replace (very) old preamp batteries with 4-yr-old batteries removed from Gastro Peak.

**Lower-voltage panels, intended to be used without a controller, 30 cells instead of the 33 cells on the 50-watt panels. Also very old.

***Capacitors are correct, yet voltage level is low. (??)

red =	To do	Jobs Remaining:	1 site replace solar panels	Panel inventory at Base:	1 M75, 4 SM50-H
orange =	Maybe do (2nd priority)		3 sites repair/test serial port		
green =	Done				

Figure 7.5: Table of power upgrade tasks undertaken since early 2005. Red indicates tasks yet to be completed as of the end of 2005. These tasks have now been completed, and as expected data drops out and gaps that had plagued the network during the winter months have been effectively eliminated.

by the HRSN, and waveforms for the small events are not typically made available. In addition, unlike the previous HRSN catalog, the additional events added by the NCSN-HRSN integration are not reviewed by an analyst nor do they generally have magnitude determinations associated with them. In some cases, the selection rules used for the integrated catalog also result in exclusion of events that are otherwise included by the NCSN.

These limitations severely hamper efforts relying on similar and characteristically repeating microearthquakes. They also reduce the effectiveness of research relying on numerous very small magnitude events in the SAFOD zone (e.g. for targeting the SAFOD targets).

To help overcome these limitations, we have embarked on an effort to develop an automated similar event cataloging scheme based on cross-correlation and pattern scanning of the continuous HRSN data now being archived. The method uses a small number of reference events whose waveforms, picks, locations, and magnitudes have been accurately determined, and it automatically detects, picks, locates and determines magnitudes for events similar to the reference event to the level of accuracy and precision that only relative event analysis can bring.

The similar event detection is also remarkably insensitive to the magnitude of the reference event used, allowing similar events ranging over several magnitude units to be fully cataloged using a single reference event. It also does a remarkably good job even when seismic energy from multiple events is superposed. Once a cluster of similar events has been cataloged, it is a relatively straight forward process to identify characteristically repeating

microearthquake sequences within the cluster (frequently a single similar event "cluster" will contain several sequences of repeating events).

Application of the method using one of the SAFOD target events as a reference is illustrated in Figure 7.6. The magnitude of the reference event is ~ 2.2 . This event was scanned through 5 years of continuous data, and 67 other events occurring within a zone of ~ 150 m were detected (including 3 very small quakes that were not even by the HRSN REDI-type system). The magnitudes of these events ranged down to magnitude -1.2 M_L . In addition to the SAFOD target sequence from which the reference was derived, several other repeating sequences within the 150m zone were also identified (5 of which had not previously been known to exist).

The procedure is still being refined to capture even smaller events, events over a larger area and for increased processing speed. Eventually, a composite catalog of similar event groups from throughout the HRSN coverage zone is planned.

The approach also holds promise in other applications where automated and precise monitoring of bursts of seismic activity to very low magnitudes is desirable (e.g. in aftershock zones or in volcanic regions) or where automated updates of preexisting repeating sequences and their associated deep slip estimates are desired.

3.5 Efforts in Support of SAFOD

An intensive and ongoing effort by the EarthScope component called SAFOD is underway to drill through, sample and monitor the active San Andreas Fault at seismogenic depths and in very close proximity (within a

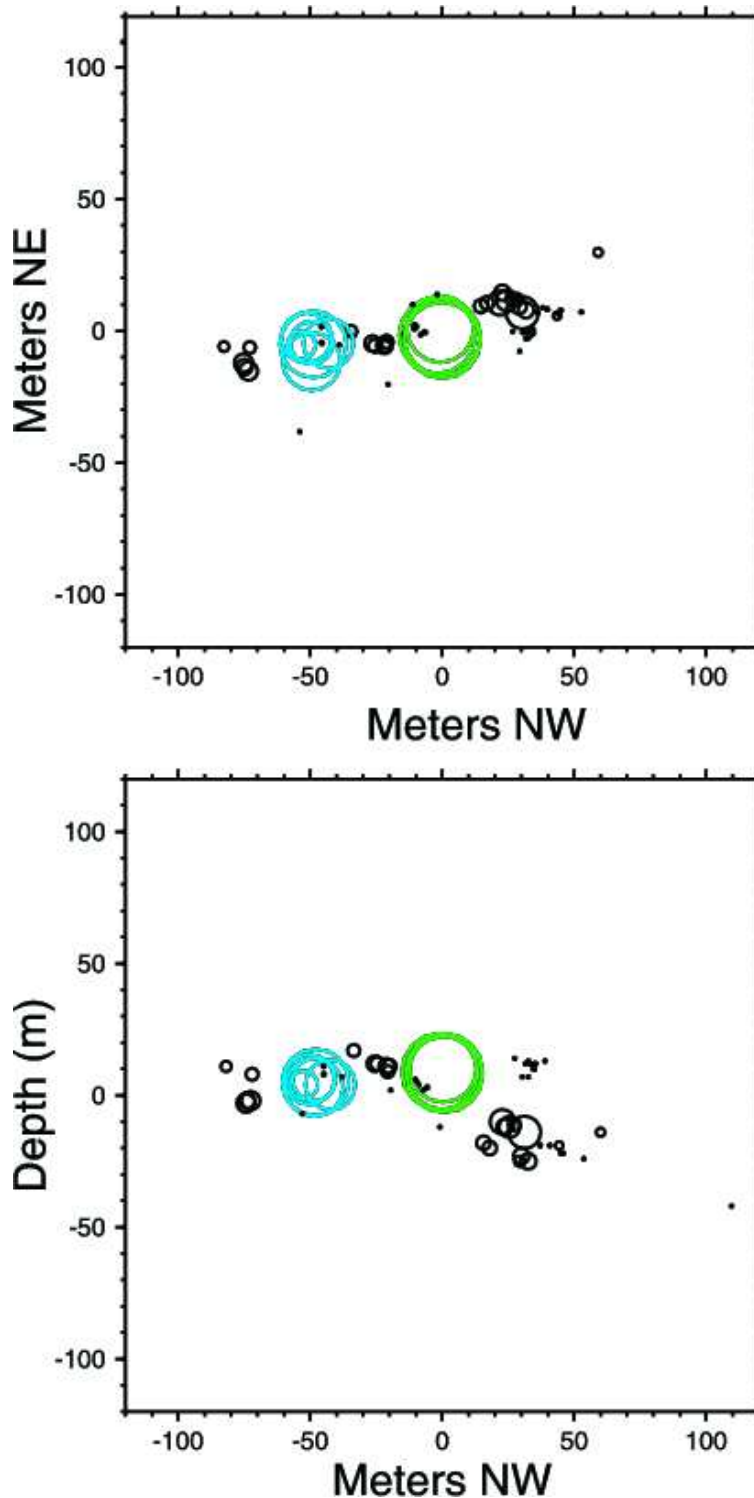


Figure 7.6: Map (top) and along fault depth section (bottom) views of double-difference locations resulting from application of the similar event pattern scanning and automated cataloging method using one of the SAFOD target events (green circles) as a reference. The magnitude of the reference event is ~ 2.2 . This event was scanned through 5 years of continuous data, and 67 other events occurring within a zone of ~ 150 m were detected (including 3 v. small quakes that were not even by the HRSN detection scheme). The magnitudes of the 67 events ranged from 2.2 down to -1.2 MI. In addition to the SAFOD target sequence from which the reference was derived, several other repeating sequences within the 150m zone were also identified (5 of which had not previously been known to exist).

few 10's of km or less) of a repeating magnitude 2 earthquake site. The HRSN data plays a key role in these efforts by providing low noise and high sensitivity seismic waveforms from active and passive sources, and by providing a backbone of earthquake and tremor detection and continuous waveform data from the numerous microearthquakes and tremors that are occurring in the general vicinity of SAFOD.

At this stage SAFOD drilling has penetrated the fault with a sub-horizontal hole slightly beneath the SAFOD target sequences, and current efforts have been focused on obtaining final estimates of the targets relative location to the existing hole to accuracies of meters if possible. This high degree of accuracy is required in order to target accurately three multi-lateral side cores for sampling and monitoring within the final target zone.

HRSN Activities this year have contributed in three principal ways to these and longer-term SAFOD monitoring efforts:

- 1) In collaboration with the USGS, we have integrated the 7 vertical HRSN channels telemetered from Parkfield into the NCSN triggering scheme (described above) to increase the sensitivity of NCSN detection in the SAFOD area. This has effectively doubled the number of small events the target location working group has for constraining the relative location of the target sequences.

- 2) Again in collaboration with the USGS, we have nearly completed a telemetry upgrade that will allow all 38 channels of the HRSN data (both 20 sps and 250 sps data streams) to flow directly from Parkfield, through the USGS Menlo Park processing center, and also to the BSL for near-real-time processing and archiving on the web based NCEDC. This will provide near immediate access of the HRSN data to the community without the week's to month's delay associated with having to transport DLT tapes to Berkeley, upload, and quality check the data.

- 3) We have also applied our prototype similar event automated catalog approach to the primary and two secondary SAFOD target zones and were able to provide the SAFOD event location working group with rapid and precise double-difference and relative magnitude catalogs of 82 similar events in the zone immediately surrounding target region occurring between 2001 day 178 and 2006 day 218 (August 6 of this year).

Figure 7.6 shows the double difference locations and estimated rupture dimensions (based on Nadeau and Johnson, 1998) of 67 of these events that were derived using one event from the SAFOD primary target sequence as the reference. Other primary target events are shown in green, and events from a secondary target located ~ 40 m to the southeast are shown in blue. Several other suspected repeating sequences can be seen as tight clusters of similarly sized events. We are in the process of confirm-

ing these events as characteristically repeating sequences members.

The SAFOD similar event catalogs are now being used by the working group to extract data from the corresponding PASO array, Pilot Hole, NCSN and mainhole data sets for integration with the HRSN data to provide as much and as detailed information as possible in the final push at locating the target sequence for the lateral side core drilling.

4. Acknowledgments

Thomas V. McEvelly, who passed away in February 2002, was the PI on the HRSN project for many years. Without his dedication, continued operation of the HRSN would not have been possible. Under Bob Nadeau's and Doug Dreger's general supervision, Rich Clymer, Bob Uhrhammer, Doug Neuhauser, Don Lippert, Bill Karavas, John Friday, Rick Lellingner and Pete Lombard all contribute to the operation of the HRSN. Bob Nadeau prepared this chapter. During this reporting period, operation, maintenance, and data processing for the HRSN project was supported by the USGS, through grant 05HQGR0080.

5. References

- Bakun, W. H., and A. G. Lindh, The Parkfield, California, prediction experiment, *Earthq. Predict. Res.*, *3*, 285-304, 1985.
- Daley, T.M. and T.V. McEvelly, Shear wave anisotropy in the Parkfield Varian Well VSP, *Bull. Seism. Soc. Am.*, *80*, 857-869, 1990.
- Hickman, S., M.D. Zoback and W. Ellsworth, Introduction to special section: Preparing for the San Andreas Fault Observatory at Depth, *Geophys. Res. Lett.*, *31*, L12S01, doi:10.1029/2004GL020688, 2004.
- Karageorgi, E., R. Clymer and T.V. McEvelly, Seismological studies at Parkfield. IV: Variations in controlled-source waveform parameters and their correlation with seismic activity, 1987-1994, *Bull. Seismol. Soc. Am.*, *87*, 39-49, 1997.
- Michelini, A. and T.V. McEvelly, Seismological studies at Parkfield: I. Simultaneous inversion for velocity structure and hypocenters using B-splines parameterization, *Bull. Seismol. Soc. Am.*, *81*, 524-552, 1991.
- Nadeau, R.M. and D. Dolenc, Nonvolcanic Tremors Deep Beneath the San Andreas Fault, *SCIENCE*, *307*, 389, 2005.
- Nadeau, R. M., and L. R. Johnson, Seismological Studies at Parkfield VI: Moment Release Rates and Estimates of Source Parameters for Small Repeating Earthquakes, *Bull. Seismol. Soc. Amer.*, *88*, 790-814, 1998.

Chapter 8

Bay Area Regional Deformation Network

1. Introduction

The last year has been a transition period for BSL, with the departure of Mark Murray in January 2006 and that of his assistant Cedric dela Beaujardiere in November 2005. We have been lucky to hire Nicolas Houlie on a post-doctoral position to assume the responsibility for the routine operations and development of the BARD network and related data acquisition and processing. Some of the field related tasks that Cedric performed have been transferred to the BSL's field engineering group. This reorganization of the tasks has caused some temporary disruption in the processing of the GPS data, but we are now back on track on all of the processing and archiving tasks. A significant effort in the last three years has been to upgrade those stations where it is possible to 1Hz continuous data acquisition, to respond to a growing interest in the community for this type of data, for the estimation of earthquake ground motions and real time earthquake quantification.

2. BARD overview

2.1 Description of the network

The BSL currently maintains and operates 30 (twenty-six bi-frequency sites and four L1 sites) BARD stations. The sampling rate vary from 1 to 30 seconds rate and the data recorded are transmitted continuously over serial connection. Most stations use frame relay technology, either alone or in combination with radio telemetry.

Of the 30 sites, ten (BRIB, CMBB, FARB, HOPB, MHCB, ORVB, PKDB, SAOB, SUTB, YBHB) are co-located with broadband seismic stations of the Berkeley Digital Seismic Network (BDSN) with which they share continuous frame-relay telemetry to UC Berkeley. These sites use the Quanterra data loggers to store and retrieve the GPS data converted to MiniSEED format (Perin et al., 1998). The MiniSEED approach provides more robust data recovery from onsite backup on the Quanterra disks following telemetry outages.

Another five stations (SVIN, MHDL, OHLN, OXMT and SBRN) have been installed in the last 3 years in the

SFBA and along the Hayward fault as the Berkeley part of a multi-institutional effort funded by the NSF/MRI program to improve strain monitoring in the SFBA using an integrated approach, with significant participation of the USGS/MP (Murray et al., 2002a). These stations include borehole tensor strainmeters, three-component borehole seismic velocity sensors, downhole pore pressure and tilt sensors and GPS receivers. This project served as a prototype for the strainmeter installations planned for PBO, which faces many of the same station installation, configuration, and data retrieval issues we have addressed. Consequently, these 5 stations have received the nickname *mini-PBO*. From July 2001 to August 2002, five boreholes were drilled to about 200-m depth and equipped with tensor strainmeters recently developed by CIW and 3-component L22 (velocity) seismometers. For this project, we developed a self-centering GPS antenna mount for the top of the borehole casings, which are mechanically isolated from the upper few meters of the ground, to provide a stable, compact monument that allows access to the top of the borehole casing for downhole maintenance. The 5 GPS receivers were progressively installed and connected to Quanterra 4120 data loggers, which provide backup and telemetry capabilities. The completion of the last station (MHDL), located in the Marin Headlands, took longer because it required AC power, which PG&E installed in December 2005. The site is operational as of Sept 1, 2006. In addition, 10-minute interval data, which are retrieved from all the sites by the USGS via a backup GOES satellite system, show that all the sites are successfully measuring strains due to tidal effects and to local and teleseismic earthquakes (Murray et al., 2002b). The remaining BSL/BARD stations only record C-GPS data. Each BSL/BARD station uses a low-multipath choke-ring antenna, most of which (except the mini-PBO ones discussed above) are mounted to a reinforced concrete pillar approximately 0.5-1.0 meter above the ground level. The reinforcing steel bars of the pillar are drilled and cemented into rock outcrop to improve long-term monument stability. A low-loss antenna cable is used to minimize signal degradation on the longer cable setups

that normally would require signal amplification. Low-voltage cutoff devices are installed to improve receiver performance following power outages. Most stations are equipped with aging Z-12 receivers, which were originally programmed to record data once every 30 s and observe up to 12 satellites simultaneously at elevations down to the horizon. The antennas are equipped with SCIGN antenna adapters and hemispherical domes, designed to provide security and protection from weather and other natural phenomena, and to minimize differential radio propagation delays. The BSL acquired 7 Ashtech MicroZ-CGRS (uZ) receivers with NSF funding for the Mini-PBO project. These have been installed at the mini-PBO stations, and two have been used to replace failing Z12 at other stations (CMBB and MODB). At these sites, the data are collected using only direct serial connections and are susceptible to data loss during telemetry outages.

There is growing interest in collecting higher rates of data for a variety of applications. For example, GPS measurements can accurately track the propagation of earthquake dynamic motions both on the ground (e.g., Larson et al., 2003) and in the atmosphere (e.g., Artru et al., 2001, Ducic et al., 2003), providing complementary information to seismic observations (calibration of integrated acceleration and velocity sensor data) and estimates of earth structure (direct observation of surface wave propagation over the oceans). We started collecting 1 Hz observations at 2 stations (DIAB and MONB) in 2003. In the last year, we have progressively upgraded the telemetry to continuous 1 Hz telemetry at 9 additional stations (CMBB, MHCN, OHLN, OXMT, SBRN, SVIN, TIBB and two new stations, SRB1, see below, and MHDL), where the bandwidth of the existing telemetry system allowed it. At stations collocated with broadband seismic sensors, the seismic data has priority for telemetry, because it is used in the Northern California real-time earthquake notification system (see <http://www.cisn.org/ncmc/>) making this upgrade more difficult and in general not feasible with the current Z12 receivers because of insufficient data compression. All data collected from BARD/BSL, including the 1Hz data are publicly available at the Northern California Earthquake Data Center (NCEDC; <http://www.ncedc.org/bard/>).

Between 1993 and 2001, the BSL acquired 29 Ashtech Z-12 and Micro-Z receivers from a variety of funding sources, including from federal (NSF and USGS), state (CLC), and private (EPRI) agencies. The network enhances continuous strain measurements in the Bay Area and includes several profiles between the Farallon Islands and the Sierra Nevada in order to better characterize the larger scale deformation field in northern California (Figure 8.1).

The number of continuous GPS stations in northern

California is significantly increasing with over 250 new site installations planned by 2008 as part of the Plate Boundary Observatory (PBO) component of the NSF-funded Earthscope project. UNAVCO and researchers from BARD and the other regional networks, such as SCIGN, BARGEN, and PANGA, are funded by NSF to fold operation and maintenance of about 200 existing stations, which constitute the PBO Nucleus network, into the PBO array by 2008. Two BSL-maintained stations (SUTB and MUSB) are included in the PBO Nucleus network. The other BSL stations are either collocated with seismic instrumentation or are located near the San Andreas Fault where real-time processing of the GPS data for earthquake notification is a high priority. Another 23 northern California stations, including most of the Parkfield network, will be included in the PBO Nucleus, and we are working with UNAVCO to facilitate their transition to UNAVCO control.

2.2 BARD Stations

The majority of the BSL BARD stations use a low-multipath choke-ring antenna, most of which are mounted to a reinforced concrete pillar approximately 0.5–1.0 meter above local ground level. The reinforcing steel bars of the pillar are drilled and cemented into rock outcrop to improve long-term monument stability. A low-loss antenna cable is used to minimize signal degradation on the longer cable setups that normally would require signal amplification. Low-voltage cutoff devices are installed to improve receiver performance following power outages. Most use Ashtech Z-12 receivers that are programmed to record data once every 30 seconds and observe up to 12 satellites simultaneously at elevations down to the horizon. The antennas are equipped with SCIGN antenna adapters and hemispherical domes, designed to provide security and protection from weather and other natural phenomena, and to minimize differential radio propagation delays.

Data from most BSL-maintained stations are collected at 15 or 30-second intervals and transmitted continuously over serial connections (Table 2.1). Station TIBB uses a direct radio link to Berkeley, and MODB uses VSAT satellite telemetry. Most stations use frame relay technology, either alone or in combination with radio telemetry. Fourteen GPS stations are collocated with broadband seismometers and Quanterra data loggers (Table 4.2). With the support of IRIS we developed software that converts continuous GPS data to MiniSEED opaque blockettes that are stored and retrieved from the Quanterra data loggers (*Perin et al., 1998*), providing more robust data recovery from onsite disks following telemetry outages.

Data from DIAB, MHCN, MONB, OHLN, OXMT, SBRN, SRB1, SVIN, and TIBB in the Bay Area, and 13 stations in the Parkfield region (all but PKDB), are now

	Sites	Lat. (deg.)	Lon. (deg)	Receiver	Telem.	Sampling rate	Collocated Network	Location
1	BRIB	37.91	237.84	A-Z12	FR	30 s	BDSN	Briones Reservation, Orinda
2	CMBB	38.03	239.61	A-UZ12	FR	1Hz	BDSN	Columbia College, Columbia
3	DIAB	37.87	238.08	A-Z12	FR	1Hz		Mt. Diablo
4	FARB	37.69	236.99	A-Z12	R-FR/R	15 s	BDSN	Farallon Island
5	EBMD	37.81	237.71	T-SSI	WEB	1Hz		East Bay Mud Headquarter
6	HOPB	38.99	236.92	A-Z12	FR	15 s	BDSN	Hopland Field Stat., Hopland
7	LUTZ	37.28	238.13	A-Z12	FR	30 s		SCC Comm., Santa Clara
8	MHCB	37.34	238.35	A-Z12	FR	1Hz	BDSN	Lick Obs., Mt. Hamilton
9	MHDL	37.84	237.50	T-NETRS	FR	1Hz	mini-PBO	Marin Headland
10	MODB	41.90	239.69	A-UZ12	NSN	15 s		Modoc Plateau
11	MONB	37.48	238.13	A-Z12	FR	1Hz		Monument Peak, Milpitas
12	MUSB	37.16	240.69	A-Z12	R-Mi-FR	30 s		Musick Mt.
13	OHLN	38.00	237.72	A-UZ12	FR	1Hz	mini-PBO	Ohlone Park, Hercules
14	ORVB	39.55	238.49	A-Z12	FR	15 s	BDSN	Oroville
15	OXMT	37.49	237.57	A-UZ12	FR	1Hz	mini-PBO	Ox Mountain
16	PKDB	35.94	239.45	A-Z12	FR	30 s	BDSN	Bear Valley Ranch, Parkfield
17	PTRB	37.99	236.98	A-Z12	R-FR	15 s		Point Reyes Lighthouse
18	SAOB	36.76	238.55	A-Z12	FR	30 s	BDSN	San Andreas Obs., Hollister
19	SBRN	37.68	237.58	A-Z12	FR	1Hz	mini-PBO	San Bruno
20	SODB	37.16	238.07	A-Z12	R-FR	30 s		Soda Springs, Los Gatos
21	SRB1	37.87	237.73	T-SSE	FR	1Hz		SRB building, Berkeley
22	SUTB	39.20	238.17	A-Z12	R-FR	30 s	BDSN	Sutter Buttes
23	SVIN	38.03	237.47	A-UZ12	R-FR	1Hz	mini-PBO	St Vincents
24	TIBB	37.89	237.55	A-UZ12	R	1Hz		Tiburon
25	UCD1	38.53	238.248	T-SSE	WEB	1Hz		UC - Davis
26	YBHB	41.73	237.289	A-Z12	FR	15 s	BDSN	Yreka Blue Horn Mine, Yreka

Table 8.1: List of the BARD maintained by the BSL. Five models of receiver are operating now: Trimble 4000 SSE (T-SSE), Trimble 4000 SSI (T-SSI), Trimble NETRS, (T-NETRS), Ashtech Z12 and Ashtech Micro Z (A-UZ12). The replacement of the Ashtech Z12 by Trimble NETRS will make the receiver park more homogeneous. The telemetry types are listed in column 6. FR = Frame Relay, R = Radio, Mi= Microwave, WEB = DSL line. Some sites are transmitting data over several legs with different telemetry.

being collected at 1-second intervals. All high-rate observations collected by these stations are currently available from the NCEDC. Collecting at such high-frequency (for GPS) allows dynamic displacements due to large earthquakes to be better measured; however, this 30-fold increase in data can pose telemetry bandwidth limitations. We are planning to convert additional stations to 1-second sampling where possible during the next year. The acquisition of the 5 NETRS bundles will help to complete this project (see subsection 3.1). In the Bay Area, we have converted stations that have sufficient bandwidth and are currently assessing bandwidth issues at other stations. Prior to the September 28, 2004 M6 Parkfield earthquake, data from the Parkfield stations were collected on an on-site computer, written to removable disk once per month, and sent to SOPAC for long-term archiving (decimated 30-sec data is acquired daily via the BSL frame relay circuit). In response to the earthquake, we modified the procedures to download 1-second data converted to compact RINEX format at hourly intervals, which does not significantly impact the telemetry bandwidth.

2.3 Data archival

The Northern California Earthquake Data Center (NCEDC), operated jointly by the BSL and USGS, archives all permanent-site GPS data currently being collected in northern California. In the past months, and due to the transition to PBO, some sites are not present in the NCEDC archive (PPT1 for instance). All the sites available will be as soon as possible archived as in the past. We archive the Federal Aviation Administration (FAA) sites all over the west pacific coast (the closest one is ZOA1). Data importation and quality assurance are automated, although some manual correction of unusual data problems is still required.

As part of the activities funded by the USGS through the BARD network, the NCEDC has established an archive of the 7000+ survey-mode occupations collected by the USGS since 1992. The NCEDC continues to archive non-continuous survey GPS data. The initial dataset archived is the survey GPS data collected by the USGS Menlo Park for northern California and other locations. The NCEDC is the principal archive for this dataset. Significant quality control efforts were implemented by the NCEDC (Romanowicz et al., 1994) to ensure that the raw data, scanned site log sheets, and RINEX data are archived for each survey. All of the USGS MP GPS data has been transferred to the NCEDC and virtually all of the data from 1992 to the present has been archived and is available for distribution. We are also archiving additional high-precision GPS data sets from northern California (mainly Parkfield measurements). Together with students in the department who are now using the GAMIT software to process survey-

mode data in the San Francisco Bay area, we are working to combine the survey-mode and C-GPS solutions into a self-consistent velocity field for northern California. The campaign velocity field computed from campaign measurements by university and USGS groups has been published by *dAlessio et al.*, (2005).

We also participate in the UNAVCO-sponsored GPS Seamless Archive Center (GSAC) project, which provides access to survey-mode and continuous GPS data distributed over many archives. We helped to define database schema and file formats for the GSAC project, and produce monumentation and data holdings records for the data archived at the NCEDC to provide GSAC with up-to-date information about our holdings. Currently, the NCEDC is the primary provider for over 74,000 data files from over 1400 continuous and survey-mode monuments. The records for these data have been incorporated into the retailer system that became publicly available in early 2003.

Data from five of our sites (HOPB, MHCN, CMBB, OHLN, YBHB) are sent to the National Geodetic Survey (NGS) in the framework of the CORS (Continuous Operating Reference Stations) project (<http://www.ngs.noaa.gov/CORS/>). The data from these five sites are also distributed to the public through the CORS ftp site.

3. 2005-2006 Activities

3.1 New stations and upgrades

During the last year we have installed one additional site on the SRB1 building on the Berkeley Campus, a building built to emergency grade standards that are designed to withstand the next M7 earthquake on the Hayward Fault. This site is equipped with a TRIMBLE 4000 SSE with a Zephyr Geodetic Antenna and is in a good location to reduce the baseline length between surrounding sites (OHLN, BRIB, TIBB, and EBM1, see Figure 2.1) and increase the accuracy of the real-time processing application. It is providing 1Hz data in real time and has been archived at the NCEDC since day 210 in 2006.

We have also assisted collaborators in installations and upgrades of several continuous stations, including at Thales Navigation (THAL), Hat Creek Radio Observatory (HCRO), and EBMD in downtown Oakland, which is being upgraded to real-time 1 Hz telemetry with a direct radio link to the BSL. This site, which belongs to East Bay Municipal Utilities District (EBMUD) has been renamed EBM1 was operated for part of 2004-2005 at 30s sampling rate. It was upgraded to 1Hz using a new DSL line provided by EBMUD. It is not currently operating because the PC failed and EBMUD is looking for ways to restore the data flow. EBM1 will be the reference station for the East Bay Park surveyor teams for real time kinematic positioning (RTK) applications.

A similar collaboration has been engaged with East Bay Parks in collaboration with Mr. Jim Swanson in order to get, archive and process data from the PBO-East Bay Mud GPS sites in real time (Figure 2.1). The site P222 located south of the bay will be equipped to become a RTK reference base during the next year. This site will help define the standard used by East Bay Parks to upgrade (to real time and 1Hz) the PBO sites in the SFBA.

In the last year, we also performed routine maintenance at several sites replacement of a failing receiver at CMBB (lightning), MODB, TIBB (lightning), YBHB and repair of the failing receivers at mini-PBO stations (SBRN, SVIN). Cylink radios used for FARB were replaced by a Wi-Lan radio as part of a reconfiguration of the telemetry paths through UC San Francisco rather than Mount Tamalpais (2005). As part of this reconfiguration and coincident with the replacement of a badly rusted antenna mast, the Freewave radio path at PTRB was adjusted to be routed through UCSF. In February 2003, the BSL assumed responsibility for data telemetry from a 14-station GPS network in the Parkfield region, in addition to the BSL station PKDB. Most of these stations were constructed using Mini-PBO funding with contributions from the USGS and SCIGN. We replaced a computer at Carr Hill with the appropriate scripts to sequentially download the stations over radio connections, and then retrieve the data over our existing frame relay circuit. All the Parkfield GPS sites are being transferred to the PBO network except the PKDB site, which remains at BSL/BARD site, as it is collocated with a long-term BDSN station.

Five Ashtech receivers (Ashtech μZ) purchased by the *mini PBO* project have been repaired during the Fall 2005. The whole series was delivered with factory defects by Ashtech corp. However, the replacement of the capacitor and shipment fees have been covered by Ashtech corp. These receivers have been installed mainly at the mini-PBO sites. The first site affected was SVIN in September 2005. The receiver was able to see fewer and fewer satellites every day at the same time. After a few hours the number of visible satellites increased again until the next day. This problem increased dramatically with time and the state of the capacitor.

BSL acquired five NETRS Bundle pack that will be dispatched in the next year over sites where a internet DSL connection access will be available and where telemetry bandwidth does not allow to increase the sampling rate without changing the receiver (BRIB is one the priority site).

Sites	Lon. (deg.)	Lat. (deg.)	dV_e (mm/y)	dV_n (mm/y)
BAY1	197 .293	55 .19	-0 .03	0 .01
GOLD	243 .111	35 .425	1 .20	-0 .11
JPLM	241 .827	34 .205	0 .50	0 .59
PPT1	237 .61	37 .187	0 .82	0.27
VNDP	239 .384	34 .556	-0 .05	-0 .81

Table 8.2: Comparison between previous published values and recomputed values. The adjustment with the ITRF2000 is good. The errors provided here are formal and cannot be qualified as realistic (From *Houlié and Romanowicz*, in prep).

4. Data Analysis and Results

4.1 CALREF, a stable reference frame for northern California

The BARD dataset have been processed in the ITRF2000 (*Altamimi et al.*, 2002). The solutions (*Houlié and Romanowicz*, in prep) are in good agreement with previous campaign solutions (BAVU and USGS) previously released (*d’Alessio et al.*, 2005). The new coordinates release of the BARD network includes the presently operating site and the velocity of the sites already transferred from BSL to PBO during the last two years.

All the BARD sites have been processed jointly with IGS sites in California. No *a priori* constraints have been assumed during the processing. A specific troposphere study is under progress to estimate the troposphere gradient over the bay area. The velocities computed for a small selection of sites (Table 8.2) are accurate and well compatible with ITRF2000 solutions (*Altamimi et al.*, 2002). All the velocities included in the first release of California Reference Frame (CALREF) are given in Table 8.3. The CALREF will provide velocities and coordinates of sites located in the bay area at specific epochs. Each solution will be associated to discussed error estimations (formal and real). Every surveyor will be able to control the reference site coordinates for a given survey.

5. Acknowledgements

Since the departure of Mark Murray at the end of 2005, Barbara Romanowicz oversees the BARD program. Rich Clymer, Cedric de La Beaujardiere, Bill Karavas, Rick Lellinger, John Friday, Nicolas Houlié and Doug Neuhauser contributed to the operation of the BARD network. The operation of the BARD network is partially supported by funding from the USGS/NEHRP program and funding from the NSF/UNAVCO *PBO nucleus* grant

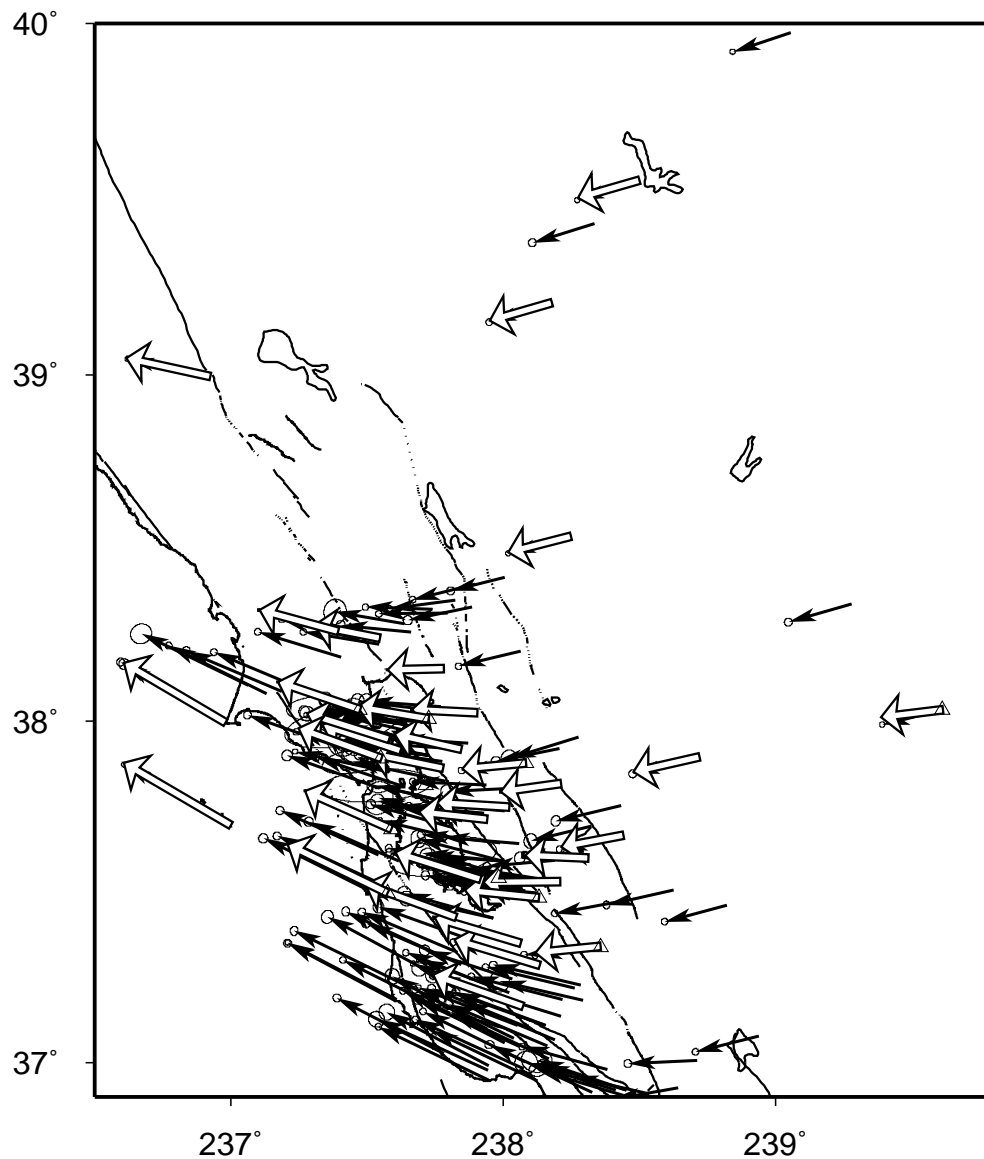


Figure 8.2: Comparison of the BARD solutions (white arrows) with the Bay Area Velocity Unification (BAVU) solutions (black arrows). All the data available at the BSL between 1994 and 2006 have been reprocessed (From Houlié and Romanowicz, in prep). BAVU website: <http://seismo.berkeley.edu/burgmann/RESEARCH/BAVU/>

6. References

Altamimi, Z., P. Sillard, and C. Boucher, ITRF2000: A new release of the International Terrestrial Reference Frame for earth science applications, *J. Geophys. Res.*, 107(B10), 2214, doi:10.1029/2001JB000561, 2002

Bürgmann, R., D. Schmidt, R.M. Nadeau, M. d'Alessio, E. Fielding, D. Manaker, T. V. McEvilly, and M. H. Murray, Earthquake potential along the northern Hayward fault, California, *Science*, 289, 1178–1182, 2000.

d'Alessio, M. A., I. A. Johanson, R. Bürgmann, D. A. Schmidt, and M. H. Murray, Slicing up the San Fran-

cisco Bay Area: Block kinematics from GPS-derived surface velocities, *J. Geophys. Res.*, 110, B06403, doi:10.1029/2004JB003496, 2005.

Dreger, D. S., L. Gee, P. Lombard, M. H. Murray, and B. Romanowicz, Rapid finite-source analysis and near-fault strong ground motions: Application to the 2003 Mw 6.5 San Simeon and 2004 Mw 6.0 Parkfield earthquakes, *Seismol. Res. Lett.*, 76(1), 40–48, 2005.

Houlié, N. and P. Briole, Laterally heterogeneous troposphere: a potential explanation for seasonality in GPS coordinates time series, *J. Geophys. Res.*, submitted.

Houlié, N., G. Occhipinti, P. Lognonné, and M. Murakami (2006), Rayleigh seismic waves detected by GPS.

Application to the 2003 September 25th, Hokkaido earthquake, *Geophys. Res. Lett.*, submitted.

Houlié, N. and Romanowicz, B., CALREF, a stable reference frame for the Northern California, in prep.

King, N. E., J. L. Svarc, E. B. Fogleman, W. K. Gross, K. W. Clark, G. D. Hamilton, C. H. Stiffler, and J. M. Sutton, Continuous GPS observations across the Hayward fault, California, 1991-1994, *J. Geophys. Res.*, *100*, 20,271–20,283, 1995.

Langbein et al., Preliminary report on the 28 September 2004, M 6.0 Parkfield, California earthquake, *Seismol. Res. Lett.*, *76(1)*, 10–26, 2005.

Murray, M. H., and P. Segall, Continuous GPS measurement of Pacific–North America plate boundary deformation in northern California and Nevada, *Geophys. Res. Lett.*, *28*, 4315–4318, 2001.

Murray, M. H., R. Bürgmann, W. H. Prescott, B. Romanowicz, S. Schwartz, P. Segall, and E. Silver, The Bay Area Regional Deformation (BARD) permanent GPS network in northern California, *EOS Trans. AGU*, *79(45)*, Fall Meeting Suppl., F206, 1998.

Murray, M., Neuhauser D., Gee, L., Dreger, D., Basset, A., and Romanowicz, B., Combining real-time seismic and geodetic data to improve rapid earthquake information, *EOS. Trans. AGU*, *83(47)*, G52A-0957, 2002.

Murray, M.H., D.C. Agnew, R. Bürgmann, K. Hurst, R.W. King, F. Rolandone, J. Svarc, GPS Deformation measurements of the 2003 San Simeon earthquake, *Seism. Res. Lett.*, *75*, 295, 2004.

Perin, B. J., C. M. Meertens, D. S. Neuhauser, D. R. Baxter, M. H. Murray, and R. Butler, Institutional collaborations for joint seismic and GPS measurements, *Seismol. Res. Lett.*, *69*, 159, 1998.

Rhie, J., D. Dreger, and M. H. Murray, A prediction of strong ground motions from geodetic data for PGV ShakeMaps, *Geophys. Res. Lett.*, in prep., 2005.

Rolandone, F., I. Johanson, and R. Bürgmann, Geodetic observations of the M6.5 San Simeon earthquake with focus on the response of the creeping segment of the San Andreas fault, *Seism. Res. Lett.*, *75*, 293, 2004.

Romanowicz, B., B. Bogaert, D. Neuhauser, and D. Oppenheimer, Accessing northern California earthquake data via Internet, *EOS Trans. AGU*, *75*, 257–260, 1994.

Uhrhammer, R., L. S. Gee, M. Murray, D. Dreger, and B. Romanowicz, The M_w 5.1 San Juan Bautista, California earthquake of 12 August 1998, *Seismol. Res. Lett.*, *70*, 10–18, 1999.

Site	Lon.	Lat	Ve (mm/y)	Vn (mm/y)	σ_e (mm/y)	σ_n (mm/y)	Start
BAY1*	197.29	55.19	-6.3	-25.5	0.0000	0.0000	1996.08
BAY2	197.29	55.19	-5.6	-25.2	0.0400	0.0300	1996.08
BRIB	237.85	37.92	-24.8	5.6	0.0100	0.0100	1993.58
CMBB	239.61	38.03	-22.9	-2.8	0.0100	0.0100	1993.92
CNDR	238.72	37.90	-24.4	-5.5	0.0200	0.0200	1999.27
DIAB	238.08	37.88	-23.7	-2.2	0.0100	0.0100	1998.33
FARB	237.00	37.70	-39.8	23.3	0.0100	0.0100	1994.00
GOLD*	243.11	35.43	-18.2	-5.4	0.0000	0.0000	1989.95
HCRO	238.53	40.82	-18.0	-8.7	0.1400	0.1500	2003.50
HOPB	236.93	39.00	-31.1	6.8	0.0100	0.0100	1995.58
JPLM*	241.83	34.21	-36.6	11.8	0.0000	0.0000	1989.44
LUTZ	238.14	37.29	-31.7	9.5	0.0100	0.0100	1996.33
MHCB	238.36	37.34	-24.2	-2.4	0.0100	0.0100	1996.33
MODB	239.70	41.90	-16.9	-9.1	0.0200	0.0200	1999.83
MOLA	237.58	37.95	-30.5	9.7	0.0100	0.0100	1993.75-2002.22
MONB	238.13	37.49	-27.5	2.7	0.0100	0.0100	1998.50
MUSB	240.69	37.17	-22.3	-4.0	0.0100	0.0100	1997.83
OHLN	237.73	38.01	-26.4	4.4	0.0200	0.0200	2001.83
ORVB	238.50	39.56	-22.7	-6.6	0.0100	0.0100	1996.83
OXMT	237.58	37.50	-36.9	18.0	0.0600	0.0600	2004.12
P181(PBO)	237.62	37.92	-29.0	9.6	0.3800	0.4000	2005.09
P198 (PBO)	237.39	38.26	-29.2	7.9	0.0900	0.1000	2004.77
P200 (PBO)	237.55	38.24	-24.3	4.7	0.2000	0.2200	2005.73
P222 (PBO)	237.92	37.54	-31.5	10.0	0.1100	0.1200	2005.26
P224 (PBO)	237.78	37.86	-26.9	5.5	0.1000	0.1100	2005.25
P225 (PBO)	237.94	37.71	-25.2	2.7	0.0900	0.1000	2005.14
P227 (PBO)	238.21	37.53	-28.6	-0.4	0.5800	0.6300	2006.20
P228 (PBO)	238.31	37.60	-23.5	1.0	0.4300	0.4700	2005.93
P229 (PBO)	238.02	37.75	-26.8	1.6	0.1100	0.1200	2005.29
P230 (PBO)	238.21	37.82	-22.5	-3.1	0.1100	0.1200	2005.15
P261 (PBO)	237.78	38.15	-21.0	-0.5	0.0900	0.1000	2004.50
P262 (PBO)	237.90	38.03	-24.2	1.2	0.1100	0.1200	2005.32
PKDB	239.46	35.95	-43.0	18.7	0.0100	0.0100	1996.67
PPT1*	237.61	37.19	-40.7	22.1	0.0000	0.0000	1996.14
PTRB	236.98	38.00	-37.7	22.2	0.0100	0.0100	1998.58
S300	238.44	37.67	-22.9	-4.4	0.0200	0.0200	1998.48
SAOB	238.55	36.77	-41.4	22.0	0.0100	0.0100	1997.58
SBRN	237.59	37.69	-32.0	14.2	0.0300	0.0300	2003.18
SODA	26.39	67.42	18.7	34.1	0.1400	0.1600	1994.70
SODB	238.07	37.17	-33.1	11.7	0.0100	0.0100	1996.33
SUAA	237.83	37.43	-33.7	12.4	0.0100	0.0100	1994.30
SUTB	238.18	39.21	-23.1	-6.7	0.0100	0.0100	1997.33
SVIN	237.47	38.03	-30.5	10.3	0.0400	0.0400	2003.89
THAL	238.07	37.35	-32.0	9.5	0.2000	0.2200	2003.00
TIBB	237.55	37.89	-30.8	11.2	0.0100	0.0100	1994.42
UCD1	238.25	38.54	-23.1	-6.0	0.0100	0.0100	1996.38
VNDP*	239.38	34.56	-42.2	20.9	0.0000	0.0000	1992.48
YBHB	237.29	41.73	-15.8	-6.7	0.0100	0.0100	1996.75

Table 8.3: CALREF 2006 official velocities. All velocities and estimated errors (σ) are indicated in mm per year. For each site, the relevant time-span and the network are specified. The sites with a star are the sites for which the velocities have been used during the combination of the daily solutions.

Chapter 9

Northern California Earthquake Data Center

1. Introduction

The Northern California Earthquake Data Center (NCEDC), a joint project of the Berkeley Seismological Laboratory (BSL) and the U.S. Geological Survey at Menlo Park, serves as an online archive for various types of digital data relating to earthquakes in central and northern California. The NCEDC is located at the Berkeley Seismological Laboratory, and has been accessible to users via the internet since mid-1992.

The primary goal of the NCEDC is to provide a stable and permanent archival and distribution center of digital geophysical data for networks in northern and central California. These data include seismic waveforms, electromagnetic data, GPS data, strain, creep, and earthquake parameters. The seismic data comes principally from the Berkeley Digital Seismic Network (BDSN) operated by the Seismological Laboratory, the Northern California Seismic Network (NCSN) operated by the USGS, the Berkeley High Resolution Seismic Network (HRSN) at Parkfield, the EarthScope USArray Transportable Array stations in northern California, the various Geysers networks, and selected stations from adjacent networks such as the University of Reno, Nevada network and the Southern California Seismic Network (SCSN). GPS data are primarily from the Bay Area Regional Deformation (BARD) GPS network and the USGS/Menlo Park GPS surveys. The collection of NCSN digital waveforms dates from 1984 to the present, the BDSN digital waveforms date from 1987 to the present, and the BARD GPS data date from 1993 to the present. The BDSN includes stations that form the specialized Northern Hayward Fault Network (NHFN) and the MiniPBO (MPBO) borehole seismic and strain stations in the SF Bay Region.

The NCEDC also provides support for earthquake processing and archiving activities of the Northern California Earthquake Management Center (NCEMC), a component of the California Integrated Seismic Network (CISN). The CISN is the California regional organization of the Advanced National Seismic Network (ANSS).

2. 2005-2006 Activities

By its nature, data archiving is an ongoing activity. In 2005-2006, the NCEDC continued to expand its data holdings and enhance access to the data. Projects and activities of particular note include:

- Began continuous archiving of the entire NCSN network, This includes data from all USGS NC stations, continuous telemetry stations in northern California from the USGS National Strong Motion Program (NSMP), and continuous data from contributing networks.
- Developed and implemented the NCEDC DART (Data Available in Real Time), a system that provides access to real-time timeseries data.
- Developed software and procedures to read and archive continuous NCSN seismograms from tapes for 2001-2005.
- Expanded archiving of data from EarthScope US-Array (network TA) stations for northern California.
- Support NCEMC database efforts to supply the NCEDC with real-time earthquake parameters.

These activities and projects are described in detail below.

3. Data Collections

The bulk of the data at the NCEDC consists of waveform and GPS data from northern California. Figure 9.1 shows the geographic distribution of data archived by the NCEDC. Figure 9.2 shows the relative proportion of each data set at the NCEDC. The total size of the datasets archived at the NCEDC is shown in Table 9.1. Figure 9.3 shows the amount of data for each year that is archived at the NCEDC.

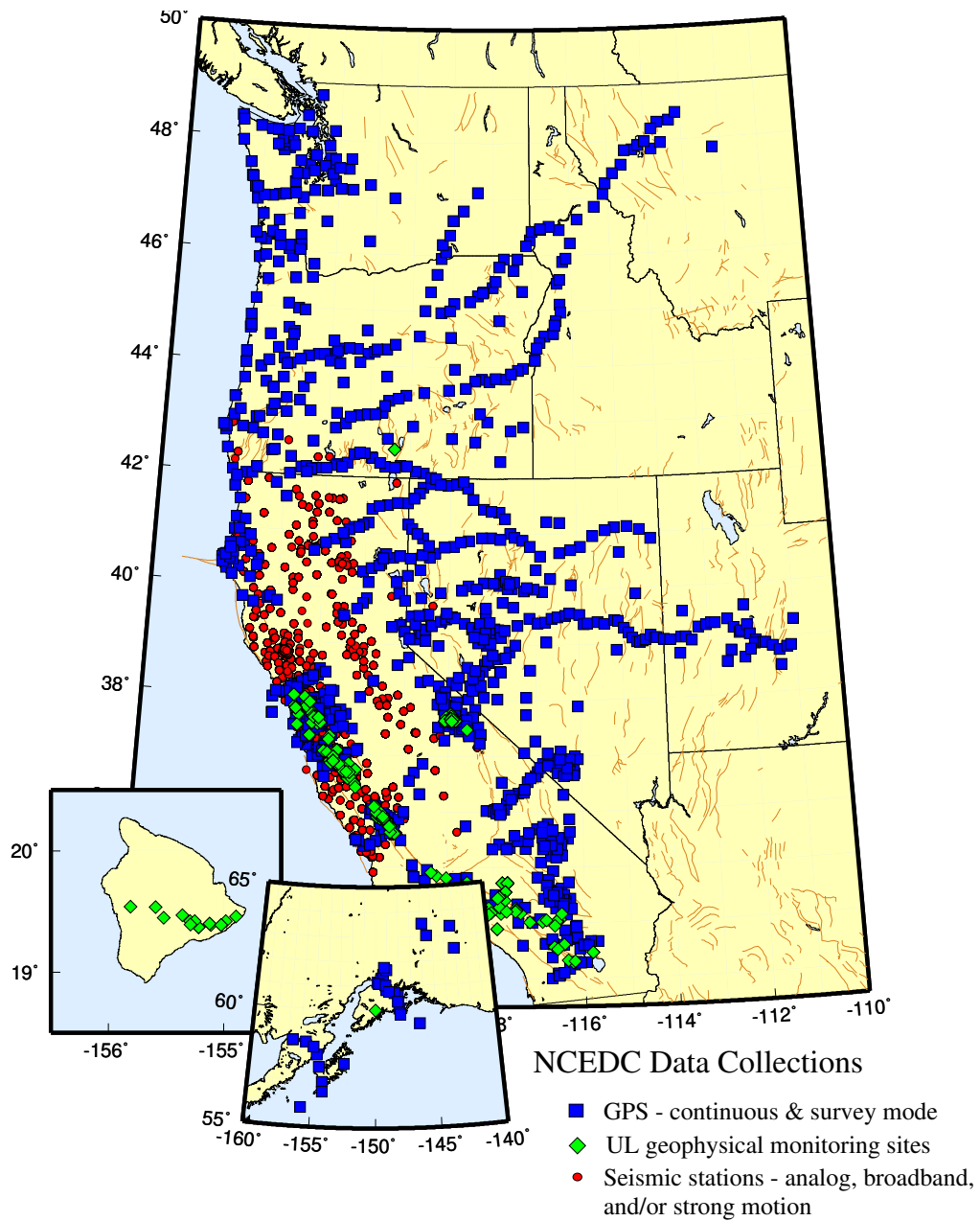


Figure 9.1: Map showing the location of stations whose data are archived at the NCEDC. Circles are seismic sites; squares are GPS sites, and diamonds are the locations of USGS Low-frequency experiments.

Volume of Data archived at the NCEDC

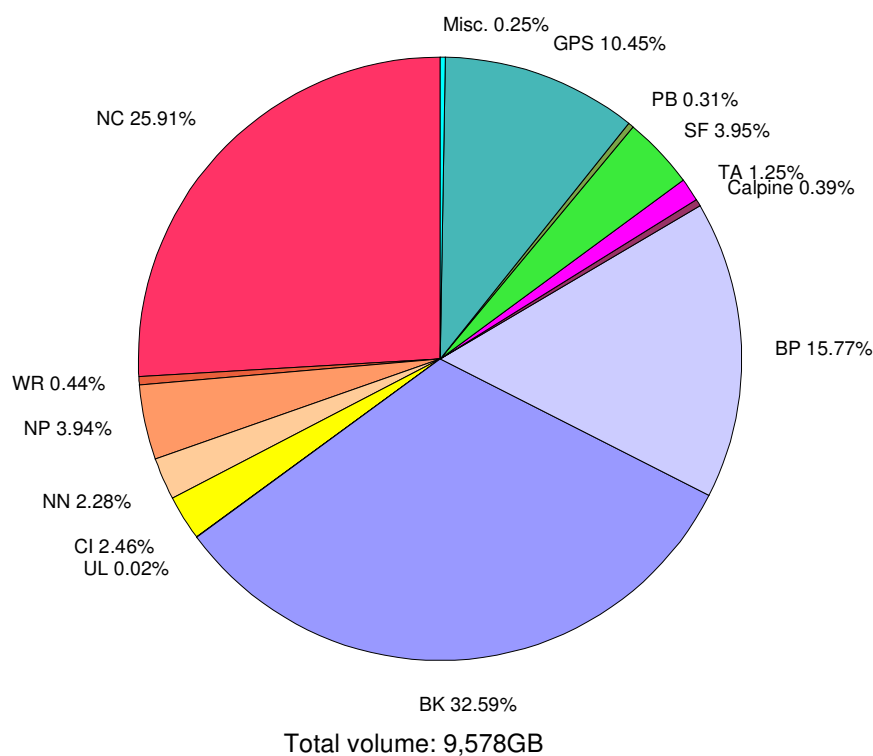


Figure 9.2: Chart showing the relative proportion of each data set at the NCEDC.

Data Type	GBytes
BDSN/NHFN/MPBO (broadband, electric and magnetic field, strain) waveforms	3,111
NCSN seismograms	2,463
Parkfield HRSN seismograms	1,536
BARD GPS (RINEX and raw data)	998
UNR Nevada seismograms	216
SCSN seismograms	234
Calpine/Unocal Geysers region seismograms	37
EarthScope SAFOD seismograms	378
EarthScope USArray seismograms	119
EarthScope PBO strain waveforms	3
USGS Low frequency geophysical waveforms	2
Misc data	24
Total size of archived data	9,534

Table 9.1: Volume of Data Archived at the NCEDC by network

NCEDC Total Volume by Year of Data

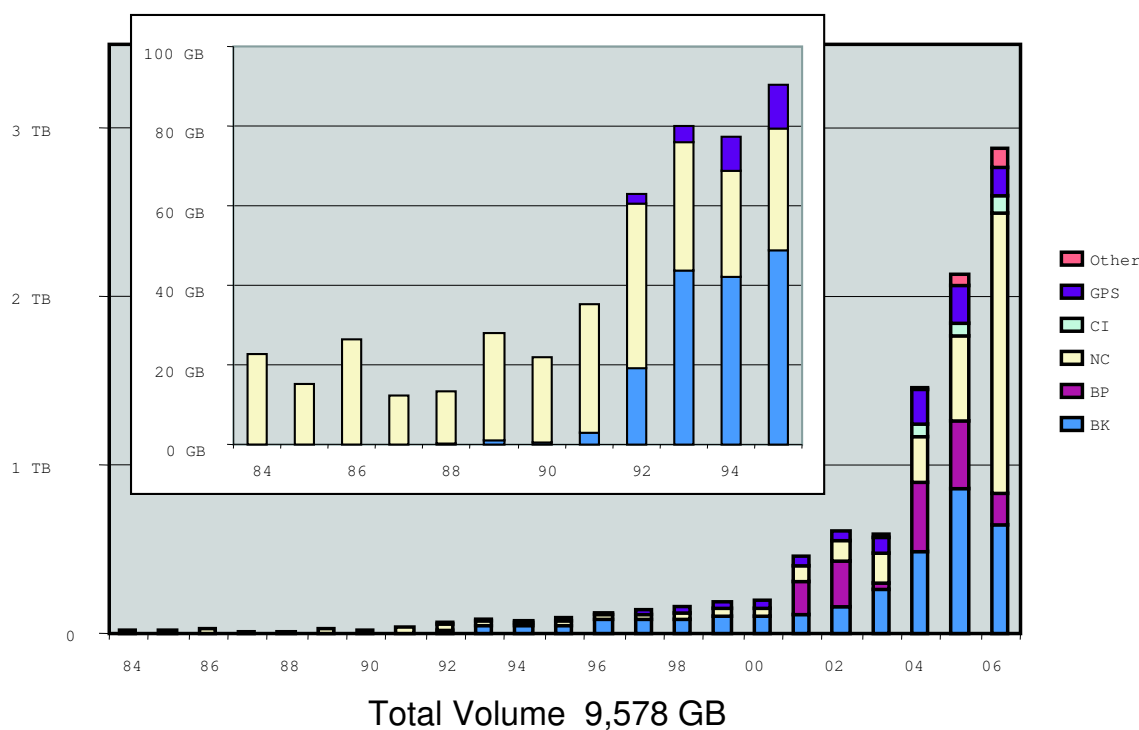


Figure 9.3: Figure showing the total volume of data archived at the NCEDC, broken down by data year.

3.1 BDSN/NHFN/MPBO Seismic Data

Archiving current BDSN (Chapter 4), NHFN (Chapter 6), and Mini-PBO (Chapter ??) (all stations using the network code BK) seismic data is an ongoing task. These data are telemetered from 47 seismic dataloggers in real-time to the BSL, where they are written to disk files, used for CISN real-time earthquake processing, and delivered in real-time to the DART (Data Available in Real Time) system on the NCEDC, where they immediately available to anyone on the internet. In September 2004, the NCEDC began to archive continuous high frequency data (80 Hz and 100 Hz) from all of the BDSN broadband, strong motion, and strainmeter sensors. Previously, 20 Hz and lower rate data channels were archived continuously, and high frequency data was archived only for events. In early 2006, the NCEDC started to receive all of the BK stations in real-time and making them available to users through the DART. All timeseries data from the Berkeley networks continue to be process and archived by an NCEDC analyst using *calqc* in order to provide the highest quality and complete data stream to the NCEDC.

3.2 NCSN Seismic Data

NCSN continuous and event waveform data are sent to the NCEDC via the internet and/or private IP network. The NCSN event waveform files are currently assembled and analyzed at Menlo Park, and are then delivered to the NCEDC, where they are automatically converted to MiniSEED and archived.

The NCEDC maintains a list of teleseismic events recorded by the NCSN, which is updated automatically whenever a new NCSN event file is received at the NCEDC, since these events do not appear in the NCSN catalog.

Since 2002 the NCEDC has archived continuous data from the 15 continuously telemetered digital NCSN broadband stations: 11 stations in northwest California and southwest Oregon in support of the USGS/NOAA Consolidated Reporting of EarthquakeS and Tsunamis (CREST) system, two digital broadband stations in the Mammoth region, and two digital broadband stations in the Parkfield region. At the USGS's request, we also continuously archived the 3 component 500 Hz data from the Mammoth Deep Hole.

In January 2005, in response to interest in non-volcanic tremors detected in northern and central California, the NCEDC began archiving continuous high frequency data

from 21 additional NCSN stations in selected regions of northern California and Parkfield. In response to requests for additional continuous NCSN data, we received approval to rebudget funds to purchase disk and tape systems to support the reading and archiving of continuous waveforms from the entire NCSN from 2001 to the present and to establish procedures continuous archiving of current NCSN data. We purchased the require hardware, and developed procedures to read, convert, and archive the continuous data from the NCSN tapes.

In December 2005, the NCEDC began archiving all available continuous data from the NCSN continuously telemetered stations. We initially started with the stations owned and operated by the USGS Menlo Park (USGS/MP) NCSN (network code NC), and in early 2006, and after discussions with the other cooperating networks that supply data to the NCSN, we expanded the continuous archive to include data from all stations that are contributed to the NCSN.

The NCEDC installed a freeorb server at the USGS in Menlo Park to acquire and buffer the NCSN data for delivery to the NCEDC over the internet. The orbserver currently provides 2 hours of storage in the memory-mapped ring buffer file at Menlo Park. The NCEDC developed an Earthworm-to-Orb-MiniSEED acquisition program to acquire all NCSN waveform data from an Earthworm ring on a USGS/MP, convert the data to MiniSEED format, and insert the data into the observer's ring buffer. We created an orbserver client that runs on the NCEDC computer that connects to the orbserver in Menlo Park, retrieves the the NCSN waveform data records, and writes them to daily channel files in the NCEDC DART.

Most of the NCSN data are automatically archived at the NCEDC, but data from the NCSN broadband stations and Mammoth Deep Hole, most of which can deliver out-of-order data through the USGS Nanometrics satellite system, are processed by an NCEDC analyst using *calqc*.

3.3 Parkfield High Resolution Seismic Network Data

Event seismograms from the Parkfield High Resolution Seismic Network (HRSN) from 1987 through June 1998 are available in their raw SEG Y format via NCEDC research accounts. A number of events have faulty timing due to the lack or failure of a precision timesource for the network. Due to funding limitations, there is currently no ongoing work to correct the timing problems in the older events or to create MiniSEED volumes for these events. However, a preliminary catalog for a significant number of these events has been constructed, and the catalog is available via the web at the NCEDC.

As described in Chapter 7, the original HRSN acquisition system died in late 1998, and an interim system of

portable RefTek recorders were installed at some of the sites. Data from this interim system are not currently available online.

Starting in 2000, the HRSN was upgraded with Quanterra Q730 dataloggers and digital telemetry, and 3 new borehole stations were added to the network. In 2000-2003 the PASO array, a temporary IRIS PASS-CAL broadband network with real-time telemetry, was installed in the Parkfield area and its recording system was housed at the HRSN recording site in Parkfield. During this time, the HRSN collected event data from both the HRSN and PASO array and provided this integrated data set to researchers in near-real-time. The HRSN detected triggers using the HRSN stations and delivered triggered high-rate data from the HRSN and the PASO stations in real-time to the NCEDC, where they were made available to the research community via anonymous ftp until they are reviewed and permanently archived. In addition, the HRSN 20 Hz (BP) and state-of-health channels were archived continuously at the NCEDC. As an interim measure, the NCEDC also archived the continuous 250 Hz (DP) data channels through late 2002 in order to help researchers retrieve events that were not detected during the network upgrade.

The increased seismic activity related to the magnitude 6.5 earthquake in nearby San Simeon on December 22, 2003 drastically increased the number of triggers by the HRSN network. From December 2003 through August 2004, the HRSN had over 70,000 triggers. The 56Kb frame relay connection from Parkfield to UC Berkeley, which was installed to transmit continuous 20 Hz data, selected 250 Hz channels, and event triggered 250 Hz waveforms from the network, was saturated from the increased activity. The HRSN stopped telemetering the event-triggered waveforms, and the NCEDC started to archive continuous 20 and 250 Hz data from the entire network from tapes created at the HRSN operations center in Parkfield in order to preserve this unique dataset. The seismicity again increased after the magnitude 6.0 Parkfield earthquake on September 28, 2004.

In early 2006 the NCEDC started to receive the HRSN 20 Hz data and a subset of the 250 Hz data in real-time for distribution through the DART. The NCEDC continues to archive continuous 250 Hz and 20 Hz data streams from the HRSN tapes written in Parkfield and processed at the NCEDC.

3.4 EarthScope USArray Transportable Array

EarthScope began installing broadband stations for the Transportable Array component of USArray in California in 2005. The NCEDC started acquiring telemetered continuous data from the northern California and surrounding stations as they were installed, and is archiving these data to support users working with northern

California seismic data. These data are made available to users using the same data request methods as all other continuous data waveform data at the NCEDC. The Transportable Array stations have a limited operational timespan of 18 to 24 months, after which they will be relocated to new sites across the country. Data from these stations are delivered to the NCEDC as they are received by the BSL for distribution through the DART.

3.5 EarthScope Plate Boundary Observatory (PBO) strain data

The NCEDC has been designated by EarthScope as one of two archives for PBO borehole and laser strain data. Strain data are collected from all of the PBO strain sites and are processed by UNAVCO. MiniSEED data are delivered to the NCEDC using SeedLink, and raw and XML processed data are delivered to the NCEDC using Unidata's Local Data Manager (LDM). The MiniSEED data are inserted into the NCEDC DART, and are subsequently archived from the DART. UNAVCO provides EarthScope funding to the NCEDC to help cover the processing, archiving, and distribution costs for these data.

3.6 EarthScope SAFOD

The NCEDC is designated as the primary archive center for the SAFOD event data, and will also process the continuous SAFOD data. Starting in July 2002, scientists from Duke University successfully installed a three component 32 level downhole-seismic array in the pilot hole at the EarthScope SAFOD site in collaboration with Steve Hickman (USGS), Mark Zoback (Stanford University) and the Oyo Geospace Engineering Resources International (GERI) Corporation. High frequency event recordings from this array have been provided by Duke University for archiving at the NCEDC. We converted data from the original SEG-2 format data files to MiniSEED, and have developed the SEED instrument responses for this data set. We continue to receive data from the various SAFOD seismic deployments in the Pilot Hole and Main Hole, and will convert, archive, and distributed these data. SAFOD will provide EarthScope funding to the NCEDC to cover the processing, archiving, and distribution costs for these data. A small subset of the continuous SAFOD data channels are also incorporated into the NCSN, and are available in real-time from the NCEDC DART.

3.7 UNR Broadband data

The University of Reno in Nevada (UNR) operates several broadband stations in western Nevada and eastern California that are important for northern California earthquake processing and analysis. Starting in August 2000, the NCEDC has been receiving and archiving continuous broadband data from four UNR stations. The

data are transmitted in real-time from UNR to UC Berkeley, where they are made available for CISN real-time earthquake processing and for archiving. Initially, some of the stations were sampled at 20 Hz, but all stations are now sampled and archived continuously at 100 Hz.

The NCEDC installed Simple Wave Server (SWS) software at UNR, which provides an interface to UNR's recent collection of waveforms. The SWS is used by the NCEDC to retrieve waveforms from UNR that were missing at the NCEDC due to real-time telemetry outages between UNR and UC Berkeley.

In early 2006 the NCEDC started to archive continuous data from the UNR short-period stations that are contributed to the NCSN. Both the broadband and short-period UNR stations contributed to the CISN are available in real-time through the NCEDC DART.

3.8 Electro-Magnetic Data

The NCEDC continues to archive and process electric and magnetic field data acquired at several UC Berkeley sites. dataloggers at PKD, SAO, and JRSC acquire data from 3 components of magnetic field and 2 or 4 components of electric field at 40 Hz, 1 Hz, and 0.1 Hz, and are telemetered in real-time along with seismic data to the Berkeley Seismological Laboratory, where they are processed and archived at the NCEDC in a similar fashion to the seismic data (Section 3.17.).

Using programs developed by Dr. Martin Fullerkrug at the Stanford University STAR Laboratory (now at the University of Bath), the NCEDC has computed and archived magnetic activity and Schumann resonance analysis using the 40 Hz data from this dataset. The magnetic activity and Schumann resonance data can be accessed from the Web.

The NCEDC also archives data from a low-frequency, long-baseline electric field project operated by Dr. Steve Park of UC Riverside at site PKD2. These data are acquired and archived in an identical manner to the other electric field data at the NCEDC.

3.9 GPS Data

The NCEDC continues to archive GPS data through the BARD (Bay Area Regional Deformation) network of continuously monitored GPS receivers in northern California (Chapter 8). The NCEDC GPS archive now includes 67 continuous sites in northern California. There are approximately 50 core BARD sites owned and operated by UC Berkeley, USGS (Menlo Park and Cascade Volcano Observatory), LLNL, UC Davis, UC Santa Cruz, Trimble Navigation, and Stanford. Data are also archived from sites operated by other agencies including East Bay Municipal Utilities District, the City of Modesto, the National Geodetic Survey, and the Jet Propulsion Laboratory.

In addition to the standard 15 second or 30 second continuous GPS datastream, the NCEDC is now archiving and distributing high-rate 1 Hz continuous GPS data from the 14 stations in Parkfield and from 10 BARD stations. These high-rate data are available via anonymous FTP from the NCEDC but are currently not included in the GPS Seamless Archive (GSAC), since the GSAC does not currently handle both high-rate and low-rate data from the same site and day.

The NCEDC continues to archive non-continuous survey GPS data. The initial dataset archived is the survey GPS data collected by the USGS Menlo Park for northern California and other locations. The NCEDC is the principal archive for this dataset. Significant quality control efforts were implemented by the NCEDC to ensure that the raw data, scanned site log sheets, and RINEX data are archived for each survey. All of the USGS/MP GPS data has been transferred to the NCEDC and virtually all of the data from 1992 to the present has been archived and is available for distribution.

3.10 Geysers Seismic Data

The Calpine Corporation currently operates a micro-seismic monitoring network in the Geysers region of northern California. Prior to 1999 this network was operated by Unocal. Through various agreements, both Unocal and Calpine have released triggered event waveform data from 1989 through 2000 along with preliminary event catalogs for the same time period for archiving and distribution through the NCEDC. This dataset represents over 296,000 events that were recorded by Calpine/Unocal Geysers network, and are available via research accounts at the NCEDC.

The Lawrence Berkeley National Laboratory (LBNL), with funding from the California Energy Commission, operates a 22 station network in the Geysers region with an emphasis on monitoring seismicity related to well water injection. The earthquake locations and waveforms from this network are sent to the NCEDC, and the locations are forwarded to the NCSN so that they can be merged into the NCSN earthquake catalog. The LBNL Geysers waveforms will be available at the NCEDC after the NCSN catalog has been migrated from flat files to the database.

3.11 USGS Low Frequency Data

Over the last 30 years, the USGS at Menlo Park, in collaboration with other principal investigators, has collected an extensive low-frequency geophysical data set that contains over 1300 channels of tilt, tensor strain, dilatational strain, creep, magnetic field, water level, and auxiliary channels such as temperature, pore pressure, rain and snow accumulation, and wind speed. In collaboration with the USGS, we assembled the requisite

information for the hardware representation of the stations and the instrument responses for many channels of this diverse dataset, and developed the required programs to populate and update the hardware database and generate the instrument responses. We developed the programs and procedures to automate the process of importing the raw waveform data and convert it to MiniSEED format. Since these data are delivered to the NCEDC on a daily basis and immediately archived, these data are not inserted into the NCEDC DART.

We have currently archived timeseries data from 887 data channels from 167 sites, and have instrument response information for 542 channels at 139 sites. The waveform archive is updated on a daily basis with data from 350 currently operating data channels. We will augment the raw data archive as additional instrument response information is assembled by the USGS for the channels, and will work with the USGS to clearly define the attributes of the "processed" data channels.

3.12 SCSN/Statewide seismic data

In 2004 the NCEDC started to archive broadband and strong motion data from 15 SCSN (network CI) stations that are telemetered to the NCEMC. These data are used in the prototype real-time state-wide earthquake processing system and also provide increased coverage for northern California events. Since the data are telemetered directly from the stations in real-time to both the SCSN and to the NCEMC, the NCEDC archives the NCEMC's copy of the data to ensure that at least one copy of the data will be preserved.

In early 2006 the NCEDC started to continuously archive all of the selected SCSN short-period stations that are contributed to the NCSN. All of these data are available in real-time from the NCEDC DART.

3.13 Northern California Seismicity Project

The objective of Northern California Seismicity Project is to characterize the spatial and temporal evolution of the northern and Central California seismicity during the initial part of the earthquake cycle as the region emerges from the stress shadow of the great 1906 San Francisco earthquake. Although the current BSL catalog of earthquakes for the region appears to be a simple list of events, one must remember that it really is a very complex data set. The existing catalog is inhomogeneous in that it suffers from the three types of man-made seismicity changes: namely detection changes, reporting changes, and magnitude shifts. The inherent catalog inhomogeneity exists because the location and magnitude determination methodologies have changed as the instrumentation and computational capabilities improved over the past century. It is easy to misinterpret observed vari-

ations in seismicity if we do not understand these inherent limitations of the catalog. As a result, the northern and central California seismicity since 1906 is poorly understood.

Creation of a northern and central California catalog of seismicity that is homogeneous, that spans as many years as possible, and that includes formal estimates of the parameters and their uncertainty is a fundamental prerequisite for probabilistic studies of the seismicity. The existence of the invaluable BSL seismological archive, containing the original seismograms as well as the original reading/analysis sheets allows the application of modern analytical algorithms towards the problem of determining the source parameters of the historical earthquakes.

Our approach is to systematically re-analyze the data acquired from the reading/analysis sheet archive to develop a homogeneous catalog of earthquake location and local magnitude (M_L) including formal uncertainties on all parameters which extends as far back in time as the instrumental records allow and which is complete above appropriate threshold magnitudes. We anticipate being able to compile a new catalog of location and M_L which spans 1930 to the present and is which complete at the M_L 3 threshold.

During the year 2005-2006 we have completed the transcription of the original reading/analysis sheets to computer readable flat files for all M_L 3.0 and larger earthquakes which have occurred in northern and central California and vicinity back to January 1, 1951. We started with the events that occurred in 1983 and worked backwards in time. The events from January 1, 1984 onwards were already in computer readable form. Data were transcribed from the original reading/analysis sheets for 5204 earthquakes and preliminary locations and local magnitudes have been calculated. We plan to transcribe reading/analysis sheet data back to at least 1932 but the process is more complicated and time consuming since we will have to pull the original Wood-Anderson seismograms from the archive to read the maximum trace amplitudes in order to calculate the local magnitude of the events. The research reports (Sections 3.12. and 3.13.) by R. Uhrhammer discuss these projects in more detail.

3.14 Earthquake Catalogs

Northern California

The NCEDC provides searchable access to both the USGS and BSL earthquake catalogs for northern and central California. The "official" UC Berkeley earthquake catalog begins in 1910 and runs through 2003, and the "official" USGS catalog begins in 1966. Both of these catalogs are archived and available through the NCEDC, but the existence of 2 catalogs has caused confusion among both researchers and the public.

In late 2006, the NCEMC will begin providing a single unified northern California earthquake catalog in real-

time to the NCEDC through database replication from the NCEMC's real-time systems. The NCEDC has developed and is testing the required programs that will be used to enter all previous NCSN catalog data into the NCEDC database. We will then merge the the BSL catalog with the NCEMC catalog to form a single unified northern California catalog from 1910 to the present. The BSL and the USGS have spent considerable effort over the past years to define procedures for merging the data from the two catalogs into a single northern and central California earthquake catalog in order to present a unified view of northern California seismicity. The differences in time period, variations in data availability, and mismatches in regions of coverage all complicate the task.

Worldwide

The NCEDC, in conjunction with the Council of the National Seismic System (CNSS), produced and distributed a world-wide composite catalog of earthquakes based on the catalogs of the national and various U.S. regional networks for several years. Each network updates their earthquake catalog on a daily basis at the NCEDC, and the NCEDC constructs a composite world-wide earthquake catalog by combining the data, removing duplicate entries that may occur from multiple networks recording an event, and giving priority to the data from each network's *authoritative region*. The catalog, which includes data from 14 regional and national networks, is searchable using a Web interface at the NCEDC. The catalog is also freely available to anyone via ftp over the internet.

With the demise of the CNSS and the development of the Advanced National Seismic System (ANSS), the NCEDC was asked to update its Web pages to present the composite catalog as a product of the ANSS. This conversion was completed in the fall of 2002. We continue to create, house, distribute, and provide a searchable web interface to the ANSS composite catalog, and to aid the regional networks in submitting data to the catalog.

4. NCEDC Operations

In 2005, the NCEDC relocated its archive and distribution system from McCone Hall to a new state-of-the-art computer facility in a new seismically braced building on the Berkeley campus. The facility provides seismically braced equipment racks, gigabit ethernet network, air conditioning and power conditioning. The entire facility is powered by a UPS with generator backup.

The currently installed NCEDC facilities consist of a mass storage environment hosted by a Sun V240 host computer, a 100 slot LTO-2 tape library with two tape drives and a 20 TByte capacity, and 30 TBytes of RAID

storage, all managed with the SAM-FS hierarchical storage management (HSM) software. A dual processor Sun Ultra 60 provides Web services and research account access to the NCEDC, a dual Sun 280R processor provide data import and export services, and a Sun Ultra 450 computer is used for quality control procedures. Two AIT tape libraries will be used to read NCSN continuous data tapes. An 64-bit Linux system hosts a database dedicated to providing data to external users. A new Sun Opteron processor has recently been purchased to upgrade the NCEDC web server.

The hardware and software system is configured to automatically create multiple copies of each timeseries file. The NCEDC creates an online copy of each file on online RAID, a second copy on LTO-2 tape which is stored online in the tape library, and a third copy on LTO-2 tape which is stored offline and offsite. All NCEDC data are online and rapidly accessible by users.

The NCEDC operates two instances of its Oracle database, one for internal operations, and one for external use for user data queries and data distribution programs. The databases are synchronized using multi-master replication.

5. Data Quality Control

The NCEDC developed a GUI-based state-driven system *calqc* to facilitate the quality control processing that is applied to the continuously archived data sets at the NCEDC.

The quality control procedures for these datasets include the following tasks:

- data extraction of a full day of data,
- quickcheck program to summarize the quality and stability of the stations' clocks,
- determine if there is missing data for any data channel,
- provided procedures to retrieve missing data from the stations and incorporate it into the day's data,
- optional creation of multi-day timeseries plots for state-of-health data channels,
- optional timing corrections for data,
- optional extraction of event-based waveforms from continuous data channels,
- optional repacking of MiniSEED data,
- creating waveform inventory entries in the NCEDC database,

- publishing the data for remote access on the NCEDC.

Calqc uses previously developed programs to perform each function, but it provides a graphical point-and-click interface to automate these procedures, and to provide the analyst with a record of when each process was started, whether it executed correctly, and whether the analyst has indicated that a step has been completed. *Calqc* is used to process all data from the BDSN network, and all continuous broadband data from the NCSN, UNR, SCSN, and HRSN networks that are archived by the NCEDC. The remainder of the continuously archived data are automatically archived without any analyst interaction.

6. Database Development

Due to restrictions imposed by the USGS/MP NCSN CUSP event analysis system, the NCEDC still stores the official NCSN earthquake catalog, phase, amplitude, and coda readings in flat text files. However, the NCEDC has worked closely with the NCEMC to develop and test procedures that will allow the USGS/MP to replace the CUSP analysis system with *jiggle*, the analysis tool developed by the SCSN and to deliver earthquake parametric data in real-time to the NCEDC database. We have developed the database tools to insert the NCEMC earthquake parametric information into databases in the real-time earthquake analysis systems, and have extensively tested database replication between the NCEMC databases and the NCEDC database. We have developed the programs necessary to migrate the NCSN catalog into the CISN parametric schema and to search and retrieve earthquake data from the database. In fall 2006, we will coordinate the retirement of CUSP with the migration of the NCEMC system to the replicated database environment.

During 2002-2004, the NCEDC and NCSN jointly developed a system consisting of an extensive spreadsheet containing per-channel information that describes the hardware of each NCSN data channel and provides each channel with a SEED-compliant channel name. This spreadsheet, combined with a limited number of files that describe the central-site analog digitizer, FIR decimation filters, and general characteristics of digital acquisition systems, allow the NCSN to assemble its station history in a format that the NCEDC can use to populate the hardware tracking and instrument response database tables for the NCSN.

The NCEDC instrument response schema represents full multi-stage instrument responses (including filter coefficients) for the broadband dataloggers. The hardware tracking schema represents the interconnection of instruments, amplifiers, filters, and dataloggers over time, and is used to describe all of the UC Berkeley and

USGS stations and channels archived at the NCEDC. All NCSN event waveform and continuous timeseries data has been converted from CUSP and Earthworm format to MiniSEED, and are available along with the UC Berkeley data and data from the other networks archived at the NCEDC in full SEED format.

The NCEDC has developed XML import and export procedures to provide better maintenance of the hardware tracking information and resulting instrument responses for stations in our database. When changes are made to either existing hardware or to station configurations, we export the current view in XML format, use a GUI-based XML editor to easily update the information, and import the changes back into the database. When adding new stations or hardware, we can easily use information from existing hardware or stations as templates for the new information. This allows us to treat the database as the authoritative source of information, and to use off-the-shelf tools such as the XML editor and XML differencing programs as part of our database maintenance procedures.

Additional details on the joint catalog effort and database schema development may be found at <http://www.ncedc.org/db>

7. Data Distribution

The NCEDC continues to use the World Wide Web as a principal interface for users to request, search, and receive data from the NCEDC. In fall 2005 the NCEDC acquired the domain name *ncedc.org*. The NCEDC's Web address is now <http://www.ncedc.org/>

Earthquake Catalogs

The NCEDC provides users with searchable access to northern California earthquake catalogs and to the ANSS world-wide catalog via the web. Users can search the catalogs by time, magnitude, and geographic region, and can retrieve either hypocenter and magnitude information or a full set of earthquake parameters including phase readings, amplitudes, and codas.

Station Metadata

In addition to the metadata returned through the various data request methods, the NCEDC provides dataless SEED volumes and SEED RESP file for all data channels archived at the NCEDC. The NCEDC currently has full SEED instrument responses for 8462 data channels from 1379 stations in 14 networks. This includes stations from the California Geological Survey (CGS) strong motion stations that will contribute seismic waveform data for significant earthquake to the NCEDC and SCEDC.

SeismiQuery

We have ported and installed the IRIS *SeismiQuery* program at the NCEDC, which provides a common interface to query network, station, and channel attributes and query the availability of archived timeseries data. We have provided both IRIS and the SCEC Data Center with our modified version of *SeismiQuery*.

DART (Data Available in Real Time)

The DART (Data Available in Real Time) represents the first step in NCEDC's effort to make current and recent timeseries data from all networks, stations, and channels available to users in real-time. The NCEDC developed DART in December 2005 to provide a mechanism for users to obtain access to real-time data from the NCEDC. All real-time timeseries data stream delivered to the NCEDC are placed in MiniSEED files in a web-accessible directory structure. The DART waveforms can be accessed by web browsers or http command-line programs such as *wget*, a *FISSURES* waveform server, and a Berkeley-developed Simple Wave Server (SWS) which provides programmatic access to the DART data by specified SEED channel and time interval. We will be providing users with a client program to retrieve data from the SWS in the near future. The DART currently provide access to the most recent 30 days of data.

We are using the Freeorb software, an enhanced version of the open-source orb software developed by the IRIS-funded Joint Seismic Project (JSP), as the primary method for delivering real-time data to the NCEDC and into the DART. The freeorb package implements an object ring buffer (ORB) and orbserver, which provides a reliable storage ringbuffer and an interface for orb client programs to read, write, and query the orbserver. Orbserver clients running at the NCEDC computer connect to remote orbserver at the BSL and USGS/Menlo Park, retrieve the MiniSEED timeseries data records, and write them to daily channel files in the NCEDC DART. Strain data from the EarthScope PBO network are delivered to the NCEDC using SeedLink, and are inserted into the DART using a similar SeedLink client program.

The NCEDC developed an automated data archiving system to archive data from the DART on a daily basis. It allows us to specify which stations should be automatically archived, and which stations should be handled by the NCEDC's Quality Control program *calqc*, which allow an analyst to review the waveforms, retrieve missing data from stations or waveservers that may have contain late arriving out-of-order data, and perform timing corrections on the waveform data. The majority of data channels are currently archived automatically from the DART.

NetDC

In a collaborative project with the IRIS DMC and other worldwide datacenters, the NCEDC helped develop and implement *NetDC*, a protocol which will provide a seamless user interface to multiple datacenters for geophysical network and station inventory, instrument responses, and data retrieval requests. The *NetDC* builds upon the foundation and concepts of the IRIS *BREQ_FAST* data request system. The *NetDC* system was put into production in January 2000, and is currently operational at several datacenters worldwide, including NCEDC, IRIS DMC, ORFEUS, Geoscope, and SCEDC. The *NetDC* system receives user requests via email, automatically routes the appropriate portion of the requests to the appropriate datacenter, optionally aggregates the responses from the various datacenters, and delivers the data (or ftp pointers to the data) to the users via email.

STP

In 2002, the NCEDC wrote a collaborative proposal with the SCEDC to the Southern California Earthquake Center, with the goal of unifying data access between the two data centers. As part of this project, the NCEDC and SCEDC are working to support a common set of 3 tools for accessing waveform and parametric data: *Seis-miQuery*, *NetDC*, and *STP*.

The *Seismogram Transfer Program* or *STP* is a simple client-server program, developed at the SCEDC. Access to *STP* is either through a simple direct interface that is available for Sun or Linux platforms, or through a GUI Web interface. With the direct interface, the data are placed directly on a user's computer in several possible formats, with the byte-swap conversion performed automatically. With the Web interface, the selected and converted data are retrieved with a single ftp command. The *STP* interface also allows rapid access to parametric data such as hypocenters and phases.

The NCEDC has continued work on *STP*, working with the SCEDC on extensions and needed additions. We added support for the full SEED channel name (Station, Network, Channel, and Location), and are now able to return event-associated waveforms from the NCSN waveform archive.

EVT_FAST

In order to provide Web access to the NCSN waveform before the SEED conversion and instrument response for the NCSN has been completed, the NCEDC implemented *EVT_FAST*, an interim email-based waveform request system similar to the *BREQ_FAST* email request system. Users email *EVT_FAST* requests to the NCEDC and request NCSN waveform data based on the NCSN event id. Initially the NCSN waveform data was converted to either SAC ASCII, SAC binary, or AH format, and placed

in the anonymous ftp directory for retrieval by the users. *EVT_FAST* event waveforms can now also be provided in MiniSEED format, and are now named with their SEED channel names.

FISSURES

The *FISSURES* project developed from an initiative by IRIS to improve earth scientists' efficiency by developing a unified environment that can provide interactive or programmatic access to waveform data and the corresponding metadata for instrument response, as well as station and channel inventory information. *FISSURES* was developed using CORBA (Common Object Request Broker Architecture) as the architecture to implement a system-independent method for the exchange of this binary data. The IRIS DMC developed a series of services, referred to as the *Data Handling Interface (DHI)*, using the *FISSURES* architecture to provide waveform and metadata from the IRIS DMC.

The NCEDC has implemented the *FISSURES Data Handling Interface (DHI)* services at the NCEDC, which involves interfacing the DHI servers with the NCEDC database schema. These services interact with the NCEDC database and data storage system, and can deliver NCEDC channel metadata as well as waveforms using the *FISSURES* interfaces. We have separate *FISSURES DHI* waveform servers to serve archived and DART data stream. Our *FISSURES* servers are registered with the IRIS *FISSURES naming services*, which ensures that all *FISSURES* users have transparent access to data from the NCEDC.

GSAC

Since 1997, the NCEDC has collaborated with UNAVCO and other members of the GPS community on the development of the *GPS Seamless Archive Centers (GSAC)* project. This project allows a user to access the most current version of GPS data and metadata from distributed archive locations. The NCEDC is participating at several levels in the *GSAC* project: as a primary provider of data collected from core BARD stations and USGS MP surveys, and as a wholesale collection point for other data collected in northern California. We helped to define database schema and file formats for the *GSAC* project, and have produced complete and incremental monumentation and data holdings files describing the data sets that are produced by the BARD project or archived at the NCEDC so that other members of the *GSAC* community can provide up-to-date information about our holdings. Currently, the NCEDC is the primary provider for over 138,000 data files from over 1400 continuous and survey-mode monuments. The data holdings records for these data have been incorporated into the *GSAC* retailer system, which became publicly available in late 2002.

In addition, the NCEDC is archiving and distributing high-rate 1 Hz GPS data from 10 BARD stations in addition to the normally sampled 15 second or 30 second data. These high-rate data are available by FTP from the NCEDC, but are not available through GSAC due to GSAC's inability to distinguish multiple data streams with different sample rates for the same day and station.

8. Acknowledgements

The NCEDC is a joint project of the BSL and the USGS Menlo Park and is funded primarily by the BSL and the USGS. Additional funding for the handling and archiving of the EarthScope PBO and SAFOD data is provided through subawards from the respective NSF EarthScope projects.

Doug Neuhauser is the manager of the NCEDC. Stephane Zuzlewski, Rick McKenzie, Nicolas Houlie, Bob Uhrhammer, and Peggy Hellweg of the BSL and David Oppenheimer, Hal Macbeth, and Fred Klein of the USGS Menlo Park contribute to the operation of the NCEDC. Doug Neuhauser, Peggy Hellweg, Stephane Zuzlewski, and Bob Uhrhammer contributed to the preparation of this chapter.

Chapter 10

Data Acquisition and Quality Control

1. Introduction

Stations from most networks operated by the BSL transmit data continuously to the BSL facilities on the UC Berkeley campus for analysis and archive. In this chapter, we describe activities and facilities which cross-cut the individual networks described in Chapters 4, 6 and 7, including procedures for data acquisition and quality control, and sensor testing capabilities and procedures. This year the computer and networking facilities used for data acquisition moved from McCone Hall to the University's seismically safe building at 2195 Hearst Ave.

While some of these activities are continuous from year to year, we have identified changes or activities which are specific to 2005-2006.

2. Data Acquisition Facilities

Until 2005-2006, both the BSL staff monitoring routine data acquisition, and the computers and facilities to acquire, process, and archive the data were situated in McCone Hall. There the BSL has facilities designed to provide air conditioning, 100-bit switched network, and reliable power with UPS and generator. During this year, the computers and telemetry equipment associated with data collection and archival were moved to the new campus computer facility in 2195 Hearst Avenue.

2.1 The Move to 2195 Hearst Avenue

After several years of actively working with the campus, the BSL has finally relocated the infrastructure supporting the critical operations of data acquisition, processing, archiving, and data distribution to a more robust facility than McCone Hall. With assistance from the Office of the Vice Chancellor for Research, the BSL has been granted space in 2195 Hearst, a recently completed building on the Oxford Tract. 2195 Hearst was constructed to current seismic codes, and the hardened campus computer facility within was designed with special attention for post-earthquake operations. The computer center contains state-of-the art seismic bracing, UPS power and

air conditioning with generator backup, and extensive security and equipment monitoring.

During 2005-2006, the BSL completed the relocation of equipment to the new facilities in 2195 Hearst. This includes all of its data acquisition and real-time earthquake processing computers, as well as the data archive and distribution computers. Following the computer move, all telemetry equipment (5 T1s lines, dedicated leased phone circuit to our paging service, dialin/dialout modems, as well as various radio and VSAT communication equipment) were also transferred to the new location over the course of several months. The final elements were moved in February, 2006. During the transition, the private network used for seismic data acquisition and earthquake processing was temporarily bridged between McCone Hall and 2195 Hearst using an encrypted tunnel across the campus backbone network.

2.2 Power and Air Conditioning in McCone Hall

In the past, mission-critical earthquake monitoring and review processes ran on several computers in McCone Hall. Thus, these computer systems run on circuits with both UPS and generator power. Air conditioning is provided through both "building air" and two additional AC units. Over the years, the BSL has experienced problems with both the McCone generator system and the air conditioning.

With the move of many BSL and NCEDC operations servers to the campus computer center at 2195 Hearst (SRB1), our generator power and air conditioning resources in the BSL server room in 237 McCone have better matched our needs over the past year. The BSL generator and UPS battery system supported servers during one brief power outage this year. The air conditioning systems for room 237 required maintenance and some parts replacement, but no serious problems resulted during these events. The BSL generator is maintained by Physical Plant Capital Services and was run without load twice monthly.

BSL is developing a long range plan with UCB Communications Network Services (CNS), a division of Infor-

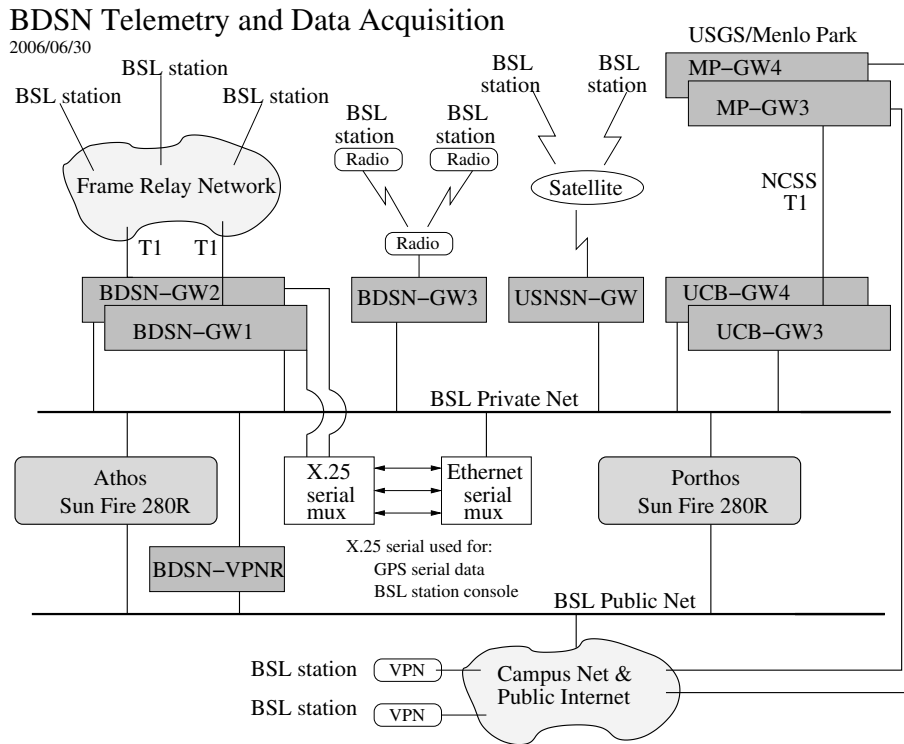


Figure 10.1: Data flow from the BDSN, NHFN, MPBO, HRSN, and BARD network into the BSL central processing facility.

mation Services and Technology, to replace the generator with a larger, 100 kW unit, and to upgrade the UPS battery backup systems. This joint project is designed to provide generator/UPS power for the two CNS-operated network equipment closets serving all of McCone Hall, in addition to providing emergency power to the BSL suite and the BSL engineering lab in room 298 McCone. BSL and CNS will present this plan to the Vice Chancellor Academic Council for approval and assistance with funding for this proposal.

3. Data Acquisition

Central-site data acquisition for the BDSN/NHFN/MPBO is performed by two computer systems located at the BSL (Figure 10.1). These acquisition systems are also used for the Parkfield-Hollister electromagnetic array and for the BARD network. A third system is used primarily as data exchange system with the USNSN and transmits data to the USNSN from HOPS, CMB, SAO, WDC, HUMO, MOD, MCCM, and YBH. Data acquisition for the HRSN follows a more complicated path, as described in Chapter 7.

3.1 Comserv

The BSL uses the **comserv** program for central data acquisition, which was developed by Quanterra. The **comserv** program receives data from a remote Quanterra data logger, and redistributes the data to one or more **comserv** client programs. The **comserv** clients used by REDI include **datalog**, which writes the data to disk files for archival purposes, **cdafill**, which writes the data to the shared memory region for REDI analysis, and other programs such as the seismic alarm process, the DAC480 system, and the feed for the Memento Mori Web page (Figure 10.2).

The two computers that perform data acquisition also serve as REDI processing systems. In order to facilitate REDI processing, each system maintains a shared memory region that contains the most recent 30 minutes of data for each channel used by the REDI analysis system. All REDI analysis routines first attempt to use data in the shared memory region, and will only revert to retrieving data from disk files if the requested data is unavailable in the shared memory region.

Each BDSN datalogger that uses frame relay telemetry is configured to enable data transmission simultaneously to two different computers over two different frame relay T1 circuits to UCB. However, the BSL normally actively enables and uses only one of these data stream from each

early diagnoses of instrumental problems. A PSD estimation algorithm was developed in the early 1990's at the BSL for characterizing the background seismic noise and as a tool for quality control. As presently implemented, the algorithm sends the results via email to the engineering and some research staff members and generates a bargraph output which compares all the BDSN broadband stations by components. A summary of the results for 2005-2006 is displayed in Figure 4.2. Other PSD plots for the NHFN, HRSN, and MPBO are shown in Figures 6.2, 7.3, respectively.

Four years ago, we expanded our use of the weekly PSD results to monitor trends in the noise level at each station. In addition to the weekly bar graph, additional figures showing the analysis for the current year are produced. These cumulative PSD plots are generated for each station and show the noise level in 5 frequency bands for the broadband channels. These cumulative plots make it easier to spot certain problems, such as failure of a sensor. In addition to the station-based plots, a summary plot for each channel is produced, comparing all stations. These figures are presented as part of a noise analysis of the BDSN on the WWW at <http://www.seismo.berkeley.edu/seismo/bdsn/psd/>.

The PSD algorithm has been documented in previous annual reports.

4.1 PDF Noise Analysis

In addition to the PSD analysis developed by Bob Uhrhammer, the BSL has implemented the Ambient Noise Probability Density Function (PDF) analysis system developed by *McNamara and Buland* (2004). This system does its noise analysis over all the data of a given time period (week or year), including earthquakes, calibration pulses, and cultural noise. This is in contrast to Bob Uhrhammer's PSD analysis, which looks at only the quietest portion of data within a day or week. Pete Lombard of the BSL extended the McNamara code to cover a larger frequency range and support the many different types of sensors employed by the BSL. Besides the originally supported broadband sensors, our PDF analysis now includes surface and bore-hole accelerometers, strain meters, and electric and magnetic field sensors. These enhancements to the PDF code, plus a number of bug fixes, were provided back to the McNamara team for incorporation in their work. The results of the PDF analysis are presented on the web at <http://moho/seismo/PDF/>. Figure 10.3 shows noise analysis results for a typical week. We review these plots as part of our assessment of station health.

5. Sensor Testing Facility

The BSL has set up an instrumentation test facility in the Byerly Seismographic Vault in order to systemati-

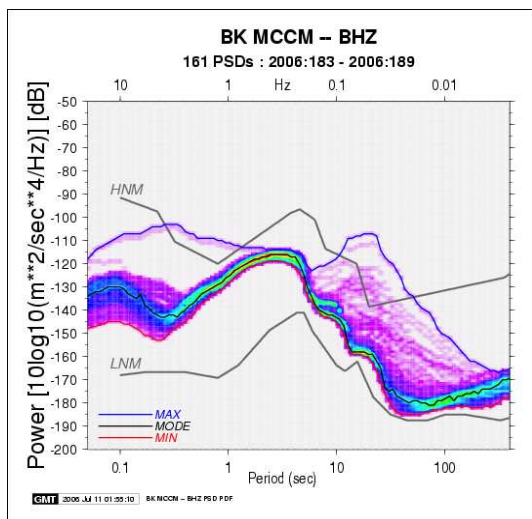


Figure 10.3: Noise analysis results for the week of 07/02/06 at the newest BDSN station MCCM, on the BHZ component. The prominent feature at short periods are produced by waves from the nearby earthquake offshore of Fort Ross, California, (2006/07/06, 20:43 UTC; M_L 3.7). At long periods, the surface waves of a M_w 6.6 earthquake in the Aleutian Islands (2006/07/08, 20:40 UTC) dominate the spectrum.

cally determine and to compare the characteristics of up to eight sensors at a time. The test equipment consists of an eight-channel Quanterra Q4120 high-resolution data logger and a custom interconnect panel that provides isolated power and preamplification, when required, to facilitate the connection and routing of signals from the sensors to the data logger with shielded signal lines. This year a GPS rebroadcaster was installed, so that all data loggers in the Byerly vault will operate on the same time base. Upon acquisition of the 100 samples-per-second (sps) data from the instruments under test, PSD analysis and spectral phase coherency analysis are used to characterize and compare the performance of each sensor. Tilt tests and seismic signals with a sufficient signal level above the background seismic noise are also used to verify the absolute calibration of the sensors. A simple vertical shake table is used to assess the linearity of a seismic sensor.

The sensor testing facility of the BSL is described in detail in the 2001-2002 Annual Report.

6. STS-1 Electronics Development

In February 2006, we embarked on a project to develop new electronics for the STS-1 very broadband seismometer. This is a collaborative project with Tom VanZandt

of Metrozet, LLC (Redondo Beach, CA) and is funded by a grant from NSF through the IRIS/GSN program.

The STS-1 VBB (*Wielandt and Streckeisen, 1982; Wielandt and Steim, 1986*), widely viewed as the finest VBB sensor in the world, is currently the principal broadband seismometer used by the Incorporated research Institutions for Seismology (IRIS) Global Seismographic Network (GSN), GEOSCOPE, and several other global or regional seismic networks operated by members of the Federation of Digital Broad-Band Seismograph Networks (FDSN). The installed base (approximately 750 sensor axes) represents a very significant international investment for low frequency seismology. The BDSN includes 10 STS-1's in its network. Unfortunately, many of the STS-1 seismometers, which were manufactured and installed 10-20 years ago, are encountering both operational failures and age-related errors (*Ekstrm and Nettles, 2005*). This problem is exacerbated by the fact that sensors are no longer being produced or supported by the original manufacturer, G. Streckeisen AG (Pfungen, Switzerland). The nature and severity of this problem has been discussed widely. For example, a report from a recent broadband seismic sensor workshop (*Ingate et al, 2004*) highlights the unique value of the installed base of STS-1 sensors, as well as the current lack of replacements with equivalent long period performance. In the absence of focused action by the seismological community, the state-of-health of the existing STS-1 instruments will continue to decline. Numerous efforts, both commercial and government-funded, are underway to develop future replacements (*IRIS Workshop, 2004*). Regardless of how one views the potential of these new approaches to delivering a manufacturable, STS-1-equivalent product, given the present funding environment, it is clear that they all would mandate outright replacements of the existing STS-1 sensors.

In collaboration with its commercial partner, Metrozet, LLC (Redondo Beach, CA), the BSL is developing and testing new electronic hardware, and methods for mechanical repair, for the STS-1. The intent of this effort is to develop simple and economical long-term solutions to current and anticipated problems with the existing STS-1 sensors. A primary aim is to develop a fully-tested, modern electronics module that will be a drop-in replacement for the original electronics. This will provide users with a legitimate option for replacing old modules that are no longer functioning. This new electronics design will address environmental packaging problems that have led to operational errors and failures in the existing instruments. This effort will also provide the opportunity to implement a set of electronic improvements that will make the installation and operation of the sensors more efficient.

In the first half of 2006, Metrozet developed the first prototype and reverse engineered electronics for the STS-

1, while the BSL engineering staff constructed a test-bed at the Byerly Vault (BKS) and developed the capability to simultaneously test 6-8 STS-1 components. Much time was spent locating spare STS-1's and the associated environmental shields and bringing them back to Berkeley.

7. Acknowledgements

Doug Neuhauser, Bob Uhrhammer, Peggy Hellweg, Pete Lombard, and Rick McKenzie are involved in the data acquisition and quality control of BDSN/NHFN/MBPO data. Development of the sensor test facility and analysis system was a collaborative effort of Bob Uhrhammer, Tom McEvelly, John Friday, and Bill Karavas. IRIS and DTRA provided, in part, funding for and/or incentive to set up and operate the facility and we thank them for their support. Bob Uhrhammer, Peggy Hellweg, Pete Lombard Doug Neuhauser and Barbara Romanowicz contributed to the preparation of this chapter. The STS-1 project is funded by NSF through the IRIS/GSN program.

8. References

- Ekstrm, G. and M. Nettles, <http://www.seismology.harvard.edu/~ekstrom/Projects/WQC.html>, 2005.
- Ingate, S. et al, Workshop Report from Broadband Seismometer Workshop, Lake Tahoe, CA, <http://www.iris.edu/stations/seisWorkshop04/report.htm>, 2004.
- McNamara, D. and R. Buland, Ambient Noise Levels in the Continental United States *Bull. Seism. Soc. Am.*, 94, 4, 2004.
- Scherbaum, Frank. Of Poles and Zeros: Fundamentals in Digital Seismology, Volume 15 of Modern Approaches in Geophysics, G. Nolet, Managing Editor, Kluwer Academic Press, Dordrecht, xi + 257 pp., 1996.
- Tapley, W. C. and J. E. Tull, SAC - Seismic Analysis Code: Users Manual, *Lawrence Livermore National Laboratory*, Revision 4, 388 pp., March 20, 1992.
- Wielandt, E. and G. Streckeisen, The leaf spring seismometer: design and performance, *Bull. Seis. Soc. Am.*, 72, 2349-2367, 1982.
- Wielandt, E. and Steim, J. M., A digital very broad band seismograph, *Annales Geophysicae*, 4 B(3), 227-232, 1986.

Chapter 11

Northern California Earthquake Monitoring

1. Introduction

Routine analysis of the data produced by BSL networks begins as the waveforms are acquired by computers at UC Berkeley, and ranges from automatic processing for earthquake response to analyst review for earthquake catalogs and quality control.

Over the last 12 years, the BSL has invested in the development of the hardware and software necessary for an automated earthquake notification system (*Gee et al.*, 1996; 2003a). The Rapid Earthquake Data Integration (REDI) project is a research program at the BSL for the rapid determination of earthquake parameters with three major objectives: to provide near real-time locations and magnitudes of northern and central California earthquakes, to provide estimates of the rupture characteristics and the distribution of ground shaking following significant earthquakes, and to develop better tools for the rapid assessment of damage and estimation of loss.

In 1996, the BSL and USGS began collaboration on a joint notification system for northern and central California earthquakes. The current system merges the programs in Menlo Park and Berkeley into a single earthquake notification system, combining data from the NCSN and the BDSN. Today, the joint BSL and USGS system forms the Northern California Earthquake Management Center (NCEMC) of the California Integrated Seismic Network (Chapter 5).

With partial support from the USGS, the BSL is currently embarking on the development and assessment of a system to warn of imminent ground shaking in the seconds after an earthquake has initiated but before strong motions begin at sites that may be damaged (Chapter 9.).

2. Northern California Earthquake Management Center

The details of the Northern California processing system and the REDI project have been described in previ-

ous annual reports. In this section, we describe how the Northern California Earthquake Management Center fits within the CISN system, detail recent developments, and discuss plans for the future development.

Figure 5.3 in Chapter 5 illustrates the NCEMC as part of the the CISN communications ring. The NCEMC is a distributed center, with elements in Berkeley and in Menlo Park. The 35 mile separation between these two centers is in sharp contrast to the Southern California Management Center, where the USGS Pasadena is located across the street from the Caltech Seismological Laboratory. As described in Chapter 5, the CISN partners are connected by a dedicated T1 communications link, with the capability of falling back to the Internet. In addition to the CISN ring, the BSL and the USGS Menlo Park have a second dedicated communications link to provide bandwidth for shipping waveform data and other information between their processing systems.

Figure 11.1 provides more detail on the current system at the NCEMC. At present, two Earthworm-Earlybird systems in Menlo Park feed two “standard” REDI processing systems at UC Berkeley. One of these systems is the production or paging system; the other is set up as a hot backup. The second system is frequently used to test new software developments before migrating them to the production environment. The Earthworm-Earlybird-REDI systems perform standard detection and location, and estimate M_d , M_L , and M_w , as well as processing ground motion data. The computation of ShakeMaps is also performed on two systems, one in Menlo Park and one in Berkeley, as described below. An additional system performs finite-fault processing and the computation of higher level ShakeMaps.

The dense network and Earthworm-Earlybird processing environment of the NCSN provides rapid and accurate earthquake locations, low magnitude detection thresholds, and first-motion mechanisms for small quakes. The high dynamic range data loggers, digital telemetry, and broadband and strong-motion sensors of the BDSN along with the REDI analysis software provide

Northern California Management Center Current Implementation

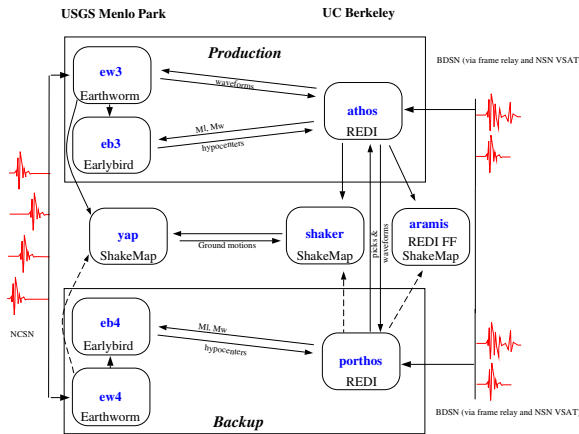


Figure 11.1: Detailed view of the current Northern California processing system, showing the two Earthworm-Earlybird-REDI systems, the two ShakeMap systems, and the finite-fault system.

reliable magnitude determination, moment tensor estimation, peak ground motions, and source rupture characteristics. Robust preliminary hypocenters are available about 25 seconds after the origin time, while preliminary coda magnitudes follow within 2-4 minutes. Estimates of local magnitude are generally available 30-120 seconds later, and other parameters, such as the peak ground acceleration and moment magnitude, follow within 1-4 minutes (Figure 11.2).

Earthquake information from the joint notification system is distributed by pager/cellphone, e-mail, and the WWW. The first two mechanisms “push” the information to recipients, while the current Web interface requires interested parties to actively seek the information. Consequently, paging and, to a lesser extent, e-mail are the preferred methods for emergency response notification. The *recenteqs* site has enjoyed enormous popularity since its introduction and provides a valuable resource for information whose bandwidth exceeds the limits of wireless systems and for access to information which is useful not only in the seconds immediately after an earthquake, but in the following hours and days as well.

3. 2005-2006 Activities

3.1 System Development

As part of ongoing efforts to improve the monitoring systems in northern California, the BSL and the USGS Menlo Park made progress in the development of the next generation of the northern California joint noti-

fication system or the Northern California Seismic System (NCSS).

Figure 11.1 illustrates the current organization of the two systems. As described above, each Earthworm/Earlybird component is tied to a REDI component and the pair form a single “joint notification system.” Although this approach has functioned reasonably well over the last eight years, there are a number of potential problems associated with the separation of critical system elements by ~35 miles of San Francisco Bay.

Recognizing this, we are redesigning the Northern California operations so that identical, complete systems operate independently at the USGS and UC Berkeley. In FY01/02, specifications were established and the details required for design were determined. In the interim, however, much of the development effort focused on statewide CISM activities, and specific plans for the “next generation” Northern California system were put on hold. The enforced wait provided the opportunity for some ideas to mature and the current plans for the NCEMC are somewhat different from those envisioned in 2001.

The current design draws strongly on the experience in Southern California for the development of TriNet (Figure 11.3), with modifications to allow for local differences (such as very different forms of data acquisition and variability in network distribution). In addition, the BSL and the USGS want to minimize use of proprietary software in the system. The TriNet software used three forms of proprietary software: Talerian Smart Sockets (TSS) for inter-module communication via a “publish and subscribe” method, RogueWave software for database communication, and Oracle as the database management system. As part of the development of the Northern California Earthquake Data Center, the USGS and BSL have worked extensively with Oracle databases and extending this to the real-time system is not viewed as a major issue. However, we did take the opportunity to review options for replacing Smart Sockets and RogueWave with Southern California, resulting in joint agreement on replacement packages and shared development effort.

In the last four years, BSL staff, particularly Pete Lombard, have become extremely familiar with portions of the TriNet software. We have continued to adapt the software for Northern California, making adjustments and modifications along the way. For example, Pete Lombard has adapted the TriNet magnitude module to northern California, where it is running on a test system. Pete made a number of suggestions on how to improve the performance of the magnitude module and has worked closely with Caltech and the USGS/Pasadena on modifications.

The BSL and the USGS Menlo Park have developed and tested a design to exchange “reduced amplitude timeseries.” One of the important innovations of the TriNet software development is the concept of contin-

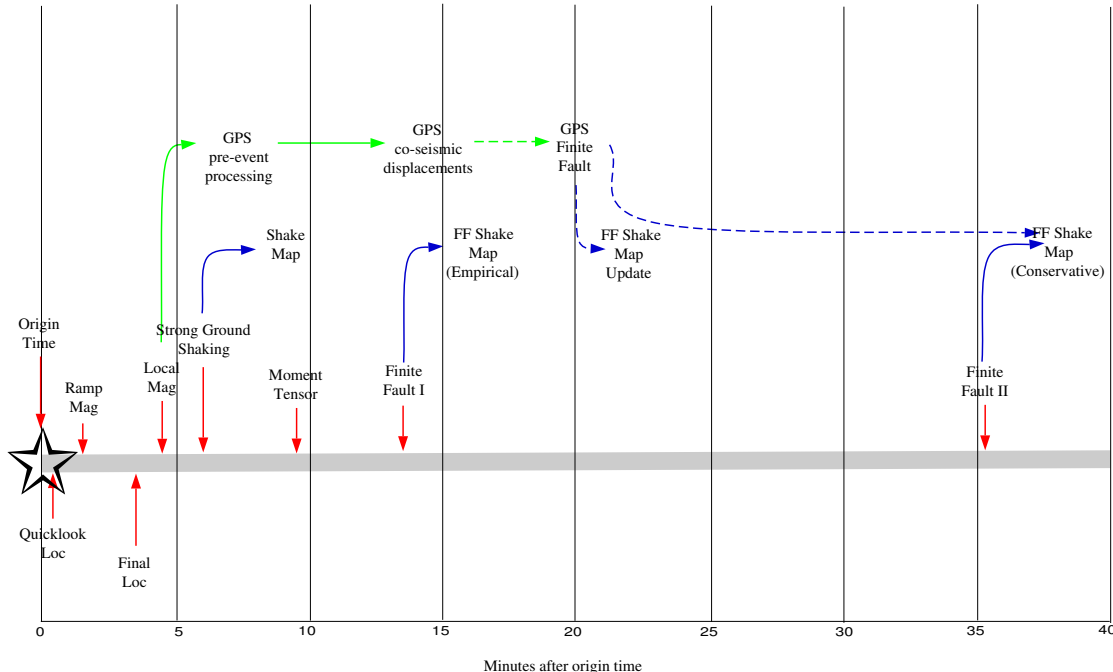


Figure 11.2: Illustration of the current (solid lines) and planned/proposed (dotted lines) development of real-time processing in northern California. The Finite Fault I and II are fully implemented within the REDI system at UC Berkeley and are integrated with ShakeMap. The resulting maps are still being evaluated and are not currently available to the public.

uous processing (*Kanamori et al., 1999*). Waveform data are constantly processed to produce Wood Anderson synthetic amplitudes and peak ground motions. A program called `rad` produces a reduced timeseries, sampled every 5 secs, and stores it in a memory area called an “Amplitude Data Area” or ADA. Other modules can access the ADA to retrieve amplitudes to calculate magnitude and ShakeMaps as needed. The BSL and the USGS Menlo Park have collaborated to establish the tools for the ADA-based exchange. As part of the software development in northern California, a number of modules have been developed.

During 2005-2006, progress has continued toward the retirement of `CUSP` - the system used by the USGS Menlo Park to time earthquakes. `CUSP` was initially developed in Southern California during the late 1970s - early 1980s and has been used for a number of years in Northern California. However, the `CUSP` system is becoming increasingly outdated.

The NCEMC has implemented a plan to retire `CUSP`, using some components of the Southern California system. The primary responsibility for the necessary programming and development rest on the shoulders of BSL staff. They have implemented the

`RequestCardGenerator` (a module that decides which channels to archive, given a particular earthquake), a waveform archiving module, and `iiggle` (the earthquake timing interface). The NCEMC and SCMC collaborated on modifications to `jiggle` for use in Northern California such as the computation of M_d . The test system is operating, and USGS timers have begun to assess `jiggle`.

Also during the past year, Northern and Southern California developers spent a day in Pasadena discussing issues of joint interest.

3.2 M_L and M_w

The REDI system has routinely produced automatic estimates of moment magnitude (M_w) for many years. However, wary of complications caused by the publication of multiple magnitudes, these estimates were not routinely used as the “official” magnitude until after the 05/14/2002 Gilroy earthquake (M_w 4.9, M_L 5.1).

In a past annual report, we discussed the question of when to report M_w . As currently implemented, solutions that meet a minimum quality criterion are automatically reported (a variance reduction of 40% or higher). This criterion appears to work very well and screens out events contaminated by teleseisms. Over the last few years,

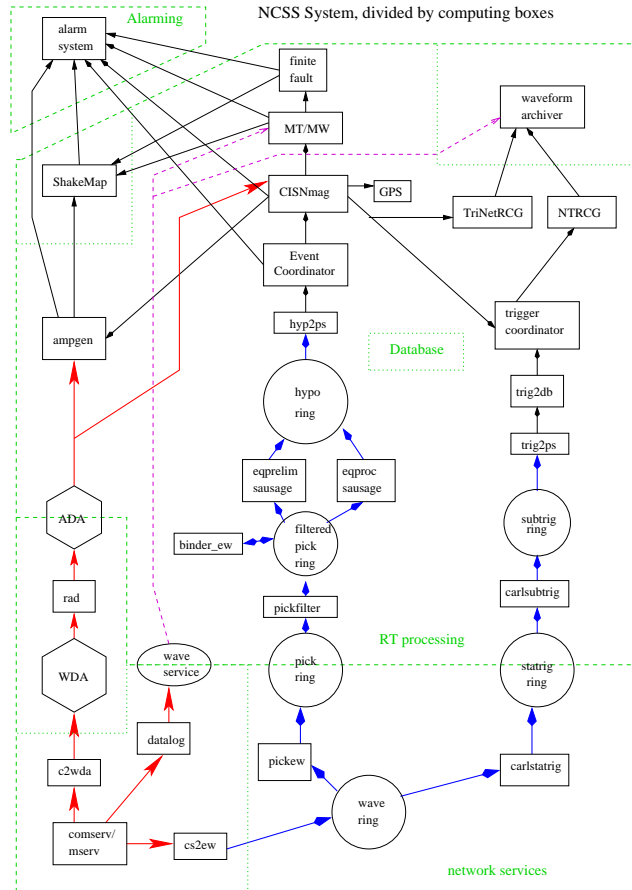


Figure 11.3: Schematic diagram of the planned NCSS system. The design combines elements of the Earthworm, TriNet, and REDI systems

nearly all events over 4.5 have met this criterion, as have a number of events in the M3.5-4.5 range. As part of the effort to establish a statewide magnitude reporting hierarchy, we have looked more closely at the estimates of M_w (Gee *et al.*, 2003b; 2004) and the comparison between M_w and M_L .

Two methods of determining regional moment tensor (RMT) solutions are part of the REDI system - the complete waveform modeling technique (CW) of Dreger and Romanowicz (1994) and the surface wave inversion (SW) of Romanowicz *et al.* (1993). In the past year processing for the SW algorithm was discontinued, however CW moment tensors continue to be calculated, reviewed and reported. Comparison between the results of the CW method and other regional moment tensor studies in northern California and the western United States show excellent agreement in the estimate of seismic moment and M_w . Over 128 events, the average difference in M_w is 0.002 magnitude units.

As we transition toward statewide reporting of earthquake information, a comparison of magnitudes calculated for southern and northern becomes important. We have collected a set of events recorded well by digital broadband and and strong motion stations of the Northern California (NC), Berkeley (BK) and Southern California (CI) networks and are assessing the computation of local magnitude for each station.

4. Routine Earthquake Analysis

In fiscal year 2005-2006, more than 30,000 earthquakes were detected and located by the automatic systems in northern California. This compares with over 38,800 in 2004-2005, and 12,000 in 2003-2004. Many of the large number of events in 2004-2005 are aftershocks of the 2004 Parkfield earthquakes. The number of events continues to remain high, because we are now receiving data from a network of seismometers in the Geysers, a region with

a high level of small magnitude seismicity. Of the more than 30,000 events, over 170 had preliminary magnitudes greater than 3. Fourteen events had M_L greater than 4. The largest event recorded by the system occurred on 12 May 2006 with M_w 4.6. This earthquake near the Geysers, California was actually two events within 70 seconds of each other.

As described in the 2003-2004 Annual Report, the BSL staff are no longer reading BDSN records for local and regional earthquakes (as of March 2004). This decision was in part intended to reduce duplication of effort between Berkeley and Menlo Park.

The BSL continues to focus on the unique contributions that can be made from the broadband network. From July 2005 through June 2006, BSL analysts reviewed nearly 30 earthquakes in northern California and adjoining areas of magnitude 3.5 and higher. Reviewed moment tensor solutions were obtained for 11 events (through 6/30/2006). Figure 11.4 and Table 11.1 display the earthquakes located in the BSL catalog and the moment tensor solutions.

4.1 Seismic Background Noise PSD in Northern and Central California

The density and distribution of broadband seismic stations located in Northern and Central California increased during the past year, with two new BK stations and additional broadband seismic stations installed as the USArray transportable array completes its station coverage in the region. One design goal of the transportable network is to complement the existing BDSN broadband stations and cover the region with an average interstation spacing of ~ 70 km. Our motivation for characterizing the seismic background noise PSD level observed at the transportable stations is, in part, that we would like to occupy the best sites after the transportable array moves out of the region, in order to improve the coverage of the BDSN network.

PSD algorithm

We have been characterizing the vertical and horizontal seismic background noise levels observed in Northern and Central California via Power Spectral Density (PSD) analysis of the seismic background signals recorded by the BDSN broadband seismic stations (BK network), NCSN broadband stations (NC network) and by the US-Array broadband seismic stations (TA network). Two frequency bands, the 1-5 Hz short-period (SP) band and the 30-60 second long-period (LP) band, are analyzed to characterize the background noise in the seismic bands of interest, particularly for the study of the seismic signals from local and regional seismic events.

The PSD algorithm uses a statistical approach to robustly estimate the background noise PSD. The PSD estimates are reported in dB relative to $1 \text{ (m/s}^2\text{)}^2/\text{Hz}$. The

input time series is parsed into eight (possibly overlapping) time series and each of the resulting time series are appropriately windowed prior to calculating their PSD estimates. For short time series, less than 1.5 hours in length, the time series are detrended and sine tapered while for longer time series the dominant semi-diurnal gravitational tide signal is also removed to avoid biasing the long-period PSD estimates. The PSD estimates are smoothed and reported at twenty logarithmically spaced intervals per decade in period.

Owing to the statistical nature of the PSD algorithm, the time series processed must contain at least 65,635 (216) contiguous samples. Shorter time series are not processed and a warning is issued. The PSD algorithm can process data with a wide variety of sampling rates (from < 0.01 sps to > 500 sps). A typical usage with broadband data is for the time series to contain one day of continuous LH (1 sps) data (86,400 samples), say. Since the sensor transfer function representation in the SEED data volume for a typical inertial seismometer does not include the static component of the response, the background noise PSD estimates for periods longer than approximately an hour will be biased high; and hence, they will be unreliable.

The PSD code distribution along with examples of its usage are available via the Web at <http://seismo.berkeley.edu/algorithms/>.

Seismic Background Noise Analysis

We acquired SEED data volumes containing a network day (2006.022) of 1 Hz three-component broadband data from the broadband stations of the NC network, the TA transportable network and from the BK permanent network. This data was used to characterize the seismic background noise in the long period (LP) band between 30-60 seconds. We also acquired SEED data volumes containing two network hours (2006.022.0000-0200) of 40 Hz three-component broadband data from the same stations of all three networks. (day 2006.022.0000-0200). This data was used to characterize the seismic background noise in the short period (SP) band, between 1-5 Hz. This study was done to assess the broadband NC stations and to help identify TA sites that would be good candidates for upgrading to permanent BDSN sites once TA moves away from Northern California.

The vertical-component LP (30-60 second period) seismic background noise PSD is shown in Figure 11.5A and the corresponding horizontal-component noise is shown in Figure 11.5B. The spread between the quietest and noisiest stations on the vertical-component is ~ 20 dB. Stations of both the BK and TA are relatively quiet. The spread between the quietest and noisiest stations on the horizontal-components in the LP band is ~ 30 dB with a larger percentage of noisy stations. The stations with the lowest noise levels are situated on bedrock or in hard rock

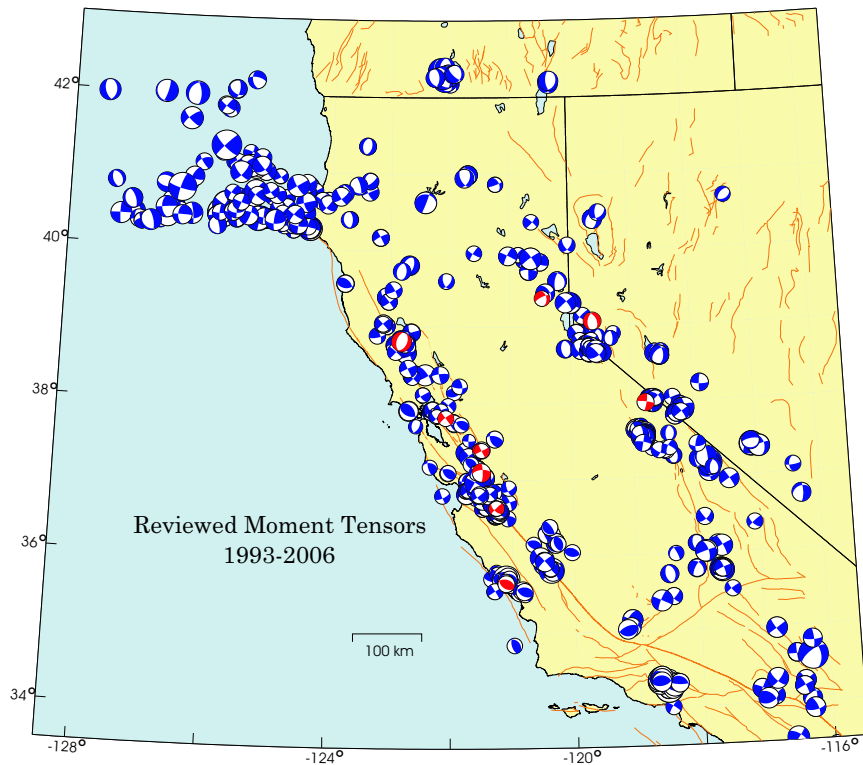


Figure 11.4: Map comparing reviewed moment tensor solutions determined by the BSL in the last 12 years (blue) with those from the fiscal year 2005-2006 (red).

mines and are far from cultural noise sources. Stations with high PSD noise levels on the horizontal components may either be on thick alluvium or have high ambient cultural noise levels.

The vertical-component SP (1-5 Hz) seismic background noise PSD is shown in Figure 11.5C and the corresponding horizontal-component noise is shown in Figure 11.5D. Here the spread between the quietest and noisiest stations on the vertical-component is larger than in the LP band, ~ 50 dB. The spread between the quietest and noisiest stations on the horizontal-component is likewise ~ 50 dB. Again, the stations with high horizontal-component PSD noise levels in the SP band are generally either sites with thick alluvial deposits or high ambient cultural noise levels.

Based on this analysis as well as criteria such as ownership, and access to power and telemetry, seven stations have been selected for upgrade to permanent sites within the next 18 months. These are: V04C (RAMR), HAST, O01C and P01C, as well as HATC, HELL and SUTB.

5. Acknowledgements

Peggy Hellweg oversees the REDI system and directs the routine analysis. Peter Lombard and Doug Neuhauser contribute to the development of software.

Rick McKenzie, Doug Dreger, David Dolenc, Ayhi Kim, Ved Lekic, Mark Panning, Junkee Rhie, Dennise Templeton, and Akiko Toh contribute to the routine analysis. Peggy Hellweg, Doug Neuhauser and Bob Uhrhammer contributed to the writing of this chapter.

Partial support for the development and maintenance of the REDI system is provided by the USGS.

The facilities of the IRIS Data Management System, and specifically the IRIS Data Management Center, were used by Bob Uhrhammer for access to the TA network (USArray) waveform and metadata required in the noise comparison study.

6. References

- Dreger, D., and B. Romanowicz, Source characteristics of events in the San Francisco Bay region, *USGS Open File Report 94-176*, 301-309, 1994.
- Gee, L., J. Polet, R. Uhrhammer, and K. Hutton, Earthquake Magnitudes in California, *Seism. Res. Lett.*, 75(2), 272, 2004.
- Gee, L., D. Neuhauser, D. Dreger, M. Pasyanos, R. Uhrhammer, and B. Romanowicz, The Rapid Earthquake Data Integration Project, *Handbook of Earthquake and Engineering Seismology*, IASPEI, 1261-1273, 2003a.
- Gee, L., D. Dreger, G. Wurman, Y. Gung, B. Uhrham-

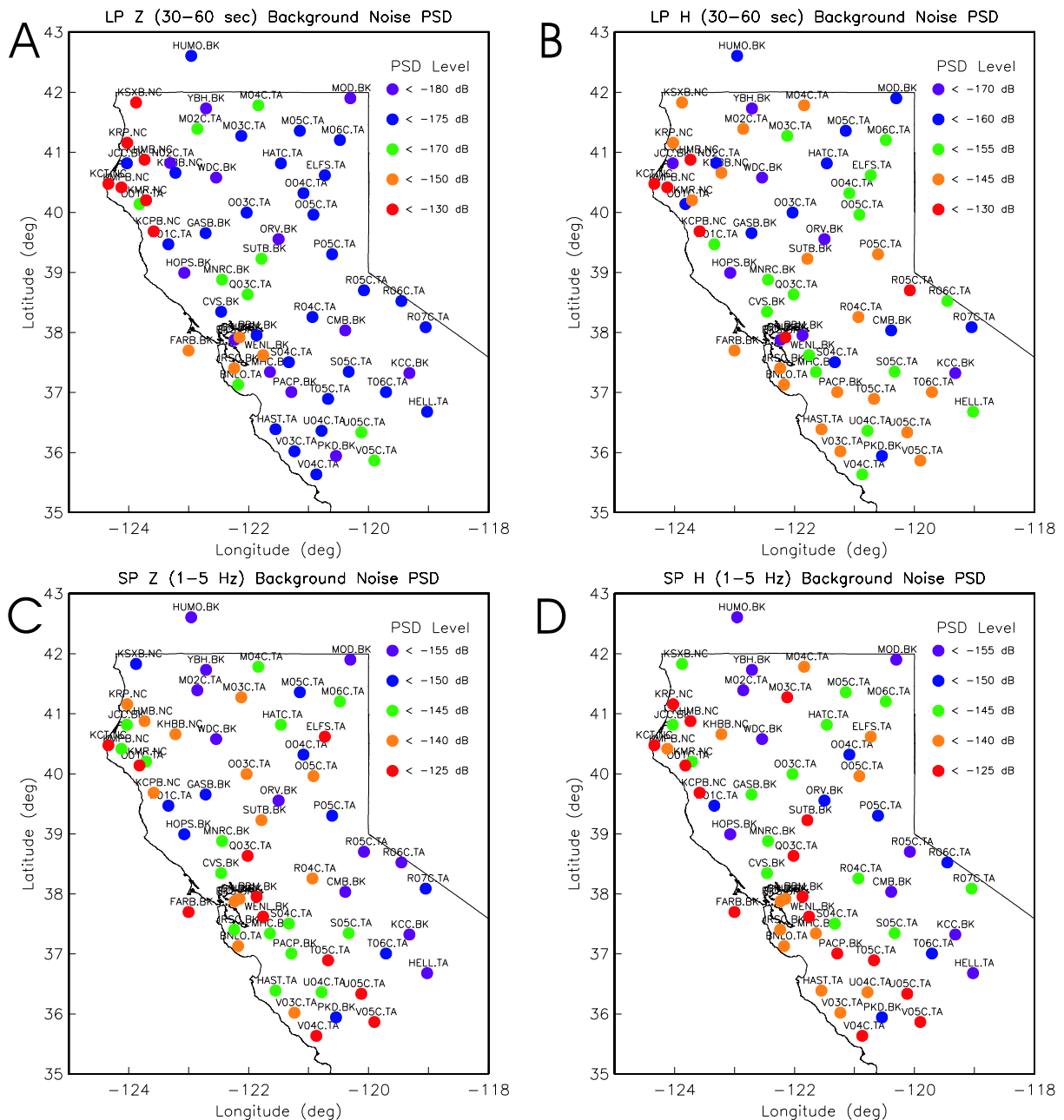


Figure 11.5: Results of seismic background noise PSD analysis for BK, broadband NC and TA network stations in Northern and Central California. A and B show results for the vertical and horizontal-components in the long period (LP) band (30-60 second), respectively. C and D show corresponding results for the short period (SP) band (1-5 Hz).

mer, and B. Romanowicz, A Decade of Regional Moment Tensor Analysis at UC Berkeley, *Eos Trans. AGU*, 84(46), Fall Meet. Suppl., Abstract S52C-0148, 2003b.

Gee, L., D. Neuhauser, D. Dreger, M. Pasyanos, B. Romanowicz, and R. Uhrhammer, The Rapid Earthquake Data Integration System, *Bull. Seis. Soc. Am.*, 86, 936-945, 1996.

Pasyanos, M., D. Dreger, and B. Romanowicz, Toward

real-time estimation of regional moment tensors, *Bull. Seis. Soc. Am.*, 86, 1255-1269, 1996.

Romanowicz, B., D. Dreger, M. Pasyanos, and R. Uhrhammer, Monitoring of strain release in central and northern California using broadband data, *Geophys. Res. Lett.*, 20, 1643-1646, 1993.

Location	Date	UTC Time	Lat.	Lon.	MT Depth	M_l	M_w	Str.	Dip	Rake	Mo
Pinnacles	08/13/05	19:13:20.20	36.634	-121.25	8	3.7	3.7	226	85	29	3.17E+21
SE Carson City, NV	09/16/05	15:09:44.44	39.066	-119.624	11	4.2	4.2	336	48	-114	2.26E+22
San Simeon	10/02/05	13:48:09.9	35.648	-121.104	5	4.4	4	287	47	76	1.27E+22
Geysers	11/17/05	08:55:05.5	38.814	-122.782	5	3.9	3.9	42	83	-7	7.04E+21
Alum Rock	01/15/06	10:42:07.7	37.388	-121.514	8	3.6	3.6	75	87	-26	2.18E+21
Morgan Hill	01/25/06	15:29:57.57	37.389	-121.485	14	3.7	3.6	153	88	180	2.99E+21
Bodie	02/16/06	17:47:59.59	37.985	-118.775	11	4.3	4.1	279	82	-9	1.52E+22
Morgan Hill	03/21/06	21:41:42.42	37.812	-122.074	14	3.8	3.8	323	90	-170	5.15E+21
Geysers	05/12/06	10:37:29.29	38.814	-122.814	5	4.4	4.6	195	48	-97	1.13E+23
Truckee	05/29/06	10:38:44.44	39.371	-120.455	14	4	3.7	244	74	-49	3.97E+21
San Martin	06/15/06	12:24:51.51	37.102	-121.492	5	4.7	4.4	360	78	-152	4.18E+22

Table 11.1: Moment tensor solutions for significant events from July 1, 2005 through June 30, 2006 using a complete waveform fitting inversion. Epicentral information from the UC Berkeley/USGS Northern California Earthquake Management Center. Moment is in dyne-cm and depth is in km.

Chapter 12

Outreach and Educational Activities

1. Introduction

The BSL is involved in a variety of outreach activities ranging from lectures to lab tours and educational displays. Commemorating the centennial of the 1906 San Francisco earthquake on April 18 provided the focus for many of them during this year. The BSL's earthquake information tape (510-642-2160) and an extensive set of web pages continue to provide basic information on earthquakes and seismic hazards for northern and central California.

2. Highlights of 2005-2006

Many of the BSL's outreach activities in this year were related to the centennial of the 1906 earthquake. In addition to organizing a special lecture series with Stanford University, the BSL contributed to museum exhibits and brochures. It also co-hosted the 2006 Annual Meeting of the Seismological Society of America, which took place within the framework of the *100th Anniversary Earthquake Conference Commemorating the 1906 San Francisco Earthquake*. Many of the BSL tours, lectures, school visits and media interactions which occurred during the course of the year were related to or inspired by the earthquake's anniversary.

2.1 2006 SSA

In November of 1906, after the San Francisco earthquake, the Seismological Society of America (SSA) was founded here to study earthquakes and promote public safety. Thus, it was fitting that the meeting in the year of the centennials of the earthquake and the society's founding take place in San Francisco. Together with the USGS, the BSL co-hosted the society's annual meeting, from 4/18/2006 - 4/22/2006 in San Francisco's Moscone Center. The meeting was co-convened with the Earthquake Engineering Research Institute, and California Governor's Office of Emergency Services as the *100th Anniversary Earthquake Conference*, and more than 3500 participants from all over the world attended. While offering a venue for interactions between the three profes-

sional groups who work with earthquakes, the seismologists, engineers and emergency managers, one goal of the meeting was to engender more communications between the professionals and policy makers on "Managing Risk in Earthquake Country". Thus, it was important that politicians were represented by such notables as Diane Feinstein, Arnold Schwarzenegger and Gavin Newsome. The 1906 earthquake, naturally a primary topic, was highlighted in plenary sessions each day, on "The Day of the Quake", "Learning from the Past", "Assessing the Present" and "Preparing for the Future". These sessions focused on what has been accomplished during the past century in terms of best practices and research results in science, engineering, and emergency management, as well as providing a view toward the future. The meeting also featured a *Gala Reception and Banquet* in honor of the society's centennial.

In the months leading up to the anniversary conference, first Lind Gee and later Peggy Hellweg represented the BSL on the Steering Committee participating in monthly conference calls and planning meetings, as well as in many of the other committees necessary to ensure the meeting ran well. Both contributed to the development of the overall meeting program, coordinating presentations of seismologists, engineers and emergency managers. They were also members of the SSA's program committee, along with Doug Dreger and USGS representatives.

2.2 1906 Lectures, Exhibits and Presentations

Members of the 1906 UC Berkeley community both felt the 1906 earthquake and were engaged in the response. University cadets were sent to support the police and troops in San Francisco, refugees were housed and fed on campus, and Professor Andrew Lawson chaired the State Earthquake Investigation Commission, which produced the first definitive earthquake report.

Together with Stanford University, the BSL organized the *Quake '06 Centennial Lecture Series*, a series of 8 public lectures, most held on both campuses. In the Fall of 2005, three lecturers introduced their audiences a his-

torical view of what happened in 1906. The presentations in January - March 2006 covered a modern view of earth science, earthquake engineering, preparedness and disaster response.

Following an exhibit of 1906-related documents and pictures from the Bancroft Library's collection in the Brown Gallery of the Doe Library, the BSL and other campus units presented material on *1906: The Great Quake - Legacy of a Disaster*. This exhibit explored UC Berkeley's participation in advancing society's understanding of the seismological, engineering, social, and political implications of seismic events, and highlighted ongoing efforts to prepare the campus to withstand another big quake. The BSL's cases displayed the seismic hazard in the Bay Area as represented by the faults and seismicity, as well as both historical and modern instruments used to record earthquakes and some of the scientific contributions made by Berkeley professors to understand them.

The BSL also contributed to the Oakland Museum's exhibit *Aftershock! Voices from the 1906 Earthquake and Fire*. In addition to the loan of a Wood-Anderson seismometer, we developed a sequence of webpages including maps of current earthquake activity in the Bay Area, California and the world. It also featured a very popular "Make Your Own Seismogram" demonstration.

The earthquake centennial also engendered more artistic efforts, to which the BSL contributed. Following several years the Memento Mori <http://memento.ieor.berkeley.edu/memento.html> has been an alternative way of viewing seismic data from BSL's station BKS in the Berkeley Hills. In honor of the 1906 centennial, Ken Goldberg and the San Francisco Ballet produced Ballet Mori. Ballerina Muriel Maffre danced to music created in realtime from the seismic data. The Pacific Film Archive prepared a film festival entitled *65 Seconds that Shook the Earth: Commemorating the 1906 San Francisco Earthquake*. Peggy Hellweg commented on the science in the final film of the series, *The Night the World Exploded*.

2.3 Putting Down Roots

One of the major activities associated with the 1906 Centennial is the publication of a booklet on earthquake preparedness. The last publication of this type in the Bay Area followed the 1989 Loma Prieta earthquake. *Putting Down Roots in Earthquake Country* is a collaborative effort among the American Red Cross, Association of Bay Area Governments, California Earthquake Authority, California Geological Survey, California Office of Emergency Services, Earthquake Engineering Research Center, San Francisco Office of Emergency Services and Homeland Security, Southern California Earthquake Center, Structural Engineers Association of Northern California, UC Berkeley, US Department of Homeland Security (FEMA), and the USGS. Publication of

the booklet is expected in later this year, with additional releases scheduled for 2006. (*Putting Down Roots* was released in September and is available on the Web at [http://pubs.usgs.gov/gip/2005/15/.](http://pubs.usgs.gov/gip/2005/15/))

3. On-Going Activities

3.1 Tours and Presentations

As every year, tours and presentations formed an important part of BSL's public relations activities. Each month several groups, ranging from middle-school students to scientists and engineers tour our laboratory under the guidance of a graduate student or a member of the staff.

The BSL hosted several special groups during 2005-2006. The geology class from Bishop Stopford School in England for made its annual stop for a tour of the laboratory and the Hayward Fault. Several classes at different grade levels received tours. In addition, BSL graduate students visited local elementary, middle and high schools to talk about earthquakes and how we measure them. In addition to the tours, Drs. Romanowicz, Allen, Dreger, Hellweg, and Uhrhammer presented talks on earthquakes and related phenomena to public groups and the media.

3.2 Open House

The BSL participated in *CalDay* this year on the weekend after the 1906 centennial anniversary. The attendance for the open house was good - visitors showed up before we opened the doors! The visitors learned about UC Berkeley's role in earthquake monitoring, watched a streaming feed of earthquake data, jumped up and down to "make a quake" played with the earthquake machine, made P and S-waves with springs, learned about earthquake preparedness, and were given sample seismograms. In addition, visitors had the opportunity to view several of the lectures from the *Quake '06* series.

3.3 Educational Displays

The BSL continues to make REDI earthquake data available to certain schools, universities, colleges, and museums for educational displays. Participating organizations receive a REDI pager and the Qpager software to display the earthquake information. The Qpager program maps the previous seven days of seismicity, with earthquakes shown as a dot. The size of the dot indicates the magnitude of the event, while the color of the dot indicates its age. These educational displays have been installed at UC Berkeley (McCone Hall, Earthquake Engineering Research Center, LHS), California Academy of Sciences, CSU Fresno, CSU Northridge, CSU Sacramento, Caltech, College of the Redwoods, Fresno City College, Humboldt State University, San Diego State

University, Sonoma State University, Stanford University (Blume Engineering Center, Department of Geophysics), UC Davis, UC Santa Cruz, UC San Diego, and USC. For the past three years, middle schools of the San Francisco Unified School District have participated in the program.

In addition to the seismicity displays, the BSL provides local waveform feeds for helicorders at visitor centers associated with BDSN stations (CMB and MHC). Organizations such as LHS, KRON, and KPIX receive feeds from BKS via dedicated phone lines for display, while the USGS Menlo Park uses data from CMB for display in the lobby of the seismology building. The BSL has also loaned a seismometer and helicorder display to the San Leandro Unified School District for their use in science classes.

3.4 WWW

We continue to maintain and update our presence on the WWW. The webpages are intended to provide a source of earthquake information for the public. They also present information about the networks we operate, including station profiles. This benefits the research community as well. The BSL web pages publicize seminar schedules, advertize courses, and describe our research, as well as our operations. They offer updates on recent earthquake activity, details on Bay Area seismicity and hazards, and links to other earthquake and earth science servers. We also use the WWW server to distribute information internally among BSL personnel, with such details as the computing and operational resources, rosters, and schedules for various purposes.

3.5 Earthquake Research Affiliates Program

The UC Berkeley Earthquake Research Affiliates (ERA) Program is an outreach project of the BSL, the Department of Earth and Planetary Science, and the Earthquake Engineering Research Center. The purpose is to promote the support of earthquake research while involving corporations and governmental agencies in academic investigation and education activities such as conferences and field trips. The ERA program provides an interface between the academic investigation and practical application of earthquake studies.

4. Acknowledgements

Peggy Hellweg oversees the outreach activities at the BSL. Barbara Romanowicz, Bob Uhrhammer, Rick McKenzie, and many other faculty, staff, and students at the BSL contribute to the outreach activities. Peggy Hellweg contributed to the preparation of this chapter.

Chapter 13

Glossary of Common Acronyms

Table 13.1: Standard abbreviations used in this report.

Acronym	Definition
AGU	American Geophysical Union
ANSS	Advanced National Seismic System
BARD	Bay Area Regional Deformation
BDSN	Berkeley Digital Seismic Network
BSL	Berkeley Seismological Laboratory
BSS	Berkeley Seismographic Station
CISN	California Integrated Seismic Network
CGS	California Geological Survey
CLC	Campus Laboratory Collaboration
CNSS	Council of the National Seismic System
CSRC	California Spatial Reference Center
DART	Data Available in Real Time
DRC	Disaster Resistent California
EM	Electromagnetic
EPRI	Electric Power Research Institute
EERI	Earthquake Engineering Research Institute
FBA	Force Balance Accelerometer
FEMA	Federal Emergency Management Agency
FIR	Finite Impulse Response
FRAD	Frame Relay Access Device
GPS	Global Positioning System
GSAC	GPS Seamless Archive Center
HFN	Hayward Fault Network
HRSN	High Resolution Seismic Network
IGS	International Geodetic Service
IMS	International Monitoring System
InSAR	Interferometric Synthetic Aperture Radar
IRIS	Incorporated Research Institutions for Seismology
ISC	International Seismological Center
ISTAT	Integrating Science, Teaching, and Technology
JPL	Jet Propulsion Laboratory
LBNL	Lawrence Berkeley National Laboratory
LLNL	Lawrence Livermore National Laboratory
MBARI	Monterey Bay Aquarium Research Institute
MHH	Murdock, Hutt, and Halbert
MOA	Memorandum of Agreement

continued on next page

Table 13.1: *continued*

Acronym	Definition
MOBB	Monterey Ocean Bottom Broadband observatory
MOISE	Monterey Bay Ocean Bottom International Seismic Experiment
MPBO	Mini-Plate Boundary Observatory
MRI	Major Research Initiative
MRE	Major Research Equipment
MT	Magnetotelluric
NCEDC	Northern California Earthquake Data Center
NCEMC	Northern California Earthquake Management Center
NCSN	Northern California Seismic Network
NCSS	Northern California Seismic System
NEHRP	National Earthquake Hazards Reduction Program
NEIC	National Earthquake Information Center
NHFN	Northern Hayward Fault Network
NGS	National Geodetic Survey
NOAA	National Oceanic and Atmospheric Administration
NSMP	National Strong Motion Program
NSF	National Science Foundation
NSN	National Seismic Network
OES	California Governor's Office of Emergency Services
ORU	Organized Research Unit
PBO	Plate Boundary Observatory
PEER	Pacific Earthquake Engineering Center
PH	Pilot Hole
PMG	CISN Program Management Group
PPE	Parkfield Prediction Experiment
PREM	Preliminary Reference Earth Model
PSD	Power Spectral Density
QDDS	Quake Data Distribution System
REDI	Rapid Earthquake Data Integration
SAF	San Andreas Fault
SAFOD	San Andreas Fault Observatory at Depth
SAR	Synthetic Aperture Radar
SCEC	Southern California Earthquake Center
SCEDC	Southern California Earthquake Data Center
SCIGN	Southern California Integrated GPS Network
SCMC	Southern California Management Center
SCSN	Southern California Seismic Network
SEED	Standard for the Exchange of Earthquake Data
SEM	Spectral Element Method
SHFN	Southern Hayward Fault Network
SIO	Scripps Institutions of Oceanography
SNCL	Station Network Channel Location
SSA	Seismological Society of America
STP	Seismogram Transfer Program
UCB	University of California at Berkeley
UNAVCO	University NAVSTAR Consortium
UNR	University of Nevada, Reno
UrEDAS	Urgent Earthquake Detection and Alarm System
USGS	United States Geological Survey